ABSTRACT

Title of Document: TOWARDS AN AUTONOMOUS ALGAL TURF SCRUBBER: DEVELOPMENT OF AN ECOLOGICALLY-ENGINEERED TECHNOECOSYSTEM

David M. Blersch, Ph.D., 2010

Directed By: Associate Professor Patrick C. Kangas, Department of Environmental Science and Technology

The development of an autonomous and internally-controlled technoecological hybrid is explored. The technoecosystem is based on an algal turf scrubber (ATS) system that combines engineered feedback control programming with internal feedback patterns within the ecosystem. An ATS is an engineered, high-turbulent aquatic system to cultivate benthic filamentous algae for the removal of pollutants from an overlying water stream. This research focuses on designing a feedback control system to control the primary production of algae in an ATS through monitoring of the algal turf metabolism and manipulation of the turbulence regime experienced by the algae. The primary production of algae in an ATS, and thus the potential of the waste treatment process, is known to be directly related to the level of turbulence in the flowing water stream resulting from the amplitude and frequency of the wave surge. Experiments are

performed to understand the influence of turbulence on the biomass production rate of algae in an ATS. These results show that biomass production is correlated with wave surge amplitude at a constant frequency. Further, the influence of turbulence on the net ecosystem metabolism of an algal turf in an ATS was investigated. Results showed that both net primary production and respiration, measured through the diurnal change of inorganic carbon, follow a subsidy-stress relationship with increasing wave surge frequency, although some of this trend may be explained by the transfer of metabolic gases across the air-water interface. A feedback control algorithm, developed to monitor the net primary production and manipulate a controlling parameter, was found to converge quickly on the state of maximum primary production when the variance of the input data was low, but the convergence rate was slow at only moderate levels of input variance. The elements were assembled into a physical system in which the feedback control algorithm manipulated the turbulence of the flow in an ATS system in response to measured shifts in ecosystem metabolism. Results from this testing show that the system can converge on the maximum algal productivity at the lowest level of turbulence—the most efficient state from an engineering perspective—but in practice the system was often confounded by measurement noise. Investigation into the species composition of the dominant algae showed shifting relative abundance for those units under automated control, suggesting that certain species are more suited for utilizing the technological feedback pathways for manipulating the energy signature of their environment.

TOWARDS AN AUTONOMOUS ALGAL TURF SCRUBBER: DEVELOPMENT OF AN ECOLOGICALLY-ENGINEERED TECHNOECOSYSTEM

By

David M. Blersch.

Dissertation submitted to the Faculty of the Graduate School of the
University of Maryland, College Park, in partial fulfillment
of the requirements for the degree of
Doctor of Philosophy
2010

Advisory Committee:
Associate Professor Patrick C. Kangas, Chair
Associate Professor William Lamp
Dr. Walter Mulbry
Associate Professor David Tilley
Professor Fred Wheaton

Dedication

To Emma and others of her generation—may you find ways of understanding the world that bring healing to all.

Acknowledgements

Many thanks are due to all those who helped make this research possible. Dr. Walter Mulbry was expecially gracious in helping to design the experiments, discussion results, and generally providing work space and research materials as needed. Thanks, too, are due to the staff and personnel of the U. S. Department of Agriculture's EMBUL Laboratory in Beltsville, Maryland, for providing support and assistance on laboratory analyses and care of the experiments when I could not. Special thanks are due to Shannon Kondrad Ingrahm of USDA Beltsville for many of the nutrient analyses, general caretaking of the ATS units, and overall comraderie through difficult times in the laboratory. Thank you to my advisory committee for constructive and perceptive comments on this work that helped it immensely. Thank you, too, to the faculty, staff, and students of the former Biological Resources Engineering Program at the University at Maryland. Their tutelage and advice was key in forming my ideas and thinking embodied in this research. Especially helpful was Dr. Adel Shirmohammadi for his continued encouragement and recommendation to the USDA National Needs Fellowship Program, which helped to support this research. Emphatic thanks are due to Dr. Patrick Kangas for providing much of the vision for this work; his enthusiasm was welcome during the tedious times of data collection and analysis. Finally, I give my endless thanks and love to my wife, Stacey, and daughter, Emma, whose love, patience and support helped see me through some of the most difficult times.

Table of Contents

List of Tables

List of Figures

Chapter 1: Introduction—Towards the Algal Turf Technoecosystem

Introduction

The engineering of complex self-organizing biosystems is in its infancy, having advanced from early concepts of ecological engineering centered on wetlands for wastewater treatment in the 1960's to the design and constructions of complex systems that hybridize ecological entities within or coupled to a technological envelope. The research pursued here supports the development of an autonomous and internally-controlled technoecological hybrid, based on an algal turf ecosystem that combines engineered feedback control programming with internal feedback patterns within the ecosystem. Algal turfs—communities of benthic attached filamentous algae and associated heterotrophic organisms—have been studied and employed for over two decades in an engineered stream microcosm called an algal turf scrubber (ATS) as a wastewater treatment technology to absorb nutrients from the wastewater stream flow. Not only is the development of feedback control technology for the algal turf scrubber process a potentially important development stage towards remotely deployable self-optimizing wastewater treatment technologies, but the combination of automated feedback control technology with self-organizing ecological systems is an important milestone in the advancement of autonomous ecologically-engineered systems. The combined technological-ecological system, or *technoecosystem*, that results from pairing ecological systems with technologically-derived feedback control pathways is a new type of self-organizing system, the dynamics of and theoretical underpinnings for which are not fully understood, but which have profound implications for the future of

understanding the emerging landscape-scale technoecosystems that combine large-scale ecological processes with human-dominated systems. The research undertaken here is intended to understand the basic principles of technoecosystem design, development, and the resulting behavioral and organizational characteristics. This research seeks to explore the ATS as an ecological system that can be engineered into a technoecological hybrid through the design of key information feedback control pathways. To do this, this research pursues through experimentation in the laboratory an understanding of the growth and development of the algal turf in response to various limiting factors that can be precisely controlled on the ATS in the laboratory. Based on this understanding of incident limiting factors on the algal turf ecosystem and the associated effects on systems-level metrics of algal productivity, the second stage of the research aims to design an appropriate technological envelope that automatically monitors the algal turf ecosystem primary productivity and affords automatic feedback control to optimize one of the limiting factors for maximum algal productivity. Exploratory experimentation with the combined ecological and technological systems leads to analysis of the behavior of the hybrid system for signatures of autonomy.

Importance of topic

Technoecosystems form an important subclass of ecologically-engineered systems (Kangas 2004). Most technoecosystems have been constructed at the laboratory bench scale (Beyers 1974, Petersen 2001, Cai 2002), although some ecologically-engineered systems such as living machines (Todd and Josephson 1996) or enclosed biospheres (Nelson et al. 1993) have been implemented at the greenhouse-scale and employ monitoring and control elements that make them, by definition,

technoecosystems. Technoecosystem engineering is at the forefront of the field of ecological engineering, yet their development thus far has been rudimentary, as most systems that have been built as technoecosystems (Myers and Clark 1944, Beyers 1974, Petersen 2001, Cai 2002) attain a minimal level of complexity and autonomy. Indeed, in a classification system of technoecosystems has been proposed (Blersch and Kangas 2006), in which categorization is based upon the existence and direction of flow of information and/or energy between living and non-living components, most of these systems would attain classification "b" (Figure 1. 1) representing a simple feedback control system. One of the goals of this research is to advance the understanding of technoecosystem engineering to increase levels of autonomy and complexity (classes "c" to "e", Figure 1. 1). The taxonomy suggests a pathway to autonomy through the coupling of energy signatures such that the technological and ecological components are co-dependent upon each other.

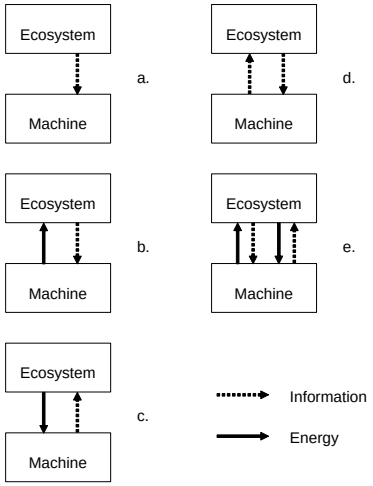

Figure 1. 1. A taxonomy of technoecosystems for a range of different kinds of systems, including some that exist and some that are theoretically possible (Blersch and Kangas 2006).

Additionally, with the advancement of artificial intelligence programming and the advent of distributed wireless networks of sensors for data acquisition (Broad 2005, Porter et al. 2005), the engineering of technoecosystems of increasing complexity and of large scales is possible. The understanding of the organizational processes of ecosystems in response to autonomous technological feedback is limited, however. Self-organization has been identified as a major component process in the design of ecologically-engineered systems (Kangas 2004, Mitsch and Jorgensen 2004), as it is inherent in biological systems (Camazine et al. 2001). This research is intended to contribute to the understanding of self-organization in systems that are hybrids of technological systems and ecosystems and exhibit system-level autonomy. The question posed in this research is thus: Does the addition of autonomous behavior in technoecosystems provide a subsidy to the self-organizing processes of the associated biosystem?

The topic of this research also has specific importance to the development of the algal turf scrubber (ATS) technology. The ATS is an ecologically-engineered system that is designed for the recovery of pollutants (typically nutrients or metals) from wastewater. The rate of recovery is dependent upon the productivity of the algal turf ecosystem, which in turn is dependent upon the balance of factors that can be limiting to the algal growth (Adey and Loveland 2007). Technological components can be strategically added for information feedback to the algal turf ecosystem, allowing the ecosystem to control its own energy inputs based upon the monitoring of a system-level metric (Blersch 2004, Blersch and Kangas 2006). It is possible to use this construct together with a self-organizing control program to allow the ecosystem to maximize its own productivity by optimizing the delivery of limiting factors. In this configuration, it would be expected

that the entire technoecosystem can self-design, in effect experimenting on itself to find the ideal conditions for productivity. From an engineering sense, it is desirable to optimize the ATS process by maximizing algal productivity while minimizing the delivery of some limiting factors (for example, light or turbulent enery) which equates directly to the cost of operation. Empirical investigation can help to answer this question. But, can an autonomous ATS answer the question for itself?

Research Questions and Objectives

There has been much interest in the construction of autonomous technoecosystems, hybrid combinations of ecological and technological components (Odum 1993, Blersch and Kangas 2006). Indeed, many ecologically-engineered systems often entail technological control networks superimposed or, sometimes, paired with ecological components for the performance of some function. Understanding how to engineer these hybrid systems for autonomous behavior is a key question for the furthering of ecological engineering. Related guiding questions for this research can be expressed. For example, can autonomy be exhibited by a combined technological-ecological system? Might autonomous operation help to increase the performance of an ecologically-engineered system?

A more specific research statement based upon these guiding questions is that an algal turf scrubber (ATS) technoecosystem can be engineered using a feedback control mechanism that monitors ecosystem productivity in realtime and influences the wave surge turbulence as the manipulated variable. Through the employment of computer-based control programming and actuating hardware, the system will organize such that it will autonomously determine the optimum level of turbulence at a given nutrient loading

rate and light level. The internal structure of the algal community in the ATS will change such that those metabolic pathways that are able to harness the additional energy input through the feedback control system will selectively persist.

Objectives

In this research, the following objectives were pursued:

1. The first objective was to investigate the effects of wave surge turbulence on algal biomass production and ecosystem metabolism in the ATS within the context of limiting factor theory via laboratory experimentation.
2. The second objective was to develop a feedback control algorithm that continuously monitors the pH level in the ATS system and calculates the metabolism of the algal turf ecosystem from the pH diurnal curve.
3. The third objective was to combine the concepts from the first and second objectives to develop a feedback control system that allows an ATS to optimize its own bed turbulence for maximum algal productivity by changing the wave surge frequency by manipulating the volumetric flow rate.
4. The final objective was to perform exploratory experimentation with the autonomous ATS system to seek signatures of autonomy. The idea is that, with such a control system, an algal turf in an ATS will automatically seek over the subsidy-stress curve of net primary productivity versus wave surge frequency to find the maximum productivity in the range.

Background

The technoecosystem

It is now possible to add artificial feedback mechanisms to ecological systems using human-created technology at a variety of scales, thereby creating new systems that are hybrids of biological and technological components (Blersch 2004). Electronic sensors and computers with control programming can be used for artificial information feedback loops to an ecosystem, possibly allowing new pathways for energy utilization within the ecosystem. Systems that combinine technological and ecological components have been called technoecosystems (Odum 1993) or, alternately, ecocyborgs (Clark et al. 1999). Odum (1993) specifically defines a technoecosystem as those systems in which "formerly wild components of ecosystems are incorporated into technological systems as hybrids of living units and hardware homeostatically coupled". The term "technoecosystem" is, however, much older, having been defined in a publication on large-scale industrial landscapes to define "large, complex, spatially or functionally distinguishable…industrial systems under conscious human control viewed as ecosystems" (Duffield 1976). This definition, important as one of the earliest published definitions of technoecosystem, was developed from concepts of systems ecology (Odum 1971) and is more akin to what is currently called industrial ecology. Key to the Odum (1993) definition, however, is the concept of homeostatic coupling, where *homeostasis* refers to the internal self-regulation of a system to maintain a quasi-steady-state despite external perturbations, and *coupling* implies a tightly-linked interdependence between internal components of the system. Thus a technoecosystem takes the form of a combined system of ecological and technological components that has internal systemic regulation

through the partial or full interdependence of its components. A way to conceptualize the technoecosystem is to recognize the necessity of internal feedback loops that affect the various sub-components, both ecological and technological, and their access to external energy sources. This perspective leads naturally to the field of feedback control engineering to inform technoecosystem design.

Another interesting permutation on the concept of the technoecosystem was provided by Clark, et al. (1999), who defined the *ecocyborg* as a system that "consist[s] of both biological and technological components that interact at the scale of an ecosystem…" (Clark et al. 1999). This definition seems to allow the possibility of technological components interacting with biological components at similar hierarchical levels and more subject to the organization and energy utilization of the entire system. Common to these definitions is the concept of some combination of technological and biological components interacting together, and thus organizing, as a whole system. In this research, the term technoecosystem will be used to descibe a system that combines technological and biological components such that the technology provides novel feedback mechanisms to the biosystems, resulting in autonomous homeostasis.

Autonomy in general systems

The concept of autonomy implies the ability for self-determination and self-perpetuation, possessing some measure of independence (Pulliam and Johnson 2002). Ruiz-Mirazo et al. (2004) use the concept of autonomy as one of two key characteristics in a universal definition of a living system. They define an autonomous system as one that "constitutes and maintains itself" in a state "far from equilibrium" by means of

> *"establishing an organizational identity of its own, a functionally integrated (homeostatic and active) unit based upon a set of endergonic-exergonic couplings between internal self-construction processes, as well as with other process of interaction with its environment."(Ruiz-Mirazo et al. 2004)*

Homeostasis is again a key point of this definition. Developing these ideas further, a definition of 'basic autonomy' was proposed as occurring when an entity "is capable of recursively generating stable novel functional constraints", where the constraint is functional if it increases the probability of system persistence in the face of external perturbations, and stable if it can be re-created in, say, successive generations (Fernando and Penn 2006). Additionally, a hierarchy of autonomy has been proposed (Vernon and Furlong 1992) in which a scale of autonomous systems is delineated into four basic types: (1) self-renewing systems; (2) self-reproducing systems; (3) self-regulating systems; and (4) self-directing systems. These ideas have been applied to living systems as well as technical systems, particularly those constructed as robots in the pursuit of research in artificial life (Brooks 2002).

Autonomy of ecosystems is a relatively new concept in ecology. In suggesting ecosystem autonomy as a key concept to be understood by ecosystem designers and managers, Pulliam and Johnson (2002) suggest that the autonomy of an ecosystem is scaled to the independence of that ecosystem from its surroundings and the inputs derived from such. No ecosystem is completely independent from its surroundings, receiving energy and matter as inputs, but the amount of autonomy of an ecosystem is established by the "relative magnitude of inputs and outputs in relationship to the size of the systems under consideration" (Pulliam and Johnson 2002). It is suggested that increased autonomy of ecosystems is sometimes desirable, for example, to limit the impacts from

external pollution sources on species within an ecosystem. It is also suggested that managers can manipulate the autonomy of ecosystems either by influencing the magnitudes of inputs and outputs to the system, or by manipulating the internal state of the system (Pulliam and Johnson 2002). Examples of naturally autonomous ecosystems are rare, but ice-covered arctic lakes have been studied and suggested as reference autonomous ecosystems (Vanriel and Johnson 1995). The authors of this study suggest that, in autonomous ecosystems, there is "a trend towards maximum energy acquisition" and conservation of that energy "in the biomass for the longest time possible". Focusing on these ideas, they deduce hypotheses concerning the determination of ecosystem autonomy that are potentially testable via observation of ecosystem properties such as species abundance, individual organism size, and energy density of organism tissues (Vanriel and Johnson 1995).

Autonomous technological systems are currently at the forefront of engineering, particularly in the fields of computer and robotic engineering, artificial intelligence, and artificial life. Many of the concepts and definitions of autonomy come from the literature regarding artificial life (Vernon and Furlong 1992, Fernando and Penn 2006) and focus on the replication of life-like properties in technical, computationally-based systems. The potential for novel autonomous systems arises at the intersection of engineering and ecology. Although few autonomous ecosystems appear in nature, many natural analogs have been engineered and studied in the form of ecological microcosms (Beyers and Odum 1993, Kangas 2004). These ecosystems have varying degree of energetic and material closure and thus fulfill the ecological conception of "autonomy". Clark et al. (1999) discuss the creation of technoecosystem hybrids in which autonomous goal

seeking is engineered in biosystems via control networks, where autonomy is understood to imply the pursuit of self-derived goals in a dynamically changing environment. Many researchers have attempted to engineer robotic systems that are powered by "food"—typically reduced organic waste products—that is digested in microbial reaction chambers (Wilkinson 2001) or supply a microbial fuel cell (Ieropoulos et al. 2009). Indeed, these researchers define the concept of "artificial symbiosis" to describe the coupling between the ecological and technological components.

Autonomous Technoecosystems

Theoretical work on the engineering and design of autonomous technoecosystems (Kok and Lacroix 1993, Clark and Kok 1998, Clark et al. 1999, Clark and Kok 1999) resulted in suggestion for a more extreme possibility for technoecosystems: the combination of ecological components with technological feedback networks exhibited as an autonomous, artificially-intelligent biosystem. An intelligent technoecosystem could process information about its internal state and take appropriate and necessary action to maintain internal homeostasis, for example, by accessing additional sources of energy or nutrients or mitigate infestations of unwanted species. The authors have proposed this type of system at the greenhouse scale for the production of agricultural crops for space exploration applications (Kok and Lacroix 1993, Clark et al. 1999). The researchers suggest parameters of complex engineered technoecosystems that might be measured to characterize a system's level of autonomy (Table 1. 1). These measures rely upon the observation of patterns and correlation between the actions of components of a system and of the entire system itself.

Table 1. 1. System properties of technoecosystems that might be used to measure the degree of system autonomy (Clark and Kok 1999).

Parameter to be Measured	Description
Order	The degree of correlation between features of the system.
Disorder	The variation in a system, either random or in a pattern.
Complexity	The variation associated with pattern, gauging the difficulty in describing the pattern.
Emergence	The degree to which global phenomena are influenced by local structure.

One of the earliest published papers on an autonomous technoecosystem (although it was not called such by the authors) was on the apparatus known as the turbidostat (Myers and Clark 1944). This apparatus was developed for the continuous growth of a suspended algal culture of *Chlorella* where the population density is automatically maintained at or near a steady state by the addition of fresh growth medium. A typical setup of the turbidostat employs an algal culture in a chamber constructed of concentric glass tubes illuminated by external lights. Fresh nutrient medium is automatically added by a solenoid valve controlled by a photocell that monitors the light transmittance of the algal culture density. As the algal culture grows denser, illumination to the photocell is blocked, creating an off-balance current in a circuit that opens the solenoid valve to allow fresh growth medium into the growth chamber. The fresh medium dilutes the suspension, restoring illumination to the photocell and closing the solenoid. The apparatus allows for the continuous culture of suspended algae at constant cell density and uniform photosynthetic rate over many months (Myers and Clark 1944). Because all sources of energy are in excess and not limiting, algal growth becomes limited only by factors internal to the alga. The rudimentary autonomy of the turbidostat is evidenced by the fact that the growth of the culture is controlled by

feedback control based upon a parameter internal to the biosystem (that is, the population density), as opposed to external control, as employed in a chemostat, in which the growth rate of a culture of microorganisms is set by the flow rate of a continuous nutrient feed into a bioreactor (Premazzi et al. 1978).

A technoecosystem was constructed using an aquatic photosynthetic microcosm in which the lights were controlled by measurement of the pH level of the solution (Kania and Beyers 1974). Dissolved carbon dioxide rises or falls because of release or uptake during respiration or photosynthesis, respectively, affecting the pH of the solution. In the technoecosystem microcosms, the level of pH was used to automatically switch on and off a light source to keep the pH within the bounds of low and high setpoints. The researchers reported that the system exhibited oscillatory behavior, alternating between periods of light and dark. In two of three replicate systems of this configuration, the light phase of the light-dark cycle was longer than the dark phase and gradually increased over time until, eventually, the light remained on constantly. Odum (1993) contends that this indicates the systems gradually organized to maximize photosynthetic power.

Another photosynthetic technoecosystem was constructed in which an artificial feedback loop was added to aquatic planktonic microcosms using dissolved oxygen sensors and a data-logging computer (Petersen 1998, 2001). When dissolved oxygen in the water column fell below a lower set point because of ecosystem respiration, a light was turned on to stimulate photosynthesis. The oxygen created in community photosynthesis increased the dissolved oxygen content of the water until it reached an upper set point, at which time the light was turned off. The nutrient uptake, primary productivity, and duration of light and dark periods were measured for all microcosms.

While the overall development of the microcosms were not seen to change much compared to fixed lighting conditions, similar patterns in energy demand and oscillatory primary productivity patterns were observed between replicate microcosms. It was found that the artificial feedback induced a partial decoupling between productivity and respiration in the planktonic community. Petersen (2001) also suggested that the novel character of the oscillations between the light and dark period was a result of the feedback structure and amounted to emergent behavior at the level of the system.

Another technoecosystem was constructed out of planktonic microcosms in which the photoperiods of experimental replicates were controlled by feedback control of pH, turning on the light when the pH level fell to a lower threshold and turning off the light at a higher threshold (Cai 2002, Cai et al. 2006). The researchers compared the behavior and internal structure of experimental replicates (that had developed under feedback control) with those of other replicates that had developed without feedback control. The researchers found that, after both types of replicates were tested under feedback control for a time, both types increased the daily light duration via that feedback, but the increase in duration was greater (506 versus 412 minutes) for those units initially developed under feedback control. Also, the increased abundance of acid-secreting blue-green algae was observed in these units, and this was suggested as the explanation for the greater photoperiod and thus greater power acquisition for these units. The authors suggest that these results demonstrate the selective persistence of power-maximizing system designs (Odum 1975) as derived from the Maximum Power Principle (Lotka 1922, Odum and Pinkerton 1955).

The design and operational dynamics of a technoecosystem investigated for a technoecosystem that consisted of a wetland soil microcosm in which redox potential was controlled by feedback (Blersch 2004, Blersch and Kangas 2006). The researchers compared microcosms with feedback control to those without it. Using platinum-tipped electrodes to measure redox potential in the microcosms, the control system could add nutrient solution to the microcosms to maintain redox potential within a defined range. A redox value greater than an upper threshold setpoint triggered the addition of a carbon solution, whereas a redox value less than a lower threshold triggered the addition of a nitrate solution. Experimental trials exhibited an oscillatory trend in redox potential over time, compared to steady decline in redox potential in the control trials. The feedback transformed the microcosms from a reduced state into an alternative state of oxidation. The researchers suggest practical applications in the optimization of denitrification rates in wastewater treatment wetlands by automatically adding the limiting nutrient. They also propose a taxonomic classification of emerging possible technoecosystems based upon the types of interactions (information exchange versus energy exchange) between living and nonliving system components (Figure 1. 1).

Algal Turf Scrubbers and the Role of Turbulence

The algal turf scrubber (ATS) has been developed as a mechanism for cultivating benthic filamentous algae under conditions of high productivity for the purpose of pollutant removal from a wastewater stream(Adey and Loveland 2007). The ATS was originally patented by Walter Adey of the Smithsonian Institution, an algae ecologist who realized that by separating out the photosynthetic component of a coral reef, the factors limiting to productivity could be managed to drive algal productivity to a maximum,

thereby providing oxygen production and nutrient uptake for coral reef microcosms (Adey 1982, Adey 1987). A typical laboratory-scale recirculating ATS is shown in Figure 1. 2. A turf of filamentous algae is grown on the screen in the shallow bed under a light source. An algal turf consists of a complex community of filamentous algae and microorganisms and is known to be among the most productive photosynthetic ecosystems in nature (Lewis 1977). When employed for wastewater treatment, pollutant-laden water is added to the reservoir of the system in batch form. Water is pumped from the reservoir to the wave surge bucket, the action of which causes wave action and turbulence in the bed. The turbulence of the flow regime selects for the benthic filamentous algae over other morphologies and contributes to the overall algal productivity (Adey and Loveland 2007). As the algal turf grows, it uptakes nutrients or adsorbs other pollutants in its biomass, and periodic harvesting of this biomass removes those pollutants from the water stream. ATS units have been examined for nitrogren and phosphorus removal from municipal wastewaters (Craggs et al. 1996), aquaria (Anonymous 1995), and dairy manure (Mulbry and Wilkie 2001, Wilkie and Mulbry 2002, Kebede-Westhead et al. 2003, Mulbry et al. 2005); metals and organics removal from industrial waters (Adey et al. 1996); and phosphorus removal from natural waters receiving agricultural runoff (Adey et al. 1993). ATS units have been employed at a variety of scales ranging from the home aquarium (Anonymous 1995) to multi-hectare facilities (Hydromentia 2005). When employed for nutrient uptake from polluted waters, the ATS technology is scaled for a particular application using estimates of algal production (in grams of biomass produced per area per unit time) and of the component biomass fraction of the nutrient of interest. The ease with which the various potential

limiting factors (most importantly, light, carbon, nitrogen, phosphorus) can be manipulated and controlled in the laboratory and the celerity of the resulting response in algal community productivity makes the ATS an ideal ecological system for research in technoecosystem engineering.

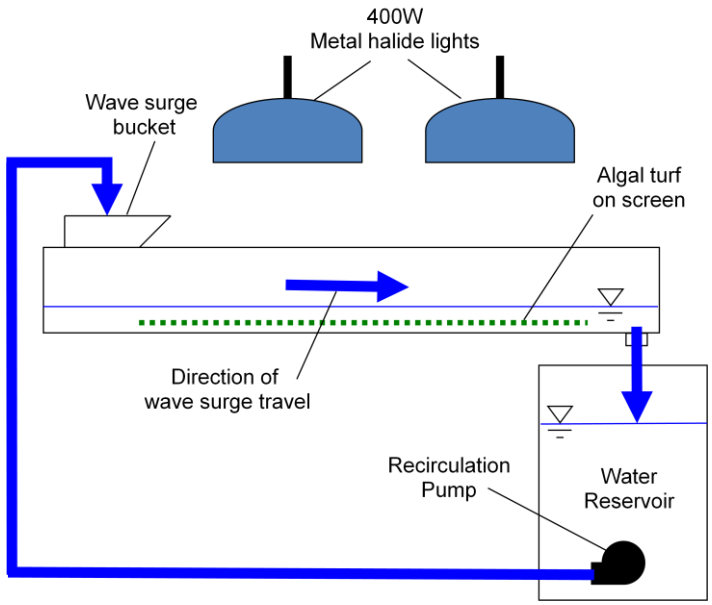

Figure 1. 2. Schematic drawing of a recirculating laboratory-scale algal turf scrubber (Adey et al. 1993).

The growth response of algae in an ATS can be described by limiting factor theory of ecology, which states that the success of an organism or community depends upon a combination of conditions, whereupon any one of which exceeds a limit of tolerance (maximum or minimum) becomes the factor that is limiting to the growth of that organism or community (Odum and Barrett 2005). Limiting factor theory extends from Liebig's Law of the Minimum (Liebig 1840), which states that the success of an organism cannot exceed the level set by the availability of the weakest component in its set of requirements. An important corollary in the consideration of algal growth in an ATS is the concept of the interaction of factors, in which the action of some factor other than the minimum may affect the utilization of the limiting factor (Odum and Barrett

2005). It is important to note that the limits of tolerance of any one factor can be in the maximum as well as the minimum, in either case causing stress in the organism or community. The classic subsidy-stress response (Odum et al. 1979) of a community to the varying availability of a factor describes that a factor low in concentration may be limiting; increasing availability of that factor may increase growth and productivity up to a maximum; and further increase may become a stressor (e.g., via toxicity interactions) which again limits productivity in some way (Figure 1. 3).

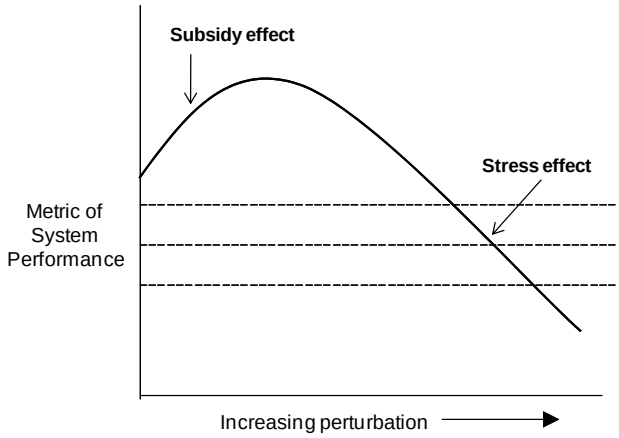

Figure 1. 3. The subsidy-stress concept in ecology, where the increase in a perturbation can initially subsidize some characteristic of system performance (being a limiting factor for that metric), but beyond a certain optimum level, the perturbation may cause increased stress effect and reduce the overall characteristic of performance (Odum and Barrett 2005).

The relationship of productivity of the benthic algal turf or periphyton to increasing velocity of the overlying fluid flow generally exhibits a subsidy-stress relationship (Odum et al. 1979, Odum and Barrett 2005) as a result of opposing mechanisms of increased availability of light and nutrient delivery to cells and increased biomass export rates due to drag forces (Stevenson 1996). Flowing water is considered to stimulate productivity of a benthic algal community for a variety of reasons (Saravia et al. 1998), including increased delivery and replenishment of nutrients from upstream; increased flushing of growth-inhibiting waste products and metabolites; and increased

import of new algal cells to open sites. Deleterious effects do exist, however, as water flow creates a drag force on cells and filaments in the periphyton matrix, increasing the scour and export of cells from a periphyton mat as a result of sloughing (Stevenson 1996). A conceptual model was developed (Whitford 1960) for understanding the general stimulatory effect of current on periphyton growth. In stagnant or non-flowing water containing a nutrient concentration, an algal cell will have surrounding it a diffusive boundary layer in which the concentration of the nutrient is lowest at the surface of the cell (because of uptake and use by cell mechanisms) and increases outward from the cell surface to equal the ambient concentration of the surrounding fluid at some defined distance away from the surface. Within this shell, diffusion kinetics dominate, and the steepness of the diffusion gradient is determined by the physical relationship between the solute (nutrients) and the solvent (water). For an attached cell in a flow environment, low-concentration water within the surrounding shell is swept away and replaced with incoming water of ambient concentration, shortening the thickness of the diffusion shell and causing the gradient to be steeper (Whitford 1960). In such a situation, the overall exchange rates of nutrients between the surface of the cell and the ambient fluid flow are increased. In a linear flowing system such as a stream, the diffusion shell is envisioned as a boundary layer overlying the base substrate in which the velocity varies from zero at the surface to the stream velocity some distance above the surface, defining the limit of the boundary layer (Silvester and Sleigh 1985). An attached periphyton community modifies the roughness of the substrate surface and, for any given flow, affects the thickness of this diffusive boundary layer.

There have been numerous attempts to model periphyton growth in flowing water which help to conceptualize the interaction of the turbulence of the flow field with the diffusive boundary layer. Many of these simulations focus on the interactions of the benthic periphyton layer with the flowing water overhead, and especially on the transport dynamics of nutrients at this interface. A simple mechanistic model was proposed (Momo 1995) that describes the growth of periphyton in streams as unstable above a critical flow velocity, resulting from the tradeoff between stimulatory and scour effects. Another model (DeAngelis et al. 1995) investigated nutrient uptake by periphyton in streams by suggesting a static diffusive boundary layer surrounding the benthic periphyton community, with nutrient availability in this layer controlled by the properties of a transient layer at its periphery. This model was improved (Nikora et al. 1998) by adding different flow conditions defined by the amount of penetration of the flow into the periphyton biomass. Further development of this model (Larned et al. 2004) showed that the height of the periphyton canopy (formed by algal filaments) in relation to the height of the boundary layer of the stream bottom was a major determinant of the controlling dynamics of nutrient uptake. That is, if the periphyton canopy extended beyond the boundary layer of the substrate, diffusive effects surrounding each algal filament controlled nutrient uptake. In general, these simulations indicate that the diffusive boundary layer can be the strongest determinant of nutrient uptake dynamics and thus periphyton productivity in flowing water. Whether the diffusive boundary layer is located at the surface of the periphyton mat (DeAngelis et al. 1995) or along the surface of algal filaments as they extend above the boundary layer of the substrate (Larned et al. 2004) is directly related to the velocity and turbulence of the overlying flow as transferred to the

forces acting upon the individual algal filaments (Son and Fujino 2003). At higher flow rates, the thickness of the diffusive boundary layer is decreased and the diffusive gradient between the uptake surface and the ambient flow becomes steeper.

Numerous empirical studies have been undertaken to verify the hypothesized effects of flow velocity on the productivity of periphyton communities. Many studies have reported an increase in the biomass accumulation rate as velocity increased, both in the laboratory (Odum 1956, Mcintire 1966a) and in the field (Horner and Welch 1981, Biggs and Hickey 1994), for flow velocities ranging from 10 to 150 cm s^{-1}. Many of these same studies also found the stimulation of metabolic measures such as primary productivity and respiration by increasing velocity levels (Odum 1956, McIntire 1966b, Marsh 1970, Biggs and Hickey 1994). Still others, however, found reduced levels of biomass accumulation at the highest levels of velocity (Antoine and Benson-Evans 1982, Horner et al. 1990, Lau and Liu 1993). These results suggest that benthic algal production in general is stimulated by increasing velocity of flow, due to the reduction of the diffusive boundary layer surrounding the benthic matrix, but that greater velocity increased rates of scour and thus export of biomass. Because of the evident impact of high flow velocities on community export rates (Antoine and Benson-Evans 1982), it can be generalized that periphyton community biomass is highest in intermediate flows. Adding complexity to the relationship, however, is the effect of other potential limiting factors (e.g., nutrient concentration, light availability) that may interact with the productivity response of periphyton communities to increasing velocity (Stevenson 1996).

These studies provide guidance as to the role of flow velocity and turbulence in stimulating the productivity of the photosynthetic benthic community it might impact. The turbulence in an ATS, however, is delivered more from the wave surge action of its design rather than the velocity of the bulk flow. Indeed, with a slope typically of 1 to 2 percent, velocities of the base flow in an ATS typically does not exceed 20 cm s^{-1}, and Reynold's numbers (an indication of the turbulent energy of a flowing fluid) are typically low (Streeter and Wylie 1975). Algal turfs in environments of periodic wave surge have been shown to be substantially more productive than the same turfs at comparable base flow velocities (Adey and Hackney 1989). An oscillatory wave flow regime was found to stimulate the primary productivity of algal turfs over 20% compared to a vortex field flow of similar velocity (Carpenter et al. 1991), and oscillatory flow was shown to have similar stimulatory effects on nitrogenase activity in an algal turf compared to unidirectional flow (Williams and Carpenter 1998). Subsequent research indicated that mass transfer of dissolved inorganic carbon (Carpenter and Williams 2007) and nutrients (Thomas and Cornelisen 2003, Barr et al. 2008) into seagrass and algal turfs can be diffusion limited at low flow velocities, and oscillatory flow plays a role in overcoming diffusive limitation caused by flow turbulence attenuation by high-canopy algal turfs (Carpenter and Williams 1993). Oscillatory flow has been shown to increase mass transfer of dissolving plaster forms up to 1.6 times over bulk flow velocities of less than 10 cm s^{-1}, although this effect was less pronounced for increased velocities beyond that (Falter et al. 2005). It is this effect which has led to the rapid development of the algal turf scrubber as an engineering system for the cultivation of a filamentous algal turf for

wastewater and pollution treatment (Adey 1982, Adey et al. 1993, Adey et al. 1996, Craggs et al. 1996).

Ecosystem Metabolism and the pH Diurnal

The measurement of ecosystem metabolism in aquatic systems entails the determination of primary production and respiration based upon the changes of gas concentrations in the overlying water. Measurement is typically performed by measuring the flux of gases dissolved in the water that are important to production and respiration, namely, oxygen and carbon dioxide. The relative rate of uptake or evolution of either of these gases (generally expressed as grams per square meter per day for the gas in question) throughout a diurnal light cycle gives an indication of the overall production of the ecosystem (Ryther 1956). For example, if carbon dioxide changes were being measured for a diurnal cycle, gross primary productivity is represented by the decline of carbon dioxide (as grams of carbon per square meter per day, or g C m^{-2} d^{-1}) during the light period; respiration is represented by the increase of carbon dioxide during the dark period; and the net primary productivity (also called the net daily metabolism) is equal to the gross primary production minus respiration (Bott 1996). The ratio of gross primary production to respiration (the P/R ratio) is often used as a functional index of the relative maturity of an ecosystem; in the successional development and maturation of ecosystems, it is generally found that the ratio of the gross primary productivity to respiration (the P/R ratio) is greater than 1 (Odum and Barrett 2005). As the ecosystem matures, the P/R ratio approaches 1 as more energy is used in respiration for the maintenance of the biomass.

Direct measurement of the metabolically important gases in aquatic systems has been performed and investigated by various researchers. A method was developed (Odum

1956) that employes the diurnal pattern of dissolved oxygen, using saturation deficits and kinetic transfer coefficients to account for the diffusion of the gas across the air-water interface. This method has since been standardized for aquatic systems (APHA 1995). Early on, this method was developed employing a Winkler titration to measure the concentration of dissolved oxygen (Odum and Hoskin 1957), and the advance of electronic probes has allowed for the automatic measurement and datalogging of metabolic gases. For example, to measure the metabolism of a natural and microcosm Caribbean coral reef flat over a number of days, researchers built and tested a computer-based data-logging system that employed oxygen sensors, current meters, light meters, and a tide gauge (Griffith et al. 1987). Continuously recorded measurements of the rise in oxygen during the day and the fall in oxygen during the night allowed calculation of the daytime net production, nighttime respiration, and total excess production. Other instruments and systems have been developed for continuous and automatic measurement of carbon dioxide concentrations in freshwater (Sellers et al. 1995, Carignan 1998) and marine systems (DeGrandpre et al. 1995).

Another method for measuring the ecosystem metabolism in aquatic systems is to track the change in carbon dioxide concentration indirectly through the measurement of pH through a diurnal cycle. Carbon dioxide dissolves in water as a weak acid via the carbonate system (Masters 1991). Thus, as the CO_2 concentration decreases during the day because of photosynthesis, pH levels increase; conversely, as the CO_2 concentration increases during the night because of respiration, pH values decrease. The method therefore requires calibration of the pH to the concentration of CO_2 in the water through analytical or empirical means (Beyers and Odum 1959). The empirical method relies

upon the construction of a pH-CO_2 curve for the water of interest to allow conversion of the pH results to CO_2 concentrations (Beyers and Odum 1959, Beyers et al. 1963, Beyers 1964). The analysis is performed by the incremental titration of distilled water saturated with CO_2 into a sample of known volume from the water body of interest from which all CO_2 has been stripped. The pH is recorded at each titration increment, and titration of precise amounts of water allows the calculation of the amount of CO_2 added at each titration step, allowing the construction of the characteristic pH-CO_2 curve for the water of interest. This method has been used to measure the metabolism of natural systems (Park et al. 1958), individual organisms (Beyers and Warwick 1968) and laboratory microcosm ecosystems (Beyers 1965). The advantage of the pH diurnal method over others results from the low cost of the near-ubiquitous pH probe, compared to other available electronic probes. Additionally, the pH method may be more appropriate for use in more turbulent environments compared to the oxygen method; because of the low partial pressure of carbon dioxide in the atmosphere, diffusion from the atmosphere into the water body is usually an insignificant component of the overall carbon budget of a productive aquatic ecosystem and thus can often be ignored in calculations of ecosystem metabolism (Park et al. 1958).

An alternate method of measuring community production is by the sacrificial harvesting of standing biomass from a substrate and measuring its ash-free dry mass (Steinman and Lamberti 1996). Calculation of production, generally expressed as grams of biomass per area per unit time, is performed by dividing the ash-free dry mass of harvested biomass by the harvest area and by the time required for the accumulation of the biomass from a barren substrate. Harvest of the standing biomass includes both

autotrophic and hetereotrophic components of the community, and no information can be determined about the partitioning of the photosynthetic and respiratory components (Steinman and Lamberti 1996). This method is fundamentally different from the gas-flux approach, inasmuch as it gives no information about the community diurnal metabolism, rather serving as an integrative index of metabolism over a of time period usually longer than 24 hours. While the method has been used for measuring productivity in natural streams (Bothwell 1988), this method has also been employed extensively for measuring the overall productivity of the algal community in algal turf scrubbers (Adey et al. 1993, Adey et al. 1996, Mulbry and Wilkie 2001, Kebede-Westhead et al. 2003).

Research Approach

Technoecosystems: The view through Odum's "Macroscope"

While the reductionist perspective is predominant in scientific inquiry, a holistic synthesizing view has value in understanding the organization of complex systems. Odum (1971, 2007) expresses the value of the holistic view through the suggestion of viewing systems through the "macroscope" of systems analysis. While details and internal mechanisms of a system are first surveyed and identified, the complexity of detail is mitigated through aggregation and classification to yield a systems-level understanding of organizational principles of the system. Principles of general systems theory translate through all real physical systems, as they are emergent from the laws of thermodynamics (Odum 2007). The macroscopic perspective guides the approach of this research. As the technological and ecological components of the ATS system under study are interpreted to be component parts of the overall ATS technoecosystem, the characteristics of each component system are investigated in isolation, yet with the

objective to understand the interaction at their interface through emergent characteristics at the systems level (Figure 1. 4). First, investigation into the response of an algal turf in an ATS to the intensity of turbulent energy is pursued. Next, based on those results, a seeking algorithm is developed and tested to serve as the core of a feedback control system. Finally, the elements are combined into a technoecosystem configuration that is tested and evaluated for efficiency of performance.

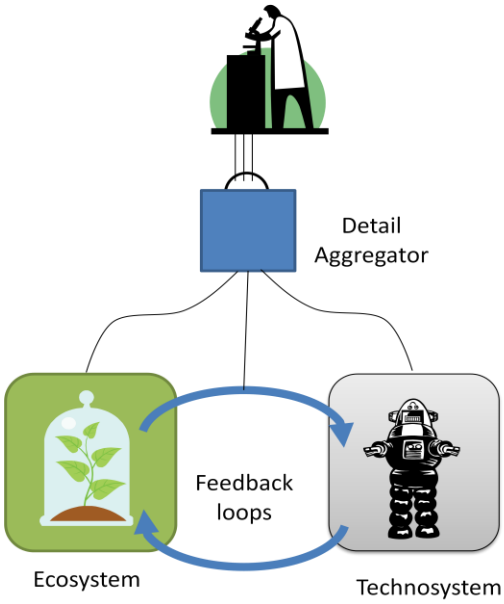

Figure 1. 4. The view through Odum's macroscope as a method of analysis for investigating the systems-level characteristics of a technoecosystem that incorporates feedback between ecological and technological components (based on Odum (2007)).

Preliminary Investigations: Pushing and Pulling the Periphyton

Following the assumption that the turbulence of a flow field overlying a benthic algal turf is a key limiting factor to the productivity of that algal community, the preliminary experiments were designed to explore the role of turbulence as a limiting factor to the productivity of the algal turf in a range of nutrient-loading environments. Volumetric flow rate and wave surge frequency were independently manipulated on a set of ATS units to establish a range of turbulence conditions. The resulting effect of

turbulence on the overall biomass production rate of algal biomass over a range of nitrogen loading rates was measured through periodic sacrificial harvesting of the algal turf. To accompany these production measures, an independent measure of turbulence intensity at the scale of the turf thickness was developed using the dissolution rate of gypsum blocks placed in the flowing water.

Investigating the Ecological: Seeking the subsidy-stress curve

The effect of turbulence on the algal turf ecosystem metabolism was investigated, with the expectation that algal net primary production and respiration should follow a subsidy-stress relationship as a function of flow turbulence. This set of experiments was undertaken to explore the possibility of using continuous monitoring of the pH diurnal to determine the ecosystem metabolism of the algal turf and measure its response to changes in levels of flow turbulence. The correlation between the metabolic measurements and overall rate of biomass production was also investigated, under the interpretation that the latter results from a integration over time of the former. Examination into the organization of the algal turf at the species level was investigated to determine the effect of interacting limiting factors on the competition between the dominant species of algae.

Investigating the Technological: Building a seeking algorithm

The research continued with the design and implementation of the supervisory control algorithm, the set of instructions that influence the technological components in response to the metabolic conditions in the ecological components. The algorithm was designed as a simple seeking algorithm that finds the maximum net primary productivity over the range of variation of volumetric flow rate, based on the results of the previous chapter. Virtual testing of the algorithm was performed by exploring its response to

hypothetical, stochastic data sets that form idealized distributions of ecosystem productivity versus flow turbulence. The convergence behavior of the algorithm—that is, the accuracy and rate of approach to the expected solution—emerged from a large number of repeated, multi-cycle trials. The results helped to inform the expected response of the system during implementation of the physical technoecosystem configuration.

Investigating the Technoecosystem: The ghost in the living machine

The engineered ATS technoecosystem was assembled and run through a series of tests for debugging and for determining the operational parameters, constraints, and protocols. Tests were performed allowing the control system to automatically change the volumetric flow rate delivered to an ATS bed in response to the changes in the algal turf net primary productivity. The resulting trace of flow rate over time and primary productivity over time were analyzed for metrics of convergence using the methods developed in virtual testing of the algorithm. The distribution of the relative abundance of the various dominant species was also analyzed for signature changes related to the presence or absence of the automated control system. These data sets together offered evidence for the self-organizational trajectory of the overall technological-ecological hybrid that was fundamentally different from the standard mode of operation for the ATS system.

Chapter 2: Preliminary Investigations—Exploring Turbulence as a Limiting Factor

Introduction

Bed turbulence, as determined by flow velocity, can be a limiting factor to the productivity of a benthic algal community (Whitford 1960, Mcintire 1966a, Horner and Welch 1981, Antoine and Benson-Evans 1982, Biggs et al. 1998). In an algal turf scrubber (ATS), the bed turbulence and thus the algal productivity is strongly determined by the amplitude (that is, the volume) and the frequency of the wave surge (Adey 1982, Carpenter et al. 1991, Adey et al. 1993, Craggs et al. 1996, Adey and Loveland 2007). It has been observed that too low of a flow rate in an ATS results in lower productivity (Adey 1982, Adey and Hackney 1989). The exact controlling mechanism is unclear, but possible candidates are decreased nutrient availability because of diffusion limitation, decreased light availability because of self-shading, or a combination of both. It is also known that a highly turbulent environment can damage and increase export of existing algal biomass (Mcintire 1966a, Horner et al. 1990). Therefore, there must be a range of turbulence levels in an ATS in which biomass production is maximized. Further, this range might shift for different light intensities and nitrogen loading rates.

Preliminary investigations were undertaken to understand the role of bed turbulence as a limiting factor to the productivity of an algal turf in an ATS. Volumetric flow rate and wave surge frequency were manipulated on an algal turf scrubber operating under a range of nitrogen loading rates. The turbulent environment of the resulting flow regimes were characterized via various measurements, and the resulting effects on algal biomass production rate were measured via regular periodic biomass harvest.

The expected results of these experiments are a series of subsidy-stress curves of biomass production rate versus nitrogen loading rate for a range of turbulence conditions established by a combination of volumetric flow rate and wave surge frequency. Information yielded from this research is intended to contribute to the understanding of the subsidy-stress relationship between algal biomass production and bed flow turbulence in an ATS.

Objectives and Hypotheses

The objective of this experiment is to examine the role of turbulence as a limiting factor that controls the biomass production of an algal turf community in an algal turf scrubber operating over a range of nutrient loading rates and in a high light environment.

The hypothesis for this series of experiments can be stated as such: biomass production in an ATS is a function of the turbulence regime when other limiting factors are in excess. Under these conditions, the biomass production rate, as measured by sacrificial harvest, will first increase and then decrease as the flow turbulence, set by a combination of wave frequency and amplitude, increases.

Research Approach

In an algal turf scrubber, the turbulence in the algal bed is controlled by a combination of volumetric flow rate, average water velocity, and wave frequency created by the wave surge bucket. Because of the wave surge bucket mechanism, the frequency of wave surge is coupled to the flow rate; that is, for a given wave surge bucket volume, an increase in the volumetric flow rate increases the wave surge frequency. This series of experiments was designed to decouple the turbulence generated by the wave surge

frequency from that generated by the increased volumetric flow rate and investigate the effects of each on algal biomass production.

Using a set of four algal turf scrubbers operating at ambient temperature and near-continuous light in the laboratory, various combinations of operating conditions were examined for their resulting effect on algal biomass production. All experiments had dual independent variables, the primary of which is nitrogen loading rate (NLR), supplied by daily additions of digested dairy manure. By changing the effective volume of the wave surge bucket through the addition of foam baffles, different combinations of wave surge frequency and volume were tested. One set of experiments had volumetric flow rate as its independent variable, holding wave surge frequency constant; another set of experiments had the wave surge frequency as its independent variable, holding the flow rate constant. All other environmental variables (light, temperature, pH level) were held constant. The independent variables were increased incrementally for different NLRs. Algal biomass was harvested weekly, dried and weighed, and used to calculate average daily biomass production rates. The relationships between biomass production rate, turbulence level (set by a combination of flow rate and wave surge frequency), and nitrogen loading rate was analyzed. Flow turbulence was measured independently by measuring the rate of dissolution of gypsum blocks deployed in the ATS units.

Equipment

Overview

The main equipment features of this set of experiments were the algal turf scrubber (ATS) units, the lights under which the ATS units operated, and the nutrients supplied to the ATS units. In addition, gypsum blocks (hereafter called clods) were

manufactured in the lab for deployment in the ATS beds to provide an independent measure of flow turbulence.

ATS Units

Four separate ATS units were employed throughout all experiments, were identical in construction to each other and are described in (Mulbry and Wilkie 2001) and (Kebede-Westhead et al. 2003). Each ATS bed was constructed out of white molded fiberglass with dimensions of 130 cm long by 101 cm wide by 15 cm deep. Two drain holes of 5 cm diameter were installed at one end of the ATS bed, and small segments of PVC pipe could be installed in these drains to set the depth of water in the ATS bed. A wave surge bucket with trapezoidal cross-section was mounted on pivots at the bed end opposite of the drains. Polyethylene mesh (3mm by 4mm spacing) was installed on the bottom of the bed (Mulbry and Wilkie 2001) to serve as a substrate on which the benthic filamentous algal turf grows. The effective growth area in the bed for the algal turf was that in between the wave surge bucket and drain holes at the opposite end, with an area of 1 m^2.

All units were operated in recirculation mode in which process water was continuously pumped from a reservoir into the wave surge bucket, flowing through the ATS bed and returning via the drain holes back into the reservoir (see Figure 1.2). The wave surge bucket tips when filled with a nominal 11 liters of water, creating a wave surge in the ATS bed with a frequency that depends on the volumetric flow rate of the recirculation pump and the effective volume of the wave surge bucket. Each ATS was paired with its own reservoir, a white semi-translucent polyethylene 200 liter drum open to the atmosphere at the top. The total volume of water in the entire ATS-reservoir

system was maintained at 150 liters through daily additions of fresh distilled water to replace evaporative losses, typically around 5 liters.

Lights

Each ATS unit was operated under its own set of two 400W metal halide lights. For all trials, the height of the lights above the ATS bed (typically around 50 cm) was adjusted to yield a light intensity of approximately equivalent intensity at the center of the ATS bed. Incident light averaged 390 (range 240–633) µmol photons m^{-2} s^{-1} over the entire ATS bed measured with a quantum flux meter and probe (LI-250 Light Meter and LI-190 Quantum Sensor, LI-COR Biosciences, Lincoln, Nebraska). All units were operated under nearly continuous light (23:1 h light-dark cycle) to maximize production. Water temperature was controlled and maintained within 2°C of ambient (23–26 °C) by activating cooling fans when high.

Nutrient Supply

All tests were run using digested dairy manure as the nutrient source. The dairy manure was collected periodically as needed from an anaerobic digester at the USDA ARS Beltsville (Maryland) dairy. The manure was collected approximately monthly in 5-gallon closed plastic containers and stored in a cold room (at approximately 4°C) until used. Upon collection, a sample of the manure was analyzed for nitrogen and N and P content. Total Kjeldahl nitrogen (TKN) and total phosphorus (TP) were determined using flow injection analysis (Model 8000, Lachat Instruments, Milwaukee, WI) after acid persulfate digestion (APHA 1995). The characteristics of Beltsville dairy manure effluent have been described (Wilkie and Mulbry, 2002) and are included (Table 2. 1). The mean manure effluent nutrient values were 1600 mg L^{-1} total N (TN) and 230 mg L^{-1}

total P (TP). The carbon content of the manure effluents was not measured routinely, but varied with manure. The C/N ratios of raw solid-separated and anaerobically digested dairy manure effluents ranged from 9 to 12 and 4 to 6.5, respectively. The variation observed in the manure characteristics was due to the water content of the manure as a result of the water use in the dairy. Typically, 0.5 to 1.5 L of manure effluent (containing 500–2300 mg L^{-1} TN and 85–300 mg L^{-1} TP) were added each day to each ATS to achieve loading rates corresponding to 0.3–2.5 g TN and 0.08–0.42 g TP m^{-2} d^{-1}.

Table 2. 1. Typical characteristics of the USDA dairy manure (undigested and digested), as reported by (Wilkie and Mulbry 2002).

Characteristics	Manure Source	
	USDA Undigested	USDA Digested
Manure management	Scraped and separated	Scraped, separated and anaerobically digested
Type of anaerobic digester	--	Full-scale suspended growth
Digester retention time (d)	--	23
Digester operating temperature (°C)	--	35
TS (mg L^{-1})	53200 (±116)	31600 (±195)
VS (mg L^{-1})	40300 (±84)	20900 (±154)
SS (mg L^{-1})	39300 (±1430)	23700 (±579)
COD_t (mg L^{-1})	71800 (±1240)	32700 (±1990)
COD_s (mg L^{-1})	19300 (±913)	4900 (±45)
TN (mg L^{-1})	1210 (±194)	2370 (±123)
TKN (mg L^{-1})	1210 (±194)	2370 (±123)
NH_4-N (mg L^{-1})	306 (±49)	1620 (±341)
NO_3-N (mg L^{-1})	< 1	< 1
TP (mg L^{-1})	303 (±55)	240
COD:N:P ratio	237:4:1	136:10:1
pH	6.95	7.83
Conductivity (mS cm^{-1})	15.60	16.20
Note: values in parentheses represent standard deviations of triplicate subsamples.		

Gypsum clods

A relative measure of turbulence for each flow condition was performed via the gypsum clod dissolution technique (Doty 1971, Jokiel 1993, Sanford 1997, Porter et al. 2000). Clods were constructed using a mixture of 104 g of laboratory-grade Plaster of Paris (calcium sulfate hemihydrate, Fisher Scientific) with 75 ml of distilled water. The solution was stirred continuously as a 50-mL pipette was used to measure 8.0 ml of the solution into the cups of a miniature muffin pan. After drying, the clods decanted from the muffin pan, and 1/16" holes were drilled into the center. A schematic of the typical clod geometry is shown in Figure 2. 1.

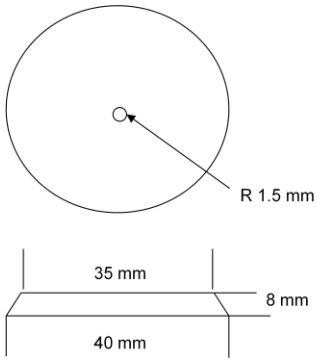

Figure 2. 1. Plan and elevation view of plaster of Paris clods designed for deployment in the ATS bed to characterize the magnitude of turbulent energy in the bed flow.

Methods

ATS Operation

Each laboratory-scale ATS unit was operated in recirculation mode with regular periodic harvest of biomass. The ATS units were previously seeded with algal consortia from a nearby stream in Beltsville, Maryland. Digested dairy manure was added daily in the morning according to the nitrogen loading rate (NLR). Over the course of the experiments the NLR ranged from 0.2 to 2.4 g TN m^{-2} d^{-1}. For all ATS units, CO_2 gas was bubbled in excess in the drum reservoir, maintaining the pH level near neutral and providing carbon in excess of photosynthetic requirements.

A series of experiments were performed on four ATS units in which the bed turbulence was manipulated via two methods: (1) through manipulation of the volumetric flow rate (ranging from 26 to 95 lpm) while the wave surge frequency was held constant; and (2) varying the wave surge frequency (from 6 to 30 min^{-1}) while the flow rate was held constant. Volumetric flow rate was measured by observing the displacement of water from a graduated reservoir. Wave surge frequency was modulated by filling the interior volume of the wave surge bucket with polystyrene foam blocks cut from commercially-available 2” closed polystyrene foam wall insulation. This reduced the

working volume of the bucket to yield the desired tipping frequency for a given volumetric flow rate. Flow rate/wave surge frequency combinations tested in this series of experiments are given in Table 2. 2. For any given volumetric flow rate, the wave surge frequency (or, inversely, the wave surge period in seconds) was a function of the wave surge bucket volume. Practical realities (such as wave surge bucket travel time) presented a constraint that prevented wave surge frequencies greater than 30 min^{-1}.

Table 2. 2. Combinations of flow rate and wave surge frequency (alternately, surge period) tested in the series of experiments.

Wave Surge Frequency (min^{-1})	Wave Surge Period (sec)	Flow Rate (lpm)		
		25	60	95
5	12		X	
8	7	X	X	X
17	3.5		X	
30	2		X	

Note: "X" = combination tested; blank implies that combination was not tested

Algal turf biomass was harvested from each ATS approximately weekly using a commercially-available shop vacuum. Harvest was performed by first powering off all recirculation pumps and allowing the water to drain from the ATS. Algal turf biomass was scraped from the ATS screen and vacuumed up immediately. The algal biomass and accompanying water were decanted from the vacuum into a 1-mm mesh polypropylene filter bag. The biomass in the bag was squeezed until no more water came through the bag. The biomass was spread out flat to air dry on a mesh screen in front of a fan. Once air dry (after approximately 48 hours), the biomass for each ATS unit was weighed using a laboratory balance. A subsample of each biomass sample was placed in a drying oven and dried for 24 hours at 50°C to determine the residual water content. Biomass

production rate was calculated as dry weight (DW) per unit time by correcting the air dry weight by the water content and dividing by the time (in days) between harvest events.

Experimental Design and Data Analysis

The ATS units were operated typically as described above with each set at a particular flow condition (Table 2. 2) and NLR. Conditions on each ATS unit were kept constant for multiple harvests until data were collected. The data collected included the weekly ATS biomass harvests for each ATS under a particular operating condition. Flow turbulence characterization included measuring the particulars about the wave environment (period of wave surge, persistence of wave front, average velocity of wave front, slope of ATS, and depth of water in ATS bed) and measuring the dissolution rate of clods strategically arranged in the bed of each ATS under a particular operating condition.

The gypsum block dissolution technique (Doty 1971, Jokiel 1993, Sanford 1997, Porter et al. 2000) was used for the determination of a relative measure of turbulence for each flow condition. This method employs the dissolution rate of standardized gypsum (plaster of Paris) blocks as an integrative measure of turbulence as it affects mass transfer across a boundary layer (Porter et al. 2000). During the operation of each ATS flow condition (that is, the combination of volumetric flow rate and wave surge frequency), gypsum blocks were deployed from 3 to 24 hours in thirteen locations regularly spaced in the ATS bed (Figure 2. 2). Clods were attached to the ATS screen using small-gage wire looped through the central hole in the clod and were placed such that they were completely submerged at all times. Upon removal from the ATS bed, all clods were rinsed with distilled water to remove any algal filaments that might be on the clod

surface. Wet weights of the clods before and after deployment, and the length of time of deployment, were measured and recorded and used to calculate the rate of dissolution. Multiple deployments (at least three) of the gypsum blocks were performed in each location in each scrubber.

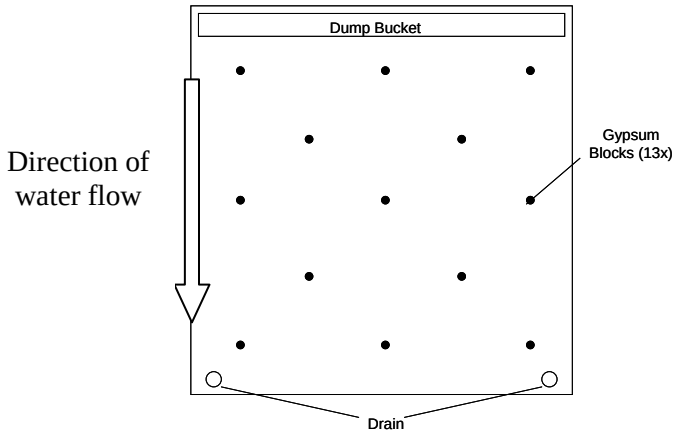

Figure 2. 2. Gypsum block deployment for measuring the turbulence in a lab-scale ATS.

Flow conditions were measured using a stopwatch and through observation. Volumetric flow rate was measured by observing the displacement of water from a graduated reservoir. Wave surge period was measured with a stopwatch as the amount of time between surge events. Wave travel time was measured with the stopwatch as the length of time for one wave surge to travel from the surge bucket to the opposite end wall of the ATS bed. Length of wave dissipation was measured as the number of lengths for the observed elevation change in the surface of the water as a result of the wave to dissipate.

For algal production measurements, comparisons were made of algal biomass production rate for each scrubber replicated in time. Algal biomass production rates were normalized as a daily production rate averaged over the harvest time period (typically 5 to 7 days). Mean values for productivity for replicate conditions were calculated. Where

independent variable conditions between individual ATS units overlap, comparisons were made across the ATS units. Gypsum clod dissolution rates were calculated as the mean of clod replicates at each location in each scrubber under each flow condition. A global mean dissolution rate for each flow condition was calculated by employing a Thiessen polygon computation (Ward and Trimble 2004), which was used to calculate a global weighted average for the entire algal growth area in an ATS. Linear regression analysis of algal productivity versus global mean dissolution rate was performed.

Results

Flow regime characterization

The flow in each ATS operating condition was characterized by baseline measurements and wave patterns of the flow, and by aggregating the clod dissolution rate measurements to produce maps of turbulence levels based on clod dissolution rates.The flow regime was characterized for the six combinations of volumetric flow rates and wave surge frequencies (Table 2. 3). It is notable that the greatest variation that accompanies the change in wave surge frequency is the approximate volume per tip, which ranges from 1.8 to 10.9 liters. This has implications for determining the amount of turbulent energy that is imparted to the base flow by the wave front. Global average gypsum clod dissolution rates are provided for each flow condition and provide a measure of average turbulence experienced in the flow regime under those conditions. Biomass production rates are also reported; the maximum production rate (30.9±1.8 g DW m^{-2} d^{-1}) is seen at the left-most flow combination (60 lpm/16 min^{-1} surge frequency), whereas the minimum biomass production rate (17.0±0.7 g DW m^{-2} d^{-1}) is listed at the right-most flow combination (60 lpm/5 min^{-1} surge frequency).

Table 2. 3. Selected measures to characterize the flow regime in the various flow rate/wave surge period combinations tested in the ATS units.

Parameter	Flow combination (Flow in lpm/Surge freq. in min^{-1})					
	60/17	95/8	60/30	60/8	25/8	60/5
ATS No.	4	7	4	5	5	7
Nom. Flow Rate (gpm)	15	25	15	15	7	15
Nom. Wave Surge Period (sec.)	3.5	7	2	7	7	11
Measured Flow Rate (gpm)	14	22	14	15	7	15
Measured Flow Rate (lpm)	51	84	51	58	27	55
Measured Surge Period (sec)	3.5	7.8	2.1	7.8	8.1	10.9
Wave Surge Frequency (min^{-1})	17.0	7.7	28.7	7.7	7.4	5.5
Appx. volume per surge (L)	3.0	10.9	1.8	7.5	3.7	10.0
Wave travel time 1st length (sec)	2.1	1.2	2.2	1.3	1.6	1.3
Wave velocity (cm/s)	51	91	50	82	66	86
No. of wave reflections	1	1	1	3	1	1
Length of wave dissipation (no. of lengths)	1.5	1.5	1.25	3.5	1.5	1.5
Slope	0.015	0.009	0.015	0.006	0.006	0.009
Avg. depth of water (mm)	10	16	10	22	13	16
Volume remaining after drainage (L)	4.8	6.6	4.8	6.9	6.9	6.6
Global Avg Clod Dissolution Rate* (g hr^{-1})	0.34	0.29	0.27	0.25	0.20	0.30
Clod Dissolution Rate SEM (g hr^{-1})	0.03	0.01	0.02	0.02	0.02	0.01
Clod Dissolution Rate n	40	52	52	40	39	40
Biomass Production Rate (g DW m^{-2} d^{-1})	30.9	29.8	25.9	22.1	21.7	17
Biomass Prod. Rate SEM (g DW m^{-2} d^{-1})	1.8	1.7	1.3	1.3	0.4	0.7
Biomass Prod. Rate no. of samples	8	5	4	5	3	2
NLR (g TN m^{-2} d^{-1})	1.4	1.6	1.7	1.3	1.7	1.4

*calculated via Thiessen weighted averaging of clods at 13 locations in three separate deployments for each ATS unit.

Gypsum clod dissolution rates were used to produce maps of turbulence within each of the ATS operating conditions, and to investigate the role of changing combinations of conditions (volumetric flow rate and wave surge frequency) on the relative turbulence level experienced in each flow regime. For the turbulence maps, gypsum clod dissolution rates were averaged for each of the 13 locations in the ATS bed under each set of flow conditions. These values were used to create interpolated contour maps of dissolution rate (Figure 2. 3 to Figure 2. 8) using MatLab version 7.10

(Mathworks, Natick, Massachusetts). These results show that, in general, all operating conditions are well-mixed laterally (perpendicular to the direction of flow) yet show a gradient of turbulence longitudinally (parallel to the direction of flow), with the greatest levels of turbulence generally closer to the wave surge bucket. The flow conditions of 60 lpm/17 min^{-1} frequency (Figure 2. 3) exhibited the greatest and most varied rates of gypsum dissolution. Most other conditions (Figure 2. 4 to Figure 2. 7) showed similar rates of clod dissolution with a similar decreasing gradient pattern from the wave surge bucket end to the drain end. An exception to this pattern is the condition for 60 lpm/5 min^{-1} frequency (Figure 2. 8), where no gradient pattern was evident, and the clod dissolution rate showed very little variation across the entire area except for a slight rise near the drain holes in the ATS bed.

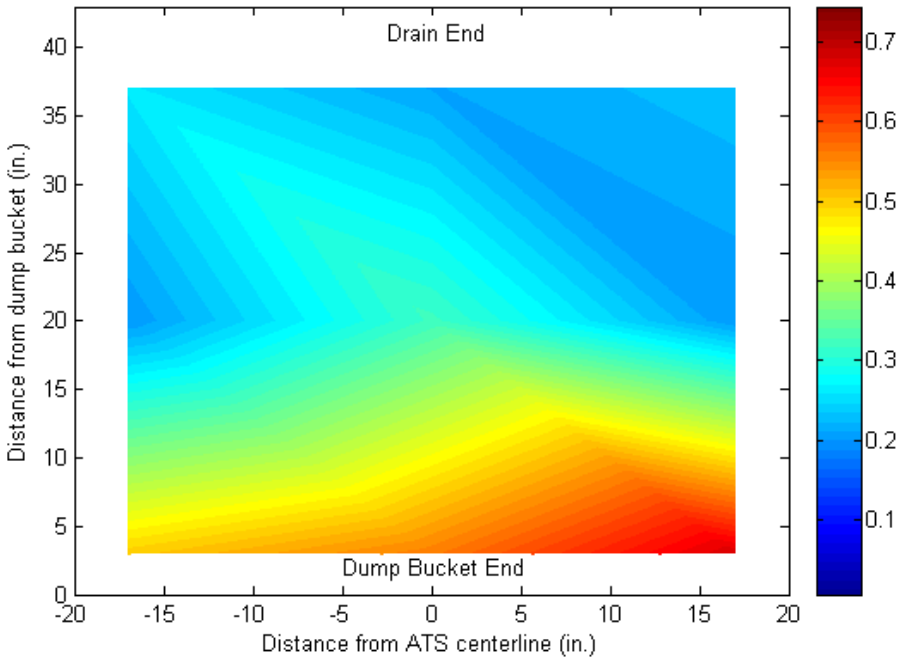

Figure 2. 3. Contour map of gypsum clod dissolution rate for flow conditions of 60 lpm/17 min^{-1} surge frequency in an ATS, expressed in g hr^{-1}.

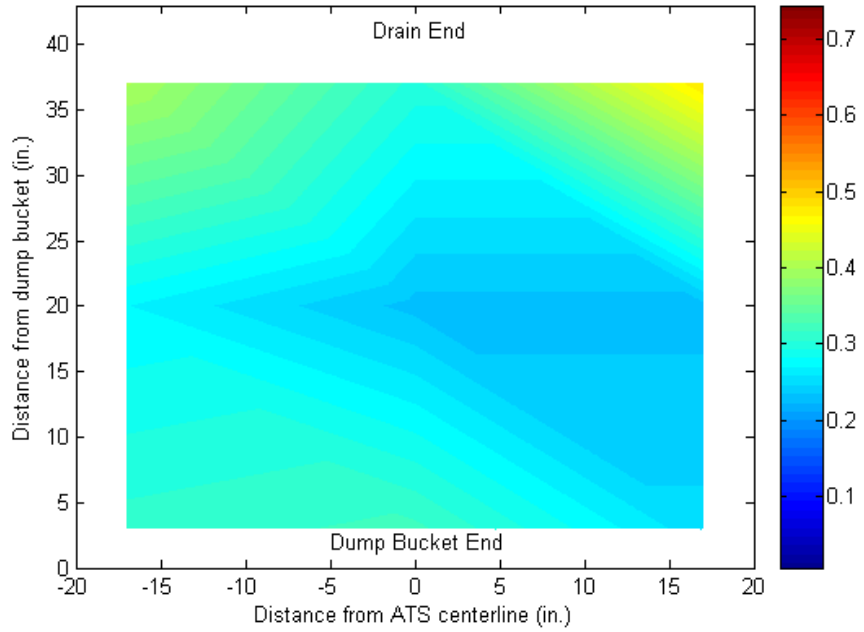

Figure 2. 4. Contour map of gypsum clod dissolution rate for flow conditions of 95 lpm/8 min^{-1} surge frequency in an ATS, expressed in g hr^{-1}.

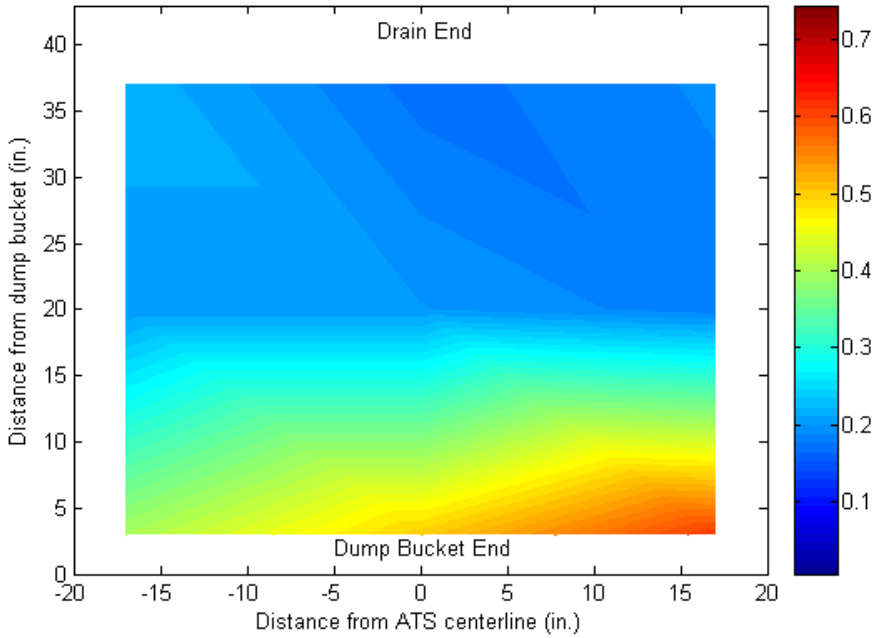

Figure 2. 5. Contour map of gypsum clod dissolution rate for flow conditions of 60 lpm/30 min^{-1} surge frequency in an ATS, expressed in g hr^{-1}.

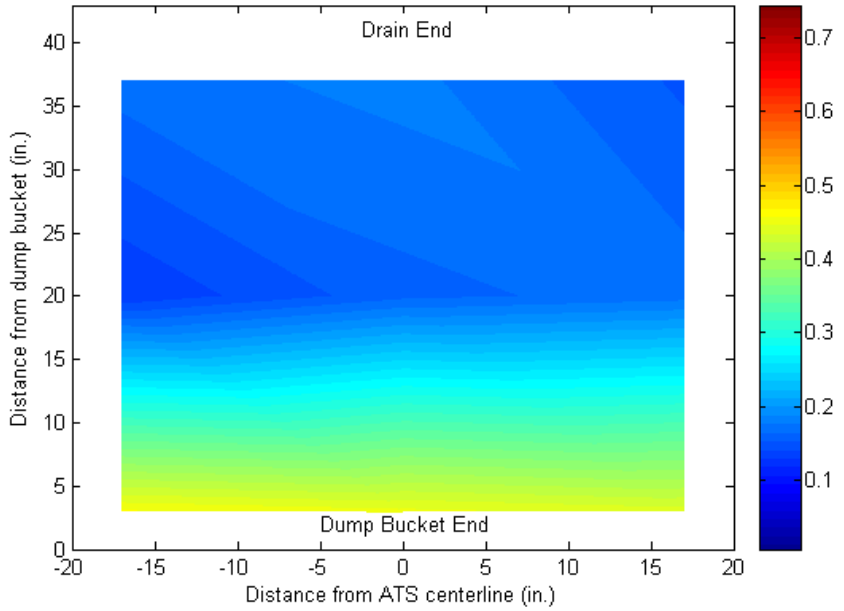

Figure 2. 6. Contour map of gypsum clod dissolution rate for flow conditions of 30 lpm/8 min^{-1} surge frequency in an ATS, expressed in g hr^{-1}.

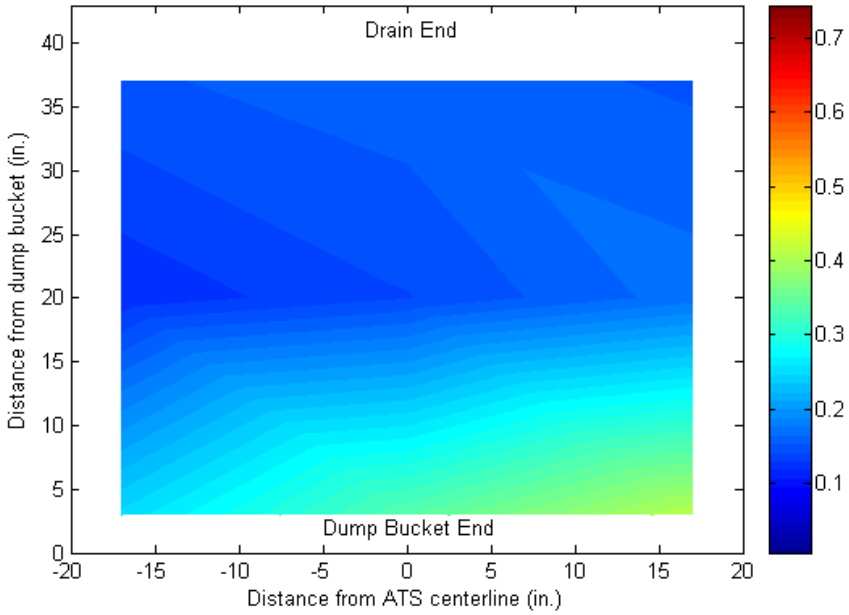

Figure 2. 7. Contour map of gypsum clod dissolution rate for flow conditions of 25 lpm/8 min^{-1} surge frequency in an ATS, expressed in g hr^{-1}.

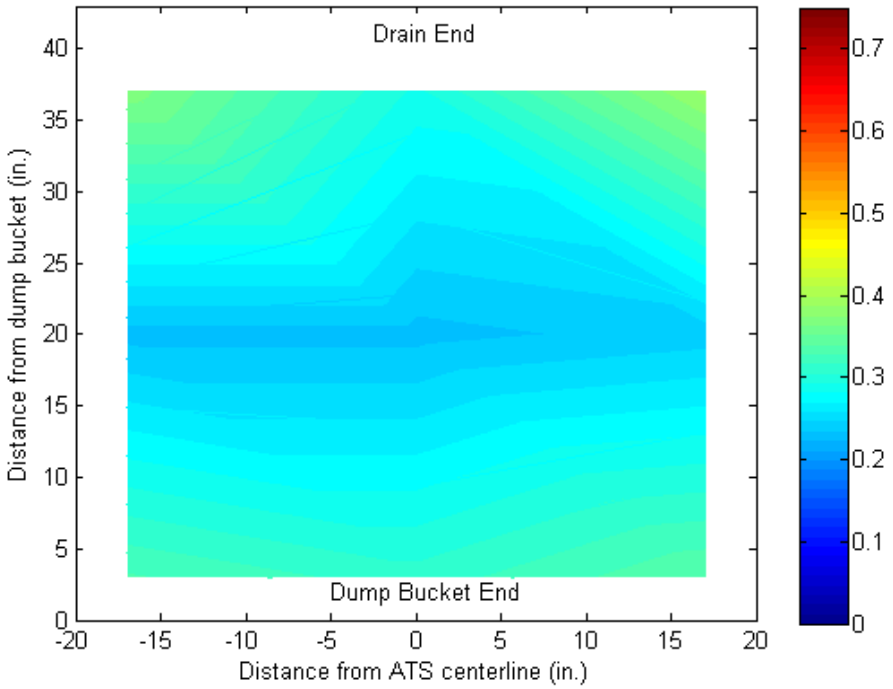

Figure 2. 8. Contour map of gypsum clod dissolution rate for flow conditions of 60 lpm/5 min^{-1} surge frequency in an ATS, expressed in g hr^{-1}.

The relationship between flow condition and clod dissolution rate was explored by analyzing the data for the clod dissolution rate as a function of wave surge tip frequency (flow rate held constant) and as a function of flow rate (wave surge frequency held constant). It was recognized that an increase in volumetric flow rate at a constant wave surge frequency increased the amplitude of the wave surge, defined by the volume per tip of the wave surge bucket. For clod dissolution rate versus wave amplitude at a constant wave surge frequency of 8 min^{-1}, a linear trend upwards is evident (Figure 2. 9). A linear regression on the relationship exhibits strong correlation (r^2 = 0.999, S_{y-x} = 0.00204) between clod dissolution rate and wave surge volume, and the slope of the regression line is significantly different than zero (P=0.0204).

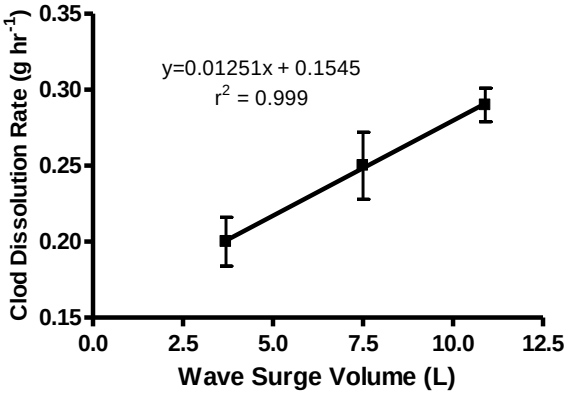

Figure 2. 9. Clod dissolution rate versus wave surge volume with wave surge frequency held constant at 8 min^{-1}.

For clod dissolution as a function of wave surge frequency, with the flow rate constant at 60 lpm (Figure 2. 10), the maximum clod dissolution rate is exhibited at a wave surge frequency of 17 min^{-1} (corresponding to a surge period of 3.5 sec), whereas the minimum dissolution rate is exhibited at a surge frequency of 8 min^{-1} (corresponding to a wave surge period of 8 sec). Clod dissolution rates at the extremes of wave surge frequency are in the middle of the range. A one-way analysis of variance (ANOVA), the null hypothesis, that there is no significant difference between the means, can be rejected at the 0.05 level of significance (F=3.023, P=0.0312).

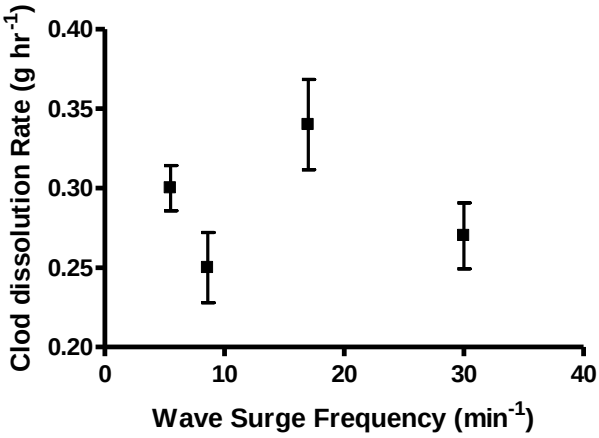

Figure 2. 10. Clod dissolution rate versus wave surge frequency, with flow constant at 60 lpm.

Biomass production for various flow conditions and NLRs

Results are shown for the series of experiments where the ATS nitrogen loading rate (NLR) and bed turbulence regime (as determined by flow rate and wave surge frequency) were manipulated and the resultant average daily algal productivity recorded. Results for four different wave surge frequencies (ranging from 5 to 30 min^{-1}) over a range of NLRs (0.25 to 2.4 g N m^{-2} d^{-1}) while holding flow rate constant at 60 lpm were generated using data collected over time (Figure 2. 11). The results trace a series of saturation-type curves, where productivity is generally lowest for all wave surge frequencies for lower NLRs (less than 1 g N d^{-1}), increases at moderate NLRs, and levels out at the highest NLR. The highest biomass production rate for all NLRs was seen consistently at a surge frequency of 17 min^{-1} with the greatest production rate (26.7 g DW m^{-2} d^{-1}) at a moderate NLR (1.4 g N m^{-2} d^{-1}), although the highest NLR was not tested at this frequency.

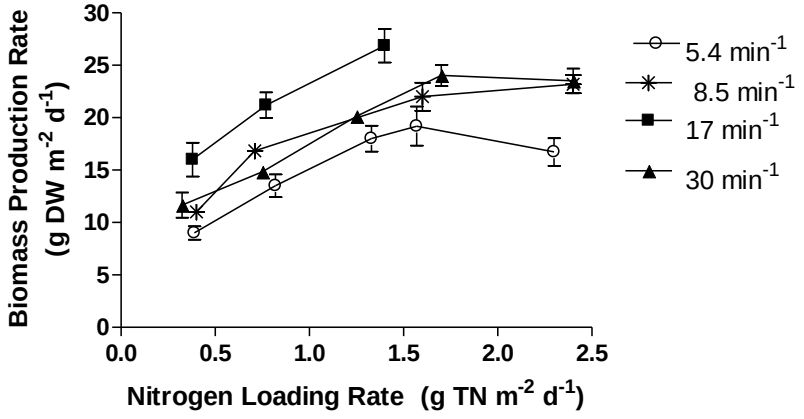

Figure 2. 11. Algal biomass production rate versus nitrogen loading rate for a range of wave surge frequencies for a flow rate of 60 lpm in an ATS.

Results of biomass production for three different wave surge volumes (4, 7.5, and 11 L, set by different volumetric flow rates) over a range of NLRs (from 0.25 to 2.4 g N

m^{-2} d^{-1}), holding wave surge frequency constant at 8.5 min^{-1}, were generated using data collected over time on another ATS. The results generally trace a series of saturation-type curves (Figure 2. 12). The pattern it shows is similar to the previous results: at a low NLR, the biomass production rate is similarly low across all wave surge volumes; it increases for all wave surge volumes at moderate NLRs; and it levels out at the highest NLRs. The highest biomass production rate is seen at a moderate NLR (1.0 to 1.5 g TN m^{-2} d^{-1}) at the highest wave surge volume of 11 L.

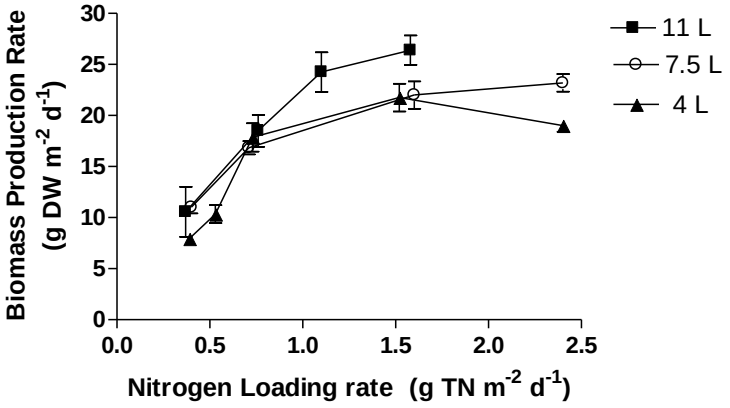

Figure 2. 12. Algal biomass production rate versus nitrogen loading rate for a range of wave surge volumes for a wave surge frequency of 8.5 min^{-1}.

These data presented above can be analyzed differently by plotting the biomass production as a function of wave surge frequency (volumetric flow rate held constant) or as a function of flow rate (surge frequency held constant) for select levels of NLR. Results for this type of analysis for biomass production versus wave surge frequency at a flow rate of 60 lpm for a range of NLRs are shown (Figure 2. 13). For all NLRs, the biomass production shows a hump-shaped pattern with increasing wave surge frequency. Biomass production is lowest at lower and higher frequencies, and is highest in the middle of the frequency range. The overall average biomass production rate at each wave surge frequency increases with increasing NLR.

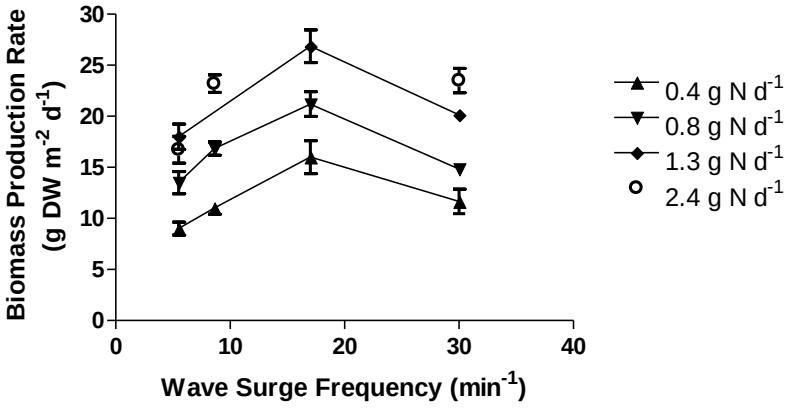

Figure 2. 13. Algal biomass productivity versus wave surge frequency for a 60 lpm flow rate for various nitrogen loading rates.

Results for this type of analysis for biomass production versus wave surge volume (as a result of changing flow rate) at a constant wave surge frequency of 8 min^{-1} for a range of NLRs are shown (Figure 2. 14). For the two lowest NLRs (0.4 and 0.7 g N d^{-1}), the biomass production rate shows almost no variation across the range of wave surge volume. For the two highest NLRs (1.6 and 2.4 g N d^{-1}), the biomass production shows an increase with increasing wave surge volume. Increasing NLR increases the overall average biomass production at each wave surge volume.

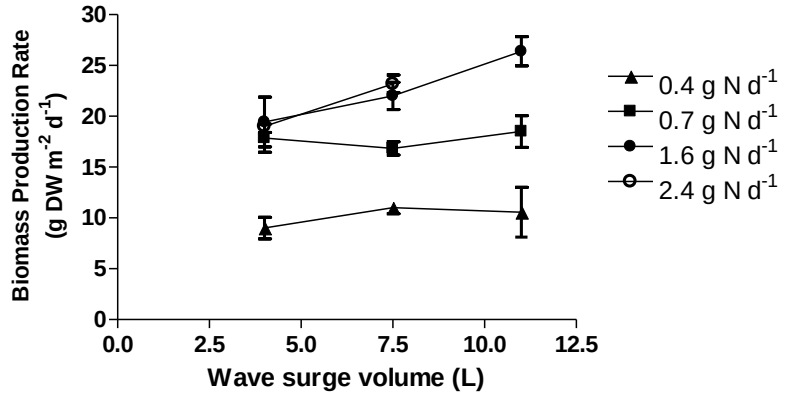

Figure 2. 14. Algal biomass productivity versus wave surge volume for a wave surge frequency of 8 min^{-1} for various nitrogen loading rates.

All the data can be pooled and analyzed for biomass production rate as a function of the mean clod dissolution rate for various NLRs. These results are presented (Figure 2. 15) and show that, for each NLR, a general increase in the biomass production rate is observed for increasing clod dissolution rate. The biomass production rate increases for each increase in NLR at each clod dissolution rate up to 1.6 g N d^{-1}, whereas no further increases in biomass production rate are seen at the highest NLR of 2.4 g N d^{-1}. The highest biomass production rate was observed at the highest NLR and the highest clod dissolution rate.

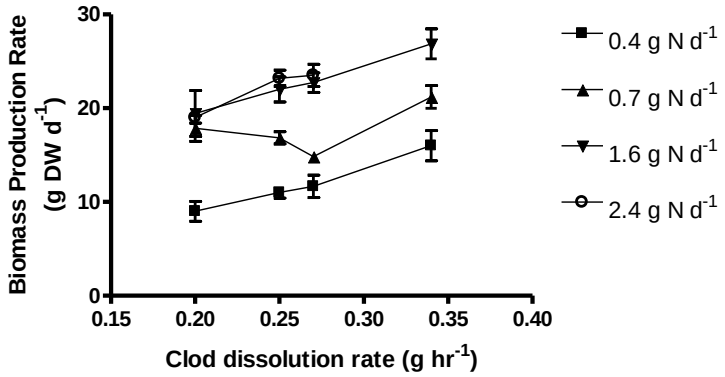

Figure 2. 15. Algal biomass production rate versus mean gypsum clod dissolution rate for various nitrogen loading rates.

Discussion

The role of turbulence as a limiting factor

Turbulence was observed to be a limiting factor to algal growth in most conditions tested in this series of experiments. From the baseline measurements on flow condition (Table 2. 3, page 42), the maximum biomass production of 30.9±1.8 g DW m^{-2} d^{-1} was observed at the flow rate/wave surge frequency combination of 60 lpm/17 min^{-1} (first column, Table 2. 3). The minimum biomass production of 17.0±0.7 g DW m^{-2} d^{-1} was observed at 60 lpm/5.5 min^{-1} (last column, Table 2. 3). The next lowest biomass

production of 21.7±0.4 g DW m^{-2} d^{-1} was observed at 25 lpm/8 min^{-1} (second last column, Table 2. 3). The volume per wave surge was similar for both of these conditions (3.0 and 3.7 liters for 60 lpm/17 min^{-1} and 25 lpm/7 min^{-1}, respectively). Hence, given that the volume per surge is the same, the increased wave surge frequency yields increased biomass production, indicating that the wave surge was limiting to production.

Additionally, it was observed that biomass production was maximized through the optimization of the combination of the wave surge frequency and the volume per surge. The two highest biomass productivities, 30.9±1.8 and 29.8±1.7 g DW m^{-2} d^{-1}, were observed at 60 lpm/17 min^{-1} and 95 lpm/8 min^{-1}, respectively (Table 2. 3, first two columns). The volume per surge for each of these conditions was significantly different, however, at 3.0 and 11 liters, respectively. This suggests that the lower wave surge frequency of the latter condition is offset by the increased volume per surge. That is, the combination of lower surge frequency and higher surge volume creates similar levels of turbulent energy over time, as experienced by the algal turf community, as the combination of the higher surge frequency and lower surge volume.

Increases in wave surge frequency at a given flow rate can yield gains in biomass production only up to a certain point. That is, there is an optimum surge frequency for a given flow rate outside of which the turbulent energy imparted to the algal turf is not as great. This was observed by comparing the biomass production at three surge frequency conditions (8, 17, and 29 min^{-1}) all at the same flow rate of 60 lpm (Table 2. 3, columns 1, 3, and 4). The biomass production was lower (22.1±1.3 g DW m^{-2} d^{-1}) for the lowest surge frequency (8 min^{-1}), was higher (30.9±1.8 g DW m^{-2} d^{-1}) for an increased surge frequency (17 min^{-1}), and was lower again (25.9±1.3 g DW m^{-2} d^{-1}) for an even further

increase in surge frequency (30 min^{-1}). This can be explained by the volume per surge, which, because there was no change in volumetric flow rate, decreased from 7.5 to 3.0 to 1.8 liters for the respective surge frequencies. The lower volume per surge lowered the mass of water injected into the flowing water in the ATS bed at each surge event. Thus there is lower energy imparted to the wavefront, which then dissipates more quickly as a function of the water depth. The maximum turbulence is thus experienced at a middle combination of surge frequency and volume per surge, and the effects of this are consequently reflected in algal biomass production.

Many of these trends were again observed in the analysis of the data in more detail (Figure 2. 11 to Figure 2. 15), providing evidence that turbulence can be a limiting factor when other potential limiting factors are in excess. When biomass production is plotted as a function of nitrogen loading rate (NLR) for different wave surge frequencies and a constant flow rate (Figure 2. 11, page 48), it displays the subsidy that increasing turbulence levels can have under conditions of increasing nitrogen availability. At low NLRs less than 1.0 g TN m^{-2} d^{-1}, the biomass production rate is similar for all wave surge frequencies, suggesting that nitrogen is limiting to algal growth. At higher NLRs, the biomass production rate diverges for different wave surge frequencies, finding a maximum at the frequency of 17 min^{-1}. A similar relationship is seen for the biomass production rate plotted as a function of NLR for different wave surge volumes at a constant wave surge frequency (Figure 2. 12, page 49), where the biomass production rate is different for different flow rates only at high NLRs, with a maximum exhibited for the highest surge volume of 11 L. This phenomenon suggests that, when nitrogen availability is no longer the limiting factor, transport of nitrogen in the bulk flow to the

algal turf and algal filaments may become limiting, and this transport is enhanced by increased turbulence.

A hump-shaped pattern emerges for the relationship of biomass production rate to wave surge frequency at a constant volumetric flow rate for different NLRs (Figure 2. 13, page 50). It cannot be interpreted here, however, as a true subsidy-stress curve. Rather, it reflects that, at a given volumetric flow rate, there is a wave surge frequency at which turbulent energy is maximized through the combination of wave surge frequency and volume of surge (the wave amplitude). Support for this interpretation comes from the similarity of the shape of these curves to the results for gypsum clod dissolution rate as a function of the wave surge frequency (Figure 2. 10, page 47). Indeed, both the maximum biomass production rates at all NLRs and the maximum clod dissolution rate were observed at a surge frequency of 17 min^{-1}. This suggests that there is a combination of wave surge frequency and surge volume that is optimum for algal growth in an ATS at a given NLR. This relationship holds for all NLR levels (Figure 2. 13), where increasing the NLR increases the overall biomass production at each wave surge frequency. The parallel relationship between biomass production and clod dissolution to wave surge frequency suggests that diffusion-limited mass transfer is at least part of the mechanism that controls algal production in the ATS environment.

The interaction of turbulence and NLR as limiting factors is again displayed by the results of biomass production rate plotted as a function of wave surge volume with frequency held constant for different NLRs (Figure 2. 14, page 50). For lower NLRs, an increase in flow rate has no effect on biomass production, and the relationship is flat, indicating that nitrogen availability is limiting. For higher nitrogen loading rates (1.6 g N

m^{-2} d^{-1} and greater), however, the increase in flow rate increases biomass production, indicating that the limiting process is not longer nitrogen concentration but transport of nitrogen to the algal cells, as moderated by flow turbulence.

Finally, the biomass production rate was seen to correlate reasonably well with clod dissolution rate (Figure 2. 15, page 51). At most NLRs, the biomass production rate increased with increasing clod dissolution rate, especially for very low (0.4 g N m^{-2} d^{-1}) and high (1.6 g N m^{-2} d^{-1} and greater) NLRs. An exception to this relationship was seen for the NLR of 0.7 g N m^{-2} d^{-1}; this may be due in part to some error in the construction or measurement of the submerged gypsum clods employed in those flow events. In all NLRs, however, the highest biomass production is seen at the highest gypsum clod dissolution rate. This again suggests the mass transfer interpretation of the role of turbulence as a limiting factor to the growth process of algae in an ATS.

Measurement of turbulence with the gypsum clod technique

The method using the dissolution of gypsum clods proved to be a fairly successful method as a predictor of turbulence in the ATS bed. The correlation between the clod dissolution rate and the flow turbulence was strong, as demonstrated by the clod dissolution rate as a function of wave surge amplitude with the frequency held constant (Figure 2. 9, page 47). The turbulence would be expected to increase with increasing wave amplitude at a constant frequency, as more mixing energy is imparted by a greater mass of the wave front. In this series of experiments, the clod dissolution rate increased linearly with increased wave amplitude (r^2=0.999), demonstrating that the clod dissolution method can provide a relative measure of turbulence in an ATS. Further experimentation would be required to adapt the method to provide a more absolute,

quantitative measure of turbulence that can be compared to other measures. The clod dissolution rate as a function of wave surge frequency with the flow rate held constant (Figure 2. 10, page 47) follows a curve that might be expected where the maximum bed turbulence is found at a combination of volume per surge and surge frequency. That is, the maximum turbulence, and thus the maximum rate of dissolution of gypsum, was found at a medium surge frequency, where any further increase in frequency reduced the volume per surge, and thus the wave amplitude, below a critical amount to create maximum turbulence. Indeed, the energy density of a wave can be described as being a function of the square of the wave amplitude (Phillips 1977), suggesting that wave amplitude is the dominant mechanism in creating the turbulence in an ATS bed.

The clod dissolution rate method was demonstrated to be useful in investigating the heterogeneity of turbulence within the bed of the ATS unit. The spatial contour maps show the distribution of turbulent energy within the ATS beds (Figure 2. 3 to Figure 2. 8). In almost all conditions of volumetric flow rate/ wave surge frequency, the turbulence regime in the ATS bed was shown to be highly zoned, exhibiting the highest levels turbulence in a zone near the wave surge bucket and dissipating rapidly in the direction of flow. The condition with the most heterogeneous distribution of clod dissolution rate was the flow rate/surge frequency combination of 60 lpm/17 min^{-1} (Figure 2. 3, page 43), the condition which also exhibited the highest average biomass production of 30.9 ± 1.8 g DW m^{-2} d^{-1} (Table 2. 3, page 36). The conditions with the most homogeneous distribution of clod dissolution rate was the flow rate/surge frequency combination of 25 lpm/7 min^{-1} (Figure 2. 7, page 45), the condition which also exhibited lower biomass production of 21.7 ± 0.4 g DW m^{-2} d^{-1} (Table 2. 3, column 5, page 42). An exception to this trend was

observed for the flow rate/tip frequency combination of 60 lpm/5.5 min^{-1} (Figure 2. 8, page 46), which showed a high amount of turbulence (a global average clod dissolution rate of 0.30 ± 0.01 g hr^{-1}; see Table 2. 3, last column) but a low biomass production of 17.0 ± 0.7 g DW m^{-2} d^{-1}. It is interesting to note that, despite the high level of turbulence, this flow condition exhibited a low amount of zonation and heterogeneity in the spatial distribution of turbulence. Could the zonation and heterogeneity found in other flow conditions be an important factor in the overall production of algal biomass? It is possible that the heterogeneity of turbulent environments within the ATS bed allows for locations of refugia characterized by lower turbulence that allow less-resilient algal species to persist, thus increasing the overall diversity of algal species that in some way translates to increased biomass production. More experimentation is required to answer this question.

The intersecting limiting factors of light, nutrients, and turbulence

A conceptual model was developed to describe the relationship between intersecting limiting factors in the production of algae in an ATS. This model can be used to explore the relationship of limiting factors (especially light, nitrogen, carbon dioxide, and turbulence) on the productivity of algae in an ATS. Some variables of importance to the productivity of algae and their relationship to each other can be described by a causal relationship model (Figure 2. 16). In this model, a pathway with a "+" indicates a direct relationship; a pathway with a "-" indicates an inverse relationship; and a pathway with a "+/-" indicates a relationship that is direct at low levels of interaction but is inverse at high levels of interaction, representative of a subsidy-stress relationship. Omitted but possibly important factors include the CO_2 concentration, temperature, frequency of nutrient feeding, frequency of harvest, and competition with suspended algal species.

In this model, the parameters that are directly controlled by the ATS operator include the wave surge bucket volume; volumetric flow rate; the water depth; light intensity; and nitrogen loading rate. The bed turbulence per unit time is directly influenced by the amplitude and frequency of the wave surge, functions of the wave surge bucket volume and volumetric flow rate. Turbulence may also be inversely affected by water depth, where deeper water may dampen the effect of the wave surge by increasing the rate of dispersion of the wave surge energy. Increased bed turbulence decreases the diffusive boundary layer at both the turf and filament scale. The decreased boundary layer increases the rate of nitrogen diffusion for a given nitrogen concentration (itself established by the user-defined nitrogen loading rate). Nitrogen diffusion rate then directly influences algal productivity, which is directly reflected in the algal biomass production. Bed turbulence directly influences light availability through increased exposure of the algal filament surface area to unidirectional light by reduction of self-shading because of increased mixing motion. Bed turbulence also directly influences scour, however, which inversely affects algal productivity by removing productive biomass from the ATS bed. While some of these relationships might better be represented by a saturation relationship or a subsidy-stress relationship, within the bounds of typical ATS operation it is assumed here that these direct or inverse relationships hold.

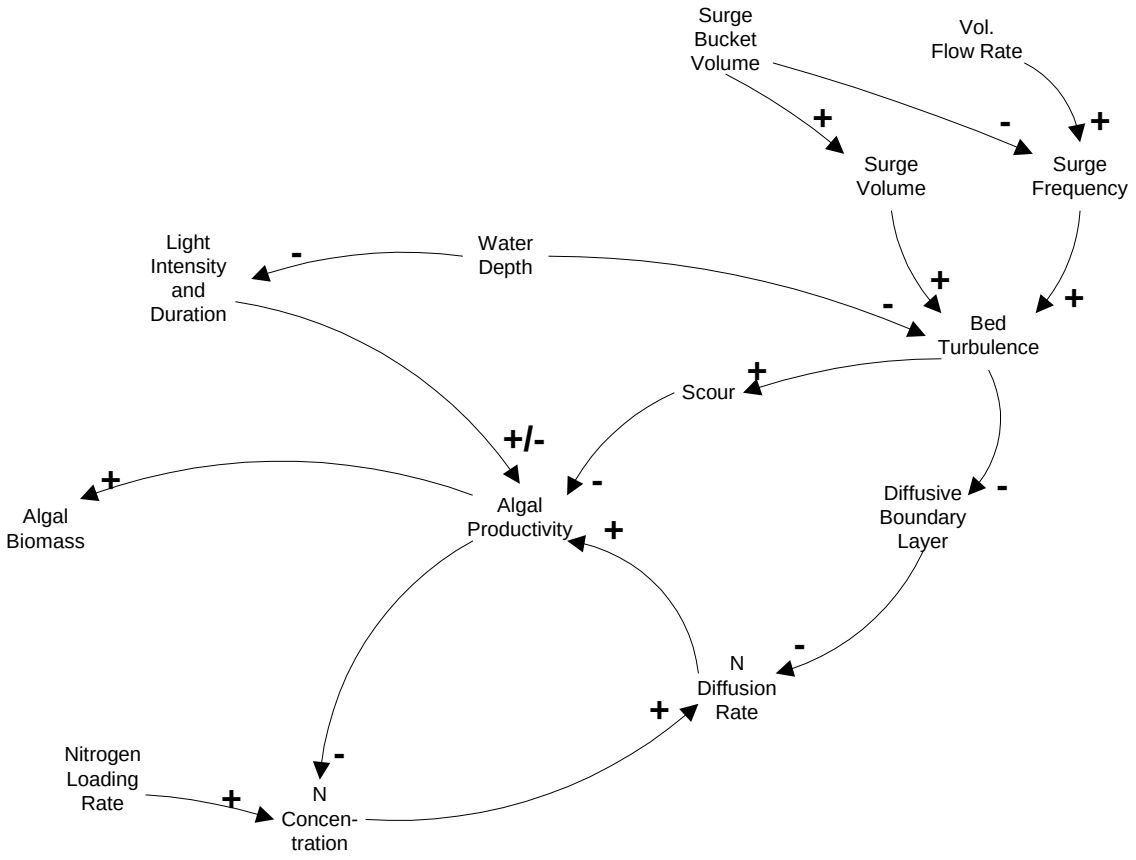

Figure 2. 16. Some causal relationships that affect algal productivity in an algal turf scrubber, showing the role of turbulence on diffusion rates and scour.

An energy systems model (Odum 1993) was developed based on the relationships outlined in the causal relationship model (Figure 2. 17 and Figure 2. 18). Processes modeled include algal community production and respiration, the associated uptake of carbon dioxide and nutrients, and the generation of turbulence by the combined action of flow rate and periodic dumping of the ATS wave surge bucket (Figure 2. 17). The energy signature of an ATS is clearly delineated by this model, which postulates that turbulent energy, as moderated by wave surge frequency and amplitude, is an important part of the energy signature. The productivity of algae in an ATS is dependent upon the availability of the primary limiting factors of light, nitrogen, and carbon dioxide, with turbulence moderating the access to all of these. Maximization of the algal production is achieved by

optimizing the availability of these limiting factors, each of which might be modeled as a subsidy-stress curve. The relative contribution of turbulence to the availability of each of these in an ATS has yet to be fully understood, however, a direction for future research.

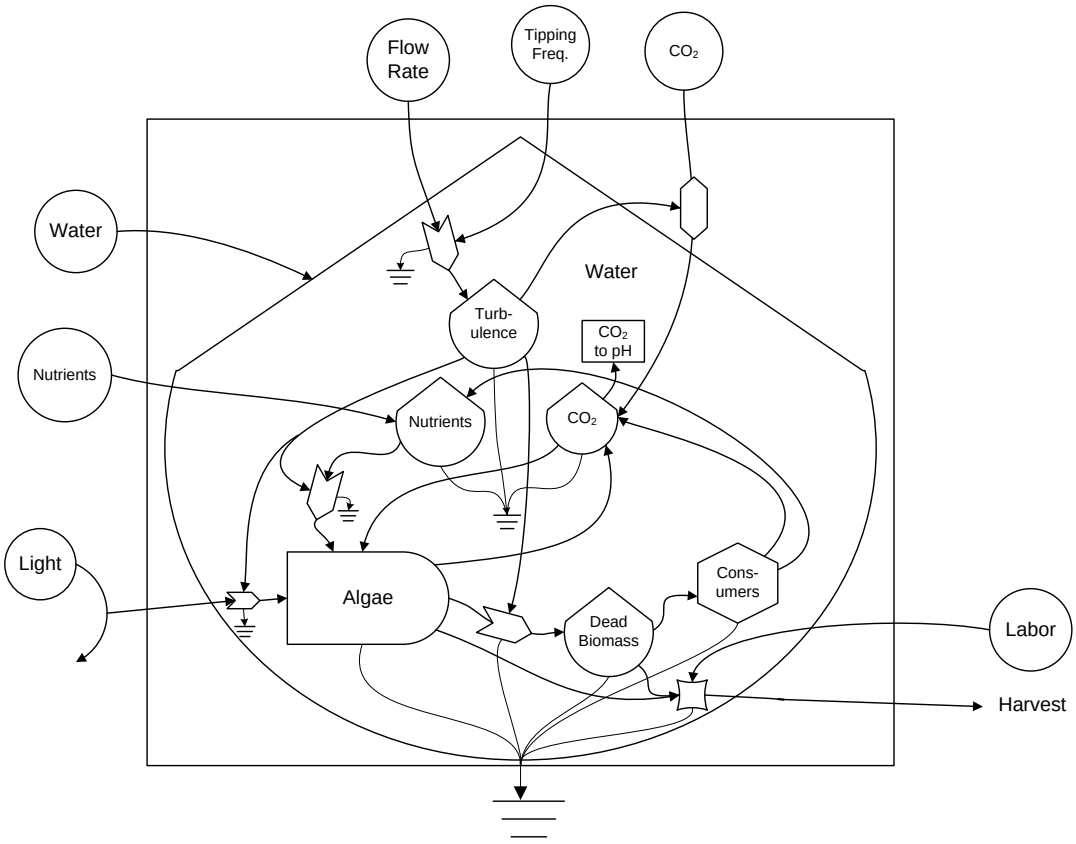

Figure 2. 17. Preliminary energy systems diagram of an algal turf scrubber, showing the effect of turbulence on the productivity of algae through moderation of the availability to other limiting factors.

Submodels of various components of the main model can further elucidate the relationship between factors and elements in the ATS ecosystem. A submodel was developed to understand the effect of turbulence on the diffusive boundary layer that surrounds the algal cell and the algal turf (Figure 2. 18). The model shows the role of engineering decisions in the design and operation of an ATS, such as drain height and volumetric flow rate, in determining the turbulent energy in the flow and resultant effect on the diffusive boundary layers surrounding the algal cells and the algal turf.

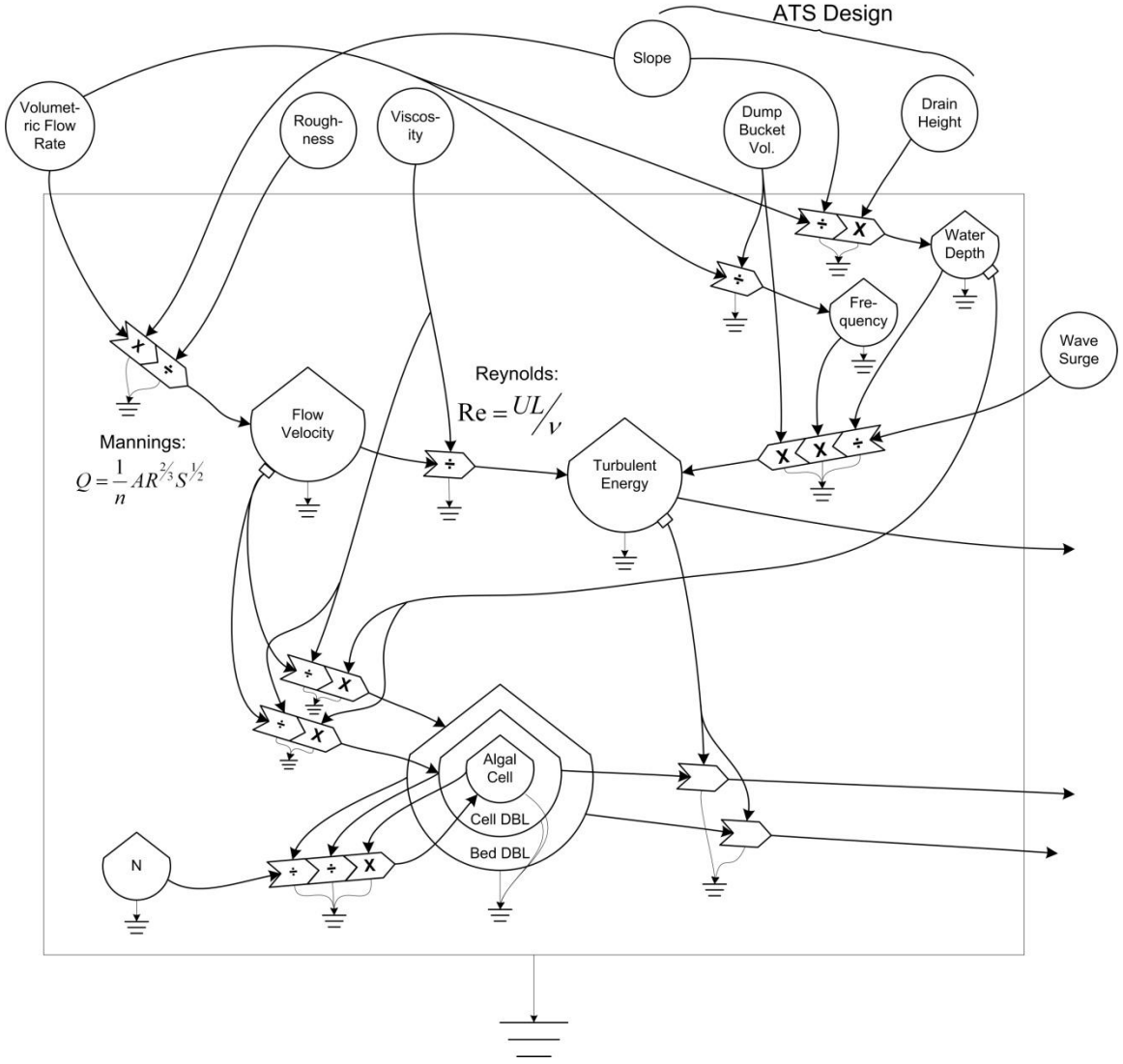

Figure 2. 18. Energy circuit diagram submodel of the effect of turbulent energy on the diffusive boundary layer (DBL) surrounding an algal turf and individual algal cell and various engineering and operational parameters that affect the turbulence regime in an ATS.

Conclusions and Implications

The following conclusions may be made for this set of experiments:

- Turbulence acts as a limiting factor to the algal biomass production in an ATS when other factors are provided in abundance.

- Wave amplitude (volume for wave surge) is a stronger factor than wave frequency on determining the biomass production of algae in an ATS. Biomass production is maximized, however, when the combination of wave surge amplitude and frequency is optimized.
- Increased turbulence affects the mass transfer at the scale of the algal turf thickness, as shown by the clod dissolution measurements. However, it cannot be concluded that this is the only mechanism that contributes to the stimulation of algal biomass production in an ATS. Further investigation is necessary to confirm the mechanism by which turbulence increases overall algal production.

Overall, the results of these experiments suggest that, coincident with biomass production, the ecosystem metabolic measures of net primary productivity and community respiration of the algal turf in an ATS as a function of flow turbulence would follow a limiting-factor relationship. Further, it is hypothesized that that relationship might have the shape of a subsidy-stress curve. This question is addressed further in subsequent sections of this research.

Chapter 3: The Ecosystem—Searching for the Subsidy-Stress Curve

Introduction

The role of turbulence in stimulating the algal biomass production in an algal turf scrubber (ATS) has been shown to be as a limiting factor when other potential limiting factors are supplied in abundance. Is this relationship reflected in the metabolic signatures of the algal turf? Can this be measured by the change in the concentration of the reactant gases (carbon dioxide or oxygen) in the ATS aquatic environment? This set of experiments was undertaken to explore these questions so that this information might inform the design of an automated process in a feedback control scenario. Measurements were designed to measure the net primary production and respiration of the ATS ecosystem and investigate responses to changes in turbulence levels. Respiration (R) is defined as the net community respiration, that is, the sum total of all respiratory processes within the ATS ecosystem. It is generally assumed to be relatively constant in light or dark (Beyers 1963). Gross primary production (GPP) is defined as the sum total of all photosynthetic processes that result in the storage of light energy as reduced organic material (Beyers 1963). In a growing ecosystem, GPP exceeds R, and the amount of excess is the net primary production (NPP); thus,

$$NPP = GPP - R$$

Also, in an early successional photosynthetic system, the ratio of NPP/R is greater than one, indicative of an autotrophic system (Odum 1956), although over the long term this ratio should approach 1 as more structure is built and system maintenance costs increase overall respiration (Odum 1969). These signatures are examined in this series of

investigations. The measurement of the metabolism of an aquatic ecosystem typically relies on monitoring the diurnal variation of the concentration of metabolically active gasses (oxygen or carbon dioxide). This necessitated the creation of a light diurnal variation, and the operation of the ATS units were changed from the continuous light environment of previous experiments to a 16 hour light/8 hour dark diurnal cycle. While this lowered the overall expected biomass production from possible light limitation, it brought the experimental setup into closer analog of typical ATS operating conditions.

Experiments were designed in which the wave surge frequency was manipulated on a set of ATS units by adjusting the volumetric flow rate to establish a range of frequencies of over two orders of magnitude. A monitoring system was designed to record the pH diurnal in each ATS unit. Monitoring the pH level of an aquatic system over a diurnal light cycle can give information about the ecosystem metabolism of the aquatic system, as pH level fluctuates inversely to the concentration of carbon dioxide (which itself fluctuates diurnally with photosynthesis and respiration). The method for determining primary production in aquatic systems is done by tracking diurnal pH fluctuations, requiring calibration by measurement of incremental changes in the pH with known incremental additions of carbon dioxide via titration (Park et al. 1958, Beyers et al. 1963, Beyers 1964). This calibration curve becomes the basis for the system to monitor net primary productivity and respiration automatically. These metrics, their ratio, and biomass production rate were measured as time replicates for each flow condition under two different light regimes and under increasing levels of nitrogen availability. Data were analyzed as a function of wave surge frequency of the ATS, with the expected result of a subsidy-stress curve evident for each. Additionally, the data were used to

investigate the relationship between the metabolic measures (NPP, R, and NPP/R ratio) and biomass production rate, under the interpretation that they should roughly correlate. Examination was performed to test the assumptions of the methodology by investigating the transfer rate of gas (oxygen and carbon dioxide) across the air-water interface in an ATS at a range of wave surge frequencies. Finally, repeated samples of algae from the growth bed of each ATS were examined and keyed for relative abundance of the dominant algal species for a preliminary investigation into their relative competitiveness under various combinations of operating conditions.

Objectives and hypothesis

The objectives of this set of experiments were as follows:

1. The first objective of this component of the research was to develop a system to monitor the metabolism of the algal ecosystem in an ATS, thereby providing information about the growth of the algal community in response to various operating conditions.
2. The second objective of this set of experiments was to determine the effect of flow turbulence, as controlled by the wave surge frequency, on the ecosystem metabolism, as evidenced by net primary productivity (NPP) and respiration (R), and biomass production rate of the algal turf community in an algal turf scrubber.

The hypothesis investigated in this set of experiments may be expressed as follows: Flow turbulence is a limiting factor to the primary productivity of an algal turf community in an algal turf scrubber when other possible limiting factors are in abundance. Algal turf metabolism, as made up of net primary production and respiration, and biomass production will follow a subsidy-stress relationship over a range of

turbulence regimes, being greatest somewhere in the middle of the range and least near the upper and lower bounds of the range, and where the turbulence regime is defined by the wave surge frequency as set by the overall volumetric flow rate in an ATS.

Research Approach

The research approach followed for investigating the subsidy-stress relationship between turbulence and algal turf productivity was performed by testing different flow rates using multiple laboratory-scale algal turf scrubbers in a laboratory. All ATS units were identical units with 1-m^2 growth area and were operated under ambient temperature conditions in the laboratory and under 16-hour light/8-hour dark diurnal light cycles. For each combination of operating conditions of light and nitrogen loading rate (NLR), a different wave surge frequency was established on each scrubber, holding wave surge volume constant. Replicates (between 4 and 8) were made in time for each surge frequency treatment. During each treatment, measurements were made of the algal turf metabolism, using the pH diurnal method, and biomass production rate through sacrificial harvesting. The measurements were analyzed for differences in these parameters between turbulence conditions under each set of operating conditions. Different combinations of light intensity and NLR operating conditions were performed to find where flow turbulence becomes limiting. Assumptions of the pH diurnal method for aquatic ecosystem metabolism were tested through investigations on the gas transfer kinetics for different turbulence conditions in the ATS units. Finally, preliminary investigation into the competition ecology of the algal consortia was performed by examining the relative abundance of dominant genera of algae under the various combinations of operating conditions.

Materials and Methods

Equipment Overview

The equipment used for this research included a data acquisition computer that monitored the pH level in the reservoir of an ATS via a pH probe and meter. Up to five separate ATS units were used in the lab to perform the experiments, and a data acquisition signal line was established for each one. The volumetric flow rate in each ATS was established by installing a combination of centrifugal pond pumps of various volumetric flow rate capacities in parallel. The overall configuration of these elements is shown in the schematic (Figure 3. 1), and the elements are described in more detail below.

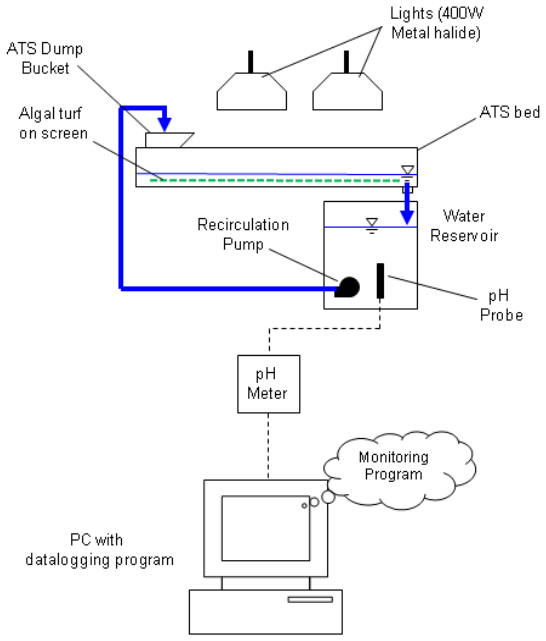

Figure 3. 1. Schematic for a PC setup for pH monitoring of an ATS operating in recirculation mode.

Algal Turf Scrubber (ATS) Units

The algal turf scrubber units used for this research were described previously in Chapter 2. The five separate ATS units employed throughout all experiments were

identical in construction and are described in (Mulbry and Wilkie 2001) and (Kebede-Westhead et al. 2003). All units were operated as previous described: they were operated in recirculation mode, each was paired with its own reservoir, and the total water volume in each system was maintained at a nominal 150 liters through daily additions of distilled water. The units were harvested regularly with a shop vacuum; after each harvest, small 5 cm square shuttle screens from each ATS unit were randomly reassigned to every other ATS unit to ensure that all units had access to the same mix of algal species types.

Lights

As described previously (Chapter 2), each ATS unit was operated under its own set of two 400W metal halide lights, except for one ATS unit for which one 1000W metal halide light was used. The height of the lights above the ATS bed was adjusted to yield a light intensity of approximately equivalent intensity at the center of the ATS bed. For this set of experiments, light intensity was measured periodically at 25 locations equally distributed across the growth area of the ATS with a quantum flux meter and probe (LI-250 Light Meter and LI-190 Quantum Sensor, LI-COR Biosciences, Lincoln, Nebraska). Near the end of one set of experiments, it was discovered that light intensity was lower than had been originally expected; presumably because of bulb age and wear, and the bulbs in all lights were replaced with new ones. This resulted in a measurable increase in light levels. Light levels were measured and checked periodically throughout all sets of experiments.

Nutrient Supply

Throughout the course of all testing and experimentation, four different types of nutrient supply were employed. For all nutrient supply types, solutions were mixed with

known nitrogen and phosphorus concentrations; aliquots of nutrient solutions were added daily to the ATS reservoir in known volumes during operation to yield the desired nitrogen loading rate (NLR). The four types of feed solution used were dairy manure, urea salt, plant-food based (Miracle Gro® solution), and modified Bristol's solution.

Manure (M)

A majority of all trials were run using undigested raw dairy manure as the nutrient source. The dairy manure was collected periodically as needed from a holding pond at the USDA ARS Beltsville (Maryland) dairy. The manure was collected approximately monthly in 5-gallon closed plastic containers and stored in a cold room (at approximately 4°C) until used. Upon collection, a sample of the manure was analyzed. A description of the results of this analysis was given in Chapter 2, Table 2.1. The manure was typically fed daily into each ATS by pouring a measured volume into the ATS reservoir to yield the intended NLR.

Urea (U) salt solution

A small number of trials were run using a urea solution as the nitrogen source and a phosphate solution for the phosphorus source. A significant die-off of algae was observed throughout these feed conditions, however, and no reportable data were collected.

Miracle Gro® solution (MG)

A number of trials were run using a solution mixed from a commercially-available chemical plant food (Miracle Gro® Water Soluble All-Purpose Plant Food, Scotts Company, Marysville, Ohio). The solution was created by dissolving 24.0 g of dry

Miracle Gro® granules in 10.5 L of distilled water, yielding a solution to yield 1.0 g N for every 50 ml of solution. The MG solution was administered to the ATS daily by decanting a measured volume of solution into the ATS reservoir. The pH level of the process water was highly unstable, however, often leading to die-off of algae, and no reportable data was collected for these feed conditions.

Modified Bristol's Solution

A number of trials were run using a solution derived from algal culture medium recipes. A modified Bristol's medium (Trainor and Shubert 1974, Lin et al. 2007) was made by dissolving known masses of inorganic salts into known volumes of distilled water (Table 3. 1). The medium was made as three separate component solutions: a nitrate solution (solution A), a phosphate solution (solution B), and a micronutrient solution (solution C). Solutions were administered to the ATS simultaneously each day by decanting measured volumes of each solution in the ratios of 25:10:10 by volume into the ATS reservoir.

Table 3. 1. Recipe for modified Bristol's solution, as the sum of three component solutions, used as an inorganic nutrient feed for some ATS operations.

Component Solution	Chemical	Mass (g)	Vol. of DI Water (ml)
A	$NaNO_3$	60.7	1000
	or		
	KNO_3	72.2	
B	K_2HPO_4	18.2	1000
	KH_2PO_4	42.5	
C	$CaCl_2$	6.05	1000
	NaCl	6.05	
	$MgSO_4 \cdot 7H_2O$	18.2	
	$FeCl_3$	0.08	
	$MnSO_4 \cdot 4H_2O$	0.09	
	$ZnSO_4 \cdot 7H_2O$	0.05	
	H_3BO_4	0.10	
	$CuSO_4 \cdot 5H_2O$	0.02	
Feed proportions:	A:B:C = 25:10:10 ml		

Monitoring System for pH diurnal

A system to monitor the pH level was constructed using a data acquisition computer connected to a pH probe and meter. For data acquisition of pH level, a custom-built Pentium 75-MHz personal computer was used with an installed National Instruments (NI) AT-MIO-16X (National Instruments Corp., Austin, Texas) data acquisition card and an external NI CB-50 I/O connector block. For all experiments involving monitoring of pH level, a pH probe (36" single junction pH electrode, Cole Parmer, catalog number c-05993-80) was installed in each ATS reservoir. Each probe was connected to a Jenco 3672 pH controller (Jenco Electronics Ltd., San Diego, California) with a 4-20 mA analog output terminal across which a 1000-Ω resistor was installed. These terminals were then connected to the respective analog input channel connectors on the CB-50 connector block. The voltage across the 1000-Ω resistor would vary directly with the pH level in a range between approximately 0 and 2.5 V. The calibration of each pH probe and controller was checked approximately every two harvest periods of their respective ATS unit.

For the pH monitoring system, LabView version 4.1 (National Instruments Corp., Austin, Texas) was used as the data acquisition software. Hardware constraints allowed recording of up to four voltage signals simultaneously, each of which was converted into pH values manually in data analysis using calibration constants determined at each recalibration event. For all trials, sampling was set at once every 5 minutes with no physical signal filtering; filtering of the pH signal was done manually during data analysis.

Titration for pH-IC conversion

The relationship between the pH level and inorganic carbon (IC) concentration for each ATS reservoir was determined through titration. Generally, this analysis was performed once each harvest period on samples taken from each ATS reservoir on the day that was the midpoint of the harvest period. Results of this analysis were applied to the pH curve for that entire harvest period, based on the assumption that the water chemistry in the reservoir did not significantly change throughout any one harvest period. Two methods were used for determining the relationship between pH and IC, summarized in the following sections.

IC analysis method

This method was used for the set of trials for the "Low light/Low NLR" operating conditions. On the day of sampling, water samples were taken from each ATS reservoir in 50-ml sample vials. Samples were taken by submerging and filling vials in the ATS reservoirs. For each ATS, the first sample was taken just before the end of the dark time period of the diel light cycle (when the pH was expected to be lowest). The time and pH of the reservoir at the time of sampling were recorded. Repeated samples were taken approximately every hour after the lights were turned on throughout the light cycle as pH continued to rise; again, the time of sample and pH were recorded for every sample. Samples were stored in the dark at 4°C until they could be analyzed (typically done at the end of the day of sampling). Samples were analyzed for total inorganic carbon (TIC), which includes carbonate, bicarbonate, and dissolved carbon dioxide, using a Phoenix 8000 TOC analyzer Tekmar Dohrman (Cincinnati, OH). Plots were made of TIC (in

ppm) versus pH. A linear regression was performed to yield an equation used to predict TIC when the pH was known for a water sample (Figure 3. 2).

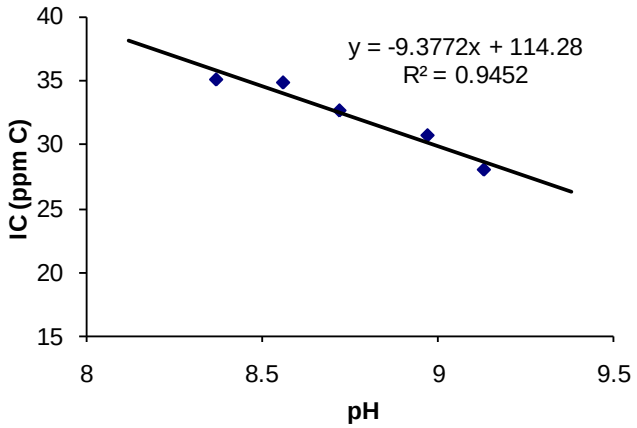

Figure 3. 2. Sample results of the relationship between total inorganic carbon (IC) and pH from the IC analysis method. A linear regression applied to sample data points relating IC to measured pH.

Titration method

The pH-CO_2 titration method was used for all remaining trial conditions and follows procedures developed in Beyers et al. (1963) and summarized in Beyers (1964). On the day of sampling, a 500 ml sample was taken from the process water in each ATS reservoir near the end of the light segment of the diel light cycle (when the pH level in the reservoir was expected to be highest). Each sample was placed in a 1-L Erlenmeyer flask and immediately sparged with nitrogen gas to remove all other dissolved gases. Sparging of samples was performed for at least 1 hour until the pH generally increased above 9.0. A titrant was prepared using HPLC distilled water in a separate Erlenmeyer flask into which compressed CO_2 gas was bubbled using an airstone, creating a titrant that was saturated with CO_2 gas. At the time of titration, the atmospheric pressure and temperature of the sample water were recorded. For the titration, the samples were gently

and continuously stirred with a magnetic stir bar. Just prior to the start of the titration of a sample, a 50-ml subsample was taken in a vial and stored in the dark at 4°C for later IC analysis. The main sample was then titrated with the titrant in which a known volume was injected below the surface of the sample using a piston-driven air displacement micropipette. The change in pH level, measured using a calibrated Jenco model 3672 pH controller (described previously) and a Corning Gel Combo pH probe (Pinnacle Electrochemistry, Woburn, Massachusetts), was recorded along with the volume of titrant added. Titration continued until the pH of the sample was below 7.0. At the end of the titration, additional 50-ml subsamples of the process water and of the titrant were taken for IC measurement. The subsamples were analyzed for inorganic carbon using a Phoenix 8000 TOC analyzer Tekmar Dohrman (Cincinnati, Ohio). The theoretical concentration of aqueous CO_2 in the titrant was determined using tables in (Beyers et al. 1963) for dissolved CO_2 concentration in water at a known barometric pressure and temperature. The beginning and ending IC concentrations were checked with those expected by the total addition of titrant. For each sample, information, a chart of IC versus pH was developed and used to convert pH to IC for that harvest period (Figure 3. 3). The curve of IC versus pH was generally described by a third order polynomial regression, and linear regression was used to extrapolate beyond the pH range measured in the titration, assumed for its ease of calculation.

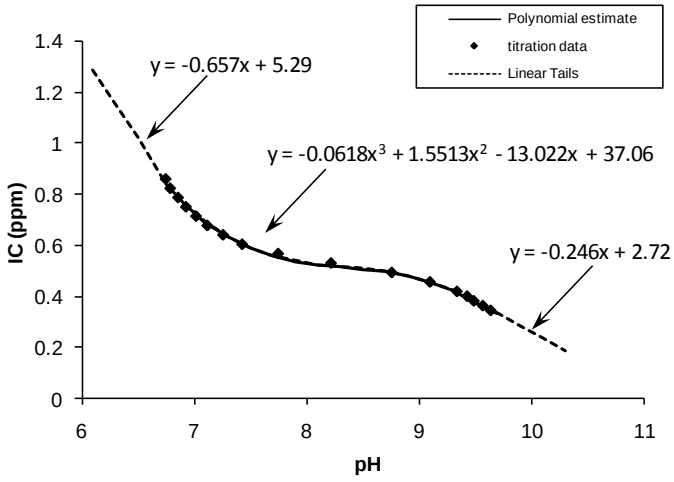

Figure 3. 3. Sample results of the pH-IC titration trial for ATS process water, which can be described by a third-order polynomial regression analysis ($r^2 = 0.998$) and linear regression to extrapolate beyond the upper and lower bounds of the titration.

System Calibration

The pH diurnal changes in an aquatic system represent an ecosystem-level parameter, the diurnal metabolism of the entire algal turf. In applying it to an ATS, the magnitude of the diurnal pH fluctuation is a function of the relationship between the area of the turf screen in an ATS and the total system volume. Thus, the calibration must be performed for different physical ATS configurations (that is, different combinations of turf area and reservoir volumes). Full calibration of the pH diurnal monitoring system required translation of the pH probe voltage to pH level using standard buffer solutions, translation of the pH level to IC concentration using the CO_2 titration method, and determination of the algal productivity by accounting for total changes in IC concentration over time. A schematic diagram of the information needed for complete calibration of the pH monitoring system for ATS productivity is given in Figure 3. 4.

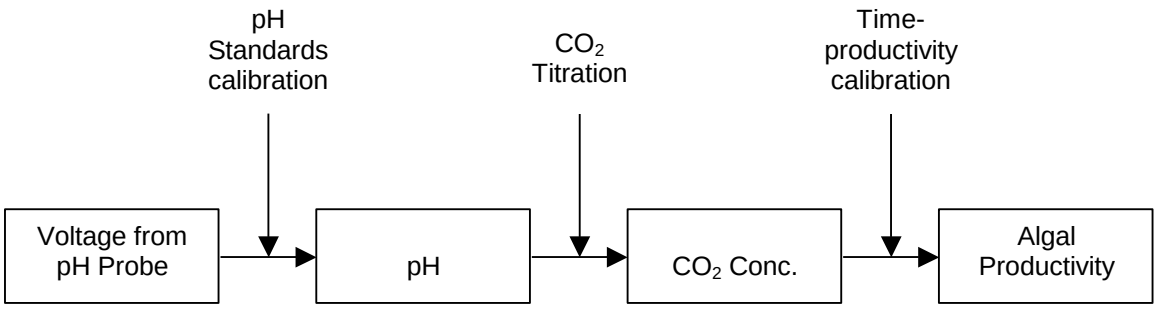

Figure 3. 4. Calibration information needed for the monitoring system to convert voltage from the pH probe to algal productivity in an ATS.

As the research progressed, it became clear that the inorganic carbon titration method was a surrogate for the net primary production, rather than serving as a measurement of the absolute value of it. The pH diurnal was clear in all trials, however, and the method was pursued assuming that it yielded a reliable and easy-to-measure parameter that was closely correlated with ecosystem metabolism. For the purposes of this research, these measurements are termed "net carbon production" (NCP).

Operating Conditions

Various combinations of light intensity, nitrogen loading rate (NLR), and wave surge frequency were tested in trials on the ATS units. The operating conditions for these parameters are summarized as follows.

Light Regimes

Measurements of the light intensity on each ATS unit were made periodically throughout all experiments. In October 2007, it was observed that the intensity of the lights was lower than had been measured previously, thought to be the result of bulb age and wear. The bulbs were replaced with new bulbs at this time, resulting in a step-wise increase in the overall light intensity incident on the algal turf. Thus, there is a division of experiments between low light and high light conditions.

To confirm light intensity levels, measurements of the light intensity were made on each ATS unit at 25 locations evenly spaced in the growth area. These were averaged for each ATS for each date of measurement using Theissen polygon weighting (Ward and Trimble 2004), the results of which are shown in Table 3. 2. A two-way ANOVA analysis (see Appendix C for ANOVA table) on ATS units 1 through 5 for April, October, and November 2007 measurements of light intensity showed that "Date" accounts for 13.5% of the variation in light intensity ($F=23.5$, $Df_n=2$, $Df_d=288$, $P<0.0001$), and that variation for "ATS no." or their interaction were not significant ($P>0.05$). A student's t-test shows that the means between April and October 2007 (Table 3. 2) were not significantly different ($P=0.0688$), but the means between October and November 2007 (after the new bulbs were installed) were significantly different ($P=0.0053$).

Table 3. 2. Weighted mean and standard deviation of light intensities for the set of ATS units in the lab measured at various times throughout the set of experiments. Means and standard deviations are calculated using Theissen polygon areal weighting of 25 measurements evenly distributed as a grid over the ATS growth area.

ATS No.	Light Intensity (μmol m^{-2} s^{-1}) at Date of Measurement			
	April 2007	**Oct. 2007**	**Nov. 2007**	**July 2008**
1	216 ± 107	186 ± 80	244 ± 129	227 ± 113
2	188 ± 84	167 ± 75	297 ± 143	--
4	259 ± 143	206 ± 108	326 ± 176	--
5	224 ± 104	169 ± 77	322 ± 166	--
7	231 ± 43	--	--	184 ± 40

The maximum light intensity levels, measured in the center of each ATS bed, are also reported (Table 3. 3). A two-way ANOVA analysis (see Appendix C for ANOVA table) on the five different ATS units for April, October, and November 2007 measurements of maximum light intensity showed that "Date" accounts for 60.95% of

the variation (F=22.0, Df_n=2, Df_d=6, P=0.0017), while "ATS no." accounts for 30.74% of the variation (F=7.40, Df_n=3, Df_d=6, P=0.0193). A student's t-test shows that the means between April and October 2007 (Table 3. 3) were not significantly different (P=0.1113), but the means between October and November 2007 (after the new bulbs were installed) were significantly different (P=0.0133).

Table 3. 3. Maximum light intensity, measured at the center of the ATS growth area, for each ATS unit in the lab measured at various times throughout the set of experiments.

ATS No.	Light Intensity (µmol m^{-2} s^{-1}) at Date of Measurement			
	April 2007	Oct. 2007	Nov. 2007	July 2008
1	357	277	378	416
2	316	270	464	--
4	477	385	553	--
5	392	265	527	--
7	272	--	--	255

Flow Regimes

Wave surge frequency in each ATS was manipulated as the independent variable by establishing different volumetric flow rates for a constant wave surge bucket volume through the use of combinations of pumps of various capacities (Table 3. 4). The pumps were submersible centrifugal pond pumps (Danner Manufacturing, Islandia, NY) and were installed in the reservoir of each ATS with flexible tubing as the conduit. Gate vales on the pump outlet were used to fine-tune the volumetric flow rate to the desired level.

Table 3. 4. Nominal pump flow rate at 2 m of head and manufacturer model number.

Pump Nominal Flow Rate	Pump Model Number*
20 lpm	MD9
40 lpm	MD12
75 lpm	MD18

*All pumps manufactured by Danner Mfg. (Islandia, NY).

For an ATS, volumetric flow rate directly influenced the wave surge frequency for a constant wave surge bucket volume. It was assumed in this set of experiments that the level of turbulence experienced by the algal turf in an ATS was directly proportional to the combination of wave surge frequency and surge volume, as indicated by previous research (Chapter 2). For this set of experiments, the wave surge volume (set by the volume of the wave surge bucket) was held constant, and wave surge frequency was manipulated by changing the overall volumetric flow rate. The lowest volumetric flow rate tested followed from equipment constraints, and larger flow rates were chosen to be approximately 5 times greater than the next lowest rate (Table 3. 5). Hence the flow rates ranged approximately two orders of magnitude. The volumetric flow rate in each trial was measured by timing the displacement of water from a graduated reservoir.

Table 3. 5. Measured flow rate (lpm) and wave surge frequency (min^{-1}) for the nominal flow rate conditions tested.

Nominal Flow Rate (lpm)	Measured Flow Rate (gpm)	Measured Tipping Frequency (min^{-1})	No. of measurements (n)
1	0.61 ± 0.34	0.06 ± 0.04	19
5	3.8 ± 0.8	0.35 ± 0.05	10
25	29 ± 1	2.7 ± 0.1	19
125	124 ± 11	11.0 ± 1.0	19

Nitrogen Loading Rates and Feed types

The various nitrogen feed types were used throughout all the trials. While undigested dairy manure was used for a majority of the testing, the other feed types made from recipes of inorganic chemicals were experimented with in attempts to more closely control the alkalinity of the process water. These inorganic feed types included a urea solution, a solution made from a commercially-available plant fertilizer (Miracle Gro®), and a modified Bristol's solution. Appreciable die-off of algae was observed for the urea

and Miracle-Gro solutions, and it was not possible to obtain meaningful biomass or metabolic data for these trials; they are hence not reported here.

Various nitrogen loading rates (NLRs) were attempted as well. The NLR was manipulated for each feed type until the maximum NLR for the set of operating conditions (light and turbulence level) was achieved. The maximum NLR was defined as that NLR just under the rate at which the daily nitrate measurements in the water column exhibited an increase. It was assumed that at rates higher than this threshold NLR, there was not enough algal growth for complete uptake of the nitrogen being supplied daily, and the nitrogen would then accumulate in the reservoir as nitrate. The NLRs are reported here as arbitrary designations "Low", "Medium", and "High" (Table 3. 6).

Table 3. 6. Feed type and nitrogen loading rate (NLR) for different nutrient feed conditions tested throughout the set of experiments.

NLR Designation	Feed Type*	NLR (g N $m^{-2}d^{-1}$)
Low	M	0.6 ± 0.0 (n=17)
Medium	M	1.7 ± 0.3 (n=9)
Hi	M	2.5 ± 0.0 (n=6)
Low	B	0.6 ± 0.3 (n=18)

*__Note:__ For "Feed Type", "M" = raw dairy manure; "B" = modified Bristol's solution.

Experimental Design: Subsidy-stress experiments

Replication of each treatment (defined as a turbulence level at a particular light level and NLR combination) was performed on individual ATS units in time. Between five and eight replicate trials of each treatment were performed. Five sets of operating conditions were tested as follows:

- Low light/Low NLR/Manure
- High light/Low NLR/Manure

- High light/Medium NLR/Manure
- High light/High NLR/Manure
- High light/Low NLR/Bristol's solution

For each condition, data were collected from 5 to 8 harvest periods. Harvest periods ranged from 7 days at Low Light/Low NLR conditions to 4 days at High Light/High NLR. Following the collection of sufficient data points at each condition, new treatments of turbulence level were randomly assigned to each ATS unit and tested under a new NLR. The scrubbers were not moved from their original and respective bank of lights. In one event, the ATS screens were cut into strips, which were then assigned randomly to a new ATS bed and reassembled. This was done to eliminate bias that might result from a history or memory of previous operating conditions experienced by each algal mat community. A time line of tests performed according to ATS number, treatment conditions, NLR designation, and light condition is shown in Figure 3. 5.

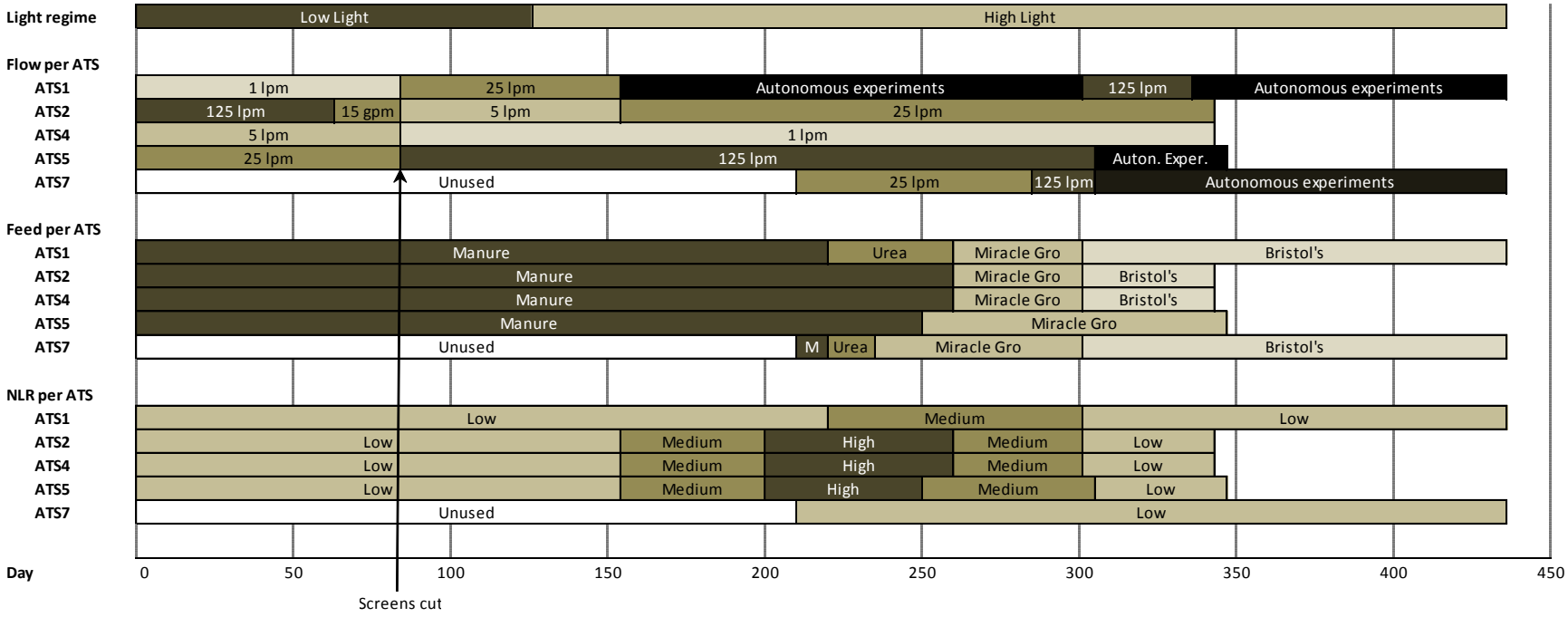

Notes: (1) Light regime was applied to all ATS units at once; other parameters (feed type and NLR) are detailed per ATS unit. (2) Experiments were started on 18 June 2007 (Day 0) and proceeded for 430 days. (3) "Screens cut" indicates when the turf screens in each bed were cut into strips and reassembled randomly in other ATS units.

Figure 3. 5. Timeline for operation of algal turf scrubber units for experiments in subsidy-stress and for autonomous experimentation.

Data Collection

During all trials, water temperature and level were monitored daily in all ATS units. Once a NLR was established, nitrate in the reservoir water was measured prior to each harvest for each ATS unit. Dried biomass from the weekly harvest event for each ATS unit was weighed using a laboratory balance to determine dry weight of biomass production per unit time. Biomass fraction was tracked for that collected from the ATS screen and that collected in the water in the vacuum accompanying each harvest. A record of the pH diurnal was collected for each scrubber for each harvest period automatically with the data acquisition computer, with data sample taken every 5 minutes. A pH-IC titration curve was performed for each ATS unit at least once each harvest period.

Data Analysis and Statistical Approach

The data collected by the computer were an analog voltage varying between 0 and 2.5 V, correlating to a pH level between 4 and 11, respectively, and a timestamp of the voltage reading for each ATS unit. The data for each ATS unit for each harvest period were imported into a spreadsheet program for processing. Processing of data included converting the timestamp to date and time, and converting the voltage to pH using the calibration values for each respective pH controller. The data were filtered and smoothed using spreadsheet software. Noise in the pH signal was reduced by eliminating unrealistically high (greater than 11) or low (less than 5) pH values assuming these resulted from electrical spikes or noise, and curve smoothing was performed by averaging every twelve pH readings to yield one averaged pH reading per hour.

The pH diurnal was translated to an IC diurnal by using the pH-IC titration curve for that respective ATS unit and harvest period. The rate of change of IC was then calculated for each hour timestep by the following relationship:

$$\frac{\Delta IC}{\Delta t} = \frac{(IC)_i - (IC)_{i-1}}{t_i - t_{i-1}}$$

where $(IC)_i$ is the IC concentration at time t_i, and $(t_i - t_{i-1})$ is the timestep of 1 hour. For each timestep, the value of ($\Delta IC/\Delta t$) was evaluated and categorized: if greater than zero, it was considered net community respiration (as the amount of IC given off); if less than zero, it was considered net primary production (as the amount of carbon taken up). These were summed for every 24-hour period to yield total production and respiration for every day. These were averaged for all days of the harvest period to yield the average net carbon production and respiration, expressed as g C m^{-2} d^{-1}. For each set of conditions, measured data from each harvest period was taken as one sample data point.

In the analysis of the data, the following statistical tests were applied:

- Summary of mean and variance of biomass production rate, production, and respiration for each treatment (that is, flow rate for an established light and NLR regime);
- Significance testing using ANOVA analysis applied to the following three relationships for significance: (a) biomass production rate versus wave surge frequency; (b) respiration versus wave surge frequency; (3) net primary production versus wave surge frequency, with the null hypothesis in each case

stated that there is no effect of wave surge frequency on these dependent variables;

- Linear regression analyses of each of net carbon production (NCP), respiration (R), and ratio of NCP to R, versus biomass production rate for each set of treatments to test if the measured biomass production rate is a predictor of the ecosystem metabolism.

The following operational assumptions were made for the experimental design:

- All scrubbers are considered equivalent. Potential differences were eliminated or minimized by locating all ATS units in the same laboratory at similar light and temperature regimes. Nutrient loads were created in batches and applied at the same time to all ATS units.
- The turbulence level experienced by the algal turf community is directly proportional to the average wave surge frequency.

The following statistical assumptions were made and incorporated into the analysis:

- Samples are independent, random, and continuous for each sample set;
- The sample means and residuals are normally distributed;
- The data are not influenced by any outlier (no censored data was assumed).

Gas Diffusion Measurements

An investigation was made into the kinetic transfer dynamics of gas diffusion across the air-water interface in an ATS system. This information is fundamental to the assumption underlying the pH-diurnal method employed in this research, in that, in operation of the ATS, it is assumed that the pH diurnal is affected solely by the biological metabolism occurring in the aquatic environment and that the effect of gas transfer of

CO_2 across the air-water interface is insignificant. This assumption is based on those originally suggested by (Park et al. 1958) in development of the method for environmental applications. Because of the high-turbulence environment of the ATS, however, the question arises: what is the effect of the turbulence level in an ATS on the transfer of gases, especially CO_2, across the air-water interface? To address this, experiments were performed to investigate gas transfer into and out of the water column in an ATS.

An ATS unit and reservoir were scrubbed clean of all algae and biofilm, and the polypropylene screen mesh was removed from the ATS bed. A solution of chlorine bleach cleanser was pumped through the ATS systems to sterilize it. The reservoir was filled with water (typically 90 to110 liters). Water chemistries approximating those employed in the subsidy-stress experiments were tested (Table 3. 7). These include distilled water (6 trials), distilled water with Bristol's solution added (4 trials), and process water from an active ATS unit (1 trial). With the ATS pumps inactive, water in the reservoir was sparged with compressed gas using air stones to remove dissolved gases from the water column. Sparging typically lasted between ½ to 1 hour until the dissolved oxygen, measured with a YSI-85 Handheld Dissolved Oxygen/Conductivity meter (YSI Corporation, Yellow Springs, Ohio), stabilized at or close to zero. Two different sparge gases were employed in separate trials for measurements on two different gas transfer scenarios:

- Compressed carbon dioxide gas (CO_2) was used as the sparge gas to supersaturate the water with CO_2 (thus lowering the pH level), yet remove oxygen from

solution, allowing measurement of dissolved CO_2 loss to the atmosphere and dissolved O_2 gain from the atmosphere;

- Compressed nitrogen gas (N_2) was used as the spare gas to remove both CO_2 (thus raising the pH level) and O_2 from solution, allowing measurement of both CO_2 and O_2 gain from the atmosphere.

Following the gas sparge, the ATS pumps were activated at a known volumetric flow rate, and dissolved oxygen concentration, pH level and time elapsed were measured periodically, with a time of zero established when the pumps were activated. Measurements of dissolved oxygen and pH level continued until they stabilized, taking from approximately 15 minutes to a few hours, depending upon the turbulence level. The trial was repeated for different wave surge frequencies as set by volumetric flow rate. Eleven trials were performed overall (Table 3. 7), each trial representing a different combination of sparge gas, wave surge frequency, and water chemistry type. Samples of water for each water type were taken from the ATS reservoir, and a pH-IC titration was performed to allow conversion of the pH readings to IC concentration values.

Table 3. 7. Operating conditions (consisting of different combinations of sparge gas, water chemistry type, volumetric flow rate, and wave surge frequency) for experimental trials for investigation of gas transfer dynamics in an ATS.

Trial No.	Sparge Gas	Total Water Volume (liters)	Water Type*	Vol. Flow rate (lpm)	Surge Freq. (min^{-1})
1	CO_2	110	D	5	0.3
2	CO_2	110	D	25	1.7
3	CO_2	110	D	60	5.0
4	CO_2	110	D	125	12
5	CO_2	110	D	125	12
6	CO_2	90	B	5	0.3
7	CO_2	90	B	125	12
8	N_2	110	D	125	12
9	N_2	110	P	125	12
10	N_2	90	B	5	0.3
11	N_2	90	B	125	12

*Water type designations: D – distilled water; B – distilled water with Bristol's solution; P – process water

Analysis of the data from the gas transfer experiment trials was performed by plotting the measured parameter versus time and fitting relevant regression curves to the data to yield the first-order gas diffusion coefficients, described by Odum (1956) as the coefficient (*K*) that solved the first-order ordinary differential equation

$$D = \frac{dC}{dt} = KS \tag{3-1}$$

where *D* is the diffusion rate per unit area, *C* is the concentration of the gas in solution (typically expressed as mass per unit volume), *S* is the saturation deficit for the gas, and *K* is the first-order gas transfer coefficient defined on an area basis (units are, for example, in g O_2 m^{-2} d^{-1}). The saturation deficit, *S*, may be defined as

$$S = 1 - \frac{C}{C_H} \tag{3-2}$$

where C_H is the saturation concentration of the gas at the temperature and atmospheric partial pressure of the solution, as predicted by Henry's Law. Combining equations (3-1) and (3-2) and solving the differential equations yields an equation for the concentration *C* of the gas at any time *t*:

$$C(t) = C_H - (C_H - C_0)e^{-Kt/C_H} \tag{3-3}$$

where C_0 is the concentration of the gas at time $t = 0$. Equation (3-3) is the general form of the equation that describes the concentration of gas as mitigated by the degree of saturation of the water. Non-linear regression was thus performed on the data to fit the curve to this general equation form. Data for different sets of measured values were analyzed differently, depending upon whether gas diffusion was into or out of the water column. The methods of analysis were as follows:

Oxygen: In all trials (1 to 11; see Table 3. 7), O_2 transfer across the air-water interface was into the water from the atmosphere. The data were expected to follow the form of an exponential saturation function (Figure 3. 6) with the ideal form as

$$Y = S\left(1 - e^{-kx}\right) + B \tag{3-4}$$

where *S* is the span; *B* is the base; *x* is time; *Y* is the concentration of the gas at time *x*; and *k* is the first-order transfer coefficient. Equating equation (3-4) with equation (3-3), it can be shown that *B* is equal to C_0 (the concentration of gas at time zero); *S* is equal to $(C_H - C_0)$ (the equilibrium concentration of the gas predicted by Henry's Law minus the initial gas concentration); and the transfer coefficient *K* (with dimensions of [Mass]/[Length]^3/[Time]) is equal to kC_H. The data were thus fit to equation (3-4) using non-linear regression, and the relevant transfer coefficients were determined.

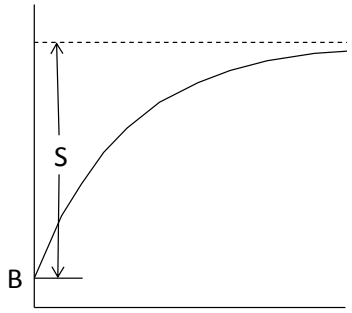

Figure 3. 6. General form of the exponential saturation function used for non-linear regression on aquatic gas concentrations over time as a result of gas diffusion into an aquatic environment with a saturation deficit, where "B" is the base or initial concentration of the gas and "S" is the span over which the gas concentration increases over time.

Carbon Dioxide: Transfer of carbon dioxide across the air-water interface was either out of or into the water to or from the atmosphere, depending upon whether the sparge gas for a trial was carbon dioxide (trials 1 through 7,Table 3. 7) or nitrogen (trials 8 through 11,Table 3. 7), respectively. Carbon dioxide concentrations were determined by converting pH measurements using the ph-IC titration data taken for each water type.

For trials in which transfer of carbon dioxide was into the water from the air (trials 8 through 11), analysis of the data was performed similarly to that used for oxygen, where non-linear regression was used to fit the data to an exponential saturation curve of the form of equation (3-4). For the trials in which transfer of carbon dioxide was out of the water to the air (trials 1 through 7), the data in most cases were close to linear, and linear regression was performed, where the slope of the linear regression equation represented the diffusion rate of carbon dioxide out to the atmosphere. In one case (Trial 7), enough data points were collected such that the carbon dioxide concentration over time followed the form of an exponential decay function (Figure 3. 7). The general form of exponential decay can be described as

$$Y = Se^{-kx} + P \tag{3-5}$$

where S is the span; P is the "plateau" to which Y trends; x is time; Y is the concentration of the gas at time x; and k is the first-order transfer coefficient. Equating equation (3-5) with equation (3-3), it can be shown that P is equal to C_H (the equilibrium concentration of the gas predicted by Henry's Law); S is equal to $(C_0 - C_H)$ (the initial concentration of the gas minus the equilibrium concentration of the gas predicted by Henry's Law); and the transfer coefficient K (with dimensions of [Mass]/[Length]^3/[Time]) is equal to kC_H. The data for trial 7 were thus fit to equation (3-5) using non-linear regression, and the relevant transfer coefficients were determined.

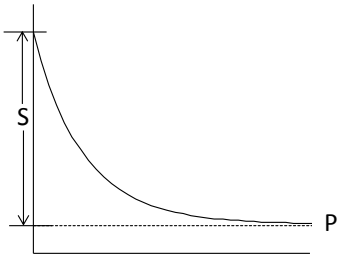

Figure 3. 7. General form of the exponential decay function used for non-linear regression of aquatic gas concentrations over time as a result of gas diffusion out of an aquatic environment with a negative saturation deficit (super-saturation), where "P" is the plateau or long-term equilibrium concentration, and "S" is the span over which the gas concentration decreases over time.

pH: Measurements of pH were taken in all trials as an indirect measure of transfer of carbon dioxide across the air-water interface. The pH level was expected to increase or decrease linearly depending upon whether carbon dioxide was transferring out of or into the water to or from the air, respectively. Thus, pH was expected to increase depending upon whether the sparge gas for a trial was carbon dioxide (trials 1 through 7, Table 3. 7) or nitrogen (trials 8 through 11,Table 3. 7), respectively. For all trials, the change in pH was expected to be approximately linear over a short interval of time. The data were thus analyzed using linear regression, and the slope of the regression function, indicating the average rate of change of pH level, were determined.

Species abundance measurements

It was observed in prior experimentation with the ATS units that certain species of algae would be dominant under certain combinations of operating conditions (turbulence level, nutrient feed type, nitrogen loading rate, etc.). To characterize this dynamic, algae were sampled periodically from each of the ATS units throughout the experiments to determine the relative abundance of the various species in the ATS bed. All sampling occurred after establishment of the high-light regime; no sampling was

performed under low-light conditions. Algae were sampled with tweezers from the screen mesh of each ATS unit in three places, typically near the center of the growth area of the ATS bed, although the specific location of sampling was haphazardly selected. Sampling occurred just prior to a harvest and was performed numerous times throughout the term of operation of the ATS units. These samples were combined in a sample vial. The vial was shaken vigorously by hand to homogenize and was sub-sampled three times with tweezers; each subsample was then mounted on a microscope slide. Using a microscope, algae was keyed to the genus level for each subsample. It was known from prior studies (Mulbry and Wilkie 2001) that the ATS units were typically dominated by benthic filamentous algae from the *Rhizoclonium*, *Microspora*, and *Oscillatoria* genera. For each subsample, an indication of the relative abundance of each of these genera of algae was made according to the following designations: (0) = Absent; (1) = Rare; (2) = Common; (3) = Abundant. Unknown genera of algae (typically one of many planktonic forms) were categorized as "Other" and ascribed an abundance designation.

Analyses of these data were performed as follows: for each sample date, the subsample mean and standard deviation were calculated for the abundance number designations for each algal genus in each ATS unit. The mean was divided by the sum of all abundance means (across all genus designations) for that ATS unit and sample day to yield a percent abundance for each genus. The recorded data included sample date, nitrogen loading rate (NLR) and feed type (i.e., manure, Miracle Gro®, urea solution, or Bristol's solution) for the harvest period, average flow rate and wave surge frequency for two weeks prior to sample date, and the relative abundance for each algal genus. Analysis included the plotting of relative abundance for each algal genus versus experiment day

for each ATS unit. The mean and the standard error were calculated for each algal genus for each ATS unit across time, and these are compared to look for trends characteristic to each ATS unit. The relative abundance for each genus was also plotted against other independent variables of interest, including feed type, nitrogen loading rate, wave surge frequency, and nitrate concentration of the ATS process water, to investigate for trends in relative abundance in response to these variables.

Results

Summary of Subsidy-Stress Data

Data are reported for five sets of operating conditions, as tested:

- Low Light/Low NLR/Manure (two separate trials);
- High Light/Low NLR/Manure;
- High Light/Medium NLR/Manure;
- High Light/High NLR/Manure;
- High Light/Low NLR/Bristol's Solution.

The data collected and used for analysis are presented in Tables B.1 to B.6 in Appendix B. For each set of operating conditions, data are reported for each of the nominal flow rate treatments, expressed in the tables as the measured wave surge frequency (in min^{-1}) and the standard deviation of those measured frequencies. At each nominal flow rate, replicate values are reported for net carbon production (NCP) and respiration (R), expressed in grams of carbon per square meter per day, the ratio of NCP to R (unitless), and the biomass production rate, expressed in grams dry weight per square meter per day. The mean, standard deviation, and number of measurements for each flow condition treatment under each set of operating conditions are reported as well.

All data were included in the statistical analyses, including no-data points (as indicated in the tables in Appendix B with a dash). These data were included to show that tests were run but that some error occasionally occurred during the data collection. Typical errors resulted from disruption of the pH diurnal record because of power outages or excessive electrical noise. For each set of operating conditions, the mean values and standard deviations for each of the measured parameters (NCP, R, NCP/R, and biomass) are plotted versus the wave surge frequency on a semi-log plot to determine if these measurements follow the expected subsidy-stress relationship to wave surge frequency. ANOVA analyses are performed on each set of data for each operating condition to test the significance of the subsidy-stress relationship. Plots are also made of NCP, R, and NCP/R versus biomass to assess the correlation between metabolic measurements and biomass measurements.

Effects of turbulence on metabolic and biomass production measurements

Results are presented for the metabolic and biomass measurements for the five sets of operating conditions in the following order:

- Low Light/Low NLR/Manure (two times);
- High Light/Low NLR/Manure;
- High Light/Medium NLR/Manure;
- High Light/High NLR/Manure;
- High Light/Low NLR/Bristol's Solution.

Low Light, Low NLR, Manure

The results for Low Light/Low NLR/Manure operating conditions are shown in Figure 3. 8. Both net carbon productivity and respiration showed first an increase and

then a decrease in magnitude as the wave surge frequency increased (Figure 3. 8-A). A steady increase in magnitude of both NCP and R was seen from the lowest wave surge frequency to a peak (-1.82 ± 0.40 and +1.93 ± 0.41 g C m^{-2} d^{-1}, for NCP and R, respectively) at a frequency of 2.7 min^{-1}. These metabolic measures were depressed at the highest level of turbulence (surge frequency of 11.5 min^{-1}). The metabolic measures exhibited a large standard deviation at all surge frequencies except the highest, where the error was smaller.

The NCP/R ratio followed a relationship opposite to the individual NCP or R measurements (Figure 3. 8-B), where its lowest value of 0.94±0.03 was seen at a surge frequency of 2.7 min^{-1}. Also, the mean NCP/R ratio was greater than 1 at the lowest and highest wave surge frequencies, and less than one at the two middle frequencies.

The biomass production rate followed a relationship (Figure 3. 8-C) similar to that seen in the metabolic measurements, with a peak in the middle of the range of wave surge frequency. The minimum mean production of 7.1 ± 3.1 g DW m^{-2} d^{-1} (n=7) occured at the highest wave surge frequency of 11.5 min^{-1}, whereas the maximum production of 11.0 ± 2.4 g DW m^{-2} d^{-1} (n=8) occured at the middle wave surge frequency of 2.7 min^{-1}. A two-tailed student's t-test on these values indicates that the means were significantly different (t=2.768, Df=13, P=0.0160). The measurements of biomass production rate have a high standard deviation as shown by the large error bars.

An analysis of variance was conducted to test whether the means of the various measures for at least one wave surge frequency was significantly different from the others. Results of this analysis are presented in Table 3. 8. In reviewing the results of the ANOVA analysis, the null hypothesis (that there is no significant difference between the

means) can be rejected at a 0.05 level of significance for all measures, including productivity ($F=13.52$, $P<0.0001$), respiration ($F=17.36$, $P<0.0001$), NCP/R ratio ($F=4.035$, $P=0.0176$), and biomass production rate ($F=4.491$, $P=0.0111$).

Table 3. 8. Results of ANOVA analysis for Low Light/Low NLR/Manure for (A) net carbon productivity (NCP); (B) respiration (R); (C) NCP/R ratio; and (D) biomass production rate.

	SS	Df	MS	F value	P value
(A) Carbon Productivity (n=8)					
Treatment (flow rate)	5.995	3	1.998	13.52	<0.0001
Residuals	3.843	26	0.147		
Total	9.838	29			
(B) Respiration (n=8)					
Treatment (flow rate)	7.455	3	2.485	17.36	<0.0001
Residuals	3.723	26	0.1432		
Total	11.18	29			
(C) NCP/R ratio (n=8)					
Treatment (flow rate)	0.04274	3	0.01425	4.035	0.0176
Residuals	0.09181	26	0.003531		
Total	0.1345	29			
(D) Biomass Prod. Rate (n=8)					
Treatment (flow rate)	61.47	3	20.49	4.491	0.0111
Residuals	123.2	27	4.562		
Total	184.7	30			

Note: “SS” = sum of squares; “Df” = degrees of freedom; “MS” = mean square

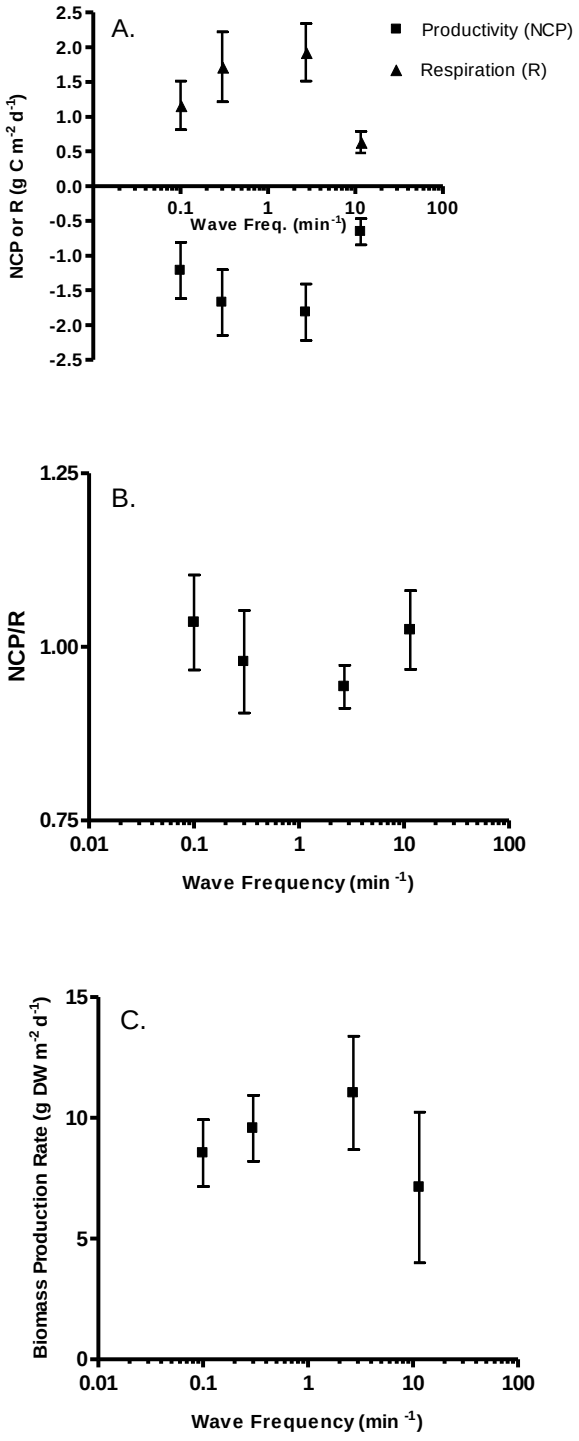

Figure 3. 8. Metabolic and biomass production rate measurements versus wave surge frequency for (Low light, Low NLR, Manure) operating conditions for an ATS: (A) net carbon productivity (NCP) and respiration (R), in g C m^{-2} d^{-1}; (B) NCP/R ratio; (C) biomass production rate, in g DW m^{-2} d^{-1}.

Low Light, Low NLR, Manure (redo)

The results for the re-testing of the Low Light/Low NLR/Manure operating conditions following the random mixing of ATS screen pieces are shown in Figure 3. 9. Both net carbon productivity (NCP) and respiration (R) showed first an increase, then a decrease over increasing wave surge frequency, although this was less pronounced than in prior tests (Figure 3. 9-A). There was a slight peak at a frequency of 2.7 min^{-1} (-0.82 ± 0.09 and +0.71 ± 0.06 g C m^{-2} d^{-1}, for NCP and R, respectively). At the highest surge frequency (11.5 min^{-1}) the metabolic measures were again depressed (-0.21 ± 0.03 and +0.19 ± 0.03 g C m^{-2} d^{-1}, for NCP and R, respectively). The metabolic measures exhibited a large standard deviation at all frequencies except the highest, where the variance appears minimized.

The ratio of NCP to R followed a slight subsidy-stress relationship (Figure 3. 9-B), showing a maximum value in the middle ranges of the wave surge frequency. The error bars representing the standard deviations of the means are, however, large compared to the previous series of tests, and the relationship does not appear significant. The mean NCP/R ratio was greater than 1 at all wave surge frequencies.

The biomass production rate showed a flat relationship (Figure 3. 9-C) for all but the highest wave surge frequency, where a drop in production was exhibited from its highest at 12.0 ± 0.9 g DW m^{-2} d^{-1} (n=5) at a frequency of 2.7 min^{-1} to 8.3 ± 1.4 g DW m^{-2} d^{-1} (n=5) at a frequency of 11.5 min^{-1}. A two-tailed student's t-test on these values indicates that the means were significantly different (t=5.087, Df=8, P=0.0009). These measurements had a high standard deviation as shown by the large error bars.

An analysis of variance was conducted to test whether the means in the various measures for at least one wave surge frequency were significantly different from the others. Results of this analysis are presented in Table 3. 9. In reviewing the results of the ANOVA analysis, the null hypothesis (that there is no significant difference between the means) can be rejected at a 0.05 level of significance for three of the measures, including net carbon productivity ($F=21.66$, $P<0.0001$), respiration ($F=28.10$, $P<0.0001$), and biomass ($F=3.711$, $P=0.0336$). The null hypothesis is accepted, however, for the NCP/R ratio ($F=0.7666$, $P=0.5315$).

Table 3. 9. Results of ANOVA analysis for the retesting of Low Light/Low NLR/Manure for (A) net carbon productivity (NCP); (B) respiration (R); (C) NCP/R ratio; and (D) biomass production rate.

	SS	Df	MS	F value	P value
(A) Carbon Productivity (n=5)					
Treatment (flow rate)	1.206	3	0.4022	21.66	<0.0001
Residuals	0.2600	14	0.01857		
Total	1.466	17			
(B) Respiration (n=5)					
Treatment (flow rate)	0.7870	3	0.2623	28.10	<0.0001
Residuals	0.1307	14	0.009334		
Total	0.9176	17			
(C) NCP/R ratio (n=5)					
Treatment (flow rate)	0.08720	3	0.02907	0.7666	0.5315
Residuals	0.5308	14	0.03792		
Total	0.6180	17			
(D) Biomass Prod. Rate (n=5)					
Treatment (flow rate)	35.01	3	11.67	3.711	0.0336
Residuals	50.31	16	3.145		
Total	85.32	19			

Note: “SS” = sum of squares; “Df” = degrees of freedom; “MS” = mean square

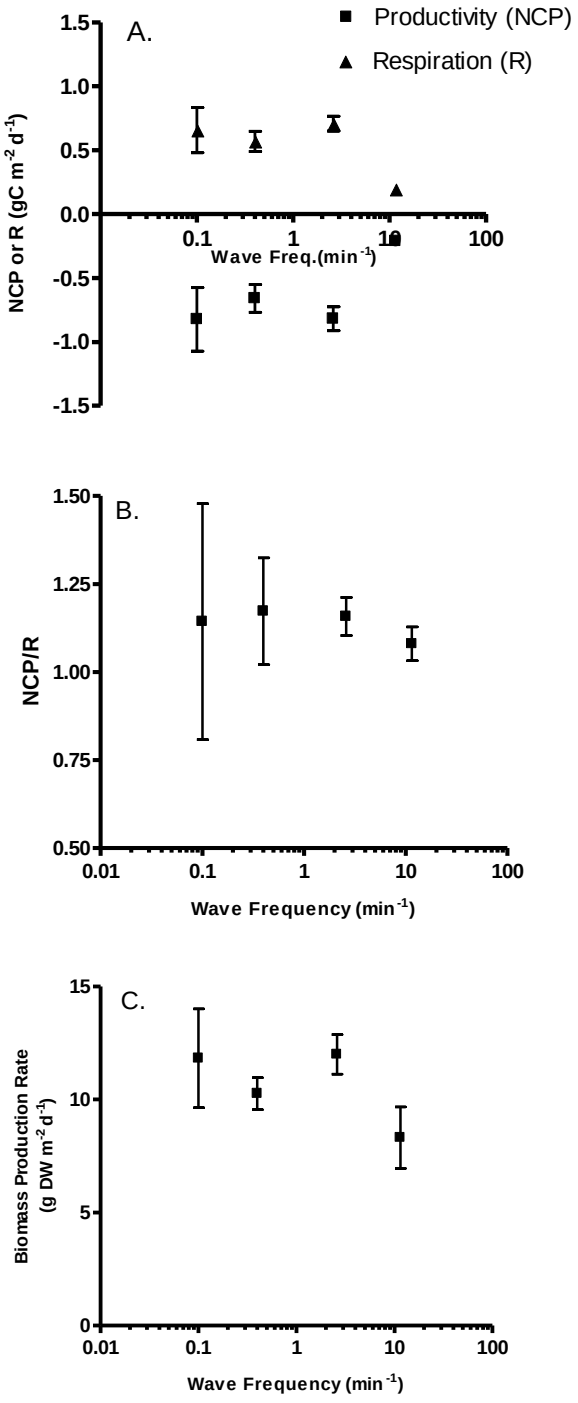

Figure 3. 9. Metabolic and biomass production measurements versus wave surge frequency for the retesting of Low Light/Low NLR/Manure operating conditions for an ATS: (A) net carbon productivity (NCP) and respiration (R), in g C m^{-2} d^{-1}; (B) NCP/R ratio; (C) biomass production rate, in g DW m^{-2} d^{-1}.

High Light, Low NLR, Manure

The results for High Light/Low NLR/Manure operating conditions are shown in Figure 3. 10. Both the net carbon productivity and respiration (Figure 3. 10-A) first increased and then decreased with increasing wave surge frequency. However, the large variance on the measurements, as represented by the error bars, makes this relationship flat. The maximum values for both NCP and R were seen at a wave surge frequency of 0.3 min^{-1} (with values of -1.77 ± 0.48 and +1.49 ± 0.41 g C m^{-2} d^{-1}, for NCP and R, respectively). These metabolic measures were depressed (with values of -0.63 ± 0.23 and +0.67 ± 0.26 g C m^{-2} d^{-1}, for NCP and R, respectively) at the highest wave surge frequency of frequency of 11.5 min^{-1}. The metabolic measures exhibited a large standard deviation at all frequencies except the highest.

The NCP/R ratio showed a steady decline from 1.35 ± 0.09 at the lowest wave surge frequency to 0.95 ± 0.10 at the highest frequency (Figure 3. 10-B). The mean NCP/R ratio was greater than 1 at all frequencies except the highest.

The mean biomass production rate showed no trend over the range of wave surge frequencies (Figure 3. 10-C) because of the high variance on the measurements. The minimum mean production rate was 12.7 ± 2.0 g DW m^{-2} d^{-1} (n=4) at the lowest surge frequency (0.04 min^{-1}), and the maximum mean production rate was 14.4 ± 2.3 g DW m^{-2} d^{-1} (n=4) at a frequency of 0.3 min^{-1}. A two-tailed student's t-test on these values indicates that the means were not significantly different (t=1.096, Df=6, P=0.3153).

An analysis of variance was conducted to test whether the means in the various measures for at least one wave surge frequency were significantly different from the others. Results of this analysis are presented in Table 3. 10. In reviewing the results of the

ANOVA analysis, the null hypothesis (that there is no significant difference between the means) can be rejected at a 0.05 level of significance for two of the measures, including net carbon productivity (F=3.720, P=0.0422), and NCP/R ratio (F=13.78; P=0.0003). The null hypothesis is accepted, however, for respiration (F=2.993, P=0.0732) and for biomass production rate (F=0.5529, P=0.6559).

Table 3. 10. Results of ANOVA analysis for the testing of High Light/Low NLR/Manure for (A) net carbon productivity (NCP); (B) respiration (R); (C) NCP/R ratio; and (D) biomass production rate.

	SS	Df	MS	F value	P value
(A) Carbon Productivity (n=4)					
Treatment (flow rate)	2.853	3	0.9509	3.720	0.0422
Residuals	3.068	12	0.2556		
Total	5.920	15			
(B) Respiration (n=4)					
Treatment (flow rate)	1.548	3	0.5158	2.993	0.0732
Residuals	2.068	12	0.1723		
Total	3.616	15			
(C) NCP/R ratio (n=4)					
Treatment (flow rate)	0.3226	3	0.1075	13.78	0.0003
Residuals	0.09367	12	0.007806		
Total	0.4163	15			
(D) Biomass Prod. Rate (n=4)					
Treatment (flow rate)	7.375	3	2.458	0.5529	0.6559
Residuals	53.36	12	4.446		
Total	60.73	15			

Note: “SS” = sum of squares; “Df” = degrees of freedom; “MS” = mean square.

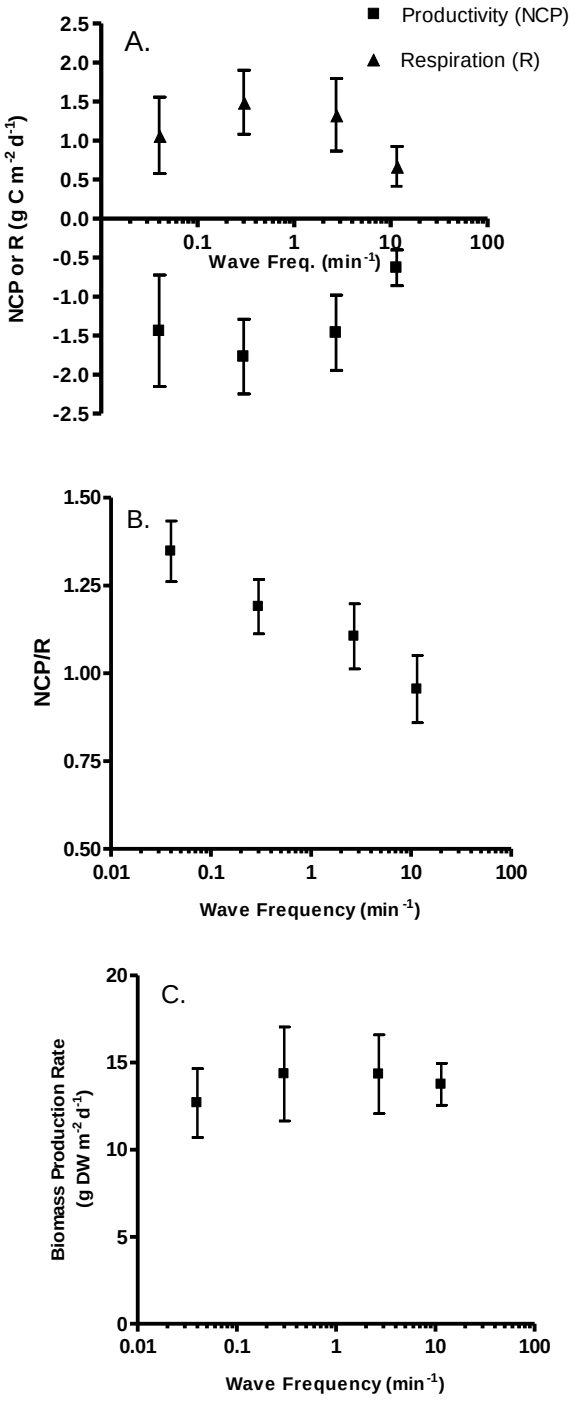

Figure 3. 10. Metabolic and biomass production measurements versus wave surge frequency for the testing of High Light/Low NLR/Manure operating conditions for an ATS: (A) net carbon productivity and respiration, in g C m^{-2} d^{-1}; (B) NCP/R ratio; (C) biomass production rate, in g DW m^{-2} d^{-1}.

High Light, Medium NLR, Manure

The results for High Light/Medium NLR/Manure operating conditions are shown in Figure 3. 11. Both net carbon productivity and respiration (Figure 3. 11-A) first increased and then decreased with increasing wave surge frequency. The maximum values for both NCP and R were seen at a wave surge frequency of 2.7 min^{-1} (with values of -1.25 ± 0.27 and +1.25 ± 0.23 g C m^{-2} d^{-1}, for NCP and R, respectively). These metabolic measures were depressed significantly at the lowest (-0.63 ± 0.20 and +0.64 ± 0.19 g C m^{-2} d^{-1}, for NCP and R, respectively) and the highest (-1.01 ± 0.19 and +0.92 ± 0.15 g C m^{-2} d^{-1}, for NCP and R, respectively) wave surge frequencies. The metabolic measures exhibited a moderate standard deviation at all surge frequencies.

The NCP/R ratio was nearly flat with a slight rise to 1.10 ± 0.14 at the highest wave surge frequency (Figure 3. 11-B). The mean NCP/R ratio was near 1 at all frequencies.

The mean biomass production rate showed a steady increase from lowest to highest wave surge frequency (Figure 3. 11-C), with a minimum mean production of 19.4 ± 2.5 g DW m^{-2} d^{-1} (n=8) at the lowest frequency, and a maximum mean production of 27.4 ± 5.1 g DW m^{-2} d^{-1} (n=8) at the highest frequency. A two-tailed student's t-test on these values indicates that the means were significantly different (t=4.019, Df=14, P=0.0013).These measurements had high standard deviations at the highest two frequencies.

An analysis of variance was conducted to test whether the means of the various measures of at least one wave surge frequency were significantly different from the others. Results of this analysis are presented in Table 3. 11. In reviewing the results of the

ANOVA analysis, the null hypothesis (that there was no significant difference between the means) can be rejected at a 0.05 level of significance for three of the measures, including net carbon productivity ($F=15.75$, $P<0.0001$), respiration ($F=19.04$, $P<0.0001$), and biomass production rate ($F=5.874$, $P=0.0094$). The null hypothesis is accepted, however, for the NCP/R ratio ($F=2.677$, $P=0.0933$).

Table 3. 11. Results of ANOVA analysis for the testing of High Light/Medium NLR/Manure for (A) net carbon productivity (NCP); (B) respiration (R); (C) NCP/R ratio; and (D) biomass production rate.

	SS	Df	MS	F value	P value
(A) Carbon Productivity (n=8)					
Treatment (flow rate)	1.513	2	0.7565	15.75	<0.0001
Residuals	0.9605	20	0.04803		
Total	2.474	22			
(B) Respiration (n=8)					
Treatment (flow rate)	1.376	2	0.6881	19.04	<0.0001
Residuals	0.7229	20	0.03614		
Total	2.099	22			
(C) NCP/R ratio (n=8)					
Treatment (flow rate)	0.06782	2	0.03391	2.677	0.0933
Residuals	0.2534	20	0.01267		
Total	0.3212	22			
(D) Biomass Prod. Rate (n=8)					
Treatment (flow rate)	255.3	2	127.6	5.874	0.0094
Residuals	456.3	21	21.73		
Total	711.5	23			

Note: “SS” = sum of squares; “Df” = degrees of freedom; “MS” = mean square.

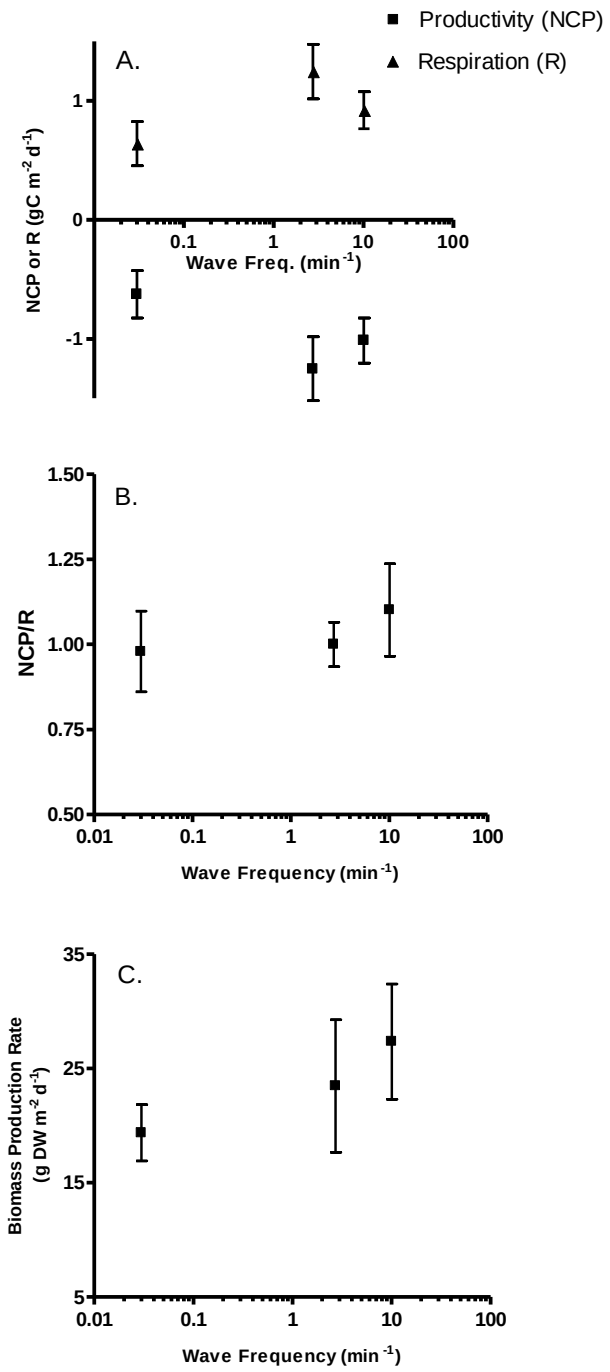

Figure 3. 11. Metabolic and biomass production measurements versus wave surge frequency for the testing of High Light/Medium NLR/Manure operating conditions for an ATS: (A) net carbon productivity (NCP) and respiration (R), in g C m^{-2} d^{-1}; (B) NCP/R ratio; (C) biomass production rate, in g DW m^{-2} d^{-1}.

High Light, High NLR, Manure

The results for High Light/High NLR/Manure operating conditions are shown in Figure 3. 12. Both net carbon productivity (NCP) and respiration (R) (Figure 3. 12-A) increased and then decreased with increasing wave surge frequency. The maximum values for both NCP and R were seen, as before, at a wave surge frequency of 2.7 min^{-1} (with values of -0.90 ± 0.20 and +0.90 ± 0.20 g C m^{-2} d^{-1}, for NCP and R, respectively). These metabolic measures were depressed at the lowest (-0.77 ± 0.53 and +0.75 ± 0.55 g C m^{-2} d^{-1}, for NCP and R, respectively) and highest (-0.77 ± 0.30 and +0.72 ± 0.33 g C m^{-2} d^{-1}, for NCP and R, respectively) surge frequencies of 0.04 and 11 min^{-1}, respectively. However, the metabolic measures exhibited a moderate standard deviation at all frequencies, and the relationship appears relatively flat.

As before, the NCP/R ratio was flat with a slight decline to 0.99 ± 0.09 at the middle surge frequency of 2.7 min^{-1} (Figure 3. 12-B). The mean NCP/R ratio is near 1 at all frequencies.

The mean biomass production rate showed a steady increase from lowest to highest wave surge frequency (Figure 3. 12-C), with a minimum mean production rate of 23.2 ± 4.6 g DW m^{-2} d^{-1} (n=6) at the lowest frequency, and a maximum mean production rate of 36.6 ± 5.6 g DW m^{-2} d^{-1} (n=5) at the highest frequency; this was the highest mean biomass production rate observed throughout all tests. A two-tailed student's t-test on these values indicates that the means were significantly different (t=4.375, Df=9, P=0.0018). The measurements of the biomass production rate have a relatively high standard deviation at all frequencies.

An analysis of variance was conducted to test whether the means of the various measures of at least one wave surge frequency were significantly different from the others. Results of this analysis are presented in Table 3. 12. In reviewing the results of the ANOVA analysis, the null hypothesis (that there was no significant difference between the means) can be rejected at a 0.05 level of significance only for biomass production rate (F=8.178; P=0.0044). The null hypothesis is accepted, however, for all other measures, including net carbon productivity (F=0.2291, P=0.7980), respiration (F=0.3907, P=0.6833), and the NCP/R ratio (F=0.6893, P=0.5171).

Table 3. 12. Results of ANOVA analysis for the testing of High Light/High NLR/Manure for (A) net carbon productivity (NCP); (B) respiration (R); (C) NCP/R ratio; and (D) biomass production rate.

	SS	Df	MS	F value	P value
(A) Net Carbon Productivity (n=6)					
Treatment (flow rate)	0.06188	2	0.03094	0.2291	0.7980
Residuals	2.026	15	0.1351		
Total	2.088	17			
(B) Respiration (n=6)					
Treatment (flow rate)	0.1177	2	0.05887	0.3907	0.6833
Residuals	2.260	15	0.1507		
Total	2.378	17			
(C) NCP/R ratio (n=6)					
Treatment (flow rate)	0.02843	2	0.01422	0.6893	0.5171
Residuals	0.3094	15	0.02062		
Total	0.3378	17			
(D) Biomass Prod. Rate (n=6)					
Treatment (flow rate)	492.7	2	246.4	8.178	0.0044
Residuals	421.7	14	30.12		
Total	914.5	16			

Note: SS = sum of squares; Df = degrees of freedom; MS = mean square.

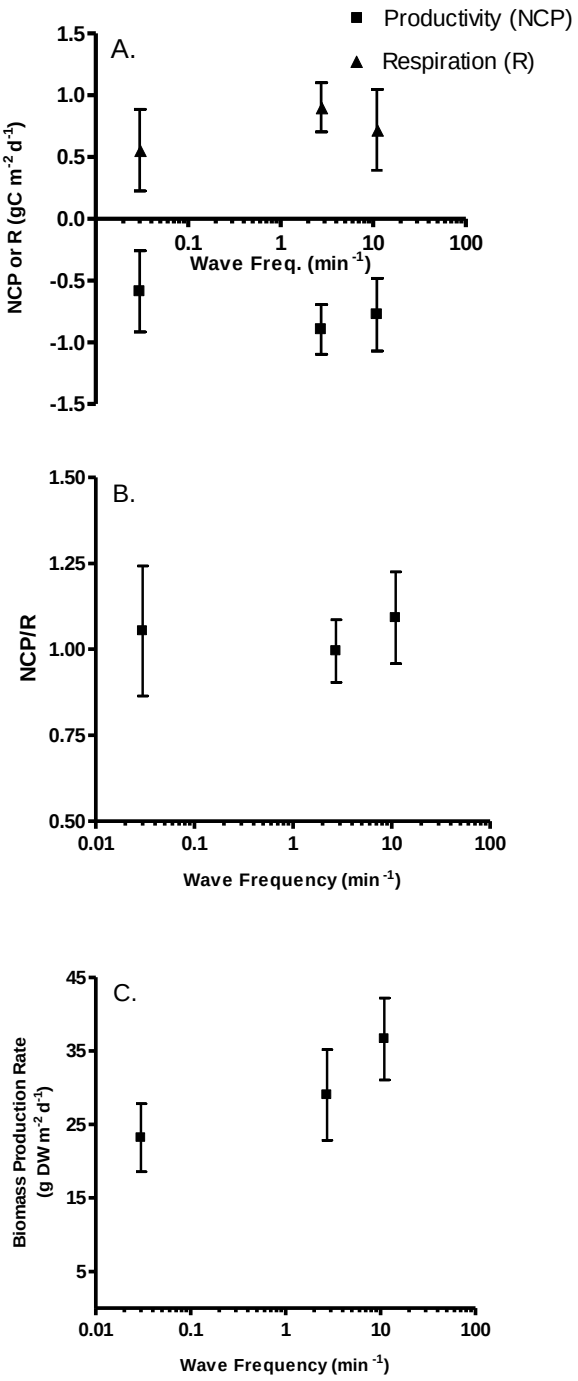

Figure 3. 12. Metabolic and biomass production measurements versus wave surge frequency for the testing of High Light/High NLR/Manure operating conditions for an ATS: (A) net carbon productivity (NCP) and respiration (R), in g C m^{-2} d^{-1}; (B) NCP/R ratio; (C) biomass production rate, in g DW m^{-2} d^{-1}.

High Light, Low NLR, Bristol's

The results for High Light/Low NLR/Bristol's operating conditions are shown in Figure 3. 13. Both the net carbon productivity (NCP) and respiration (R) (Figure 3. 13-A) increased and then decreased with increasing wave surge frequency. The maximum values for both NCP and R were seen at a wave surge frequency of 2.7 min^{-1} (with values of -0.65 ± 0.29 and +0.60 ± 0.25 g C m^{-2} d^{-1}, for NCP and R, respectively). These metabolic measures were depressed at the lowest (-0.44 ± 0.13 and +0.42 ± 0.12 g C m^{-2} d^{-1}, for NCP and R, respectively) and highest (-0.22 ± 0.06 and +0.20 ± 0.05 g C m^{-2} d^{-1}, for NCP and R, respectively) surge frequencies of 0.04 and 11 min^{-1}, respectively. However, the metabolic measures exhibited a large standard deviation at the middle frequency, and the relationship appeared relatively flat. Also, these measurements were the lowest overall metabolic measurements observed in all the tests.

As before, the mean NCP/R ratio was flat with a slight increase from the lowest to the highest wave surge frequencies (Figure 3. 13-B), ranging from 1.03 ± 0.06 to 1.11 ± 0.07. A two-tailed student's t-test on these values indicates that the means were not significantly different (t=2.194, Df=10, P=0.0530).

The mean biomass production rate showed a slight increase from lowest to highest wave surge frequency (Figure 3. 13-C), with a minimum mean production rate of 5.9 ± 2.3 g DW m^{-2} d^{-1} (n=6) at the lowest frequency, and a maximum mean production rate of 8.1 ± 1.2 g DW m^{-2} d^{-1} (n=6) at the highest frequency. A two-tailed student's t-test on these values indicates that the means were not significantly different (t=2.190, Df=10, P=0.0533). The measurements of biomass production rate had a relatively high standard deviation at all frequencies.

An analysis of variance was conducted to test whether the means of the various measures of at least one wave surge frequency were significantly different from the others. Results of this analysis are presented in Table 3. 13. In reviewing the results of the ANOVA analysis, the null hypothesis (that there was no significant difference between the means) can be rejected at a 0.05 level of significance for two of the measures, including net carbon productivity (F=8.597, P=0.0042), and respiration (F=9.759, P=0.0026). The null hypothesis is accepted, however, for the NCP/R ratio (F=2.670, P=0.1068) and biomass production rate (F=2.705, P=0.0993).

Table 3. 13. Results of ANOVA analysis for the testing of High Light/Low NLR/Bristol's solution for (A) net carbon productivity (NCP); (B) respiration (R); (C) NCP/R ratio; and (D) biomass production rate.

	SS	Df	MS	F value	P value
(A) Net Carbon Productivity (n=6)					
Treatment (flow rate)	0.4599	2	0.2299	8.597	0.0042
Residuals	0.3477	13	0.02675		
Total	0.8076	15			
(B) Respiration (n=6)					
Treatment (flow rate)	0.3992	2	0.1996	9.759	0.0026
Residuals	0.2659	13	0.02045		
Total	0.6651	15			
(C) NCP/R ratio (n=6)					
Treatment (flow rate)	0.02181	2	0.01090	2.670	0.1068
Residuals	0.05309	13	0.004084		
Total	0.07490	15			
(D) Biomass Prod. Rate (n=6)					
Treatment (flow rate)	17.00	2	8.502	2.705	0.0993
Residuals	47.14	15	3.143		
Total	64.15	17			

Note: SS = sum of squares; Df = degrees of freedom; MS = mean square.

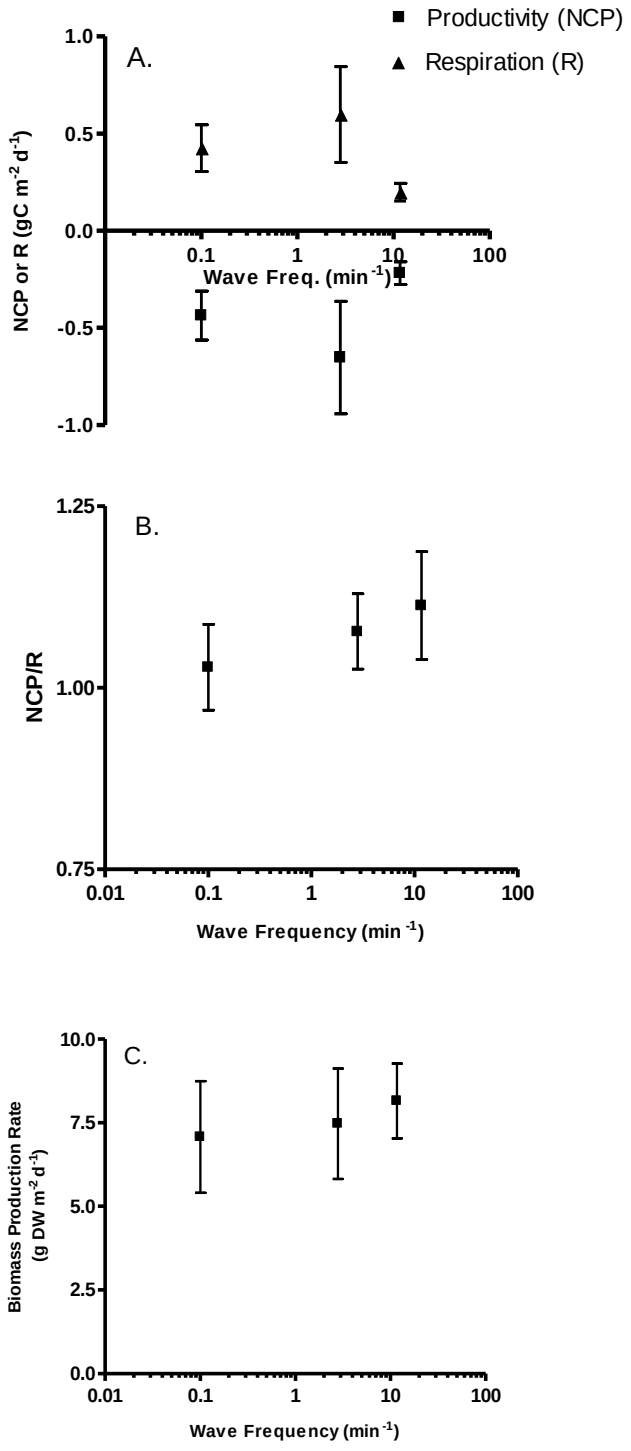

Figure 3. 13. Metabolic and biomass production measurements versus wave surge frequency for the testing of High Light/Low NLR/Bristol's operating conditions for an ATS: (A) net carbon productivity (NCP) and respiration (R), in g C m^{-2} d^{-1}; (B) NCP/R ratio; (C) biomass production rate, in g DW m^{-2} d^{-1}.

Correlation between metabolic measurements and biomass

An analysis was performed to investigate the relationship between the metabolic measurements and the biomass production rate in the ATS units. The three metabolic measures (NCP, R, and NCP/R ratio) were each plotted versus biomass production rate (B) for all flow rates at each set of operating conditions. A linear regression was performed to indicate how well the biomass production rate predicted each of the metabolic measures at that operating condition. Typical results for these regression analyses are shown in Figure 3. 14 for one set of operating conditions; graphical results for all operating conditions are given in Appendix B.

The best-fit values for the linear regression coefficients and the goodness-of-fit characteristics (coefficient of determination (r^2) and standard error of the estimate ($S_{y.x}$)), as well hypothesis testing on the significance of the slope of the regression line for each of these analyses are given in Table 3. 14. These results show that the coefficient of determination (r^2) was greater than 0.5 in only the redo trial of Low Light/Low NLR/Manure (for NCP versus B, $r^2 = 0.792$, and $S_{y-x} = 0.138$; for R versus B, $r^2 = 0.623$, $S_{y-x} = 0.147$). The same trial exhibited the largest percent in variation of the NCP/R ratio that was explained by B ($r^2 = 0.309$, $S_{y-x} = 0.164$). Only one other trial condition (number 4, High Light/Medium NLR/Manure) had any appreciable variation in NCP ($r^2 = 0.342$) and R ($r^2 = 0.282$) that was explained by B. All remaining trial conditions had coefficients of determination that were quite low (less than 0.2), indicating that any variation in the metabolic measure is not explained by biomass production. Also, hypothesis tests on the slopes of the regression lines shows that, for NCP and R versus B, the slope differs from zero in only three of the trial series (Low Light/Low NLR/Manure,

retrial of Low Light/Low NLR/Manure and High Light/Medium NLR/Manure). For the NCP/R ratio, this significance occurred in only two trial conditions (Low Light/Low NLR/Manure and its retrial). For all other trial conditions, the slope of the regression line was not significantly different than zero.

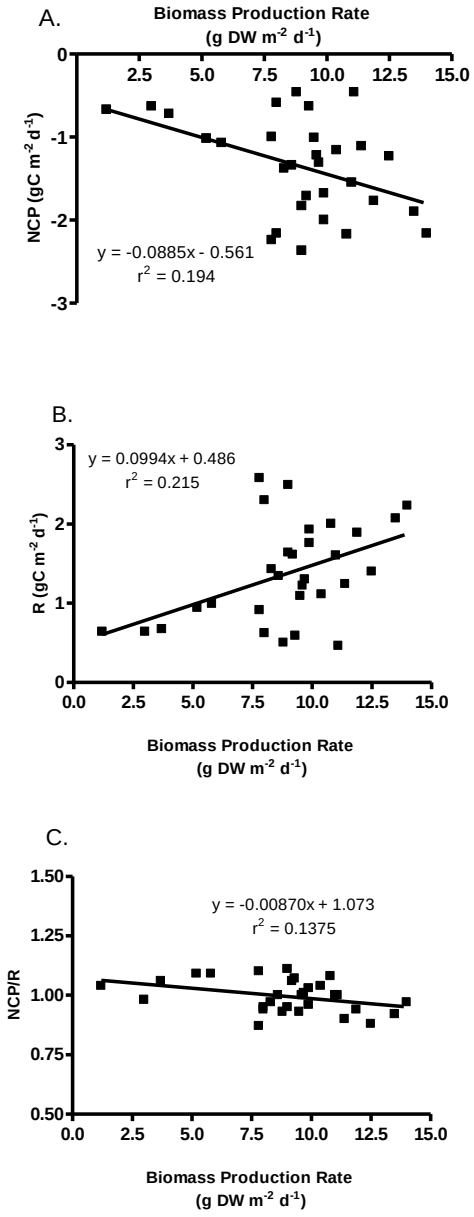

Figure 3. 14. Linear regression analysis for operating conditions of (Low light, Low NLR, Manure), showing the following metabolic measurements versus biomass production rate: (A) net carbon productivity (NCP); (B) respiration (R); (C) NCP/R ratio.

Table 3. 14. Results of linear regression analyses, including best-fit values, goodness-of-fit metrics, and hypothesis testing on the significance of the slope, on metabolic measurements versus biomass production rate (B) for all trials: (a) net carbon productivity (NCP) vs. B; (b) respiration (R) vs. B; (c) NCP/R ratio vs. B.

(a)		**Trial Number***					
Analysis:	NCP vs B	1	2	3	4	5	6

Best-fit values	Slope	-0.085 ±0.0341	-0.130 ±0.0166	-0.00447 ±0.0826	-0.0400 ±0.0127	-0.0112 ±0.00979	0.041185 ±0.0282
	Y-Int.	-0.561 ±0.0320	-0.750 ±0.178	-0.709 ±1.15	0.0137 ±0.301	-0.434 ±0.296	-0.701 ±0.208
Goodness of fit	R^2	0.194	0.792	0.0205	0.342	0.0799	0.132
	$S_{y.x}$	0.532	0.138	0.644	0.270	0.285	0.224
Significance of slope	F	6.73	60.8	0.294	9.88	1.30	2.12
	Df_n, Df_d	1,28	1,16	1,14	1,19	1,15	1,14
	P	0.0149	<0.0001	0.5965	0.0054	0.2716	0.1674
	Significantly ≠ 0?	Yes	Yes	No	Yes	No	No
	n	30	18	16	21	17	16

(b)		**Trial Number***					
Analysis:	R vs B	1	2	3	4	5	6
Best-fit values	Slope	0.0994 ±0.0359	-0.0911 ±0.0177	0.0629 ±0.0630	-0.0340 ±0.0124	-0.00735 ±0.0107	-0.0442 ±0.0248
	Y-Int.	0.486 ±0.337	-0.434 ±0.190	0.273 ±0.877	0.113 ±0.294	-0.521 ±0.323	0.697 ±0.183
Goodness of fit	R^2	0.215	0.623	0.0664	0.282	0.0305	0.185
	$S_{y.x}$	0.560	0.147	0.491	0.264	0.311	0.197
Significance of slope	F	7.66	26.4	0.996	7.46	0.473	3.17
	Df_n, Df_d	1,28	1,16	1,14	1,19	1,15	1,14
	P	0.0099	<0.0001	0.3352	0.0132	0.5023	0.0968
	Significantly ≠ 0?	Yes	Yes	No	Yes	No	No
	n	30	18	16	21	17	16

(c)		**Trial Number***					
Analysis:	NCP/R vs B	1	2	3	4	5	6
Best-fit values	Slope	-0.009 ±0.004	0.0529 ±0.0198	-0.0141 ±0.0218	0.00836 ±0.00415	0.00667 ±0.00470	0.01257 ±0.007534
	Y-Int.	1.073 ±0.0386	0.606 ±0.212	1.344 ±0.303	0.815 ±0.0982	0.855 ±0.142	0.9782 ±0.0556
Goodness of fit	R^2	0.138	0.309	0.0291	0.176	0.118	0.1658
	$S_{y.x}$	0.0642	0.164	0.1696	0.0882	0.137	0.05974
Significance of slope	F	4.463	7.152	0.4196	4.082	2.014	2.782
	Df_n, Df_d	1,28	1,16	1,14	1,19	1,15	1,14
	P	0.0437	0.0166	0.5276	0.0582	0.1763	0.1175
	Significantly ≠0?	Yes	Yes	No	No	No	No
	n	30	18	16	21	17	16

*_Trial Number_ refers to the trial conditions as follows: 1: Low light/Low NLR/Manure; 2: retest of Low light/Low NLR/Manure; 3: High light/Low NLR/Manure; 4: High light/Medium NLR/Manure; 5: High light/High NLR/Manure; 6: High light/Low NLR/Bristol's.

Results of Gas Diffusion Measurements

Results for the non-linear regression parameters for oxygen transfer into the water across the air-water interface are shown (Table 3. 15). The first-order gas diffusion constant (*K*) is calculated for per-volume and per-area bases, using the total system volume reported for each trial (Table 3. 7) and assuming a water surface area of 1.25 m^2.

Values for *K* ranged from 0.47 g O_2 m^{-2} hr^{-1} (Trial 6) for the lowest wave surge frequency (0.3 min^{-1}) to 23.8 g O_2 m^{-2} hr^{-1} (Trial 8) for the highest surge frequency (12 min^{-1}).

Table 3. 15. Results for non-linear regression on oxygen concentration over time describing gas transfer into the water column from the atmosphere for various trials defined by wave surge frequency.

Trial No.	Surge Freq. (min^{-1})	k (hr^{-1})	S (mg O_2 L^{-1})	B (mg O_2 L^{-1})	C_H (mg O_2 L^{-1})	K (mg O_2 L^{-1} hr^{-1})	K (g O_2 m^{-2} hr^{-1})	r^2
1	0.3	0.887	8.57	0.040	8.61	7.64	0.69	0.997
2	1.7	2.62	7.54	0.481	8.02	21.0	1.91	0.999
3	5.0	8.23	7.49	0.608	8.10	66.6	6.05	0.999
4	12	17.2	7.87	0.216	8.09	139	12.7	0.999
5	12	19.9	7.20	0.418	7.61	152	13.8	1.000
6	0.3	0.935	6.19	0.444	6.63	6.20	0.47	0.958
7	12	20.5	6.35	0.363	6.72	138	10.4	0.997
8	12	33.3	7.52	0.337	7.85	262	23.8	0.991
9	12	33.1	6.63	0.301	6.93	230	20.9	0.981
10	0.3	1.56	5.98	0.016	5.99	9.34	0.71	0.995
11	12	43.7	7.17	-0.082	7.08	309	23.4	0.986

Note: Parameters are as follows: "k" is the first-order parameter; "S" is the span of the change in oxygen concentration; "B" is the base or initial oxygen concentration; "C_H" is the equilibrium concentration of oxygen predicted by Henry's Law, and is calculated as the sum of S and B; "K" is the first-order transfer coefficient for oxygen into the water, expressed both on a per-volume basis and a per-area basis (assuming a reactive surface area of 1.25 m^2); and r^2 is the coefficient of determination for the non-linear regression analysis.

Results for the non-linear regression parameters for carbon dioxide transfer into the water across the air-water interface are shown (Table 3. 16). The first-order gas diffusion constant (*K*) is calculated for per-volume and per-area bases, using the total system volume reported for each trial (Table 3. 7) and assuming a water surface area of 1.25 m^{-2}. Values for *K* ranged from 0.048 g CO_2 m^{-2} hr^{-1} (Trial 10) for the lowest wave surge frequency (0.3 min^{-1}) to 2.55 g CO_2 m^{-2} hr^{-1} (Trial 11) for the highest frequency (12 min^{-1}).

Table 3. 16. Results for non-linear regression on carbon dioxide concentration over time describing gas transfer into the water column from the atmosphere for various trials defined by wave surge frequency.

Trial No.	Surge Freq. (min^{-1})	k (hr^{-1})	S (mmol CO_2 L^{-1})	B (mmol CO_2 L^{-1})	C_H (mmol CO_2 L^{-1})	K (mmol CO_2 L^{-1} hr^{-1})	K (g CO_2 m^{-2} hr^{-1})	r^2

8	12	45.6	0.081	0.000	0.081	3.7	0.134	0.989
9	12	1.99	0.086	0.622	0.707	1.4	0.051	0.975
10	0.3	0.84	0.390	1.162	1.552	1.3	0.048	0.982
11	12	54.1	0.184	1.111	1.295	70.1	2.549	0.982

Note: Parameters are as follows: "k" is the first-order parameter; "S" is the span of the change in carbon dioxide concentration; "B" is the base or initial carbon dioxide concentration; "C_H" is the equilibrium concentration of carbon dioxide predicted by Henry's Law, and is calculated as the sum of S and B; "K" is the first-order transfer coefficient for carbon dioxide into the water, expressed both on a per-volume basis and a per-area basis (assuming a reactive surface area of 1.25 m^2); and r^2 is the coefficient of determination for the non-linear regression analysis.

Results for the linear regression parameters for decreasing change in pH level, representing carbon dioxide transfer into the water across the air-water interface, for these same trials are shown (Table 3. 17). Values for this slope ("M") were negative, indicating a drop in pH over time, and ranged from -0.22 pH units hr^{-1} (Trial 10) for the lowest wave surge frequency (0.3 min^{-1}) to -12.0 pH units hr^{-1} (Trial 8) for the highest frequency (12 min^{-1}). Also, differences were seen between water chemistries operating at the same surge frequency; for example, the slope of the pH change varied from -0.82 pH units hr^{-1} for process water (Trial 9) to -12.0 pH units hr^{-1} for distilled water, both operating at a surge frequency of 12 min^{-1}.

Table 3. 17. Results for linear regression on pH level over time as a result of carbon dioxide gas transfer into the water column from the atmosphere for various trials defined by wave surge frequency.

Trial No.	Surge Freq. (min^{-1})	M (hr^{-1})	r^2
8	12	-12.00	0.937
9	12	-0.82	0.851
10	0.3	-0.22	0.909
11	12	-10.20	0.878

Note: Parameters are as follows: "M" is the slope of the regression equation, in pH units per hour, and r^2 is the coefficient of determination for the non-linear regression analysis.

Results for the linear and non-linear regression parameters for carbon dioxide transfer out of the water across the air-water interface are shown (Table 3. 18). The first-order gas diffusion constant (*K*) is calculated for per-volume and per-area bases, using the total system volume reported for each trial (Table 3. 7) and assuming a water surface area of 1.25 m^{-2}. Values for *K* ranged from 0.020 g CO_2 m^{-2} hr^{-1} (Trial 6) for the lowest wave surge frequency (0.3 min^{-1}) to 0.42 g CO_2 m^{-2} hr^{-1} (Trial 5) for the highest surge frequency (12 min^{-1}).

Table 3. 18. Results for linear and non-linear regression on carbon dioxide concentration over time describing gas transfer out of the water column to the atmosphere for various trials defined by wave surge frequency.

Trial No.	Surge Freq. (min^{-1})	Type of Regress.	M (mM CO_2 hr^{-1})	k (hr^{-1})	S (mM CO_2)	P (mM CO_2)	K (mM CO_2 hr^{-1})	K* (g CO_2 m^{-2} hr^{-1})	r^2
1	0.3	No measurements made							
2	1.7	Lin	3.1	--	--	--	--	0.113	0.988
3	5.0	Lin	5.3	--	--	--	--	0.193	0.983
4	12	Lin	9.8	--	--	--	--	0.355	0.985
5	12	Lin	11.4	--	--	--	--	0.416	0.991
6	0.3	Lin	0.5	--	--	--	--	0.020	0.987
7	12	Non-lin	--	3.03	3.509	0.4543	1.4	0.050	0.975

Note: Parameters are as follows: For the trials for which linear regression was used, "M" is the slope of the linear regression equation. For the trials in which non-linear regression is used, "k" is the first-order parameter for non-linear regression; "S" is the span of the change in CO_2 concentration; "P" is the plateau to which CO_2 concentration trends; "K" is the first-order transfer coefficient for CO_2 out of the water, expressed on a per-volume basis. For all trials, the effective transfer coefficient "K*" is calculated on a per-area basis (assuming a reactive surface area of 1.25 m2), and r2 is the coefficient of determination for the regression analysis.

Results for the linear regression parameters for increasing change in pH level, representing carbon dioxide transfer out of the water across the air-water interface, for these same trials are shown (Table 3. 19). Values for this slope ("M") ranged from 0.54 pH units hr^{-1} (Trial 6) for the lowest wave surge frequency (0.3 min^{-1}) to 6.85 pH units hr^{-1} (Trial 5) for the highest frequency (12 min^{-1}).

Table 3. 19. Results for linear regression on pH level over time as a result of carbon dioxide gas transfer out the water column from the atmosphere for various trials defined by wave surge frequency.

Trial No.	Surge Freq. (min^{-1})	M (hr^{-1})	r^2
1	0.3	No data	
2	1.7	1.74	0.988
3	5.0	2.98	0.983
4	12	5.48	0.985
5	12	6.85	0.996
6	0.3	0.54	0.985
7	12	5.70	0.930

Note: Parameters are as follows: "M" is the slope of the regression equation, in pH units per hour, and r^2 is the coefficient of determination for the regression analysis.

The data results from the gas transfer experiments as summarized in the tables (Table 3. 15 to Table 3. 19) can be analyzed graphically to show relationships and trends. The results for the first-order gas diffusion constant for oxygen transfer into the water across the air-water interface (Table 3. 15) are plotted as a function of wave surge frequency (Figure 3. 15). The diffusion constant follows a strong log-log relationship to the surge frequency, increasing directly with increasing wave surge frequency. Values for the first-order transfer coefficient and their relationship to frequency were observed to be similar for all water chemistry types.

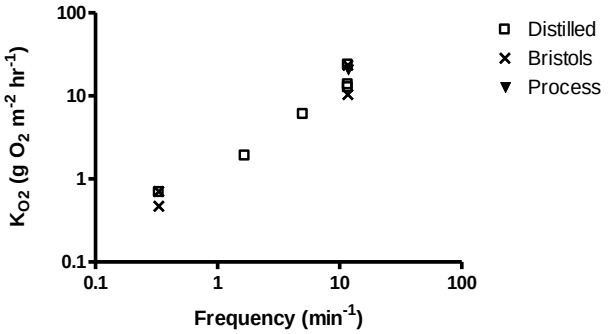

Figure 3. 15. First-order transfer coefficients for diffusion of oxygen into an ATS operating at different wave surge frequencies for different water types.

The results for the first-order gas diffusion constant for transfer of carbon dioxide into the water across the air-water interface (Table 3. 16) are plotted as a function of wave surge frequency (Figure 3. 16). The diffusion constant follows a log-log relationship to the frequency, increasing directly with an increase in frequency for the Bristol's water chemistry. Values for the first-order transfer coefficient and its relationship to wave surge frequency were observed to be dissimilar for different water chemistry types, with a decreased value exhibited for distilled water and process water as compared to Bristol's water.

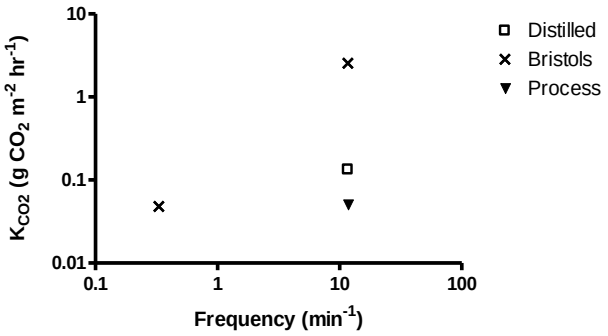

Figure 3. 16. First-order transfer coefficients for diffusion of carbon dioxide into an ATS operating at different wave surge frequencies for different water types.

The results for the rate of change of pH level representing the transfer of carbon dioxide into the water across the air-water interface (Table 3. 17) are plotted as a function of wave surge frequency (Figure 3. 17). The rate of change of pH follows a log-log relationship to the frequency, increasing directly with an increase in frequency for the Bristol's water chemistry. Values for the rate of change in pH level and its relationship to wave surge frequency were observed to be dissimilar for different water chemistry types, with similar values observed for distilled and Bristol's water and process water having a lower value.

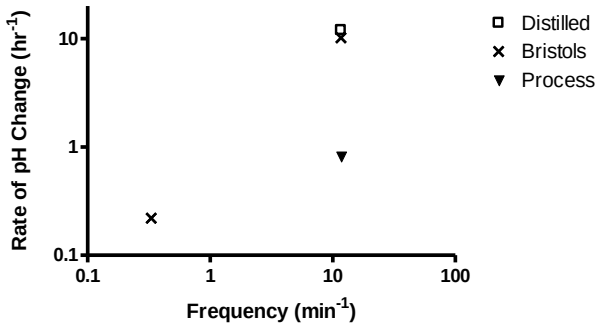

Figure 3. 17. Rate of change of pH reflecting the diffusion of carbon dioxide into an ATS operating at different wave surge frequencies for different water chemistry types.

The results for the first-order gas diffusion constant for transfer of carbon dioxide out of the water across the air-water interface (Table 3. 18) are plotted as a function of wave surge frequency (Figure 3. 18). The diffusion constant follows a log-log relationship to the frequency, increasing directly with an increase in frequency for both the distilled and the Bristol's water chemistry types. Values for the first-order transfer coefficient and its relationship to wave surge frequency were observed to be dissimilar for different water chemistry types, with a reduced effect of increasing frequency observed for Bristol's compared to distilled water types.

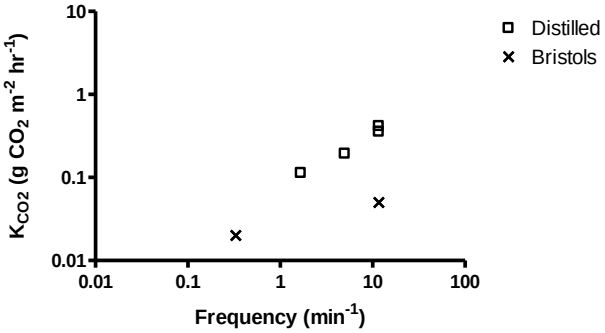

Figure 3. 18. First-order transfer coefficients for diffusion of carbon dioxide out of an ATS operating at different wave surge frequencies for different water chemistry types.

The results for the rate of change of pH level representing the transfer of carbon dioxide out of the water across the air-water interface (Table 3. 19) are plotted as a function of wave surge frequency (Figure 3. 19). The rate of change of pH level follows a log-log relationship to the frequency, increasing directly with an increase in frequency for both the distilled and the Bristol's water chemistry types. Values for the rate of change in pH and its relationship to wave surge frequency were observed to be similar for different water chemistry types, with similar values observed for distilled and Bristol's water.

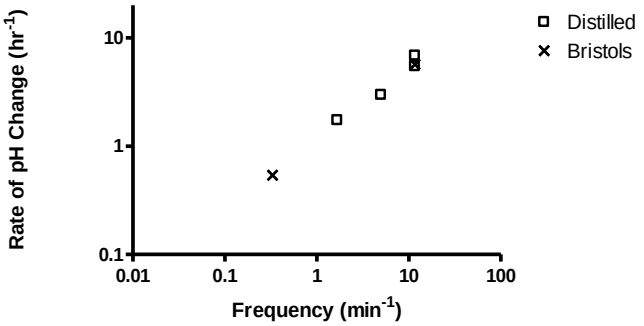

Figure 3. 19. Rate of change of pH level reflecting the diffusion of carbon dioxide out of an ATS operating at different wave surge frequencies for different water chemistry types.

Results of Species Abundance Measurements

Filamentous algal types were keyed to the genus level. In most operating conditions, benthic species from *Rhizoclonium*, *Microspora*, or *Oscillatoria* were dominant or co-dominant. The occasional presence of other species was noted; these species were typically of a planktonic morphology, and they were not identified or keyed. Micrographs of the representative algal genera are shown in Figure 3. 20. Relative abundances of the various genera of algae and the operating conditions under which they were found are reported in Table D.1 in Appendix D.

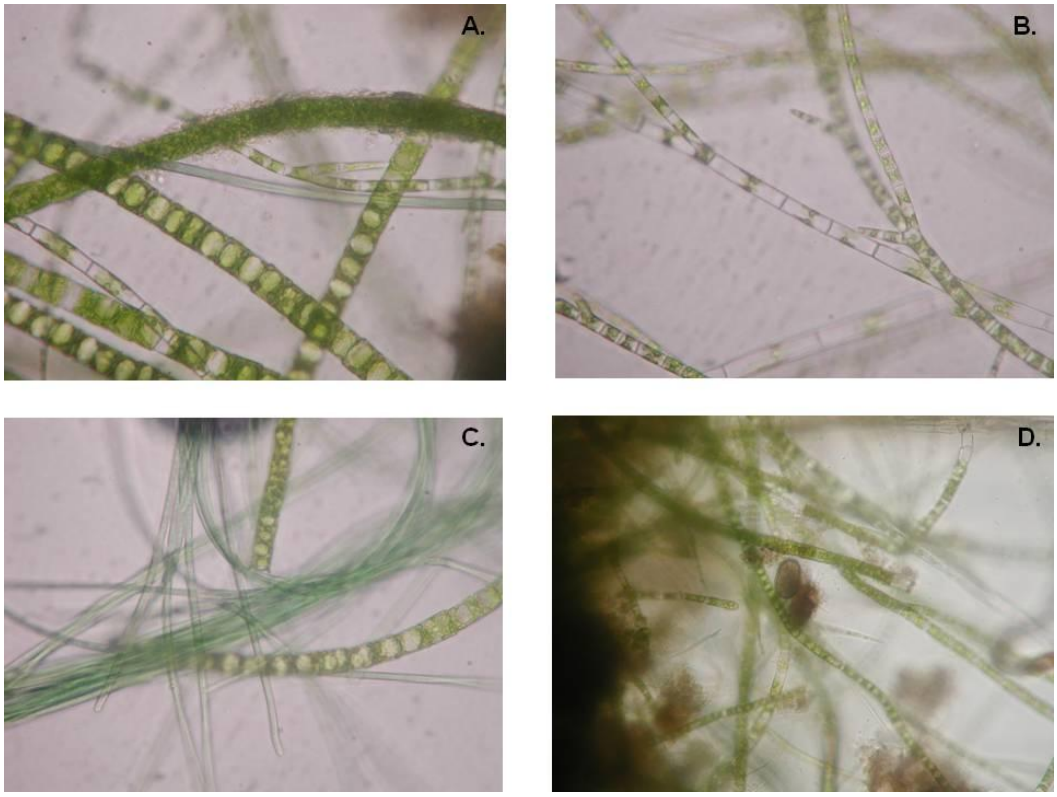

Figure 3. 20. Micrographs of representative algal genera observed in ATS units during operation. (A) *Microspora* spp. (in foreground) in ATS unit 1; (B) *Rhizoclonium* spp. in ATS unit 1; (C) *Oscillatoria* spp. (foreground) in ATS unit 5; (D) unidentified planktonic species categorized as "Other" in ATS unit 4. All micrographs taken at 40x magnification from samples collected on 16 December 2007.

Results of the species abundance measurements for each of ATS units throughout the length of the experiment are shown in Figure 3. 21. For all ATS units, the relative abundance of each of the algal genera fluctuated through time; however, some general trends are evident. For ATS unit 1, *Rhizoclonium* and *Microspora* genera were predominant throughout most of the time of operation, although *Oscillatoria* and other genera showed increasing abundances at various times. ATS unit 2 likewise showed dominance by *Rhizoclonium* and *Microspora* as well as a greater overall predominance of *Oscillatoria*. ATS unit 4 showed a much greater dominance of other planktonic species of algae. It also showed a strong dominance of *Oscillatoria* and almost no presence of *Rhizoclonium* in earlier days of operation, a situation that shifted in later days of

operation when *Rhizoclonium* and *Microspora* were more dominant and *Oscillatoria* was nearly absent. ATS unit 5 showed a fairly even distribution between *Microspora* and *Rhizoclonium* throughout latter days of operation and a strong dominance of *Oscillatoria* throughout most operation. ATS unit 7 seemed to be dominated by *Rhizoclonium* throughout much of its operation, with occasional shifts to dominance by *Oscillatoria* at times.

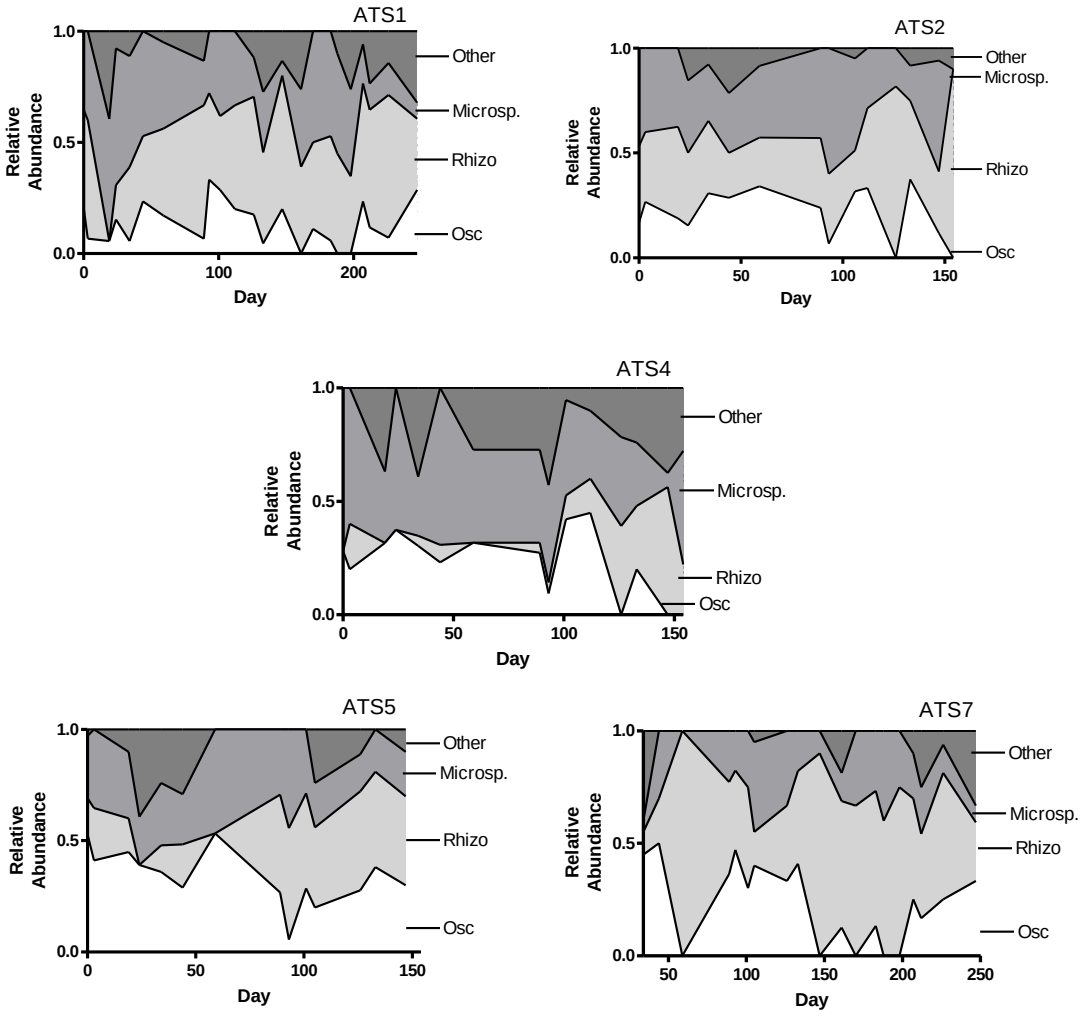

Figure 3. 21. Relative abundance of algal genera versus day of operation for each ATS unit.

The means of the relative abundance for each algal genus for each ATS unit throughout the time of operation are shown in Figure 3. 22. Although all ATS units showed similar mean abundances for most genera, some general observations may be made about trends in certain genera. ATS unit 4 generally showed a low mean abundance of *Rhizoclonium* and a high mean abundance of *Microspora*. This is a different pattern than was seen in other ATS units, which generally had a more balanced ratio between the two genera. In addition, ATS unit 4 generally had a higher mean abundance of "Other" algal genera, typically represented by planktonic algae. ATS unit 5 exhibited the highest mean proportion of *Oscillatoria* algal species. ATS unit 7 exhibited the highest proportion of *Rhizoclonium* compared to other ATS units.

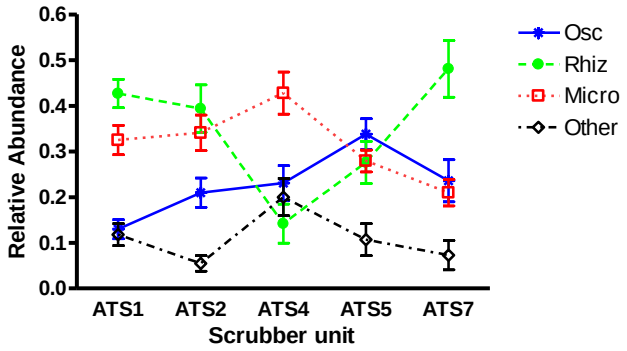

Figure 3. 22. Mean relative abundance of the various genera of algae found in each ATS unit.

The relative abundances of all algae can be plotted versus each of the independent variables of the operating conditions (Figure 3. 23) to show trends in the relative abundance of various algal genera. In relation to the type of nutrient feed (Figure 3. 23A), *Rhizoclonium* was the most abundant relative to Bristol's medium, whereas *Oscillatoria* had nearly equivalent abundance for all feed types except Bristol's medium, where it was least abundant. In relation to the nitrogen loading rate (Figure 3. 23B), only *Rhizoclonium*

was seen to have a trend that was nearly linear and significant ($r^2 = 0.6632$; $P = 0.0075$); it was the only genus seen to drop in relative abundance as NLR is increased. In relation to the wave surge frequency (Figure 3. 23C), *Rhizoclonium* showed first an increase, up to a frequency of approximately 5.5 min^{-1}, and then a decrease as surge frequency increases beyond this. *Microspora* and *Oscillatoria* both exhibited the opposite trend, decreasing to a minimum near a frequency of 5.5 min^{-1} and then increasing beyond this. No trends were seen for 'Other' algal genera.

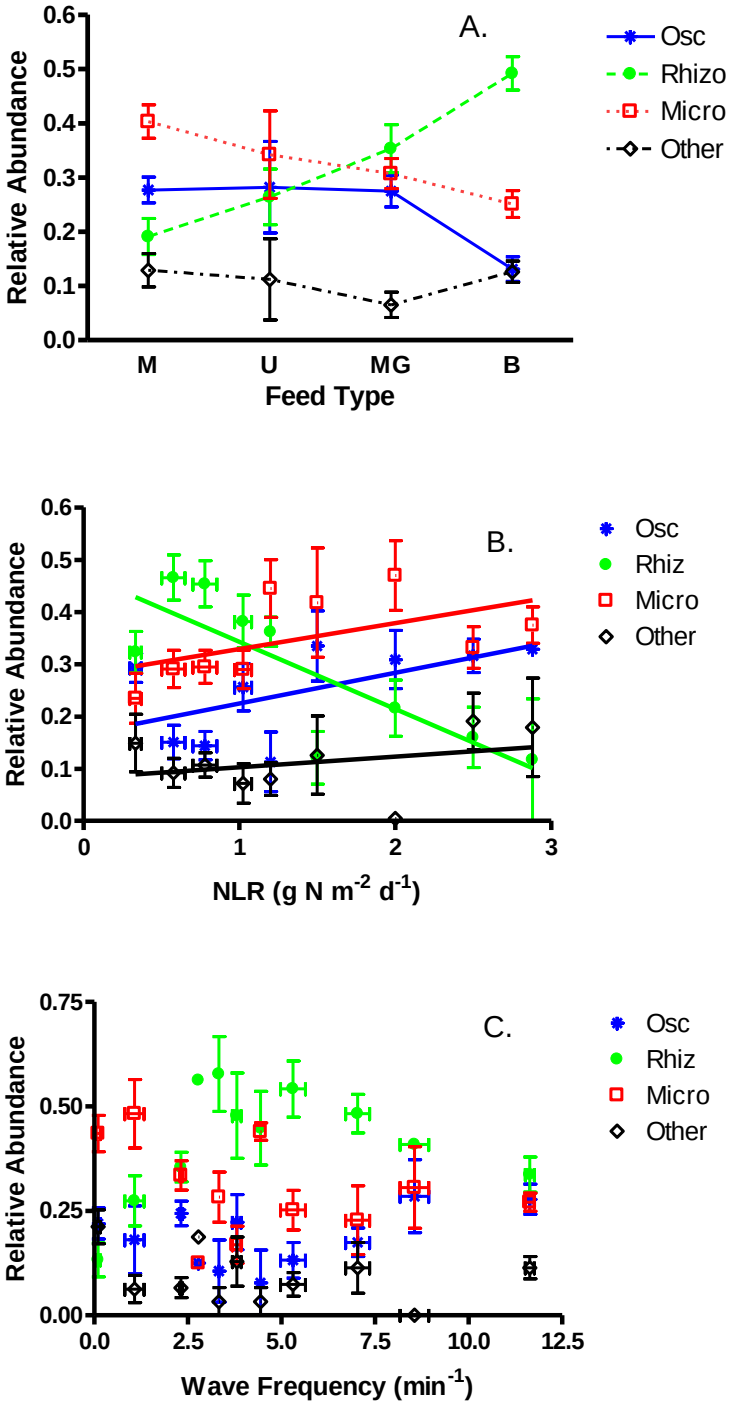

Figure 3. 23. Relative abundance of algal genera in relation to various predictor variables: (A) relative abundance versus feed type; (B) relative abundance versus nitrogen loading rate (NLR); (C) relative abundance versus wave surge frequency.

Discussion

Subsidy-stress relationships reflected in the metabolic measurements

Subsidy-stress relationships were hypothesized for the effect of flow turbulence (as set by nominal volumetric flow rate and as expressed as the wave surge frequency) on the metabolic measures of productivity and respiration, and on the ratio of these two measures. The interpretation of these results will be discussed separately.

Production and respiration measurements

A subsidy-stress relationship of flow turbulence on metabolic measurements was observed in some form for all trials. This relationship was found to be significant in most cases, but especially for Low Light/Low NLR/Manure, where the stress effect of the highest turbulence level (11.5 min^{-1}) is obvious in the NCP and R measurements. The relationship was the strongest for this case (Figure 3. 8-A, page 97). The subsidy of increasing turbulence is seen in the increase of NCP and R from the lowest wave surge frequency to the middle range, where the peak, for all cases, was typically measured at the next to highest frequency of 2.7 min^{-1}. This subsidy relationship was quite flat, however, for the retrial of these conditions (Figure 3. 9-A, page 100), a feature that is possibly indicative of light limitation of the algal growth. Also, while the peaks in NCP and R are observed in most cases at the wave surge frequency of 2.7 min^{-1}, it is possible that the true peak would be seen somewhere in the range of 5 min^{-1}, a surge frequency not tested in this series of experiments but one that was used for extensive prior experimentation with the ATS units in this lab. The “stress” of the highest surge frequency (11.5 min^{-1}) is exhibited by the depressed value of NCP and R for almost all operating conditions (Figure 3. 8 to Figure 3. 13). This was observed in all trials,

although the effect was reduced somewhat at the higher nitrogen loading rates (NLR), as evidenced in Figure 3. 11-A (page 106) and Figure 3. 12-A (page 109). This could imply that the algal community is better able to compensate for the stress of high turbulent conditions when nutrients are more available for growth and maintenance, that is, when nutrients are not limiting.

It was also noted that the variance on the NCP and R measurements for the High light/High NLR/Manure conditions (Figure 3. 12, page 109) is quite large. The ANOVA analysis (Table 3. 12, page 108) did not find any significance in the difference of the means, and a student's t-test on the lowest (NCP: -0.77 ± 0.53; R: 0.72 ± 0.33) and highest (NCP: -0.92 ± 0.20; R: 0.90 ± 0.20) of these values indicates that there is not significant difference between the means (for NCP, t=0.557, Df=6, P=0.598; for R, t=1.173, Df=8, P=0.275). The large error in this set of conditions may result from the high loading rate effect on the constancy of the water chemistry throughout the series of tests, introducing error in the pH-IC titration and thus into the CO_2 diurnal measurements. This is supported by the fact that the relative error appears to increase as the NLR is increased through subsequent trial conditions.

Ratio of NCP/R

Analyzing results from all trial conditions (Figure 3. 8-B to Figure 3. 13-B), the ratio of NCP to R had no clear trend. In some cases it showed a trend similar to the subsidy-stress curve seen in the individual NCP and R measurements for that set of trial conditions (for example, the retesting of Low Light/Low NLR/Manure conditions; Figure 3. 9-B, page 100). In many cases, the trend in the NCP/R ratio showed the inverse of the subsidy-stress curve, showing the lowest value at the middle turbulence level (for

example, in the original Low Light/Low NLR/Manure conditions; Figure 3. 8-B, page 97). In one case (High Light/Low NLR/Manure conditions; Figure 3. 10-B, page 103), the trend in the NCP/R ratio over the range of surge frequencies showed a steady and near linear trend downward with increasing turbulence level. The error in the mean NCP/R ratio was typically large, however, in most trial conditions, due to the fact that it is the ratio of two measured quantities with significant measurement error already. Given this, for most trials, any pattern or trend in the NCP/R ratio over the range of wave surge frequencies was not significant, with the ANOVA analyses indicating a significance only for the test conditions of Low Light/Low NLR/Manure (Figure 3. 8-B and Table 3. 8, pages 96 and 97) and High Light/Low NLR/Manure (Figure 3. 10-B and Table 3. 10, pages 102 and 103). In the latter case, the trend in the NCP/R ratio was a steady decrease with increasing turbulence level, decreasing from 1.35 ± 0.09 at a wave surge frequency of 0.04 min^{-1} to 0.95 ± 0.10 at a frequency of 11.5 min^{-1}. The interpretation of this is that NCP strongly exceeded R at the low turbulence levels. It is important to note that the four trials comprised by this set of conditions occurred immediately following the increase in light levels after the bulbs were replaced. Could this be a signature of a pulse of net productivity following a prolonged period of operation in light-limited conditions? If this is the case, might the lower levels of turbulence favor the photosynthetic components of the ATS system, whereas the higher levels of turbulence favor the heterotrophic components?

Overall, the values for the ratio of NCP/R ranged from a maximum of 1.35 to a minimum of 0.9. These were unexpectedly low for what is presumed to be a system dominated by an autotrophic community. Odum (1956) discusses autotrophic

communities with NPP:R ratios ranging from 1 (the windward coral reef at Eniwetok) to 3.2 (the polluted White River in Indiana), with gross primary production ranging from 9 to 21 g C m^{-2} d^{-1} (24 to 57 g O_2 m^{-2} d^{-1}) and net primary production ranging from 0 to 14.6 g C m^{-2} d^{-1} (0 to 39 g O_2 m^{-2} d^{-1}), respectively. The order of magnitude difference between the metabolic values reported here and those in the literature suggests some amount of error in the measurement of ecosystem metabolism that has not been accounted for in these analyses.

Linking metabolic measurements to biomass accrual

The subsidy-stress relationship was evident in the biomass production rate measurements at both Low Light/Low NLR/Manure conditions (Figure 3. 8-C and Figure 3. 9-C, pages 97 and 100). In both cases, the trend was relatively flat at the low end of the turbulence range, but a drop in biomass production rate was observed at the highest turbulence levels that were determined to be significant. The increase in light levels with the next series of trials (High light/Low NLR/Manure; Figure 3. 10-C, page 103) showed a flattening of this relationship, where the difference in means at all turbulence levels was not significant. Considering biomass production rate, one possible interpretation is that there was not enough light at low light levels for the algal community to build structure that could withstand the high levels of turbulence at the highest wave surge frequency. Only when the light levels were higher could the structure be maintained in the biomass to withstand the pounding at this flow rate. Anecdotal observations on algal species type throughout the various operating conditions supports this interpretation; at low light levels, the algal community at the highest turbulence levels was dominated by cyanobacteria (*Oscillatoria* sp.) that grew in compressed, mucilaginous form. At high

light levels, the algal community was dominated by the green filamentous forms (*Rhizoclonium* and *Microspora* spp.) typically found in other ATS operating conditions. Another way to interpret this phenomenon is to see the algal turf as light-limited for the low-light conditions; at that light level and NLR, the turbulence was a limiting factor and biomass production rate followed a subsidy-stress curve over its range (Figure 3. 8-C and Figure 3. 9-C, pages 97 and 100). At the high light levels in the next series of tests, biomass production rate became flat over the range of turbulence levels (Figure 3. 10-C, page 103) as nitrogen became the limiting factor.

This interpretation is then supported by the observed immediate increase in average biomass production rate with subsequent increase in NLR at the higher light levels. For the High Light/Medium NLR/Manure condition, the average biomass production rate ranged from 19.4 ± 2.5 to 27.4 ± 5.1 g DW m^{-2} d^{-1} (Figure 3. 11-C, page 106), whereas, for the High Light/Low NLR/Manure condition, the average biomass production rate ranged from 12.7 ± 2.0 to 14.4 ± 2.3 g DW m^{-2} d^{-1} (Figure 3. 10-C, page 103). The maximum average biomass production rate recorded throughout all tests was observed at even higher NLR levels under high light (Figure 3. 12-C, page 109), ranging from 23.2 ± 4.6 to 36.6 ± 5.6 g DW m^{-2} d^{-1} (the maximum individual biomass production rate measurement of 43.2 g DW m^{-2} d^{-1} was recorded for one trial under these conditions as well). At the medium and high NLR under high light, biomass production rate increased log-linearly with increasing wave surge frequency; that is, the maximum biomass production rate was seen at the highest turbulence levels (a surge frequency of 11.5 min^{-1}). In the conditions of enrichment with an abundance of light and nutrients,

turbulence was evinced to be a limiting factor. Under these conditions of plenty, the full subsidy-stress curve was not observed within the bounds of turbulence tested.[1]

For the series of tests employing Bristol's solution, the biomass production rate was observed to be flat (Figure 3. 13-C, page 112) as in other trials under a lower NLR. It should be noted that the nitrogen in Bristol's solution is primarily in the form of a nitrate salt, thus having a lower energetic return and bioavailability for the algal cells than the ammonium form found in the manure feed.

In general, summarizing the results over all test conditions, the biomass production rate followed a trend opposite of that observed for the metabolic measurements on NCP and R. That is, when NCP and R exhibited a strong subsidy-stress relationship with turbulence level, biomass production was fairly flat across the range of turbulence (see especially the results for High Light/Low NLR/Manure conditions in Figure 3. 10, page 103). Also, the trends in NCP and R over increasing turbulence levels did not match the steadily increasing trend in biomass production rate over the same range in the medium (Figure 3. 11, page 106) and high (Figure 3. 12, page 109) NLR conditions under high light. This lack of agreement was further observed in the low correlation calculated between individual measurements of biomass and corresponding metabolic measurements (Table 3. 14, page 115, and Figures B.1 to B.7 in Appendix B). The strongest correlation was seen in the retest of Low Light/Low NLR/Manure conditions, where the coefficients of determination (r^2) of the regression equation of NCP or R versus biomass were 0.792 and 0.623, respectively. All other coefficients of determination for all other conditions were low (less than 0.3), indicating a lack of

[1] Indeed, at the maximum volumetric flow rate tested, the surge frequency of the ATS wave surge bucket was near the maximum possible for the mechanics of the surge bucket mechanism.

correlation between the metabolic measures and the biomass measures. This correlation was even lower for NCP/R ratio versus B, which was generally less than 0.2 for most conditions and exhibited a maximum of 0.309 for the retest of Low Light/Low NLR/Manure. One might expect, however, that a strong correlation would exist between one or some of these measures based upon the interpretation that the integration of diurnal production over time should yield the standing biomass of the ecosystem (Odum 1969). There are multiple possible reasons for this apparent decoupling between biomass production and the metabolic measurements: (a) it represents, and is the result of, a real phenomenon inherent in ecological measurements made at different time scales; (b) it is the result of methodological errors in the implementation in the carbon titration; (c) it reflects an error in the underlying assumption that carbon exchange to and from the atmosphere is insignificant. These are discussed in greater detail.

Ecological explanation

It is possible that biomass accrual rate and the metabolic measurements are indeed inherently decoupled, as they are measurements of ecological processes that are occurring at fundamentally different time scales. For example, primary production is a diurnal measurement and reflects the rate of carbon uptake and fixation into the various molecules that compose and maintain the tissues of the algal turf community. It is the difference between the anabolic and catabolic processes occurring daily in response to the light incident upon the ecosystem. Biomass production is the sum of the growth processes over a length of time (multiple days to a week) that is up to an order of magnitude greater than that for the metabolic measurements (up to 24 hours). It is the sum of the net anabolic processes fixed in tissue (driven by the catabolic processes that release energy),

plus the net import of material minus the net export. In the ATS units, import might include the adsorption of inert organic material from the manure feed to the algal turf biomass, or the entrainment of secondary heterotrophic production material from the reservoir. Export might include the sloughing off of algal biomass that then remains in suspension in the reservoir and not counted in the regular biomass harvests. Because of these differences, it may be that the productivity and biomass production measurements should not be expected to correlate strongly. Evidence of this is supplied by the fact that the NCP measurements do not add up to the measured biomass if both are expressed in units of carbon fixed per unit time. For example, for the Low Light/Low NLR/Manure conditions (Figure 3. 8, page 97), at a turbulence level of 2.7 min^{-1}, mean biomass production rate was reported at 12.0 ± 0.9 g DW m^{-2} d^{-1}. Assuming that this biomass is 10% ash, and the remainder is 40% carbon by weight, yields an expected value for NCP of 4.3 g C m^{-2} d^{-1}. The measured NCP, however, is reported as 0.82 ± 0.9 g C m^{-2} d^{-1}, an approximate five-fold difference. This difference is more pronounced at High Light/High NLR/Manure conditions (Figure 3. 12, page 109), where the expected NCP calculated from the mean biomass production rate (29.0 ± 6.2 g DW m^{-2} d^{-1}) is 10.4 g C m^{-2} d^{-1}, yet the measured NCP is 0.90 ± 0.2 g C m^{-2} d^{-1}; an order of magnitude difference.

Methodological errors

It is possible that there were methodological errors in the measurement of metabolism or in biomass production rate. Error in measuring biomass production rate, however, is unlikely, as increasing fidelity in measurement of total biomass is assumed throughout all trial conditions as harvest methods and procedures were refined to account for all biomass components in various fractions of the harvest. It is more likely that errors

were made in measurements of net productivity and respiration; if so, the most likely source of error is in the pH-IC titration method. One source of error might be the fact that often, in the titration, it was difficult to replicate the upper extremes of the pH range seen in normal ATS operation; that is the highest pH level attained via sparging water samples with nitrogen gas was typically around 9.0, whereas, in operation of the ATS units, a pH level in excess of 9.5 was often observed. The attempt to compensate for this was to assume a linear model for the change in inorganic carbon concentration with a change in pH value. This assumption of linear ends on the titration curve could lead to underprediction of the change in CO_2 for an associated change in pH level near the margins of maximum pH observed in the experiments. It is also possible that other aquatic chemistry is not being accounted for in the titration but that occurs in the reservoir. For example, an excess of organic carbon in the manure feed may dampen the dynamics of the titration; this is a possibility, as the method was originally developed and applied in natural waters that typically were more oligotrophic (Park et al. 1958).

Error in underlying assumptions

The pH diurnal method for determining the metabolism of an aquatic ecosystem rests on the assumption that the exchange of carbon dioxide to or from the atmosphere is minimal and thus an insignificant contribution to the overall metabolic measurements. This is communicated in much of the literature summarizing this method (Park et al. 1958, Beyers et al. 1963), and is based on fact that atmospheric partial pressure of CO_2 is low (on the order of 350 ppm, three orders of magnitude lower than that for oxygen). In the operation of the ATS, this assumption may be valid only for lower turbulence levels, and increasing divergence from accuracy may occur at higher levels. The increased

mixing at higher turbulence levels could increase the transfer of CO_2 across the air-water interface. What effect might be expected from this increased rate of transfer? In the dark, when lights are off, CO_2 is produced and released into solution through community respiration. One would expect the concentration of CO_2 to build up and be lost to the atmosphere at increasingly greater rates with greater turbulence levels. Thus, at higher turbulence levels, less CO_2 remains in solution as carbonic acid, and the corresponding drop in the pH value is not as great as in the lower turbulence regime. Thus the measured change in pH may not reflect the full quantity of respiration occurring. During the day in the light, the CO_2 in solution is taken up rapidly by the autotrophic community, especially in high light conditions. In low turbulence conditions, carbon availability for algal photosynthesis is limited by diffusion across the air-water interface. One complexity of the low turbulence regime is the relative decoupling between the reservoir (where the pH measurements are taken) and the ATS bed. Any CO_2 produced by respiration in the reservoir and remaining in solution, once delivered to the algal turf bed by the periodic pulse of the wave surge bucket, is available to the algal turf and is immediately taken up. At the higher turbulence levels, any CO_2 molecule produced in respiration in the reservoir is more likely to offgas as to be taken up by an algal cell. This could possibly limit the growth of the algae (which might be reflected in biomass as well, not necessarily observed in the high NLR loading conditions). Another possibility is that the high turbulence at the air-water interface causes the entrainment of more atmospheric CO_2 than would otherwise happen at lower turbulence levels. This could help to overcome the natural carbon limitation inherent in the system at high light conditions (thus showing increased biomass production levels) but is not necessarily seen as an increase in pH

value. The ready supply of CO_2 from the atmosphere dampens the pH increase that might otherwise be seen.

Thus it is possible that, for increasing turbulence levels, a correction to the pH diurnal method, similar to the method employed for oxygen measurements (Odum 1956), should be employed, accounting for increased transfer of CO_2 across the air-water interface. Although this is typically not necessary for most environmental waters, there is likely an increasing necessity for it under conditions of increasing surface turbulence.

The measurements of gas diffusion rates across the air-water interface bear out this conclusion. The first-order gas diffusion rates measured for oxygen are strongly influenced by the turbulence of the flow regime, as evidenced by the log-log increase in value with increased wave surge frequency (Figure 3. 15, page 120). The values observed for oxygen transfer across the air-water interface are typical and on the same order as those reported in the literature. For example, Odum (1956) reports values ranging from 0.03 to 34 g O_2 m^{-2} hr^{-1} for water types ranging from still water to water drops, respectively (Table 3. 20, below), whereas values found in this research range from 0.67 to 23.8 g O_2 m^{-2} d^{-1} for lowest to highest wave surge frequencies, respectively. It is notable that the gas transfer rate for oxygen measured for the most turbulent flow condition in the ATS is significantly greater than that reported by Odum (1956) for small rivers (with a value ranging from 0.6 to 4.3 g O_2 m^{-2} d^{-1}; see Table 3. 20), an indication as to the magnitude of the turbulence possible in the ATS system in excess of that normally found in natural waters.

Table 3. 20. First-order gas diffusion constants for oxygen as reported by Odum (1956).

Water type	K (g O_2 m^{-2} hr^{-1})
Still water	0.03 – 0.08
Stirred water	0.09 – 0.74
Stream and ponds	0.08
Tank with a wave machine	0.31
Ocean surface	1.1-5.2
Small rivers	0.6-4.3
Air bubbles	2.8-28
Water drops	22-34

The first-order gas diffusion constants for the transport of carbon dioxide into the water column from the atmosphere follow a similar trend as the constants for oxygen, increasing in a log-log relationship with increasing wave surge frequency (Figure 3. 16, page 121). The magnitude of the diffusion constants for carbon dioxide is on average an order of magnitude lower than for oxygen. One would expect these to be similar, considering the similar diffusivities of the two molecules. Differences may be attributed to measurement error, possibly stemming from the pH-IC conversion. The significant dissimilarity between the carbon dioxide diffusion constants for different water chemistries at the highest wave surge frequency is possibly caused by the different base alkalinity of the water. It was expected, however, that the greatest rate of CO_2 transfer would be observed for distilled water, given that there would be no chemical buffering. The fact that this was not observed suggests possible measurement noise resulting from the pH-IC titration method; further development and refinement of this method is recommended. The first-order gas diffusion constants for the transport of carbon dioxide out of the water column to the atmosphere (Table 3. 18 and Figure 3. 18, page 122) follow an expected trend as being strongly correlated to the wave surge frequency. The magnitudes of the values of the constants for diffusion of carbon dioxide out of the

system are on the same order of magnitude as those for diffusion of carbon dioxide into the water column. The diffusion constants were lower for Bristol's than for distilled water, but remain on the same order of magnitude as those seen in the subsidy stress experiments.

The rate of pH changes as a result of carbon dioxide diffusing into or out of the water column were on the order of or greater than the magnitude of those rates observed in the subsidy-stress experiments. For example, for CO_2 diffusion into the water column, rates for decrease in the pH level were observed to range from 0.2 pH units hr^{-1} to 12.0 pH units hr^{-1} for the lowest and highest wave surge frequencies, respectively (Table 3. 17 and Figure 3. 17, pages 118 and 122), whereas rates of pH change observed in the subsidy-stress experiments were typically on the order of -0.1 pH units hr^{-1}. A similar range was observed for pH increase due to carbon dioxide diffusion out of the water (Table 3. 19 and Figure 3. 19, pages 120 and 123). This suggests the possibility that gas transfer to or from the atmosphere could affect the pH measurements in a way that is not accounted for in the metabolic measurements. The difference between water types is as expected, where the process water exhibited a smaller overall rate of pH change as a result of a greater chemical buffering.

The rate of change in pH, and thus in the concentration of carbon dioxide, was on the order of magnitude of that seen in the metabolic measurements, which raises the possibility that the accuracy of these measurements was affected by this gas exchange with the atmosphere. The differences observed between the various water chemistry types may be an artifact of the pH-IC titration method, as suggested by the inconsistency observed between the relative rates of change of pH and CO_2. An alternate way to find

the diffusion transfer rates would be to calculate those for carbon dioxide using the diffusion coefficients or molecular piston velocity for oxygen, arguably more reliably measured in this set of experiments, following an assumption that the gas transfer of inorganic gases across the air-water interface is a function primarily of the flow regime rather than of the property of the gases themselves (Stumm and Morgan 1995).

Should the atmospheric diffusion of carbon dioxide into or out of the water column be affecting the pH measurements in the subsidy-stress experiments, what does this mean for the metabolic measures determined in these experiments? During night-time measurements of respiration, carbon dioxide is produced by biological respiratory processes and is dissolved in the aqueous environment, increasing the overall inorganic carbon concentration and thus decreasing the pH value. Some of this inorganic carbon dissolved as carbon dioxide may be lost to the atmosphere, especially as aquatic concentrations increase after a few hours of darkness. This loss is shown to be greater at higher turbulence levels because of the increased gas transfer rates across the air-water interface. Thus, one might deduce that there is not as much dissolved inorganic carbon remaining in solution as was produced by biological processes, some having been lost to the atmosphere. The magnitude of the fall of pH level is therefore not as great as if all CO_2 remained in solution, and pH measurements would increasingly underpredict nighttime respiration for increasing levels of turbulence.

A similar analysis for daytime net primary production yields similar results. Assuming that daytime net primary production is positive, that is, gross primary production exceeds daytime respiration; carbon dioxide is being taken up by photosynthetic biomass and thus removed from the water column. As the concentration

of aquatic inorganic carbon decreases, the pH increases. At the higher levels of pH, the water is in extreme saturation deficit for inorganic carbon, and some carbon dioxide may be gained from the atmosphere at an order of magnitude that might be reflected in pH measurements. This gain of carbon dioxide from the atmosphere is greater at higher turbulence levels because of the increase in the diffusion across the air-water interface. Thus, more carbon dioxide is in solution than is taken up by the photosynthetic biomass, and the pH is measured to be more acidic than might be expected. The magnitude rise in pH during the light period, then, is not as great as possible, and the pH measurements may increasingly underpredict daytime net primary production at increasing levels of turbulence.

Therefore, the magnitude of the gas transfer across the air-water interface in an ATS leaves open the possibility that the loss or accrual of carbon dioxide to or from the atmosphere, respectively, is a factor that should be accounted for in the measurements of primary productivity and respiration using the pH diurnal method. The lack of this accounting is a possible explanation for the difference between the metabolic measurements and the biomass accrual measurements for conditions of highest light and nitrogen loading rate (Figure 3. 12, page 109), where the metabolic measurements exhibited a subsidy-stress relationship not reflected in the biomass measurements. Odum (1956) presents a method developed for oxygen measurements of aquatic ecosystem metabolism that amends the measured aquatic concentrations with values of air-water interface gas diffusion derived from the saturation deficit for that gas for the given atmospheric pressure and temperature. Extension of this method for use on carbon dioxide measurements here is a possible direction of future analysis.

The subsidy of hydraulic residence time

A dynamic not accounted for in conceptual models of this set of experiments is the effect on algal turf metabolism and growth of different hydraulic residence times of the ATS bed under different flow rates. The volume of the ATS bed was estimated to be approximately 25 liters, and different volumetric flow rates yield different hydraulic residence times in the ATS bed based upon the rate of displacement of water volume (Table 3. 21). It is apparent that the hydraulic residence time spans over two orders of magnitude. An increased hydraulic residence time allows the ATS process to act more as a batch reactor, as nutrient-laden water is introduced to the ATS bed periodically (displacing an equivalent volume of nutrient-poor water from the ATS bed) and allowed to remain quiescently in contact with the algal cells for a longer period of time. This could allow the partial overcoming of the limitations of material diffusion across the diffusive boundary layer surrounding the algal turf or cell. It is unclear whether or not this increased contact time can act as a subsidy partially offsetting the lower turbulence levels. Also, at low flow rates, the ATS bed and reservoir become partially decoupled, compared to the higher flow rate conditions, with the ATS bed acting as the photosynthetic component and the reservoir acting as the respiratory unit. Transport modeling of this process can help to elucidate the effect of this artifact on the overall uptake dynamics and the consequent effects on metabolic measures and on biomass production.

Table 3. 21. Hydraulic residence time for the ATS bed for different flow rates and dump bucket tip frequencies.

Nominal Flow Rate (lpm)	Dump Bucket Tip Frequency (min^{-1})	ATS Bed Hydraulic Residence Time (min)
1	0.04	28
5	0.3	7
25	2.7	1
125	11.5	0.2

Competition between algal genera in the ATS bed

The relative abundance of the various algal genera under different operating conditions in the ATS showed some interesting trends which expand the perspective on some of the results obtained in the metabolic and biomass subsidy-stress analyses. While the ATS units were expected to be dominated by *Rhizoclonium* species based upon prior experience and research with these particular units, it was observed that this was not always the case. Rather, the shifting dominance between different algal genera, based on the relative abundance numbers, was observed as a function of various combinations of operational parameters.

It might be expected that the relative abundance for each algal genus would be independent of the ATS unit. Indeed, it was assumed that the ATS units were operational replicates of each other in terms of physical configuration and light regime. Upon analysis of the relative abundance of algal genera versus scrubber unit (Figure 3. 21 and Figure 3. 22, pages 125 and 126), the data show otherwise when considering the species-level organization. For example, compared to all other units, ATS unit 4 had a high abundance of *Microspora*, while ATS unit 7 had a high abundance of *Rhizoclonium*. These inconsistencies may be explained by the fact that different ATS units were operated under different conditions at different times, and recognition of these conditions

can help elucidate some of the ecological characteristics of the various algal genera. For example, most of the ATS units generally exhibited a balance between the abundance of *Rhizoclonium* and *Microspora*. ATS unit 4, however, showed an increased dominance of *Microspora*, and "Other" algal species had a higher relative abundance in ATS unit 4 than in all other ATS units. This may be related to the predominant flow rates of ATS4, which was operated under conditions of extremely low flow (generally 4 lpm or less) for most of the time of the experiments. ATS unit 5 was operated for most of the time of the experiment at a higher flow rate than average; it was observed that *Oscillatoria* had a higher than average abundance as well. ATS unit 7 had a light source that was different than the other units (a single 1000W bulb compared to two 400-W bulbs). Although the height of the light source was adjusted such that the light intensity at the ATS growth bed matched that of the others (Table 3. 2, page 77), it is possible that there was enough of a difference in intensity or spectrum to favor one type of algal species over another. Also, ATS unit 7 had the most homogeneous turbulence pattern (Chapter 2). Could this have contributed to an increased abundance of *Rhizoclonium* in this unit?

Trends observed in the results of abundance plotted versus each of the operating parameters as a predictor variable (Figure 3. 23, page 128) can yield some generalizations about the relative competitiveness of the algal species in the ATS system. The results showing the effects of flow turbulence on the competitive relationships of the algae species in the ATS units (Figure 3. 23C) support many of the generalizations suggested by the total means of relative abundance for each ATS unit discussed previously. For example, at low turbulence levels, *Microspora* was more dominant over *Rhizoclonium*. The dominance relationship changed as turbulence level increased, as *Rhizoclonium* was

most dominant in medium turbulence levels, and *Oscillatoria* was most dominant in the highest turbulence levels. This may be related to the morphology of each algal species in relation to the turbulence regime inasmuch as how the diffusive boundary layer around the algal filament or the entire turf is moderated. In low flow and low turbulence conditions (as seen most often in ATS unit 4, for example), the planktonic species labeled as "Other" can be more competitive than at higher flow conditions. The longer-period quiescent conditions between wave surge events allow the planktonic algae more access to the light in the ATS bed, as compared to higher flow-rate conditions when the individual cells are easily swept away from the bed. *Microspora* may be more competitive in low turbulence conditions because of its larger overall filament diameter, which allows more chloroplasts per cell compared to the smaller *Rhizoclonium* and thus allows *Microspora* overall to be more productive at a given light level. At medium flow and turbulence levels, the branched design of *Rhizoclonium* may give it a competitive edge over *Microspora*, as various branches protrude at all angles in relation to the dominant flow field, thus intercepting more turbulent energy and reducing the overall diffusive boundary layer. Additionally, the smooth, cylindrical form of *Microspora* may result in its filaments aligning in parallel with the flow, encouraging clumping of the filaments (Figure 3. 24) and reducing the overall exposure of *Microspora* cells to turbulent energy.

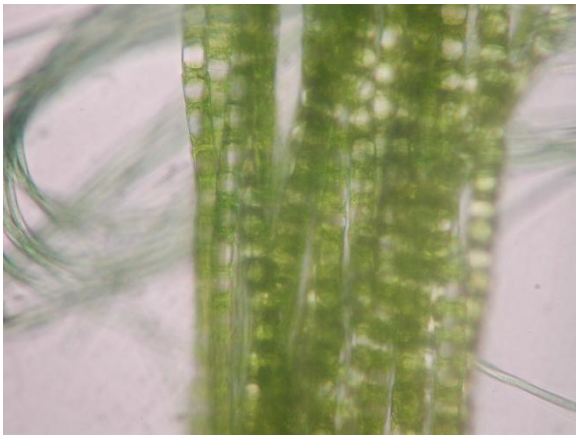

Figure 3. 24. Clumping of *Microspora* filaments observed in a sample taken from ATS unit 5 on Dec. 16, 2007. The ATS unit was operating under medium flow rate (60 lpm) conditions. Micrograph taken at 40x magnification.

In highly turbulent conditions (Figure 3. 23C), *Oscillatoria* seemed to dominate, possibly because the turf formed by *Oscillatoria* is lower and more mucilaginous than the other green algal species. In high turbulence conditions, greater breakage of the filaments of the green forms is possible; observational evidence supports this, where *Rhizoclonium* samples identified from high turbulence operating conditions were observed to have a shorter, more bifurcated branching pattern than those samples from lower turbulence operating conditions (see Figure 3. 20B, page 124), indicating the possibility of more breakage and regrowth. These relative abundance numbers may relate to the metabolic measurements or the biomass production measurements as well; for example, a lower biomass production rate was generally measured when *Oscillatoria* was dominant.

A similar pattern is observed again when investigating the relative abundance of the various algal species in relation to changes in the other operational parameters. The proportion of relative abundance among the various algal types (Figure 3. 23, page 128) seemed to fluctuate in relation to nutrient feed type (Figure 3. 23A) and nitrogen loading rate (Figure 3. 23B). For example, *Rhizoclonium* was especially dominant over

Microspora and *Oscillatoria* in conditions when Bristol's medium was used (Figure 3. 23A). In Bristol's medium, nitrogen is in its oxidized form of nitrate, as opposed to its reduced ammonia form for the other feed types; *Rhizoclonium* may be more adapted to the use of nitrate as its nitrogen source as compared to the other algal genera. In relation to nitrogen loading rate (Figure 3. 23B), *Rhizoclonium* was the only algal type for which the relationship was significant, showing a greater competitiveness at lower loading rate and becoming less so at higher loading rates. This implies higher nitrogen uptake efficiency at a lower NLR compared to the other algal genera. This may also be related to the branching morphology of *Rhizoclonium* and its smaller cell diameter than *Microspora*; these two morphological characteristics of *Rhizoclonium* may result in a greater cell surface area, and thus more sites for nitrogen uptake per unit volume of algal cell. The possibility exists that there is some cross-correlation of many of these variables, for example, NLR and feed type, as the NLR for Bristol's medium was always lower than the other feed types (possibly because of the lower uptake efficiency of the algae to use the nitrate in Bristol's). Additional analyses such as multivariate analysis are necessary to determine the strength of these cross-correlation relationships.

In all, the relative abundance of competing species of algae in the ATS display shifting patterns of dominance over the range of the independent variable of interest. This pattern is strongest for turbulence but is evident for nitrogen loading rate and even feed type. The shift in competitiveness of a species over the range of a changing variable is a classic pattern of competitive species interaction, where different species have the peak of their success at different levels of a resource over a range of that resource (Krebs 1994). In ecosystems in general, this pattern of development is seen in time in patterns of

temporal succession (Odum and Barrett 2005), or, in a stream, in a pattern of longitudinal succession (Kangas 2004) in which a species or assemblage of species is adapted and thus most competitive at a location defined by a certain distance downstream of a disturbance, pollution, or energy source. Indeed, one can imagine an algal turf scrubber raceway long enough, such as those employed in the field for nutrient recovery in waterways (Hydromentia 2005), where the energetic and nutrient regimes differ significantly downstream as compared to the upstream because of dissipation of turbulent energy and nutrient uptake. This would result in a successional pattern of species along the length of the raceway, with each species the most competitive in that location where conditions are most favorable for it[2]. The analysis presented here is merely preliminary, however, and further analysis is warranted to determine the relationship of the abundance of these algal species to the independent variables of the operating conditions and to identify cross-correlation among these parameters. This analysis has helped to indicate those operational parameters for which a strong correlation with relative abundance is expected—for example, the wave surge frequency—versus those for which little or no correlation is expected—for example, nitrate concentration of the process water. Additionally, this analysis has given an indication as to which of those relationships might be linear—for example, relative abundance versus nitrogen loading rate—and which of those might be non-linear—for example, relative abundance versus wave surge frequency. Finally, this analysis provides some context for the consideration of the role of species-level interactions at the interface of the technological components in the ATS technoecosystem, a subject to be addressed in Chapter 5.

[2] This is a good argument for ecologically-engineering such systems through initial seeding and repeated additions of as many species of algae as possible to provide the genetic diversity that allows the system to self-organize along its length to the energy signature characteristic for each location along its length.

Conclusions

The following conclusions can be made for this set of experiments:

- Turbulence of the flow is a limiting factor to the biomass production rate of algae in an ATS, and this effect becomes more pronounced as light and nutrient loading rate are greater.
- Measurements of net carbon production (NCP) and respiration (R) are also shown to follow a subsidy stress relationship in relation to flow turbulence, although the effect is more pronounced at lower light and nutrient loading conditions.
- The metabolic measurements become more decoupled from the biomass production rate measurements as light and nutrient loading rates are increased.
- The accuracy of the metabolic measurements can be refined to account for gas transfer across the air-water interface, an improvement to the analysis that could bring values of NCP and R more in line with those expected from the measured biomass production rates.
- The ratio of NCP to R showed no response to increasing level of turbulence in an ATS, exhibiting significant decoupling from the biomass production rate with lower values than expected.
- The relative abundance of the dominant genera of algae where shown to be a function of the level of turbulence, with each of the main genera most dominant within a characteristic zone of flow rate.

Implications

The effects of turbulence as a limiting factor on the metabolism and biomass production of the algae in an algal turf scrubber have been shown for conditions of high

light and nutrient availability. The information in these data contribute to the further development of the components necessary for engineering a technoecosystem based on ATS technology. The subsidy-stresss relationship to turbulence observed in the metabolic measurements help to inform parameters for design of a feedback control algorithm that can automatically control the level of turbulence to seek a range for maximum productivity. The development of this system is presented in subsequent chapters.

Chapter 4: The Technosystem—Examining the Control Algorithm

Introduction

In the design of techno-ecological hybrids, understanding the characteristics of the technological components is as important as understanding those of the ecological components. While the systems perspective of the whole technoecosystem is most desirable for understanding its behavior, the reductionist perspective is useful for understanding the expected behavior of the components in isolation from other parts of the system. That reductionist perspective is employed here to investigate the action of the control algorithm, the set of instructions that directly control the technological components in response to variation in the ecological components. The control algorithm is presented as a simple seeking algorithm designed to find the maximum of a dependent variable over the range of an independent variable subject to feedback control. The algorithm was tested virtually in response to hypothetical data sets that form idealized characteristic distributions of ecosystem productivity versus flow turbulence. These productivity-turbulence distributions are modeled as stochastic entities with different levels of variance. Virtual testing allows a brute-force approach of running the algorithm through a large number of multi-cycle trials. The convergence behavior of the algorithm—that is, accuracy and rate of algorithm convergence on the expected solution—in response to the various productivity-turbulence input distributions at three different levels of variance was analyzed. The results present implications for the rate of algorithm convergence that can help characterize the system response during implementation of the physical technoecosystem configuration.

Objectives

The objectives of this series of experiments were as follows

1. The first objective was to develop a feedback control algorithm to find the maximum of a dependent variable in an algal turf scrubber (ATS) ecosystem, such as productivity, in response to the changes in an independent variable over a range of values.
2. The second objective was to explore the dynamics and behavior of the control algorithm designed for the autonomous control experiments through virtual testing employing pre-determined data sets representing the relationship of ecosystem productivity to turbulence level in an ATS.

Research Approach

The approach for this series of experiments is to explore the activity of the control algorithm virtually and in isolation from the physical ecosystem for which it was designed. Virtual testing consists of employing a pre-determined data set in place of input monitoring data, upon which the algorithm is designed to make control decisions. The virtual data, representing idealized relationships between Pump State (a proxy for turbulence intensity) and resulting net primary productivity, is constructed in various profiles (such as step up, step down, ramp up, and ramp down) intended to test the algorithm activity at its extremes.

Methods

Control Algorithm Design

A control program was developed for the autonomous control experiments using the LabView 7 graphical programming platform (National Instruments Corp., Austin, Texas). The modular construction of the control program allows modification of the core algorithm according to data acquisition and control needs. The core algorithm used for all autonomous control experiments was designed as a basic seeking algorithm, intended to seek out the maximum or minimum of a measured parameter within an expected range via incremental change of the controlled parameter. In the case of the experiments pursued in this research, the algorithm is designed to seek out the volumetric flow rate at which net primary productivity, as measured by the pH diurnal method for ecosystem metabolism (Chapter 3), is maximized within a possible range of flow rates, assuming that productivity follows a subsidy-stress curve in relation to flow turbulence (as set by volumetric flow rate) in an ATS. Because of the design of the physical ATS systems for autonomous testing (Chapter 5), flow rate can be incremented or decremented only at discrete intervals of 5gpm over the entire range that is available (0 to 35 gpm), and each Pump State is designated a characteristic flow rate (Table 4. 1). A simplified flow chart schematic of the core algorithm is shown (Figure 4. 1), and a more detailed flow chart of the entire data acquisition and control program is provided in Appendix A.

Table 4. 1. Pump State designations and representative flow rate intended at each Pump State, based on the design of the physical system for testing autonomous behavior in an ATS.

Pump State	Intended Flow Rate (gpm)
0	0*
1	20
2	40
3	60
4	80
5	100
6	120
7	140

*In practice in the physical systems, a small flow rate (approximately 100 ml min^{-1}) is maintained via a peristaltic pump.

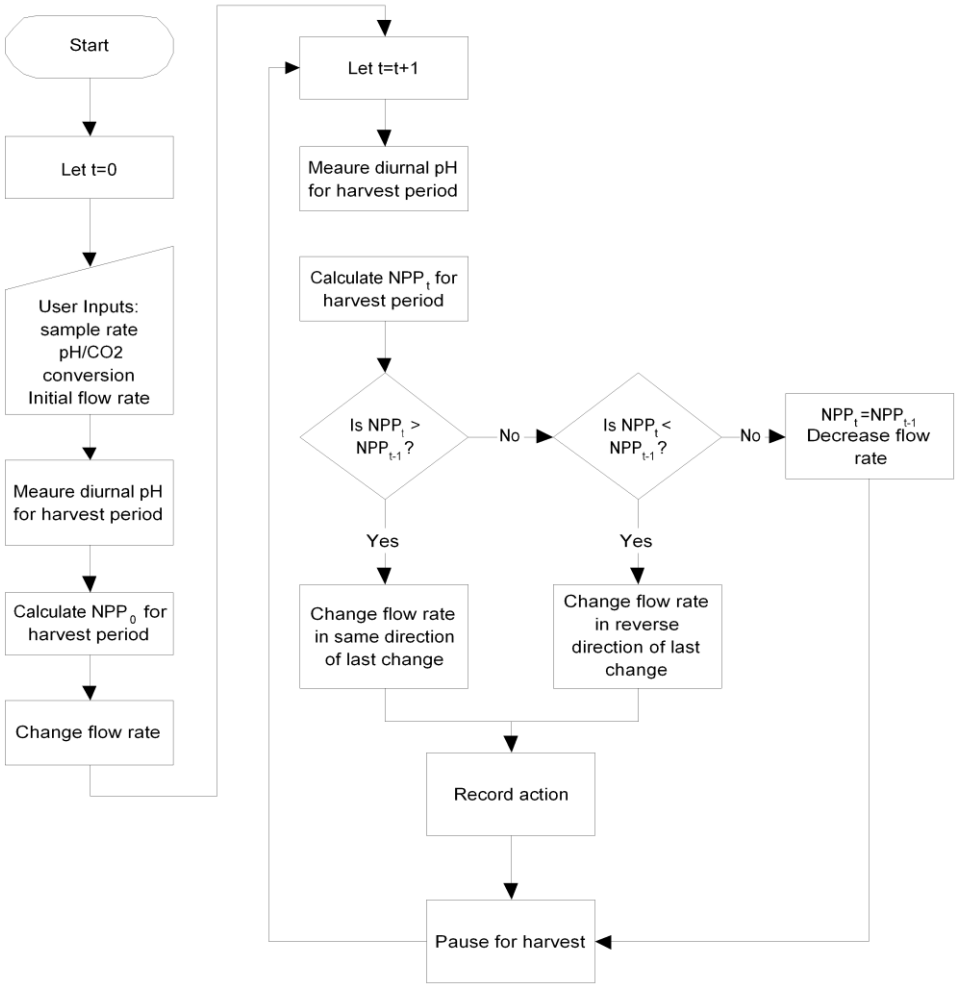

Figure 4. 1. Simplified flow chart showing the logic that underlies the basis of the control algorithm for optimizing flow for maximum net primary productivity (NPP) over time (t).

A description of the core control algorithm, as diagrammed in the simple flow chart (Figure 4. 1) follows. At the start, the user initializes parameters for the control program operation, such as the pH-IC conversion information (determined empirically from pH-CO_2 titrations in the laboratory, as described in Chapter 3), sample rates, and the initial Pump State (defining the initial flow rate). The pH is measured at a specified sample rate (typically every 15 minutes) throughout the entire harvest period (typically 96 hours); at each sampling event the pH is immediately converted to inorganic carbon (IC) concentration (using the pH-IC conversion) and stored in the computer memory. Each time the IC concentration at a sampling event is seen to decrease compared to the previous sampling event, the decrease is assumed to be the result of net primary productivity; hence the cumulative net primary production (NPP) for one harvest period is the summation of the amounts of all negative changes in IC concentration throughout the duration of the harvest period. Thus, in the algorithm, the net primary productivity (NPP_i) at any time t_i is

$$NPP_i = NPP_{i-1} + \Delta IC_i \quad , \quad (\Delta IC_i < 0)$$

where

$$\Delta IC_i = IC_i - IC_{i-1}$$

for each measurement of IC. Also, for each harvest period,

$$NPP_{total} = \sum_{i=1}^{n} NPP_i$$

At the end of the harvest period, and following harvesting, the control program changes the flow rate for the new harvest period by incrementing or decrementing the Pump State. The cumulative NPP is again and similarly monitored and calculated again for the new harvest period. At the end of this harvest period, the newly calculated NPP is compared to that of the previous harvest period. If the NPP has increased, the Pump State, and thus the flow rate, is changed again in the same direction as the last change was made; for example, if the Pump State was increased last time, it is increased again this time by one step change, increasing the flow rate accordingly. If the NPP has decreased, the Pump State is changed in the *opposite* direction as the previous change. If the NPP is in effect equivalent to the previous NPP (within a tolerance set by the user), the Pump State is decreased as a default setting. This allows the system to trend towards the energetic minimum (that is, the lowest Pump State) for the maximum productivity, presumably trending the system towards the highest engineering efficiency (that is, maximum productivity for the least amount of pumping energy). Also, if the current Pump State is at one of the extremes of its range (state 0 or state 7), the subsequent change in Pump State is always in the direction towards the center of the Pump State range, thus forcing the algorithm to continue seeking rather than becoming "pegged" in an absorbing state at the extremes of its range. All pH and IC data, and actions taken (that is, pumps activated or deactivated based on the Pump State) are recorded to a data-logging file. At the end of the user-specified time period for data collection (roughly corresponding and slightly shorter than the harvest period), all data collection is paused until manual user intervention following physical harvest of the algal turf, after which the data collection cycle begins again.

Virtual Testing of the algorithm

Extensive virtual testing of the algorithm was performed using preprogrammed data sets of total change of inorganic carbon (IC) concentration, representing primary productivity, in place of those calculated from real-time pH measurements. The use of virtual data allowed rapid testing of the program algorithm over many different hypothetical conditions with extensive replication via multiple cycles and trials.

The preprogrammed data sets used for virtual testing were in the form of hypothetical profiles of primary productivity (P), expressed in units of ppm IC, as a function of Pump State (S) that represent the discrete, incremental set points of volumetric flow rate over the anticipated available range in the physical systems (0 to 140 lpm; see Table 4. 1). These P versus S profiles were constructed in hypothetical configurations to explore the distribution of behaviors of the algorithm. The six profiles tested (Figure 4. 2) may be described as follows:

- A subsidy-stress profile (Figure 4. 2-A), based upon empirically-derived results determined in the physical subsidy-stress experiments (Chapter 3), that exhibits a peak of productivity at a moderate flow rate and reduced productivity at the extremes (both low and high) of flow rate;
- A flat profile (Figure 4. 2-B) exhibiting no change in productivity over the entire range of flow rate;
- A step-down profile (Figure 4. 2-C) exhibiting higher productivity in lower flow rates and lower productivity in higher flow rates;
- A continuous ramp-down profile (Figure 4. 2-D) exhibiting a productivity that decreases linearly with increasing flow rate;

- A continuous ramp-up profile (Figure 4. 2-E) exhibiting a productivity that increases linearly with increasing flow rate;
- A bifurcated profile (Figure 4. 2-F) exhibiting a minimum productivity at moderate flow rates and maximum productivity at the high and low extremes of flow rate.

Except for the subsidy-stress profile (Figure 4. 2-A), which was empirically determined from physical subsidy-stress experiments in the laboratory (Chapter 3), each of these profiles is entirely hypothetical, contrived to represent a possible distribution of P over S and expected to result in a unique response of the control algorithm.

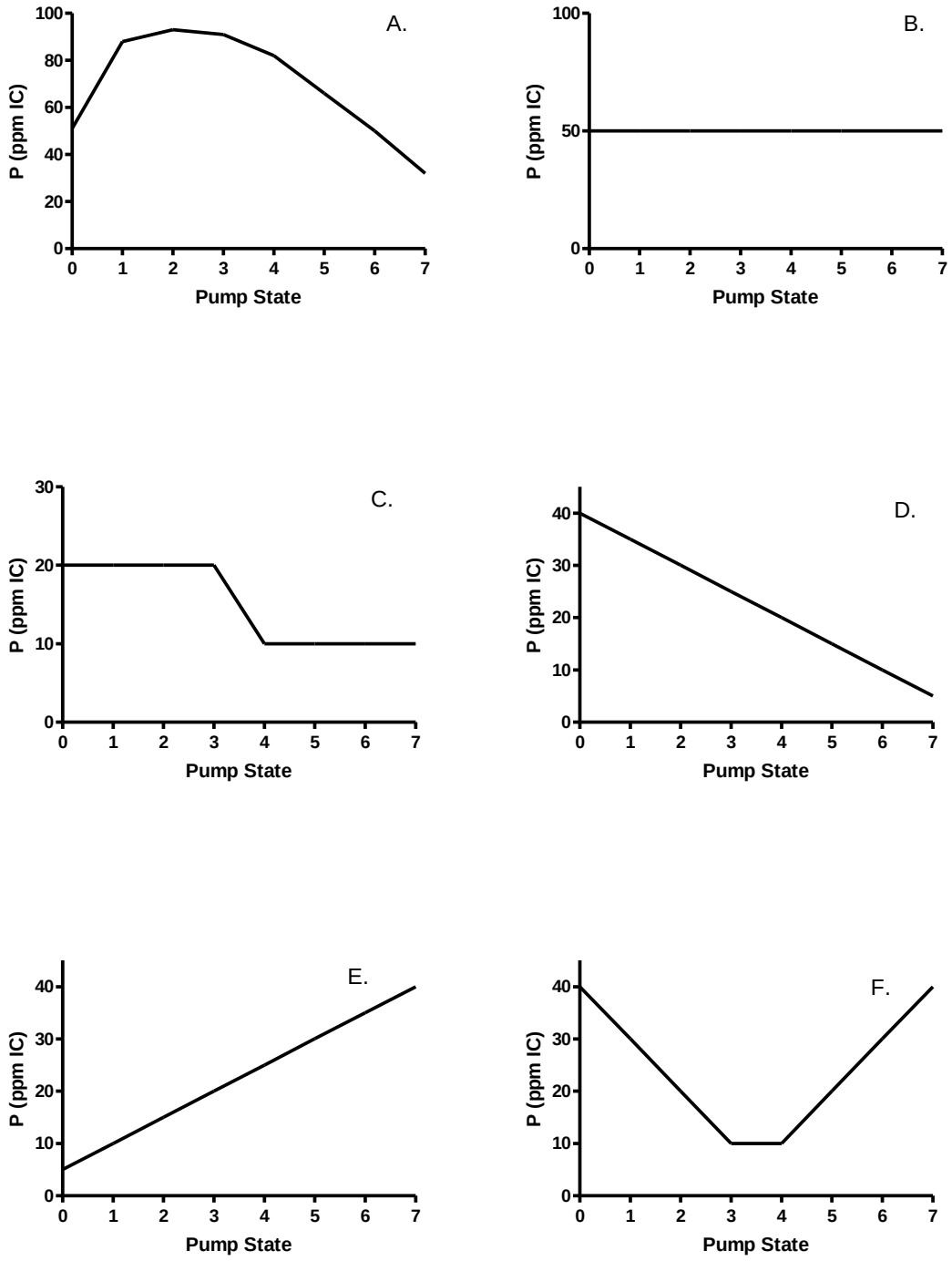

Figure 4. 2. Hypothetical profiles of productivity (P) versus Pump State (S) used as preprogrammed data sets to perform virtual testing of the optimization algorithm: (A) subsidy-stress distribution based upon prior experiments; (B) flat profile; (C) step change profile; (D) continuous ramp down profile; (E) continuous ramp up profile; (F) bifurcated maximum profile.

In addition, to simulate the variance that might be seen in physical experimentation, these hypothetical P-S profiles were applied as stochastic entities with values for P at each Pump State setpoint normally distributed about a mean. For example, in Figure 4. 2-A, the value of P at Pump State 2 might be modeled as a value normally-distributed about a mean of 93 ppm IC with a standard deviation of ±25 ppm IC (Figure 4. 3). For the virtual testing experiments reported here, the standard deviation was set at three different levels of low, medium, and high stochasticity (Table 4. 2) for each P-S profile, relative to the base mean value of the productivity P at that point, to investigate the effects of different levels of variance in productivity measurements on algorithm behavior.

Table 4. 2. Variance conditions, described as a standard deviation, tested for each of the virtual productivity/pump-state (P-S) profiles presented in Figure 4. 2.

Profile	Description of Profile	Standard Dev. % of Max.*		
		Low	Med	High
A	Subsidy-stress	1.0	11	36
B	Flat	2.0	20	100
C	Step-change down	2.5	25	50
D	Continuous ramp down	1.0	13	50
E	Continuous ramp up	1.0	13	50
F	Bifurcated maximum	1.0	25	63

*The percentage value of the standard deviation tested compared to the maximum value of the P-S function.

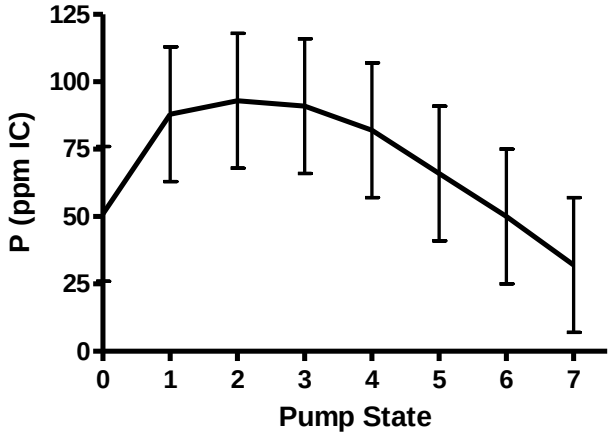

Figure 4. 3. Sample of input P-S profile A from Figure 4. 2 showing variance imposed on values for testing. Error bars represent a standard deviation of 25 ppm IC.

Testing was performed as follows: for each hypothetical P-S profile in Figure 4. 2, the profile was preprogrammed into the control program as if it were the real time primary productivity data as derived from pH measurements. The control program was allowed to make pump activation decisions based upon these preprogrammed data. For each of the profiles, the variance was set to either low, medium, or high values of standard deviation, as given in Table 4. 2. At each standard deviation for each profile, the algorithm was run 1000 times for 1000 Pump State decision cycles each run. At the start of each run, the initial Pump State (from 0 through 7) and Pump State increment (+1 or – 1) were selected randomly by a random number generator in Labview. For each run of 1000 cycles, the algorithm counted the number of times each Pump State was visited and recorded the relative frequency (number of times visited per 1000 cycles) for each. Data analysis consisted of calculating the mean and standard error of relative frequency for each Pump State for all 1000 runs and representing the data as frequency distribution plots for Pump State.

In addition, the algorithm was run 15 separate times (five for each initial Pump State of 0, 3, and 7) for each P-S profile at each input variance level, and the average cumulative mean and cumulative standard deviation was calculated for all. The relative rate of convergence of each of these was determined by calculating the percent difference between the cumulative mean or standard deviation at each cycle and the ultimate value at the limit of infinity. The cycle at which this percent difference reached less than 5% was recorded as a metric of the rate of convergence of algorithm on a solution (the ultimate cumulative average Pump State).

Results

Frequency distribution of the expected states

Virtual testing of the control program algorithm resulted in movement to multiple Pump States over time. The operation of the algorithm of the systems can be visualized by representing the changes in the Pump State on a trace of Pump State versus cycle (Figure 4. 4). The figure shows the Pump State for the first 100 cycles for hypothetical P-S profile A (see Figure 4. 2-A) for two separate runs: one with a low standard deviation (±1.0 ppm IC) and one with a high standard deviation (±32 ppm IC) on the input P-S profile data points. Results for the run with a low input standard deviation showed immediate convergence of the algorithm on Pump State 2, with continued cyclic seeking from Pump States 1 to 3. Results for the run with a high input standard deviation showed a trend towards convergence on Pump State 2 but with considerably more noise, often visiting Pump States that were higher (3-7) or lower (0) than in the case with a low input standard deviation.

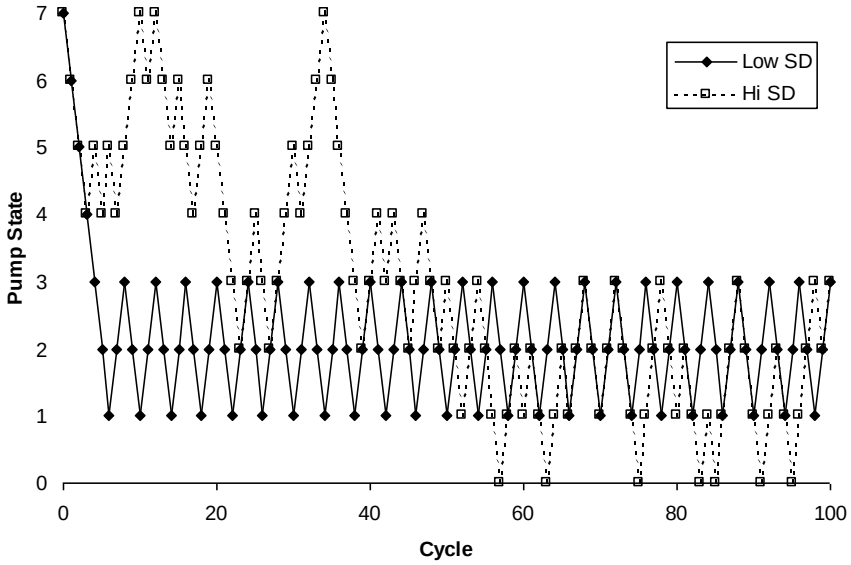

Figure 4. 4. Pump State vs. cycle for virtual testing of the control algorithm using a subsidy-stress P-S profile (Figure 4. 2-A) as input data with low and high standard deviations applied to the points on the input profile.

Results of the virtual testing experiments are summarized in the frequency distribution plots of Pump State for all six P-S input profiles each set at the three variance levels (Figure 4. 5). These distributions show the mean relative frequency of the occurrence of Pump State for 1000 runs of 1000 Pump State decision cycles each. Generally, these results show that the seeking algorithm had a strong tendency for finding the maximum of a P-S profile, although the tendency for convergence was not as definite for increasing input variance. Specific comments may be made about the results for each input distribution:

- For input P-S profile A (based upon empirical data and with a maximum at Pump State 2) with a low input standard deviation (SD), the algorithm spent a majority of its time either at State 2 (48%) or at adjacent States 1 (24%) and 3 (27%); these were reduced for higher values of input SD (for example, 33% and 25% for Pump State 2

at middle and high input SDs, respectively), and the algorithm visited all other possible Pump States more often;

- For input P-S profile B (a flat profile with no maximum) with a low input SD, the algorithm spent a majority of time at Pump State 0 (25%), 1 (39%), or 2 (19%) with lower frequencies for visiting higher Pump States; for higher values of input SD, however, the algorithm spent a near identical percent of the time (approximately 14%) at all Pump States except those at the ends of the range (0 and 7 at approximately 7%) with slightly greater percentages, on average, for the lower end of the range;
- For input P-S profile C (a step-change profile with Pump States 0-3 higher than Pump States 4-7) with a low input SD, the algorithm spent a majority of its time at State 0 (36%), 1 (46%), or 2 (14%), with lower frequencies (less than 5%) for higher Pump States; for higher values of input SD, the algorithm visited higher states more often, reducing the overall frequency for the lower states (for example, for Pump State 1, 32% and 27% at middle and high input SDs, respectively);
- For input P-S profile D (a linear ramp-down profile for higher Pump States) with a low input SD, the algorithm spent an overwhelming majority of time at Pump States 0 (49.5%) or 1 (49.5%); these were reduced (38% and 18% for state 0, and 48% and 30% for State 1 for middle and high input SDs, respectively) for higher values of input SD as the algorithm visited higher states more often;
- For input P-S profile E (a linear ramp-up profile for higher Pump States) with a low input SD, the algorithm spent an overwhelming majority of time at Pump States 6

(49.5%) or 7 (49.5%); these were reduced (35% and 15% for state 7, and 47% and 27% for state 6 for middle and high input SDs, respectively) for higher values of input SD as the algorithm visited the lower Pump States more often;

- For input P-S profile F (a bifurcated maximum profile, with maxima at Pump States 0 and 7 and minima at Pump States 3 and 4) with a low input SD, the algorithm spent a majority of time either at Pump States 0 and 1 (28% each), or slightly less at Pump States 6 and 7 (23%), with almost no visitation to the middle Pump States 2-5; these local maxima were reduced (for example, 21% and 14% for Pump State 0 for middle and high input SDs, respectively) as the algorithm visited the middle Pump States more often.

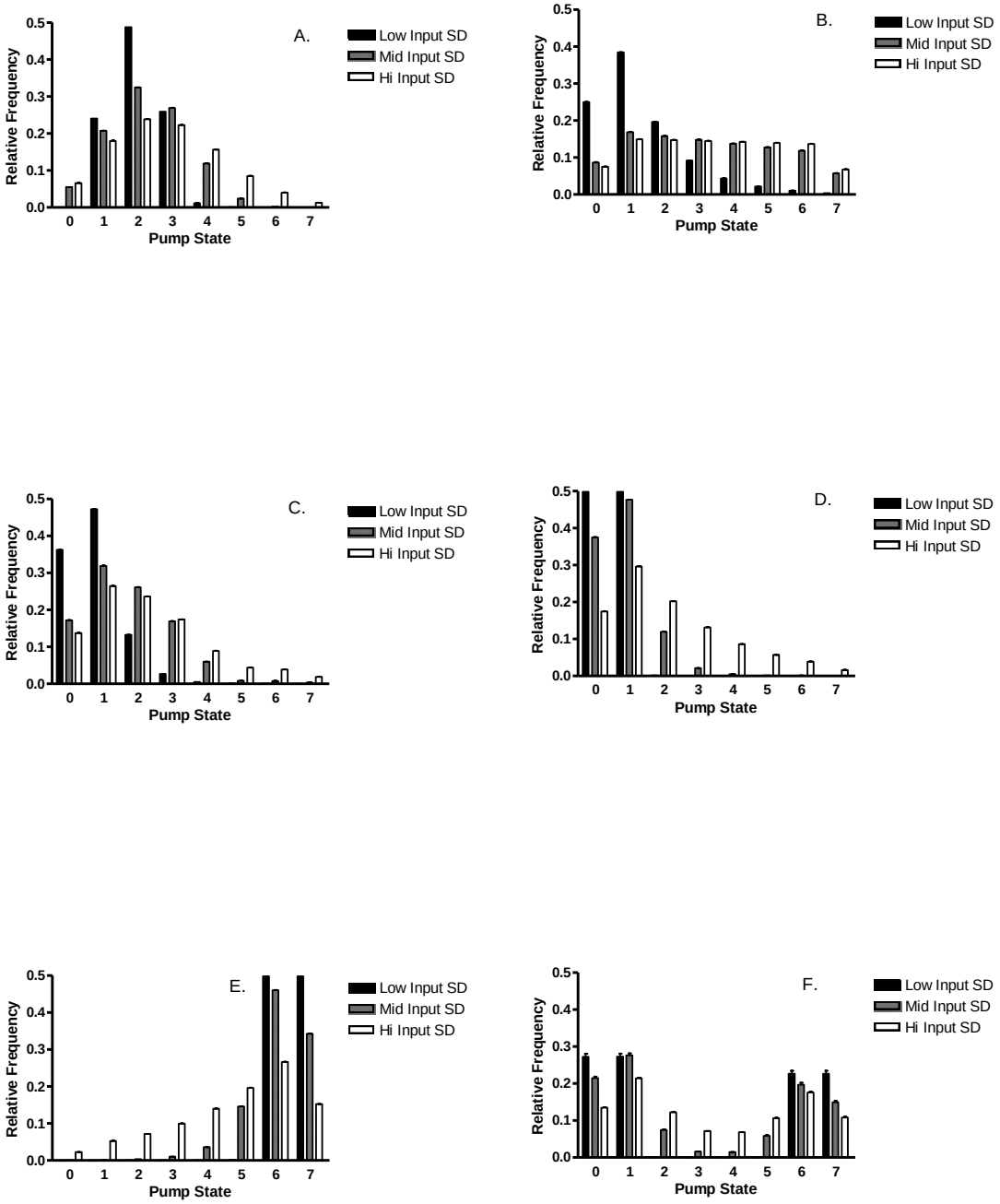

Figure 4. 5. Frequency distribution plots for results of virtual testing of the seeking control algorithm for various hypothetical preprogrammed productivity (P) vs. Pump State (S) profiles as input data. Individual distribution plots correspond to P versus S profiles as given in Figure 4. 2 as follows: (A) distribution profile based upon data collected in subsidy-stress experiments; (B) flat profile; (C) step change profile; (D) continuous ramp down profile; (E) continuous ramp up profile; (F) bifurcated maximum profile. Testing was performed at low, medium, and high standard deviation (SD) of the input profile. Frequency is expressed as a mean relative frequency of Pump State for 1000 runs of 1000 Pump State decision cycles each. Error bars represent standard error of the mean.

Rates of convergence on a solution

The cumulative mean of the Pump State over successive cycles was calculated for 15 runs of each of the input P-S profiles (Figure 4. 2) at the three levels of input variance (Table 4. 2). The general response of the cumulative mean for different levels of input variance for each of the input P-S profiles is exhibited in Figure 4. 6. In general, at low input variance levels, the cumulative mean converged quickly on the expected solution. As the input variance level increased, the cumulative mean converged on a Pump State closer to the middle of the range of Pump States (replicating the situation of complete random input with a flat P-S distribution) with a greater uncertainty, as indicated by the greater variance of the cumulative mean.

The cumulative mean of Pump State is summarized for all P-S input distribution profiles (Figure 4. 2) for the three input variance levels (Figure 4. 7). For low input variance levels, on all input profiles, the limit of the cumulative mean of the Pump State was nearly equivalent to the expected value. As the input variance level was increased, the cumulative mean of the Pump State at the limit moved towards the middle of the range of possible Pump States, more closely resembling a response to a completely flat input profile with high input variance.

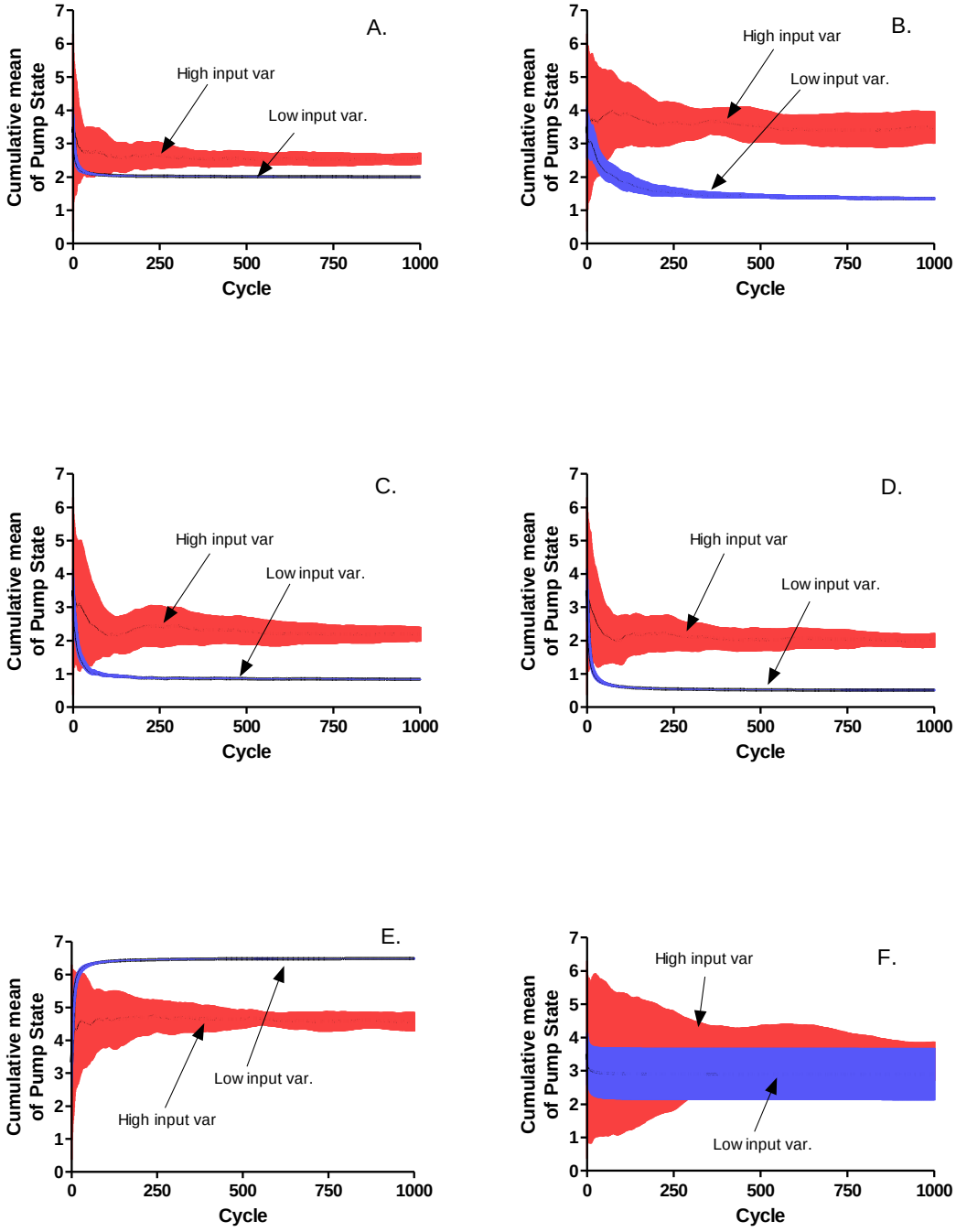

Figure 4. 6. Cumulative mean of Pump State for P-S input profiles (Figure 4. 2) for low and high levels of input variance.

Cumulative mean is calculated for 15 runs of 1000 cycles each, and error bars at each cycle are standard deviation. When the input variance is low, the cumulative mean converges quickly on the expected state. When input variance is higher, the cumulative mean converges quickly on a value closer towards the middle of the possible range of Pump States.

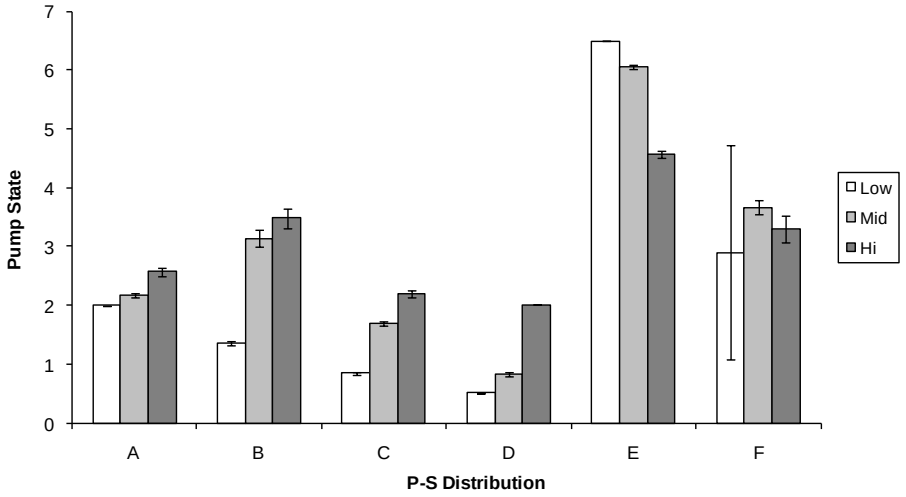

Figure 4. 7. Cumulative means of Pump State for the various P-S input distributions (Figure 4. 2), after 1000 cycles run 15 times with various starting Pump States. Error bars represent a standard error on the expected value of the mean resulting from variance by different initial Pump States at cycle 0.

The number of cycles to convergence (defined arbitrarily as within 5% of the total distance from the starting value of the cumulative mean to its value at the limit) for the cumulative mean of Pump State is summarized for all P-S input distribution profiles (Figure 4. 2) for the three input variance levels (Figure 4. 8). This metric can be considered as an indication of the rate of convergence of the algorithm on the expected state. For low input variance levels, most input profiles (all except profile B) exhibited rapid convergence (owing typically to a strong relationship, that is, comparatively steeper slope, between productivity (P) and Pump State (S)). As the input variance was increased, all input profiles showed a direct increase in the number of cycles to convergence. Those profiles that had no clear single maximum in the range of Pump States (Profile B, which was flat, and Profile F, which had dual peaks) exhibited the greatest number of cycles, and thus the slowest rates of convergence, at the higher levels of input variance.

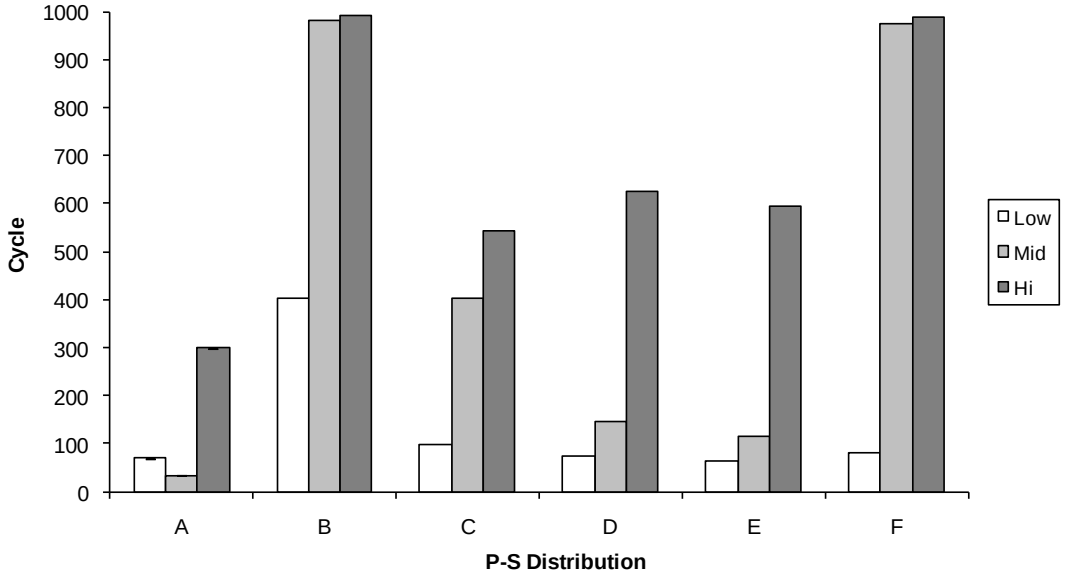

Figure 4. 8. Number of cycles to convergence (defined as within 5% of the expected value) for the cumulative mean of the Pump State for the various P-S input distributions (Figure 4. 2) after 1000 cycles run 15 times with various starting Pump States.

The cumulative standard error (the standard deviation of the Pump State, σ, divided by the square root of the cycle, n) of Pump State is summarized for all P-S input distribution profiles (Figure 4. 2) for low and high input variances (Figure 4. 9), showing that this standard error converges more rapidly for lower input variance. The overall cumulative standard error is summarized for all three input variance levels (Figure 4. 10). For low input variance levels, on all input profiles, the cumulative standard error of the Pump State at the limit was low for most cases. As the input variance level was increased, in all cases, the cumulative standard deviation of the Pump State at the limit increased.

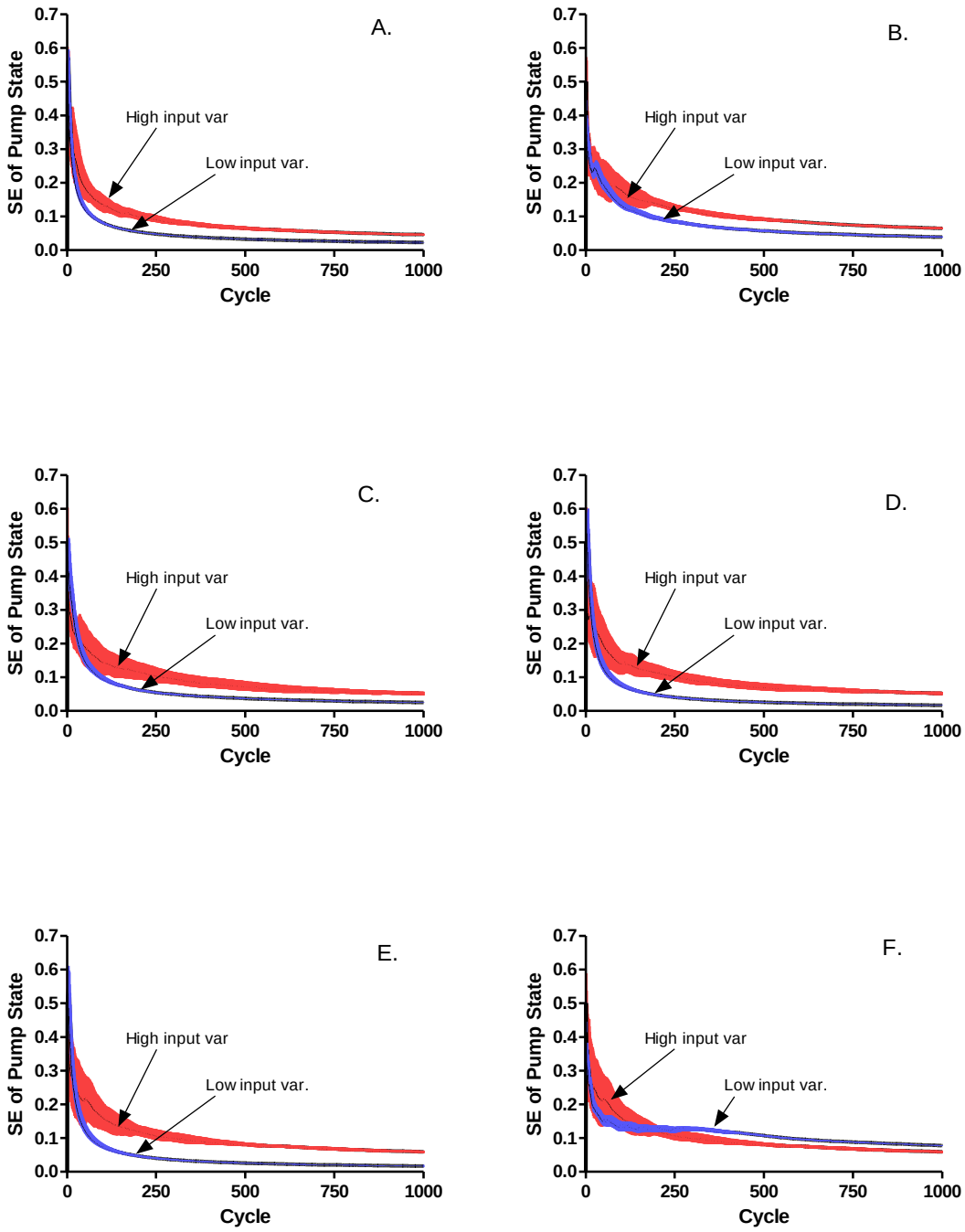

Figure 4. 9. Cumulative standard error of Pump State for P-S input profiles (Figure 4. 2) for low and high levels of input variance.

Cumulative standard error is calculated for 15 runs of 1000 cycles each, and error bars at each cycle are standard deviation. When the input variance is low, the cumulative standard error converges more quickly than when high.

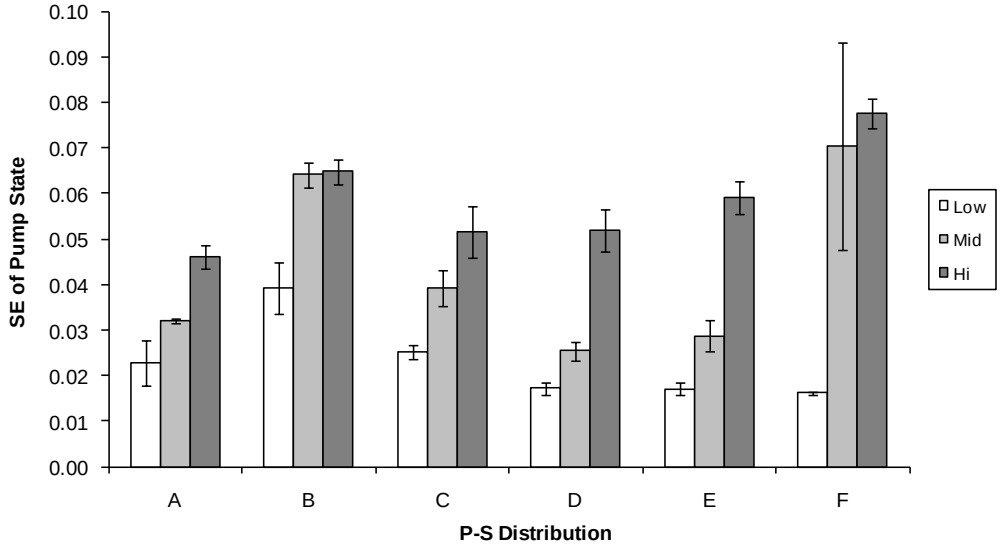

Figure 4. 10. Cumulative standard error of Pump State for the various P-S input distributions (Figure 4. 2) after 1000 cycles run 15 times with various starting Pump States. Error bars represent a standard deviation on the expected value of the standard error resulting from variance caused by different initial Pump States at cycle 0.

Discussion

Convergence of the algorithm and the expected state

Virtual testing of the control program algorithm generally exhibited convergence on the maximum productivity of a P-S distribution, although this outcome was dampened by a higher variance on the input functions. An example of the additional noise in the output of the system as a result of increased input variance is shown in the comparison of traces of Pump State versus cycle (Figure 4. 4, page 165), where immediate convergence on Pump State 2 (the expected outcome, given the input P-S profile A) was seen at low input variance, but a slower convergence to Pump State 2 with more irregular noise was seen at high input variance. Even at high input variance, however, the algorithm exhibited the ability to find the maximum of productivity over the range of Pump State over time

and on average, clearly exhibited by the probability distribution functions of Pump State (Figure 4. 5, page 168). For example, for input function A (Figure 4. 5-A), the algorithm most frequently visited Pump State 2 for the entire range of input variance. For low input variance, in which the algorithm regularly alternated only between states 1, 2, and 3 (an expected consequence due to the convention in the algorithm in which it is always seeking), the frequency distribution showed overwhelming favor to these states. At higher input variances, however, the frequency of Pump State 2 was lessened as visitation to other Pump States became more frequent, although even at the highest input variance, Pump State 2 was still favored. Convergence of the algorithm behavior on the peak productivity of the input P-S curve was also demonstrated by the ramp input functions D and E (Figure 4. 5-D and E), exhibiting a strong convergence on the peak states at low input variance and a dampening of this effect at higher input variances. This behavior was opposed to what might be expected for completely random behavior, for which one would expect, in the long term, a flat probability distribution function, in which Pump States 1 to 6 were visited equally and Pump States 0 and 7 (the end states) half as much, a condition most closely approximated by the flat P-S input profile B with high input variance conditions (Figure 4. 5-B).

Another observed and expected characteristic of the algorithm behavior is the seeking of the highest productivity in a P-S distribution at the lowest possible Pump State. This was an intentional convention programmed into the algorithm, where, should the measured productivity be equal (within a user-prescribed tolerance, typically set at 0.5 ppm IC for these experiments) at adjacent Pump States, movement towards the lower Pump State was favored. Given that a lower Pump State corresponds directly to lower

flow rate, this convention results in the algorithm seeking out the greatest mechanical efficiency for the algal production process. The effect of this convention was most clearly seen for input P-S profiles that were flat for part or all of their range, such as input profiles B and C (Figure 4. 2, page 161). The frequency distribution plots for input P-S profiles B and C (Figure 4. 5-B and C) showed that the lowest Pump States were favored overwhelmingly at the lowest values of input variance. Interestingly, for input profile B, the algorithm exhibited near complete randomness not only for the high level of input variance, as one might expect, but for the middle level of input variance as well. This is evidenced by the near flat frequency distribution (Figure 4. 5-B), indicating that an input variance of only 20% of the expected value can cause near-random behavior in the algorithm should the input P-S profile be generally flat. This may have implications for implementation of the algorithm in physical systems; given that some noise is expected in the measurement of productivity of a system, and that the productivity-flow rate relationship may be flat over a certain range, the system can be expected in the long term to visit all Pump States within that range equally and with a random trace of Pump State versus cycle, never truly converging on a maximally-efficient state.

The influence of the minimization convention on overall algorithm behavior is also exhibited by the frequency distribution for Pump State for input P-S profile E (Figure 4. 5-E). In this case, the minimization convention is in complete opposition to the prevailing P-S profile (Figure 4. 2-E), a continuous ramp-up of productivity with increasing Pump State with a maximum at Pump State 7. Without the minimization convention in the algorithm, it would be expected that the frequency distribution of profile E is a mirror image of that for profile D. Indeed, this is the case for low input

variance, where the frequencies for Pump States 6 and 7 for profile E, at 0.499 and 0.498, respectively, were equivalent to those for Pump States 1 and 0 for profile D, respectively. These frequencies dropped for profile E, however, relative to profile D for mid- and high values of input variance. For example, at high input variance, profile E had a frequency of 0.266 and 0.152 for Pump States 6 and 7, respectively, whereas profile D had a frequency of 0.296 and 0.173 for Pump States 1 and 0, respectively. The difference was evident but slight—only 3 to 4 percent—showing that the action of the algorithm is dominated in most cases by the goal to find the maximum peak of productivity over the range of the flow, with minimization of the flow rate only a secondary consideration.

The action of the minimization convention is also evident in frequency distribution F (Figure 4. 5-F), which had a bifurcated maximum with equal peak values on the input P-S profile (Figure 4. 2-F, page 161). The frequency distribution plot for this shows that, at all standard deviation levels, the algorithm favored the peak at the lowest Pump States, although this trend was dampened at a higher input variance. In this case, the higher input variance contributed to the success of the algorithm in finding the most efficient Pump State, spending more time at the lower peak of the P-S profile. This is because at the lower input variances, when the initial value for the Pump State for a run is 4 or greater, the algorithm strongly tended towards the upper peak at Pump State 7, which then, together with Pump State 6, became an absorbing state. Periodic destabilization of the seeking trends by high input variances at times allowed the algorithm to "climb down" the P-S profile to find the lower peak. However, because the higher input variance would occasionally destabilize the algorithm from the lower peak as well, one can say that, generally, some uncertainty on the productivity measurements can serve to

destabilize the seeking algorithm from absorbing states at local maxima on the P-S curve, potentially yielding opportunity to seek out and find other localized maxima.

In general, the control algorithm can be expected to find the maximum productivity for a distribution over flow rate—or any other controlled variable, for that matter. Even in most cases of relatively high uncertainty of input measurement, the algorithm can be expected to spend a majority of its time at or near the localized maxima of a productivity distribution, favoring those maxima that have lower input energies. Behavior approaching random seeking is evident when the productivity distribution is flat and uncertainty on its measurement is high (that is, standard deviations are on the order of the base value of the measurements).

Rate of convergence on the expected state

The cumulative mean gives an indication of how well the seeking algorithm converges on the expected solution. The cumulative mean of the Pump State (Figure 4. 6 and Figure 4. 7, pages 170 and 171) approached the expected value throughout many cycles of operation when input variance was low, where the expected value was the lowest Pump State where productivity (P) is maximized. Increasing the input variance moved the cumulative mean toward the middle of the range (that is, 3.5), as seen in the results for the flat P-S profile (profile B, Figure 4. 2, page 161) with a high input variance. This condition represents the state that most closely replicates a completely random input P-S profile. This activity holds for all P-S distributions. It is interesting to note that under certain conditions the ability of the algorithm to find the expected state was fairly robust. For example, the action in response to profile A (Figure 4. 2-A) with a

high input variance of 36% of the peak value of the distribution has a cumulative average of 2.55, only 20% off from the expected state of 2.

The cumulative standard error (Figure 4. 9 and Figure 4. 10, pages 173 and 174) gives an indication as to the spread of activity of the Pump State over the number of cycles. A larger cumulative standard error indicates that the program visited more Pump States outside the expected values over time. Its maximum should be found at high input variance conditions on a flat or bifurcated profile where there is a near equivalent chance to visit all possible states within the range of Pump State. In all cases, an increase in the input variance significantly increased the cumulative standard error; for example, for input profile A, the cumulative standard error increased from 0.023 to 0.046 for low to high input variance, respectively (Figure 4. 10). The greatest cumulative standard errors were seen for input profile B, because of its flat uniform profile, and for profile F, which, because of its bifurcated profile, resulted in the algorithm spending nearly equal numbers of cycles near the lower or higher ends of the Pump State range when input variance was of medium or high value.

Taken together, the cumulative means and cumulative standard errors give an indication on the convergence behavior of the algorithm. These values are summarized (Table 4. 3) for each profile for low and high input variance only. Low variance on the input profiles produced more efficient seeking results as the algorithm spent very little time at Pump States extraneous to the expected state or its adjacent states. The higher input variance significantly increased the standard errors on the output and thus skewed the cumulative mean; the distribution of states visited was broader under the higher input variance.

Table 4. 3. Cumulative mean and standard error of Pump State for various input P-S profiles (Figure 4. 2) for low and high input variance conditions.

Profile	Expected State	Low Input Var.	High Input Var.
A	2	2.01±0.023	2.55±0.046
B	0	1.34±0.039	3.48±0.065
C	0	0.84±0.025	2.19±0.052
D	0	0.51±0.017	2.01±0.052
E	7	6.49±0.017	4.57±0.059
F	0	2.90±0.016	3.29±0.078

The number of cycles to convergence can give an indication as to the rate of convergence of the algorithm on the expected solution. In most cases, convergence occurred rapidly (in less than 100 cycles) for input profiles of low variance. Only input profile B (a flat profile, Figure 4. 2, page 161) exhibited a slow rate of convergence, likely due to its flat shape which increases the likelihood that other Pump States further from the expected state would be visited over time. An increase in the input variance significantly increased the number of cycles to convergence in all cases. Those profiles which exhibited a well-defined maximum (A, C, D, and E, Figure 4. 2, page 161) showed convergence within the 1000 cycles at higher input variances. Profiles B and F showed slow convergence even at medium levels of input variance. With a flat or indeterminate P-S profile, the algorithm tended to wander over the entire range of possible Pump States. The level of variability on input data affected the variability of the output behavior of the algorithm.

One important implication of these results is the scale of the number of cycles appropriate for an experiment in the physical systems. Even at low input variance conditions, using the metrics employed here, the number of cycles required to demonstrate behavior of the control algorithm is on the order of 60 to 100. Conditions of

higher input variance would require considerably more cycles (500 to 1000) to fully characterize the activity of the algorithm with these methods of analysis. Within the context of physical testing, in which one cycle is defined by the harvest period that typically ranges from 4 to 7 days, a minimum experiment of 100 cycles would range on the order of a year, a prohibitive length of time. Other metrics are sought to adequately characterize the convergence power of the algorithm. One possibility may come from the field of Markov chain analysis, where a Markov chain or "random walk" is defined as a stochastic process where the probability of entering a state at time $t+1$ is determined only by the state at time t (Kemeny and Snell 1960). Application of Markov chain analysis to the algorithm employed here would rely upon computation of the probabilities of at each Pump State of movement to each of the adjoining states. This could be done for the virtual simulation scenarios tested here, where a stochastic measure of primary productivity is defined for each Pump State. Markov chain modeling of the implementation of the algorithm with the physical ATS units would require defining the same transition probabilities for each Pump State. These might be computed based on empirical subsidy-stress investigations as described in Chapter 3. In addition, given that Markov chain analysis has been used to simulate social situations such as competing technologies or dissemination of culture (Izquierdo et al. 2009), the mathematics used to analyze the behavior of Markov chains may be suitable for understanding dynamics of ecological systems, where subsequent states are determined solely by prior states. This is a recommendation for further analysis of these results, and development in general for a possible avenue for characterization of technoecosystem behavior.

Conclusions and Implications

The following conclusions can be made for this set of experiments:

- Analysis of the control algorithm in isolation using virtual simulation shows that the algorithm has the ability to seek for and find the maximum of a parameter at the lowest possible Pump State over a range of distribution relationships.
- The actions and effectiveness of the algorithm, as measured by the rate of convergence, are strongly influenced by the variance of the input data to which it responds and by the strength of the relationship between the controlled parameter and the measured variable. Refinement of the control process, in this scenario, would depend more on improving the fidelity of the capabilities of the system to measure the response of the ecological system.

The analysis presented here provides a procedural map for investigations into technosystem dynamics that only increases in importance as the complexity of the control algorithm is increased. This analysis also provides perspective on the expectation for the operation of the algorithm in physical testing experiments described in the next chapter. The expected action of the algorithm in response to the ecological components is inherently variable, and the measurements upon which the algorithm operates can be inherently noisy; these issues are addressed in further research effort employing the algorithm in physical ATS units.

Chapter 5: The Technoecosystem—Putting it all together

Introduction

The component systems were assembled into the full algal turf scrubber technoecosystem, and the system was tested through multiple trials using different nutrient feed recipes. Testing of the technoecosystem consisted of allowing the system to run through numerous harvest cycles and tracking the Pump State and net primary productivity through time. The expected behavior of the system was for it to track the pump state to converge over a number of cycles on the maximum productivity of the algal turf, the peak of the subsidy-stress curve of production to flow turbulence. Analysis of the system behavior consisted of examining the time-trace of Pump State and productivity for metrics of convergence that can be compared to the expected behavior as determined by the virtual experiments on the algorithm. The relative abundances of the dominant algal species were tracked throughout the operation of the system and are compared to those measured for ATS units operating in a standard mode without feedback control.

Objectives and Hypothesis

The objective of this set of experiments was to test the operational dynamics of an autonomous algal turf scrubber (ATS) that uses feedback control circuits to optimize the turbulence in the bed for maximum algal productivity through control of the volumetric flow rate. The hypothesis was that, given control circuitry (via computer) and a program algorithm, the autonomous ATS system will selectively activate pumps to modify flow rate in such a way as to follow the trajectory of a subsidy-stress curve of productivity

versus turbulence level, finding the maximum productivity while minimizing the level of turbulence.

Research Approach

An automated monitoring system was designed to measure the metabolism of an algal turf ecosystem in an ATS. The ATS water reservoir was monitored continuously using a pH meter connected to a datalogging control computer. A control program algorithm on the computer calculated then net carbon productivity and respiration (see Chapter 3) from the pH diurnal curves and changed flow rate accordingly to maximize net carbon productivity, following the assumption that, all other factors in excess, flow turbulence (as modulated by volumetric flow rate) was limiting to algal turf metabolism. Flow rate was manipulated via control circuitry that provided power to a bank of three pumps of various flow rate capacities. By activating different combinations of the three pumps, up to eight flow rate setpoints ("Pump States") across a range (from zero to 140 lpm) were attainable. In multiple trials, the system was allowed to automatically manipulate flow rate over multiple harvest periods until the optimum flow rate was converged upon for maximum algal productivity. The Pump State, net carbon productivity, and biomass production rate were converted to power acquisition, and traces of production power versus flow rate power were generated and analyzed for signatures of convergence.

Equipment

System overview

The equipment used for this research included a data acquisition computer that monitored the pH level in the reservoir of an ATS via a pH probe and meter. Digital output signal lines on the control computer activated relay-switched outlets that powered centrifugal pumps of various volumetric flow rate capacities. The overall configuration of these elements for the data acquisition mode has been shown previously (Chapter 3); the configuration for the autonomous control system mode are shown in the system schematic (Figure 5. 1), and the elements are described in more detail below.

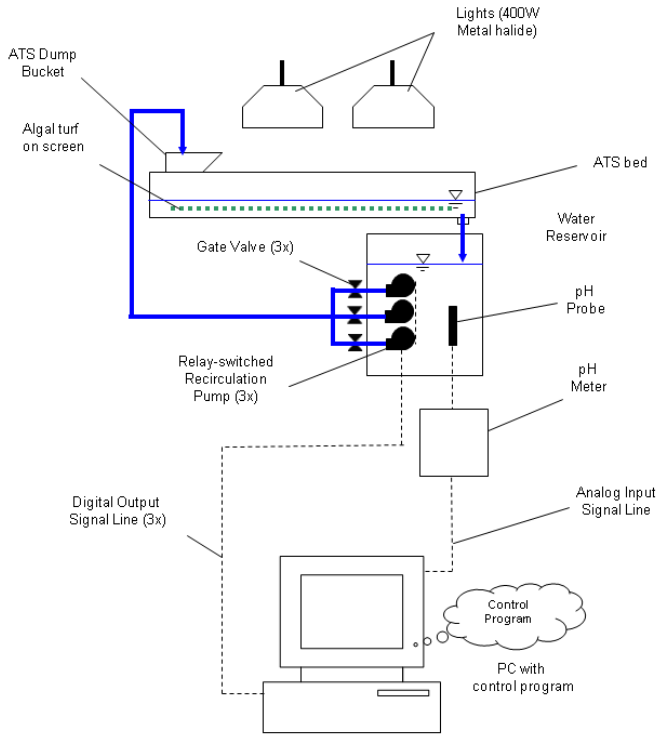

Figure 5. 1. Schematic diagram of a computer setup for feedback control of flow rate in an ATS.

ATS units

The algal turf scrubber units used for this research were nominally 1-m^2 laboratory-scale units. The five separate ATS units employed throughout all experiments were identical in construction and are described previously (Chapter 2). As described in previous experiments (Chapters 2 and 3), all units were operated in a recirculation mode in which process water was continuously pumped from a 200 liter drum reservoir into the wave surge bucket. As before, each ATS was paired with its own reservoir, and the total volume of water in the entire ATS reservoir system was maintained at a nominal 150 liters through daily additions of fresh distilled water to replace evaporative losses.

Lights

As reported previously (Chapter 3), each ATS unit was operated under two 400W metal halide lights, although one trial unit (ATS unit 7), however, operated under one 1000W metal halide light. For all autonomous experiment trials, the height of the lights above the ATS bed was adjusted to yield a light intensity of approximately 350 μmol photons m^{-2} s^{-1} measured at the center of the ATS bed area with a quantum flux meter and probe (LI-250 Light Meter and LI-190 Quantum Sensor, LI-COR Biosciences, Lincoln, Nebraska). Lights were operated under a 16 hour light/8 hour dark diurnal.

Nutrient supply

The various nutrient supply types employed in the ATS units have been described previously (Chapter 3). Throughout the course of the autonomous experiments, all four types of nutrient supply were attempted. For each of the nutrient supply types, solutions were mixed with known nitrogen and phosphorus concentrations, and aliquot volumes of nutrient solutions were added during scrubber operation to yield desired nitrogen loading

rates. The four types of feed solution used were dairy manure, urea salt, plant-food based (Miracle Gro® solution), and modified Bristol's solution (see Chapter 3 for descriptions).

Data acquisition and control system

A separate data acquisition computer was used for the autonomous control experiments than was used for data acquisition in the subsidy-stress experiments (Chapter 3). For the autonomous control experiments, a Dell Inspiron laptop computer with an installed NI DAQ-700 PCMCIA multifunction I/O card (National Instruments Corporation, Austin, Texas) and an external NI CB-50 I/O connector block was used. As in the subsidy-stress experiments that involved the monitoring of pH (Chapter 3), each ATS had a pH probe (36" single junction pH electrode, Cole Parmer) installed in its reservoir connected to a Jenco 3672 pH controller (Jenco Electronics Ltd., San Diego, California), the analog output terminals of which were then connected to the respective analog input channel connectors on the CB-50 connector block. Through this configuration, the voltage across the terminals would vary directly between 0 and 2.5 volts with the measured pH. As before, throughout the experiments, each probe and Jenco controller combination were recalibrated approximately every two ATS harvest periods.

For the autonomous control experiments, the pH monitoring system configuration used in the subsidy-stress experiments (Chapter 3) was amended with control circuitries that activated pumps on demand to establish the flow rate in each ATS (see Figure 5. 1). Three pumps of different flow rate capacities were installed in the reservoir of each ATS unit. Each pump was connected to a relay-controlled outlet, which in turn was connected to a digital output port on the computer's data acquisition card. Pumps were submersible centrifugal magnetic-drive pond pumps (Danner Manufacturing, Islandia, N.Y.), and each

was installed with a gate valve on the outlet piping to allow fine-tuning adjustment of the volumetric flow rate (Table 5. 1).

Table 5. 1. Nominal pump flow rate at 2 m of head and manufacturer model number. Pumps were generally of larger flow capacity than required and were scaled back using gate valves on the outlet.

Pump Nominal Flow Rate	Pump Model Number*
20 lpm	MD9
40 lpm	MD12
80 lpm	MD18
*All pumps manufactured by Danner Mfg. (Islandia, NY).	

Activation of multiple pumps in different combinations allowed the total flow rate delivered to the ATS bed to be set at eight discrete flow rate set points (here called Pump States) at increments of 20 lpm over the total possible range from zero to 140 lpm (Table 5. 2). Wave surge volume was held constant at approximately 11 liters for all flow rates, resulting in a different wave surge frequency at each Pump State. A low-flow peristaltic pump was installed on each experimental unit such that when all pond pumps were deactivated (Pump State 0), a small trickle-flow of typically less than 2 lpm was maintained. When the control algorithm (next section) required a pump to be activated, the computer activated a 5-V digital signal to the appropriate control line, closing the relay and activating the outlet to switch on the pump.

Table 5. 2. Pump designations, nominal flow rates, and truth table showing activation states of individual pumps and total flow rate for a given flow rate state.

Pump No. →	1	2	3		
Nom. Pump Flow Rate (gpm) →	20	40	80	**Total Flow Rate (lpm)**	**Wave surge frequency (min^{-1})**
Pump State ↓	**Activation State (0 = off, 1 = on)**				
0	0	0	0	>2**	0.1
1	1	0	0	20	1.7
2	0	1	0	40	3.3
3	1	1	0	60	5.0
4	0	0	1	80	6.7
5	1	0	1	100	8.3
6	0	1	1	120	10
7	1	1	1	140	12

** A peristaltic pump provided constant low flow at less than 2 lpm.

Just as two separate hardware configurations were used for the subsidy-stress experiments and the autonomous control experiments, separate monitoring and control programs were used. Whereas the subsidy-stress experiments (Chapter 3) used a program that was strictly for monitoring and data logging of the pH diurnal, the control program developed for the autonomous control experiments calculated incremental changes in metabolism in real-time based upon the pH diurnal, and subsequently took control actions (in the form of switching on or off pumps) based upon the values of those changes. The control algorithm was the basic seeking algorithm described previously (Chapter 4, Section 4.1). The algorithm seeks out the maximum or minimum of a variable within an expected range via incremental change of the controlled parameter. A simplified flow chart schematic of the core algorithm and description of operation was previously given (Chapter 4, Figure 4.1, page 156), and a more detailed flow chart of the entire data acquisition and control program is provided in Appendix A.

Conversion of the monitored pH diurnal to the concentration of inorganic carbon (IC) is central to the control system operation. This information was determined by subjecting periodic samples of process water to a pH-IC titration (described in Chapter 3). This titration yielded a pH versus IC concentration curve that was described by a third-order polynomial function within the upper and lower limits of pH measured (Figure 5. 2). The algorithm assumed this polynomial representation and the user has the opportunity to enter the polynomial coefficients at the beginning of each harvest cycle. For pH values above and below the limits in the titration, a linear function, based upon a linear regression of the last three points on the tail of the pH-IC relationship, was used for extrapolation.

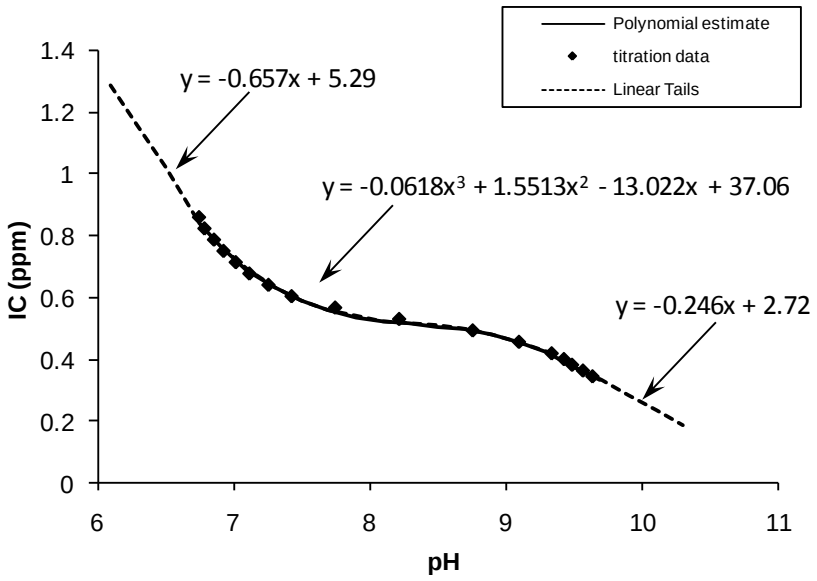

Figure 5. 2. Sample of polynomial description of an empirical pH-IC titration trial for ATS process water.

As discovered in previous experiments, it became clear that the inorganic carbon titration method as employed here was a surrogate for the net primary production, rather than serving as a measurement of the absolute value of it. The pH diurnal was clear in all

trials, however, and the method was pursued as a reliable parameter that was closely correlated with ecosystem metabolism and that could be automatically monitored for use in the feedback control system. As before, for the purposes of this research, these measurements are here referred to as "net carbon production" (NCP).

Methods

The general procedure for the physical testing of the automated control system was as follows. The control program was initialized with the user-input operational parameters, which included the following:

- File path for data logging on the computer;
- Sample rate (in Hz);
- Number of samples to average for each pH data point;
- Sample period (in minutes) for each pH data point;
- Harvest period (in hours), the length of time to integrate the pH-derived IC concentration data;
- Titration data to convert pH to IC concentration, entailing the regression coefficients for the third-order regression polynomial describing the titration curve, the upper and lower bounds of pH for which the polynomial was valid, and the constants for linear extrapolation of the pH-IC titration curve beyond the range of the titration;
- Starting Pump State for the algorithm, corresponding to the flow rate for cycle 0 (see Table 5.2) and designated as low (Pump State 0), medium (Pump State 3), and high (Pump State 7).

Typical values for many of these parameters are given in Table 5. 3.

Table 5. 3. Typical parameter values used for operation of the autonomous algorithm on physical systems.

Parameter	Value
Initial Pump State	0, 4, or 7
Pump State increment	+1 or -1
Sample Rate	1000 Hz
No. of Samples to average	3000
Data collected every	60 minutes
IC Tolerance	5 ppm
Evaluate NCP for	92 hours

For at least two harvest periods prior to the initialization of an automated run, the ATS was run at the flow rate corresponding to the starting Pump State to allow the algal community to become conditioned to the flow regime. After all parameters were input into the algorithm, and following harvest of the scrubber and calibration of the pH probe, the control algorithm was started immediately. Typically, the algorithm was started during the dark period of the diurnal light cycle. The control algorithm was allowed to run uninterrupted for the extent of the designated harvest period, typically established from 92 to 96 hours (four complete day/night cycles), the minimum amount of time and number of diurnal cycles estimated as necessary for adequate sampling of the ATS metabolism for any single operating condition. The data collection of the control algorithm automatically paused at the end of the harvest period time awaiting operator intervention and instructing the operator to harvest. During this pause, the ATS was harvested by the operator. Typically the harvest was performed within 12 hours of the initiation of the pause in data acquisition.

ATS Operation

For all automated ATS trials, the light diurnal was set via timer to 16 hour light/8 hour dark cycle. Also, each ATS was operated as previously described (Chapters 2 and 3), with daily nutrient feed additions and distilled water additions as necessary to make up for evaporative losses. For each ATS, the nutrient feed addition was automated using a peristaltic pump on a timer, set to activate daily approximately 1 hour before the end of the dark period of the diurnal light cycle. For this, the necessary volume of feed solution for the following day's feeding requirement was placed into a plastic jug into which a tube from the feed pump was inserted, and the other end of this feed tube was placed inside the ATS reservoir just above the water surface.

Harvest Procedures

For each harvest performed at the end of each harvest cycle, the following procedures were followed in this order. First, samples of algae were taken from three places haphazardly chosen on the ATS bed; these samples were placed in process water in 50-ml plastic vials and placed in cold (4°C) storage for later taxonomic analysis. All pumps were then turned off and the ATS bed was allowed to drain. Water samples were taken from the reservoir, some of which were used for immediate nitrate analyses and some were placed in cold storage for later pH-IC titration analyses. Nitrate analysis was performed with Reflectoquant nitrate strips (EM Science, Gibbstown, NJ). Algae biomass was then harvested by first scraping all algal biofilm from the dump bucket, and then removing all algal biomass and dump bucket scrapings from the ATS bed and screen using a wet-dry vacuum.

Following harvest of the algal biomass from the ATS bed, approximately one-third of the water in the reservoir was wasted and replaced with fresh distilled water. This was performed to maintain relatively constant water chemistry over time and to prevent the excessive buildup of constituents in the water to levels potentially deleterious to algal growth. On the day of harvest for that harvest period, the nutrient feed was input into the reservoir at the time of distilled water addition. Following this, the calibration of the pH probe in the ATS reservoir was checked. Power was reactivated to the bank of pumps, and the data acquisition and control program was reinitialized, whereupon any automated changes in pump activation state were performed.

Algae processing

After harvest, the algae/water suspension in the vacuum was decanted into a 1.5-mm polyethylene mesh filter bag inside a bucket; the water was allowed to pass through the filter mesh, retaining a majority of the algae filaments in the bag. The algal biomass in the bag was gently squeezed and pressed by hand to remove excess water (which was collected into the bucket), and spread flat on a rack in front of a fan for air-drying. The water was kept in the bucket for 24 to 48 hours to allow floating particulates to settle. After settling, the supernatant water was siphoned off the top, and the remaining sludge was spread out in a shallow pan, placed in front of the fan, and allowed to air dry. Drying typically required between 24 to 48 hours. Upon air drying, the biomass harvested from the screen and from the harvest water were combined and weighed with a balance. Numbers were reported as the total biomass produced for that harvest period. Samples were taken periodically from the biomass harvests for oven-drying to calculate the

average per cent moisture for all samples. Samples were also taken periodically for ashing to calculate the average per cent ash for all samples.

Recorded data

The data collected for all trials and recorded to the data logging computer comprised the following:

- Timestamp (indicating date and time);
- Time elapsed since program start (in seconds);
- Harvest cycle elapsed since program start;
- Measured pH level;
- Calculated IC concentration (in ppm);
- Average rate of change in IC concentration in past timestep;
- Calculated change in IC concentration based on average rate of change;
- Cumulative negative change in IC concentration this harvest period;
- On/off state of pump 1 in most recent time step;
- On/off state of pump 2 in most recent time step;
- On/off state of pump 3 in most recent time step;
- Pump State of most recent time step.

Data Analysis

Analysis of the data entailed plotting the Pump State and the net carbon productivity (NCP) associated with that Pump State versus harvest cycle. The trend in

Pump State over repeated cycles and NCP were qualitatively assessed for directional trends for finding the expected state. The expected state was derived from the predicted maximum NCP within the range of flow rates (that is, Pump States) as determined in the subsidy stress experiments (Chapter 3). For both types of nutrient feed used (undigested dairy manure and Bristol's medium), the maximum NCP was expected to be seen at a flow rate between 5 and 25 lpm (wave surge frequencies of 0.3 and 2.7 min^{-1}, respectively; see Figure 3.10, page 103), corresponding to a Pump State between 0 and 2, respectively (see Table 5. 2, page 189). Also, for all trials, the NCP was plotted versus biomass production rate; linear regression analysis was performed on NCP versus biomass production rate to examine the correlation between the two. One might expect the NCP and biomass production rate to correlate, as the integration of NCP (the total amount of carbon fixed by the photosynthetic community minus that respired by heterotrophic community) over the harvest period should predict the biomass yield.

The algae samples were identified and keyed to the genus level. The relative abundance of the three major genera of algae (Rhizoclonium, Microspora, and Oscillatoria) were calculated and plotted versus day of operation for the autonomously controlled ATS units. Mean relative abundance was calculated for each of the autonomously controlled ATS units and compared to the mean relative abundance calculated for ATS units similarly operated but not on autonomous control.

Trials

Each automated scrubber trial was allowed to operate as long as possible to ensure the completion of as many harvest cycles as possible. A harvest cycle was defined as the time period from one harvest to the next, as set by the user-delineated "Harvest

Period" parameter in the control program. A trial is defined here as a set of harvest cycles on one individual automated ATS for which all operating conditions (light, nitrogen loading rate) are constant except the flow rate being changed by the automated program. Three different ATS units were used to perform a total of 16 different trials of the automated control system. The trials were conducted as exploratory investigation to elucidate the operating parameters of the system, establish the operational protocols for the system, and experiment with different nutrient feed sources. The parameters that were modified through this exploration included the nutrient feed type, the nitrogen loading rate, the harvest period, the measurement tolerance on productivity, and the starting Pump State. A summation of trials and their defining parameter values are shown in Table 5. 4.

Table 5. 4. List of physical tests of the automated ATS system.

ATS No.	Test No.	Dates	Feed[a]	Mean NLR[b] (g N d^{-1})	Harvest period (d)	Toler-ance[c]	Starting Pump State/Flow rate (lpm)	Notes
1	1-1	11/20/07 - 12/1/07	M	0.7±0.0	7	5	7/140	Initiating test of system
	1-2	12/1/07 - 2/2/08	M	0.8±0.2	5	5	7/140	System reprogrammed with signal filtering
	1-3	2/3/08 - 3/3/08	U	1.2±0.3	4	5	3/60	Test of alternate feed solution
	1-4	3/4/08 - 3/18/08	MG	0.7±0.3	4	5	3/60	Test of second alternate feed solution
	1-5	3/29/08 - 4/18/08	MG	0.9±0.2	4	5	3/60	
	1-6	5/30/08 - 6/23/08	B	0.7±0.1	4	1	7/140	Test of third alternate feed solution
	1-7	6/25/08 – 9/3/08	B	0.6±0.1	4	1	3/60	Continuation of prior run with minimization convention reprogrammed
5	5-1	4/18/08 - 4/23/08	MG	0.8±0.0	4	5	7/140	Test of alternate feed solution at high flow initiating Pump State.
	5-2	4/23/08 - 5/2/08	MG	0.8±0.2	4	5	7/140	
	5-3	5/2/08 - 6/3/08	MG	0.8±0.3	4	5	7/140	
7	7-1	4/18/08 - 4/23/08	B	0.4±0.0	4	5	0/2	Test of third alternate feed solution at low flow rate
	7-2	4/23/08 - 5/2/08	B	0.4±0.03	4	5	0/2	Restart of prior trial.
	7-3	5/2/08 - 6/23/08	B	0.8±0.2	4	5	1/20	Continuation of prior trial
	7-4	6/25/08 – 9/3/08	B	0.6±0.1	4	0.5	4/80	Continuation of prior trial with minimization convention reprogrammed

Notes: (a) Feedstocks used: “M”, raw dairy manure; “U”, urea-phosphate solution mix; “MG”, Miracle-Gro solution; “B”, modified Bristol’s solution; (b) “NLR” is the nitrogen loading rate (mean ± standard deviation); (c) “Tolerance” is the equivalence tolerance for successive measurements of productivity; that is, the algorithm assumes $P_i = P_{i-1}$ when $|Pi – Pi\text{-}1| < T$, where P_i is the productivity measured at time t_i, and T is the tolerance (in ppm IC).

Results

Overview

Results of all the trials performed in the physical testing of the control algorithm are shown in Table 5. 5. Most trials were run for only a few cycles because of various failure reasons, yielding a catalog of possible failure scenarios and pitfalls for operation of such a system. The high number of trials that ended in failure is reflective of the exploratory nature of this set of experimental trials. The failure scenarios can be categorized into three types: programming errors (trials 1-1, 1-6, and 7-3), power failures or mechanical errors (trials 5-1, 7-1, and 7-2), and feedstock "instability" errors (trials 1-3 to 1-5, 5-1 to 5-3). The programming errors were generally expected as part of the debugging process for new programs and amounted to the incorrect application of the minimization convention (trial 1-6) or running of the algorithm from a saved set of data rather than real-time monitoring data (trial 7-3). Power or mechanical errors were typically the result of power spikes or failures, due to laboratory electrical problems, that would cause errant pH measurements (for example, in Trials 1-1 and 7-2). Nutrient feed errors were particular to the individual feed type. When manure was used as the nutrient feed, there was concern that the feed was variable through time and thus affecting the veracity of the pH-IC titration curves (e.g., Trials 1-1 and 1-2). When urea was the nutrient feed, the main concern was that the algae were not growing, exhibiting very low biomass production numbers for this trial (Trial 1-3). When Miracle Gro® was the nutrient feed (Trials 1-4, 1-5, and 5-1 to 5-3), the pH level in the ATS reservoir often showed considerable instability, often dropping below 7.0 and seeming to impact the growth of the algae. It was observed that this would often happen if excess nitrogen was supplied, following which an increase in nitrate concentration in the reservoir was noted.

Table 5. 5. List of physical tests and results of the automated ATS system.

ATS and Test No.		Dates	Feed[a]	Mean NLR[b] (g N d^{-1})	Harvest period (d)	Tolerance[c]	Starting Pump State	Cycles completed	Success or Failure?	Notes
1	1-1	11/20/07 - 12/1/07	M	0.7±0.0	7	5	7	5	F	Errant pH signals from electrical noise; some measurement cycles only 1 day long.
	1-2	12/1/07 - 2/2/08	M	0.8±0.2	5	5	7	10	S	New program eliminating errant pH signal, but no minimization convention.
	1-3	2/3/08 - 3/3/08	U	1.2±0.3	4	5	3	5	F	Algae did not grow with this feedstock.
	1-4	3/4/08 - 3/18/08	MG	0.7±0.3	4	5	3	3	F	Instability in pH with this feedstock; low pH necessitated amendment with NaOH.
	1-5	3/29/08 - 4/18/08	MG	0.9±0.2	4	5	3	5	F	Instability in pH with this feedstock; low pH necessitated amendment with NaOH.
	1-6	5/30/08 - 6/23/08	B	0.7±0.1	4	1	7	5	S	Adequate run, although minimization convention not applied correctly.
	1-7	6/25/08 – 9/3/08	B	0.6±0.1	4	1	3	11	S	Successful continuation of previous run with minimization convention applied correctly.
5	5-1	4/18/08 - 4/23/08	MG	0.8±0.0	4	5	7	1	F	Two-day power outage shut off lights and compromised pH diurnal.
	5-2	4/23/08 - 5/2/08	MG	0.8±0.2	4	5	7	2	F	Instability in pH with this feedstock; low pH necessitated amendment with NaOH.
	5-3	5/2/08 - 6/3/08	MG	0.8±0.3	4	5	7	6	F	Instability in pH with this feedstock; low pH necessitated amendment with NaOH.
7	7-1	4/18/08 - 4/23/08	B	0.4±0.0	4	5	0	1	F	Two-day power outage shut off lights and compromised pH diurnal.
	7-2	4/23/08 - 5/2/08	B	0.4±0.03	4	5	0	2	F	Power outage invalidated second half of data.
	7-3	5/2/08 - 6/23/08	B	0.8±0.2	4	5	1	10	S/F	Continuation of previous file; decisions being made from saved data rather than real-time.
	7-4	6/25/08 – 9/3/08	B	0.6±0.1	4	0.5	4	11	S	Successful test of new algorithm with corrected minimization convention.

Notes: (a) Feedstocks used: “M”, raw dairy manure; “U”, urea-phosphate solution mix; “MG”, Miracle-Gro solution; “B”, modified Bristol’s solution; (b) “NLR” is the nitrogen loading rate; error is standard deviation; (c) “Tolerance” is the equivalence tolerance for successive measurements of productivity; that is, the algorithm assumes $P_i = P_{i-1}$ when $|P_i - P_{i-1}| < T$, where P_i is the productivity measured at time t_i, and T is the tolerance in ppm IC.

Results by individual trial

The trials discussed here are representative of those that exhibited dynamic behavior in a way that was expected and thus can be considered as having moderate success, or they are representative of a typical failure situation. Not all the trials are discussed, as some were failures because of bugs in the program or because of mechanical failures of the ATS units in the lab.

Trial 1-2: The Launch

Trial 1-2 can be considered as the inaugural trial that first exhibited the dynamics of the control algorithm in response to a physical system. The trial was performed from 12/1/07 to 2/2/08, using undigested dairy manure as the nutrient feed at a nitrogen loading rate of 0.8±0.2 g N m^{-2} d^{-1}. It was operated using a harvest period of 5 days, and completed a total of 10 cycles starting from a Pump State of 7 (Figure 5. 3). During its operation, the Pump State decreased steadily through 7 cycles to Pump State 0, and the measured net carbon productivity (NCP) at each cycle was either the same or greater than the prior cycle. Overall, the Pump State was directed to and remained in lower values (0 or 1) by the end of the trial.

An excessive value for the NCP was measured at cycle 6 (Figure 5. 3), likely due to errant pH measurements because of signal noise. The trial, however, exhibited an error or "bug" in the program: whereas the NCP at cycle 7 was less than that at cycle 6, the Pump State did not change in the other direction in cycle 8, as would be expected. Also, when the Pump State was at 0, it should have increased to 1 by the default "rebound" convention included in the algorithm with the intention to always destabilize the

algorithm from possible attractor states. This exhibits that there were errors in the algorithm programming that was corrected in later versions of the control program.

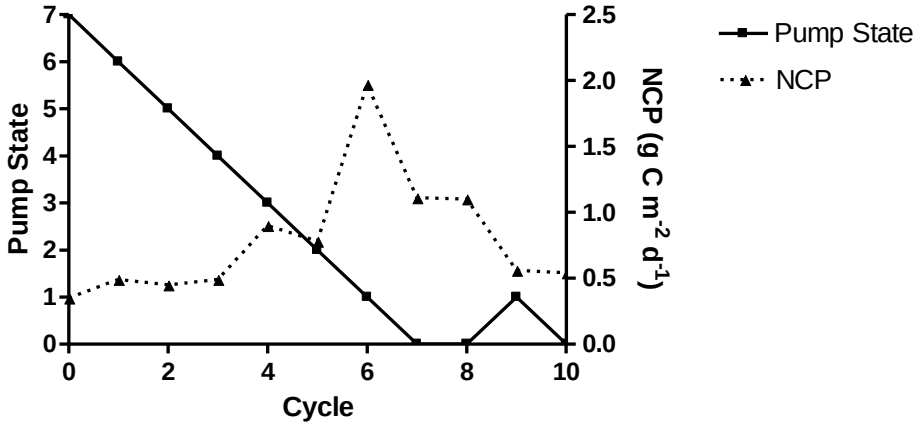

Figure 5. 3. Pump State and average net carbon productivity (NCP) versus cycle from Trial 1-2.

A comparison of the measured average NCP versus the biomass production rate, with the errant NCP at cycle 6 removed because of measurement error (Figure 5. 4), showed no correlation ($R^2 = 0.0115$) with a slope that was not significantly different than zero ($F(1,9) = 0.105$, $p = 0.753$).

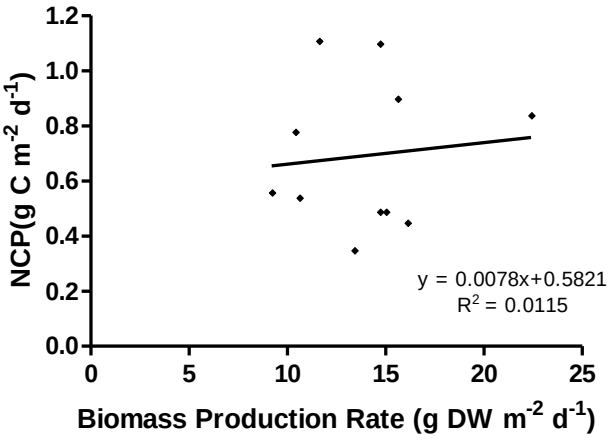

Figure 5. 4. Net carbon productivity (NCP) versus biomass production rate for Trial 1-2, showing no correlation between productivity and biomass production.

Trials 1-6 and 1-7: A new recipe

Trial 1-6 was stopped for algorithm and system maintenance, and trial 1-7 was started at the Pump State where trial 1-6 left off; hence, results from trials 1-6 and 1-7 can be combined and treated as the same trial run. Trial 1-6 was performed from 5/30/08 to 6/23/08, and trial 1-7 was performed from 6/25/08 to 9/3/08, using modified Bristol's solution as the nutrient feed at a nitrogen loading rate of 0.6 ± 0.1 g N m^{-2} d^{-1}. The trials were operated at a harvest period of 4 days, and completed a total of 16 cycles (5 for Trial 1-6 and 11 for Trial 1-7) starting in Trial 1-6 from a Pump State of 7 (Figure 5. 5). During its operation, the Pump State decreased steadily through 4 cycles as measured NCP increased at each subsequent cycle. As a demonstration of the minimization convention, the Pump State continued to decrease from cycle 4 to cycle 5 as the NCP for cycle 4 was approximately the same as the previous cycle. A significant decrease in the measured NCP for cycle 5 at Pump State 2 (compared to cycle 4 at Pump State 3) initiated a change in direction of Pump State increments, as expected. This dynamic continued through the extent of the trial, as the Pump State continues to vacillate yet showed a general decrease from Pump State 7 to Pump State 2 after 15 cycles.

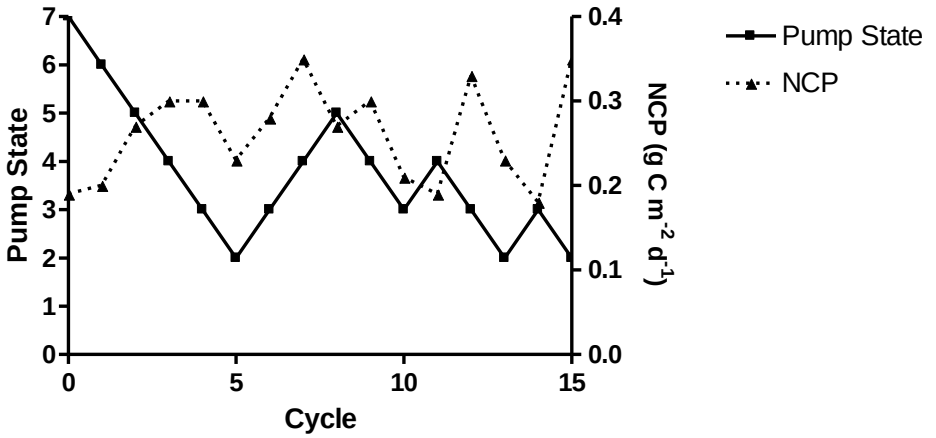

Figure 5. 5. Pump State and average net carbon productivity versus cycle for combined Trials 1-6/1-7.

A comparison of the measured average NCP versus the biomass production rate (Figure 5. 6) for the combined data of trials 1-6 and 1-7 showed low positive correlation ($r^2 = 0.267$) with a slope that is significantly non-zero ($F(1,14) = 5.308$, $p = 0.0371$).

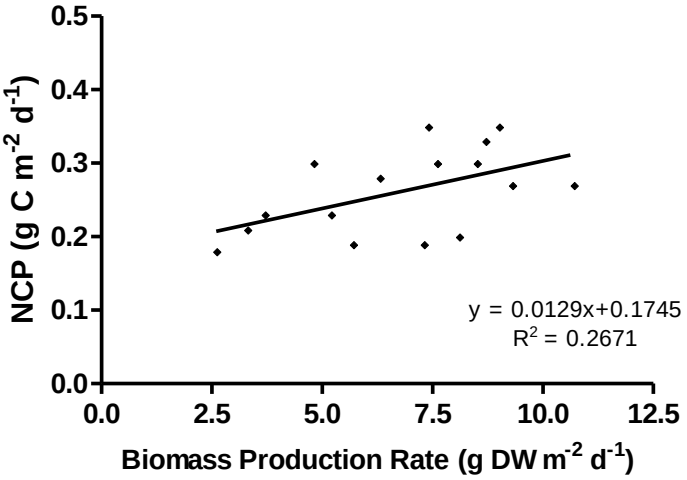

Figure 5. 6. Net carbon productivity (NCP) versus biomass production rate for combined Trials 1-6/1-7.

Trial 5-3: A trial with inorganic feed

Trial 5-3 can be considered as representing a typical failure condition, as the inorganic feed used in this trial created unstable pH chemistry in the reservoir water,

unrelated to the metabolism of the algal turf, that affected the outcome of the control algorithm. The trial was performed from 5/2/09 to 6/3/09, using Miracle Gro® solution as the nutrient feed at a nitrogen loading rate of 0.8 ± 0.3 g N m^{-2} d^{-1}. It was operated at a harvest period of 4 days, and completed a total of 6 cycles starting from a Pump State of 7 (Figure 5. 7). During its operation, the Pump State decreased steadily through 7 cycles to Pump State 0, and the measured net carbon productivity (NCP) at each cycle (except for the final cycle) was either the same or greater than the prior cycle. In this trial, the NCP increased at every cycle except the last. The Pump State continued on its trajectory (decreasing) at each cycle, and the trend in the Pump State was downward for the entire trial.

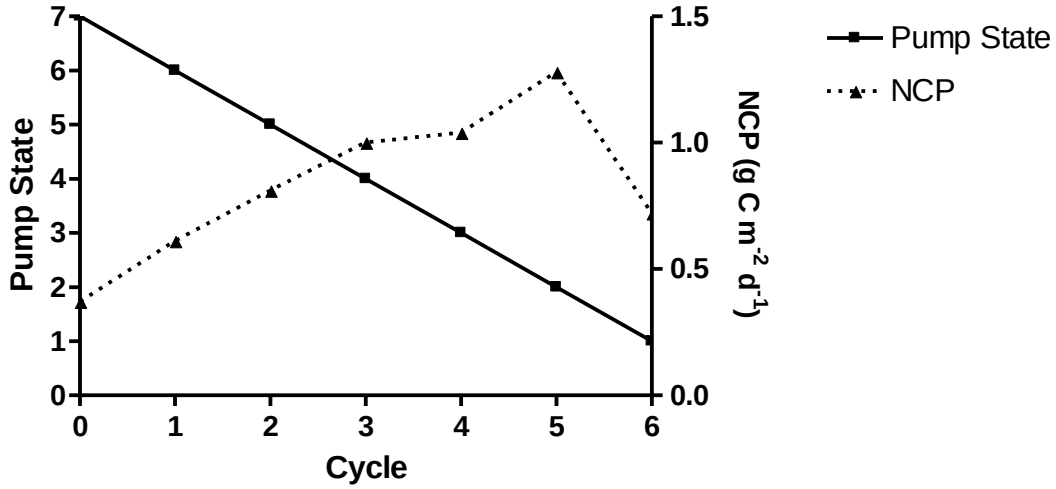

Figure 5. 7. Pump State and average net carbon productivity (NCP) versus cycle for Trial 5-3.

A comparison of the measured average NCP versus the biomass production rate (Figure 5. 8) for Trial 5-3 shows high correlation ($R^2 = 0.9024$) with a slope that is significantly non-zero ($F(1,4) = 36.67$, $p = 0.0038$).

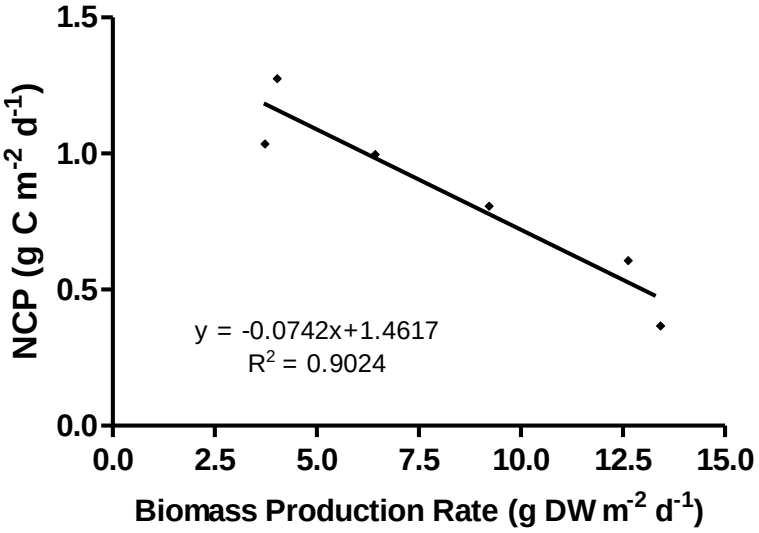

Figure 5. 8. Net carbon productivity (NCP) versus biomass production rate for Trial 5-3.

Trial 7-4: Bristol's solution

Trial 7-4 can be considered as representing as close to successful algorithm operation on a physical system as was attained in this set of trials. The trial was performed from 6/25/08 to 9/3/08, using Bristol's modified solution as the nutrient feed at a nitrogen loading rate of 0.6 ± 0.1 g N m^{-2} d^{-1}. It was operated at a harvest period of 4 days, and completed a total of 11 cycles starting from a Pump State of 4 (Figure 5. 9). During its operation, the Pump State trended towards lower Pump States. The measured net carbon productivity (NCP) varied at each cycle, but there was a general lower trend in NCP in later cycles.

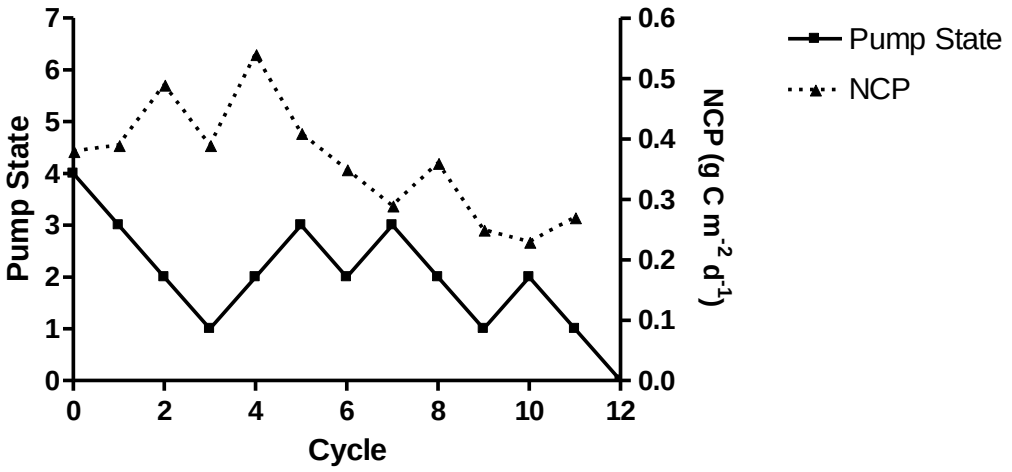

Figure 5. 9. Pump State and average net carbon productivity (NCP) versus cycle for Trial 7-4.

A comparison of the measured average NCP versus the biomass production rate (Figure 5. 10) for the combined data of trials 7-3 (for which data were collected but not used by the algorithm to make Pump State change decisions) and 7-4 showed low positive correlation ($R^2 = 0.267$) with a slope that is significantly non-zero ($F(1,24) = 8.603$, $p = 0.0073$). The two lowest biomass production rate values may skew this analysisk, however, and removal of these from the regression analysis as possible outliers results in no correlation ($R^2 = 0.0458$) with a slope that is not significantly different than zero ($F(1,22) = 1.057$, $p = 0.315$).

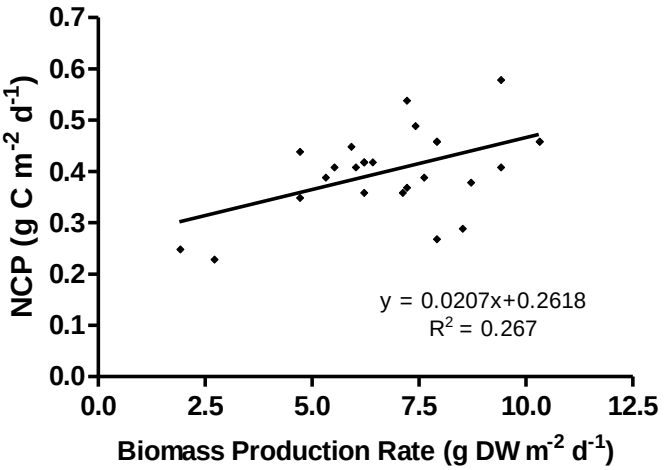

Figure 5. 10. Net carbon productivity (NCP) versus biomass production for Trials 7-3/7-4.

The combined data set of trials 7-3 and 7-4 provides a large enough sample size (n=24) to investigate the effects of different Pump States on the productivity. A mean and standard error of NCP measured at different Pump States shows a slight maximum at Pump State 2, with decreasing values for higher and lower Pump States (Figure 5. 11). An analysis of variance revealed no significant difference ($F(2,21) = 0.672$; $p = 0.52$; $R^2 = 0.061$) between the mean NCP for any Pump States.

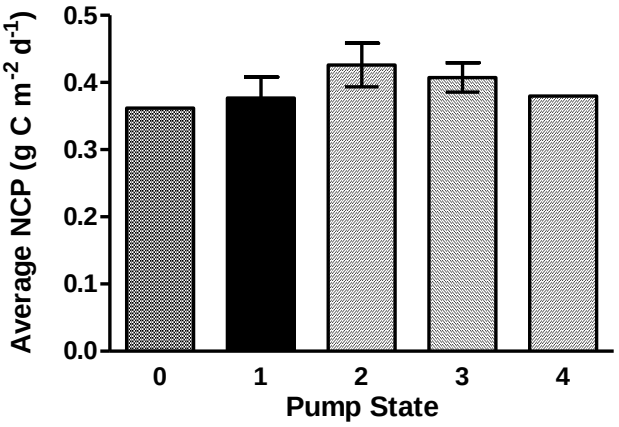

Figure 5. 11. Mean and standard error of net carbon productivity (NCP) versus Pump State for trials 7-3 and 7-4.

The mean and standard error of the biomass production rate for the combined trials 7-3 and 7-4 measured at different Pump States shows a slight maximum at Pump State 4 and a decreased value a Pump State 1 (Figure 5. 12). An analysis of variance revealed no significant difference ($F(2,21) = 2.326$; $p = 0.12$; $R^2 = 0.183$) between the mean biomass production rate for any Pump States.

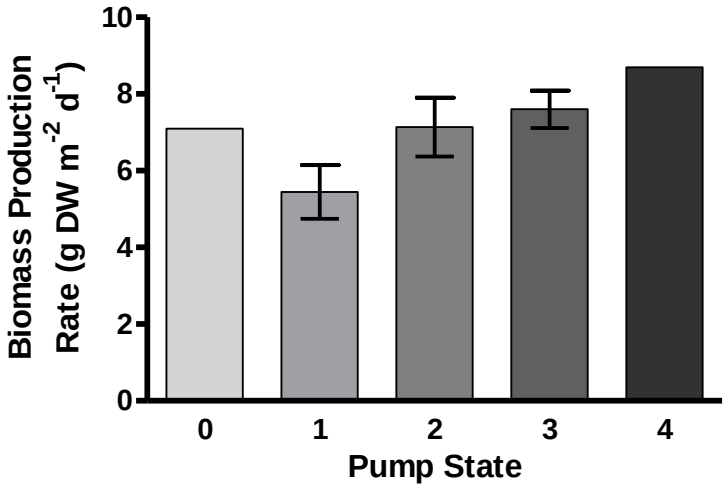

Figure 5. 12. Mean and standard error of biomass production rate versus Pump State for trials 7-3 and 7-4.

Cumulative means and standard errors of trials

The cumulative means and standard errors of the Pump State were calculated for the trials that showed moderate success in exhibiting control behavior (trial 1-2, trial 1-6/1-7, and trial 7-4). These results are given in Table 5. 6.

Table 5. 6. Number of cycles, cumulative mean, and cumulative standard error for successful phyical trials of the automated control system for the ATS units.

Trial number	Total cycles	Cumulative Mean of Pump State	Cumulative Standard Error of Pump State
1-2	10	2.50	0.71
1-6/1-7	15	3.75	0.36
7-4	12	1.88	0.27

These results were plotted on the cumulative mean and cumulative standard error versus cycle number plots that were developed using virtual data sets in Chapter 4 (Figure 4.6 and Figure 4.9, pages 170 and 173, respectively) as a means of comparison to expected outcome. Only the results from virtual data sets representing a subsidy-stress distribution (Figure 4.2A) and a flat distribution (Figure 4.2B) of net carbon productivity versus Pump State are used for comparison, as it was expected that results of the physical experiments would follow one of these two distributions. Results for this analysis for the cumulative mean of Pump State versus cycle are shown (Figure 5. 13). For all three trials, the cumulative mean of the Pump State fell within the bounds of the expected Pump State for the high input variance conditions for both the subsidy-stress input distribution (Figure 5. 13A) and the flat distribution (Figure 5. 13B). Only trial 1-2 falls within the bounds of the expected value for the low input variance conditions on the subsidy-stress input distribution (Figure 5. 13A).

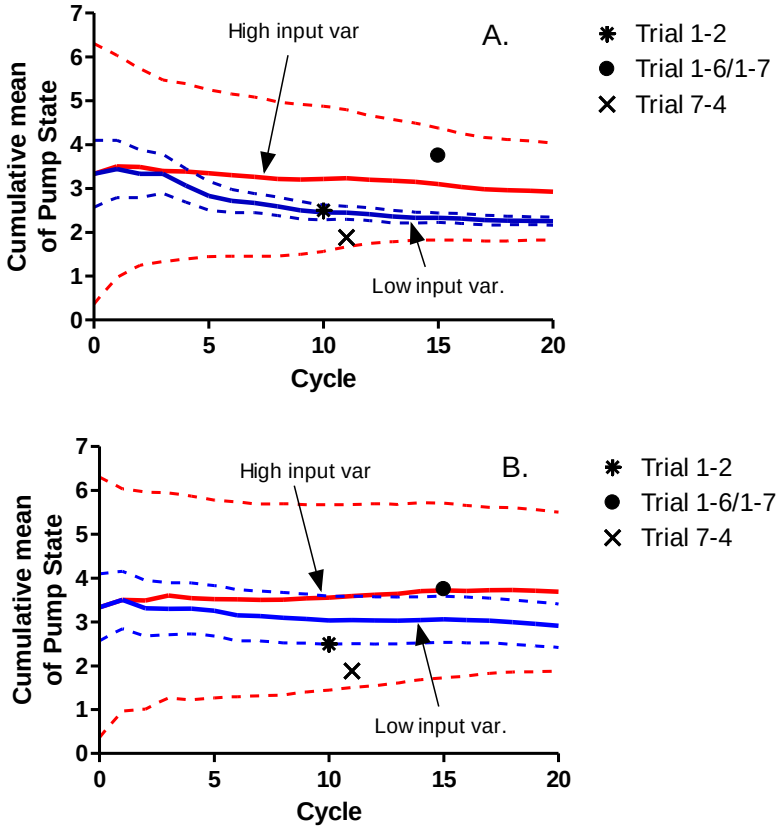

Figure 5. 13. Cumulative mean for physical autonomous trials compared against virtual results generated for (A) a subsidy-stress distribution and (B) a flat distribution of net carbon productivity versus Pump State for low and high values of input variance. Error bars represent standard deviation of the expected state based on uncertainty resulting from the initial Pump State.

Results for this analysis for the cumulative standard error of Pump State versus cycle are shown (Figure 5. 14). For two trials (1-6/1-7 and 7-4), the cumulative standard error of the Pump State fell within the bounds of the expected Pump State for the high input variance conditions for the subsidy-stress input distribution (Figure 5. 14A), and only one trial (trial 7-4) fell within the bounds of the expected solution of the flat distribution (Figure 5. 14B). The standard error of Trial 1-2 falls well outside the bounds of the expected value for all input variance conditions on both input distributions (Figure 5. 14A and B).

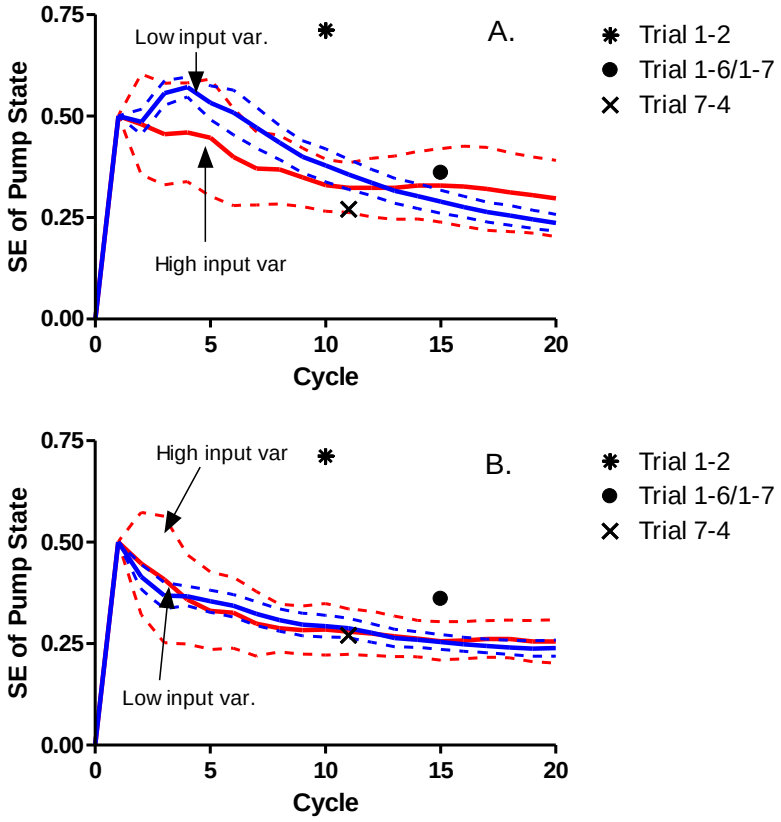

Figure 5. 14. Cumulative standard error for physical autonomous trials compared against virtual results generated for (A) a subsidy-stress distribution and (B) a flat distribution of net carbon productivity versus Pump State for low and high values of input variance. Error bars represent standard deviation of the expected state based on uncertainty resulting from the initial Pump State.

Algal Species Relative Abundance in Autonomous Systems

The relative abundances of the various algal species were plotted versus day of operation for the autonomously controlled ATS units 1 and 7 to look for trends related to their operational conditions (Figure 5. 15 and Figure 5. 16). These data are a subset of the relative abundance data presented in Chapter 3 (Figure 3.21, page 125). For ATS unit 1 (Figure 5. 15), there is no obvious trend throughout the entire time period, although near the end of the trial there is an apparent decline in *Microspora* and *Rhizoclonium* and an apparent increase in other species. ATS unit 7 (Figure 5. 16) shows a similar pattern,

with *Oscillatoria* and other species increasing and *Microspora* and *Rhizoclonium* decreasing.

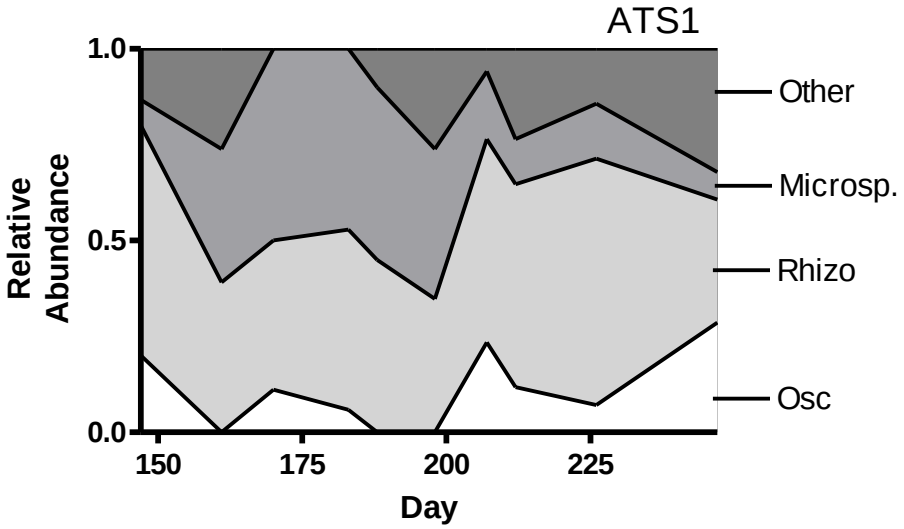

Figure 5. 15. Relative abundance of various algal genera versus day for ATS unit 1 while operating under the automated system and Bristol's nutrient medium.

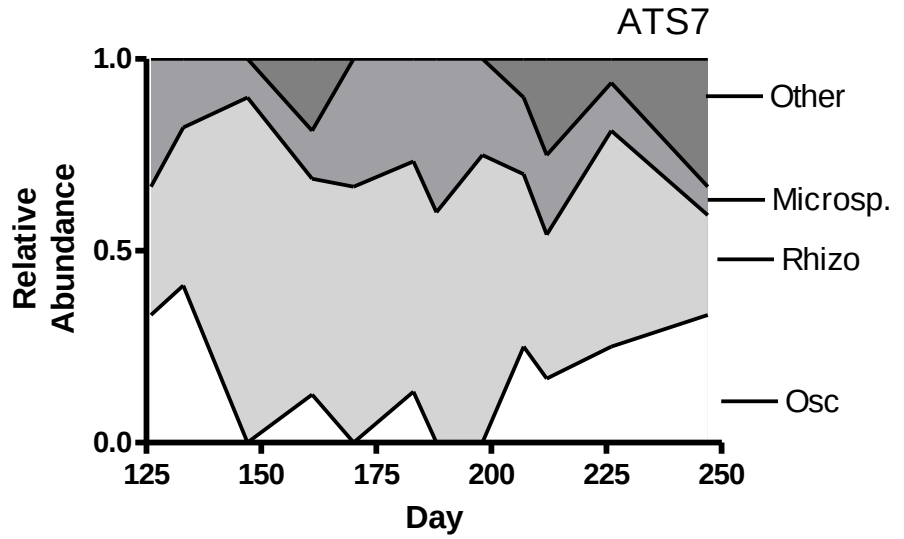

Figure 5. 16. Relative abundance of various algal genera versus day for ATS unit 7 while operating under the automated system and Bristol's nutrient medium.

The mean relative abundance of each of the dominant algal species was calculated for all ATS units operating under Bristol's medium, which included those under standard operating conditions at various set flow rates and those under autonomous control operating conditions. Results are shown in Figure 5. 17. The algae *Rhizoclonium* showed the highest mean relative abundance in ATS unit 2 operating at a flow rate of 25 lpm, which also showed the lowest relative abundance of other species. *Rhizoclonium* and *Oscillatoria* had the lowest mean relative abundance in ATS unit 4 operating at a flow rate of 1 lpm, which also had the highest relative abundance of other algal species. ATS units 1 and 7 operating under autonomous control were both dominated by *Rhizoclonium* at a measured relative abundance that was similar to those measured for the ATS units operating under standard conditions. The distribution of abundance in autonomous ATS1 and ATS7 resembled most closely those observed in ATS1 operating under standard conditions at a flow rate of 125 lpm.

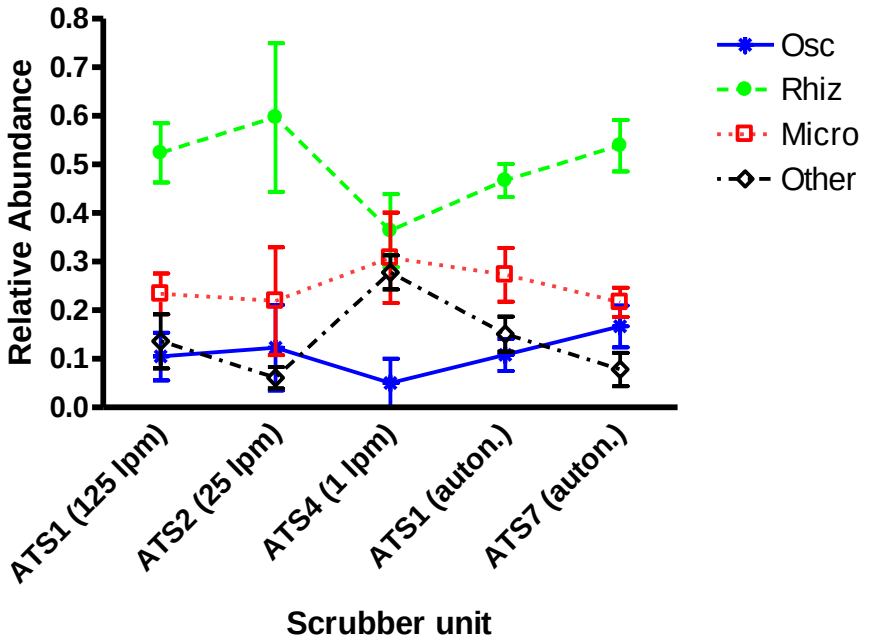

Figure 5. 17. Mean relative abundance for algal genera in ATS units under standard and autonomous operation. All units operated under similar nitrogen loading rates using Bristol's medium.

The aggregated mean of relative abundance for the various species were calculated for the standard and autonomous operational modes and compared to each other (Figure 5. 18). Results show that there is no apparent difference in the relative abundance of the various algal genera between standard and autonomous operation. From standard to autonomous operation, there is a slight rise in the mean relative abundance of *Oscillatoria* and a slight decline in the mean relative abundance of other algal genera. A student's t-test was performed for each of the species comparing the mean relative abundance between standard and autonomous operational modes. In no case were the means significantly different (Table 5. 7).

Table 5. 7. Results of t-tests for cumulative mean and SEM of relative abundances of various algal genera for autonomous and standard operating modes.

Algal Genus	Autonomous			Standard			t	Df	P
	μ	SEM	n	μ	SEM	n			
Osc	0.140	0.0278	22	0.0928	0.0353	12	1.032	32	0.310
Rhiz	0.506	0.0330	22	0.495	0.0638	12	0.1788	32	0.859
Micro	0.242	0.0298	22	0.254	0.470	12	0.2215	32	0.826
Other	0.111	0.0253	22	0.158	0.343	12	1.099	32	0.280

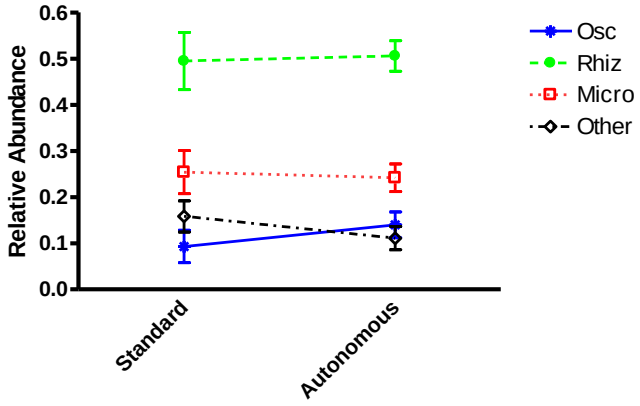

Figure 5. 18. Aggregated mean relative abundance for algal genera in ATS units under standard and autonomous operation. All units operated under similar nitrogen loading rates using Bristol's medium.

Discussion

Evolution and display of the seeking behavior

The operation of the control system employing the seeking algorithm operated as expected when programming bugs and operational protocols were worked out. The algorithm focused on seeking the lowest possible Pump State for the highest measured productivity, the convention of minimization of pump state programmed into the algorithm. This was shown in the operation of many of the operational trials considered as successful. For example, for Trials 1-6 and 1-7 (Figure 5. 5, page 204), the operation of the algorithm, throughout the trace of the Pump State versus cycle, exhibited the

expected behavior in all cases: it maintained the direction of Pump State increment as NCP was found to increase (for example, cycles 1, 2, and 3); reduced the Pump State when NCP was found to stay the same (for example, cycle 4 to 5); and changed the direction of Pump State increment when NCP was found to decrease (for example, cycle 5 to 6). After numerous cycles, the Pump State in general decreased as a result of the algorithm's minimization convention.

Another nearly successful trial of the control algorithm was exhibited in Trial 7-4 (Figure 5. 9, page 207). In this trial, the Pump State started at state 4, and over the next 11 cycles it circulated around the middle and low Pump States but trending towards lower Pump States. The NCP also varied, which explains the variation in Pump States. The variation in NCP was not entirely explained by the Pump State, however—for example, the peak at cycle 4 was higher than any other NCP. There also appears to be a general net trend downward in NCP over time, where one would expect the system to converge on the highest NCP within the range of Pump States. This trial therefore exhibited the action of the minimization convention, where the NCP at successive states fell within the tolerance for measurement error. The reduction in NCP over successive cycles was possibly the result of some other factor (either limiting or a pollutant) that had accumulating effects over time that was not measured.

The algorithm was demonstrated to be susceptible to failure situations resulting from "false" interpretations of input data. An example of this was observed in trial 5-3, where the average NCP increased at almost every cycle and Pump State change (Figure 5. 7, page 205). These are, however, false readings of NCP, as increasingly large fluctuations in pH level were created because of acidification of the reservoir

(presumably because of nitrification of excess mineral nitrogen in cycles that were overfed) and subsequent pH increase through the manual addition of sodium hydroxide. The large fluctuations in pH contributed to the increased measured change in inorganic carbon (IC) for each diurnal cycle. This was attributed incorrectly by the automated system to algal primary productivity, when a majority of the pH changes were attributable to the pH increases caused by the sodium hydroxide amendments. The resulting effect on algorithm operations on Pump State was the steady decrease in Pump State (Figure 5. 7) as the NCP measured at each subsequent cycle was greater than the last because of ever-increasing pH swings due to acidification and NaOH chemical amendment. This was also evident in the strong negative correlation between biomass and NCP for Trial 5-3 (Figure 5. 8, page 206), explained by the reduced biomass production along with increased swings in pH level created chemically from NaOH addition. The hypothesized mechanism by which this occurs is as follows: when the algal community is stressed, it exhibits less than ideal growth rates, and thus does not completely uptake all the ammonia nitrogen from the water column. With excess ammonia nitrogen in an aerobic environment, nitrification occurs, causing acidification of the water in the reservoir. This more acid environment further stresses the algae and restricts its growth, a positive feedback loop that further prevents the uptake of ammonia-N into the algal biomass. Operator interference to correct the increasingly acid aquatic environment, by way of amendment with sodium hydroxide, caused large sudden increases in pH that the monitoring program interpreted as a sudden decrease in dissolved inorganic carbon and thus registered as a spike in productivity. In this way, the largest measured NCP was associated with the lowest biomass production, and the Pump State

change decisions were made from false information. Overall, the algorithm was shown to operate sufficiently on a physical system but was susceptible to errors, false readings, and general measurement noise on the input data. Further development of the algorithm might entail more smoothing and noise reduction of the pH diurnal signal; assessment of the veracity of productivity values in relation to those expected, based on past performance; and improvement of the fidelity and accuracy of productivity measurements.

A way to visualize the ability of the algorithm to converge on a solution is to generate a phase plot of net carbon productivity or biomass production rate versus pump state. Further, if these data are used to calculate the power of each of these processes, then the phase plots give an indication of a type of efficiency of the system. This type of efficiency—termed the transformity of the of the bioproduction—is thought to trend towards a minimum value in a self-organizing system (Odum 1996). The calculation of the power of the various components focuses on accounting for the energy inputs to the system (lights, turbulent flow energy, nutrients, human intervention) and the bioproduction outputs from the system.

The net energy inputs to the ATS technoecosystem include the lights, turbulent energy, nutrients, human intervention, and material/matter support infrastructure. Because all ATS units were identical in construction and operation during the autonomous experiments and thus the power in the turbulent flow in the ATS bed was the only energetic variable changing throughout, only the power of the flow for each Pump State need be calculated for use in the phase plots. The total power of the turbulent water environment (E_T) is equal to the sum of the power of the base flow rate (E_f) and the energy of the wave surge (E_w):

$$E_T = E_f + E_w$$

The power of the base flow rate is a function of the water velocity, density, and the cross-sectional area of the flow. This can be derived from the equations of the kinetic energy of motion ($E = ½\ mv^2$) and may be expressed as follows:

$$E_f = \frac{1}{2}\rho A v^3$$

where ρ = density of water (1000 kg m^{-3})

A = cross-sectional area of flow (1 m wide by 0.015m deep)

v = velocity of flow (estimated at 0.2 m s^{-1})

The power of the wave surge turbulence can be calculated as a function of the density of water, average wave height, and frequency of the wave surge (Phillips 1977), and may be expressed as follows:

$$E_w = \frac{1}{2}\rho g a^2 f$$

where

ρ = density of water (1000 kg m^{-3})

g = acceleration of gravity (9.8 m s^{-2})

a = average wave height (estimated at 0.075m)

f = frequency of wave (varies for volumetric flow rate)

For the ATS process, estimates for the parameters of the flow include an average water depth of 0.015 m, bed width of 1 m, base flow velocity of 0.2 m s^{-1}, and an average wave height of 0.075 m. With these parameters, the power for each of the Pump State can

be calculated (Table 5. 8) and show that the power delivered is linearly related to the Pump State as a result in the linear increase in wave surge frequency (Figure 5. 19).

Table 5. 8. Total power calculated per second and per day for the flow condition at each Pump State.

Pump state	Flow rate (lpm)	f (min^{-1})	Total energy E_T ($E_f + E_w$) ($J\ m^{-2}\ s^{-1}$)	Total energy E_T ($E_f + E_w$) ($J\ m^{-2}\ d^{-1}$)
0	1	0.09	0.621	5.36E+04
1	20	1.8	1.393	1.20E+05
2	40	3.6	2.206	1.91E+05
3	60	5.5	3.019	2.61E+05
4	80	7.3	3.832	3.31E+05
5	100	9.1	4.646	4.01E+05
6	120	10.9	5.459	4.72E+05
7	140	12.7	6.272	5.42E+05

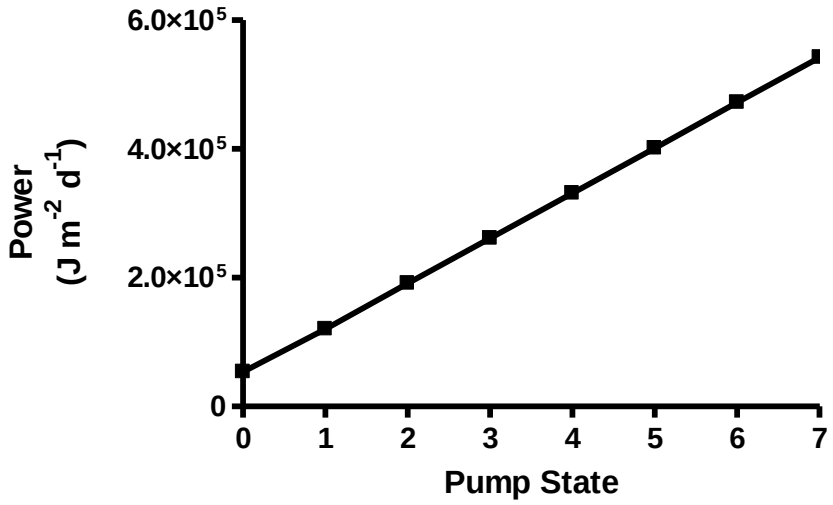

Figure 5. 19. Total power, a combination of that from the wave surge and and base flow velocity, for each Pump State.

The power of bioproduction in the ATS can be calculated from the measurements of the biomass production rate, using the energetic equivalence relationships of 4 kcal g^{-1} of dry weight of biomass (Odum 1996). These calculations were applied to the biomass production rate and corresponding pump state for each of the autonomous experiment

trial runs, and the results were plotted as phase plots of the power of bioproduction versus the power of the Pump State. The results for Trial 1-2 (Figure 5. 3, page 202) were recalculated as the power of bioproduction and plotted versus power of Pump State. These results (Figure 5. 20) show that the pump state converges towards an attractor state where bioproduction is maximized for the lowest possible Pump State.

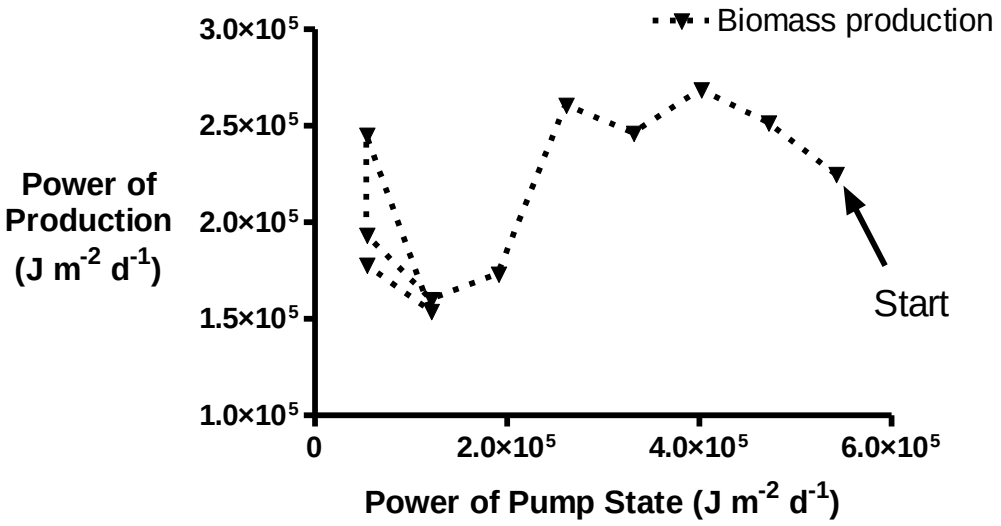

Figure 5. 20. Power of biomass production versus power of Pump State for Trial 1-2.

This analysis was performed on the results from other trials that were deemed as successful (Trial 1-6/7, Figure 5. 5, page 204, and Trial 7-4, Figure 5. 9, page 207), and a similar pattern of convergence is seen for each (Figure 5. 21 and Figure 5. 22).

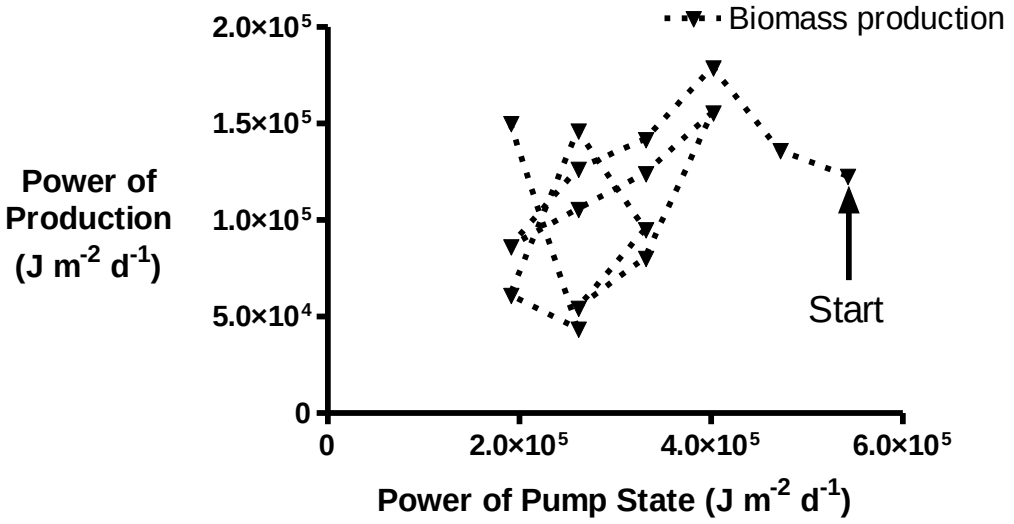

Figure 5. 21. Power of biomass production versus power of Pump State for combined Trials 1-6/1-7.

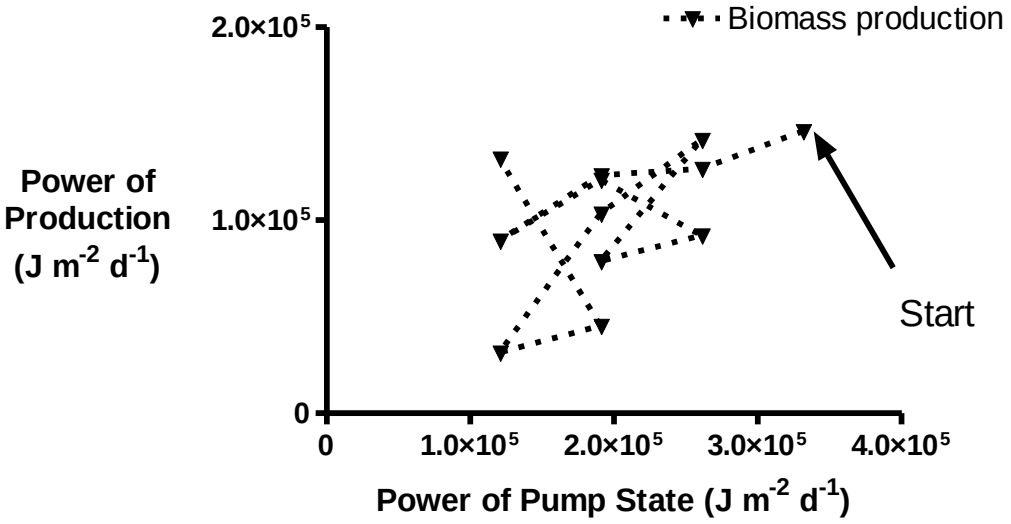

Figure 5. 22. Power of biomass production versus power of Pump State for Trial 7-4.

In each of these trials, results show a converence on the lowest power of Pump State as the power of the bioproduction of the system circulates around and approaches a maximum. The visualization of the ratio of the power of pump state to the power of bioproduction is analogous to the transformity of the bioproduction, that is, the amount of

pumping energy required to produce a certain amount of bioproduction energy (Odum 1996). In each of these trials, the state of the system is attracted around a similar ratio of pump power to production. Each of these plots indicates that the autonomous system seeks a state of lower transformity, but the circulation around an attractor state indicates that it reaches a threshold in that seeking process. This would seem to support the contention that, in the organization of complex systems, self-organization seeks the maximum empower and leads to a thermodynamic minimum for the transformity of an energy storage, in this case, the energy embodied in the algal biomass (Odum 1996).

Difficulties and challenges with system implementation

In many of the trials, it was observed that the correlation between NCP and biomass production rate was low throughout the autonomous trials. The trial with the highest correlation between NCP and biomass production was Trial 5-3 (Figure 5. 8, page 206; $r^2 = 0.9024$), but it was determined that this was based on the false values of NCP interpreted from user manipulation of the reservoir pH through NaOH amendments in times of deleteriously low pH levels. The next highest correlation between NCP and biomass was observed in Trial 7-3/7-4 (Figure 5. 10, page 208; $r^2 = 0.267$), where potential outliers on the low end of biomass production likely skewed the regression analysis. Biomass production rates were comparatively low (5 to 10 g DW m^{-2} d^{-1}) throughout most trials using Bristol's medium with no significant difference observed between Pump States, however, suggesting the likelihood that the distribution of NCP to Pump State under which the physical experiments were operating was closer to a flat distribution with large error rather than the presumed subsidy-stress distribution.

Throughout the operation of the control algorithm on the physical systems, it was observed that the shape and measurement noise of the input distribution (the expected relationship between Pump State and NCP) was an important determinant of the behavior of the control system, as suggested by the virtual trials explained in Chapter 4. A subsidy-stress curve of NCP versus Pump State was expected for the operation of the physical systems, as predicted by the subsidy-stress experiments (for example, Chapter 3, Figure 3.8A, page 97) and idealized in the virtual experiments (see Chapter 4, Figure 4.2A, page 161). It is possible, however, that the distribution of NCP over Pump State more closely resembled a flat distribution (Chapter 4, Figure 4.2B, page 161), as suggested by the rather flat subsidy-stress relationship determined for ATS units operating under Bristol's medium at low turbulence levels (Chapter 3, Figure 3.13, page 112). Also, the results of the subsidy-stress experiments (Figure 3.13) suggest that the variance on the measurements of NCP is rather large compared to the base value of the measurements, further supporting the view that the operation of the algorithm in the physical systems more closely resembles that in response to a flat input distribution with large input error. This is further supported by the mean of NCP and biomass production rate for each of the Pump States and the associated ANOVA analyses (Figure 5. 11 and Figure 5. 12, page 208 and 209, respectively), which indicate a flat relationship between both NCP and biomass production and Pump State (at least for those Pump States—0 through 3—for which data were available). The analysis of the cumulative means and standard errors (Figure 5. 13 and Figure 5. 14, pages 211 and 212), intended to clarify which input NCP-Pump State distribution was most representative of the operational conditions, was inconclusive. All cumulative means of the physical trials fell within the bounds of the

standard error of the Pump State for both the idealized subsidy-stress (Figure 5. 13A) and flat (Figure 5. 13B) input distributions with high input variance. Comparison of the cumulative standard errors of the Pump State from the physical systems trials to those of the virtual trials would seem to indicate a closer relationship with the subsidy-stress Pump State distribution (Figure 5. 14A) than with the flat distribution (Figure 5. 14B), as two of the trials (Trial 1-6/1-7 and Trial 7-4) fell within the bounds of the expected value for the former but only one (Trial 7-4) fell within the bounds of the latter. This analysis remains inconclusive, however, as there is too much overlap between the expected values of the means or the standard errors of the Pump State for the two input distributions because of the overall low number of cycles. One would need from 50 to 100 cycles of the control algorithm on a physical system to be able to discern the trend in Pump State where the metrics of cumulative mean and standard error would yield enough information to allow this comparison.

Other possible failures of the system can point to ways to improve the methodology and the overall automated control system. The measured NCP was seen to be sensitive to other factors besides bed turbulence (as set by the Pump State). However, noise was often generated in the pH signal, and NCP was itself very noisy when measurements were of high fidelity. Thus there is a high amount of variation that can be expected at any one Pump State. The actions of Pump State changes are thus not appreciably different from operating on random input data. Given this amount of variation, one would expect a general trend downward in the Pump State because of the algorithm's minimization convention. Another potential flaw was exhibited by Trial 7-4 (Figure 5. 9, page 207), which showed a downward trend in NCP throughout many

cycles, even though a general increase in NCP was expected as a general result of the operation of the algorithm. This may possibly be because of inadequate frequency of pH-IC titration. The NCP numbers are calculated using the IC titration from cycle 2 near the beginning of the trial. Possible changes in water chemistry through time (as certain constituents possibly build up in concentration) may cause a drift in the pH-IC relationship that was not accounted for here. Finally, the lack of strong correlation between biomass production rate and measured NCP is not entirely unexpected; this reflected the decoupling of biomass production rate and NCP exhibited in the subsidy-stress experiments (Chapter 3), and noise in the NCP measurements may outweigh the variation seen through the variation of Pump State.

The relationship between species-level organization and technological feedback

In the analysis of the relative abundance of species in the autonomous systems, there was no signal seen in the mean relative abundance and no significant difference seen between autonomously controlled ATS units and the standard operating ATS units. ATS units 1 and 7 showed similar mean relative abundances of all measured algal genera to ATS unit 1 operating in standard mode at 125 lpm (Figure 5. 17, page 215). These values for the autonomously controlled ATS units were also within the middle of the range for all ATS units. This explains why there is no significant difference between the aggregated mean relative abundance of the automated and standard operating modes (Figure 5. 18, page 216). One might expect this, however, due to the change in species mix over time (as shown by the trends in Figure 5. 15 and Figure 5. 16, page 213) in response to the changes in the energy signature of the ATS system (through the changes in the turbulence level), which itself changes in response to change in the net metabolism

of the ecosystem. The system affords the opportunity for autocatalytic feedback to occur until the system finds an absorbing state, which should include a characteristic mix of species ideally adapted to the energy signature incident on the algal turf.

Despite the lack of significant difference in the relative abundance of species between autonomous control and standard operating modes, there is some evidence that the autonomous systems were in the process of organizing to a new state that is particular to the autonomously controlled technological envelope. For both ATS unit 1 and ATS unit 7, an increase in *Oscillatoria* and other species and a decrease in *Rhizoclonium* and *Microspora* were observed near the end of the time period of operation under autonomous control (Figure 5. 15 and Figure 5. 16, pages 213 and 213). Might *Oscillatoria* and other species be more competitive in the autonomously controlled environment? It is possible that some characteristic of the physiology or ecology of *Oscillatoria* positions it to better utilize the information feedback afforded by the control system, allowing this genera to affect change in conditions of the energy signature that are most advantageous for it. Indeed, this phenomenon was observed by Cai (2006), who observed an increased abundance in acid-secreting blue-green algae in those microcosms that developed under automatic control of lights compared to those that did not. Additionally, *Oscillatoria* was already seen to be more competitive at very high or very low range of turbulence levels (Chapter 3, Figure 3. 23C, page 128). Through the minimization convention programmed into the control algorithm, the control system automatically favors the lower end of the turbulence range. One can interpret the overall system as the components internal to it, both technological and ecological, are self-organizing in such a way that the energy signature and ecosystem at the species level are

organizing around each other to find the optimum level of operation. This amounts to a demonstration of the Maximum Power Principle (Odum and Pinkerton 1955), which describes that those subsystems that maximize power—energy use per unit time by the ecosystem—within a self-organizing system will be selected for over time.

Designing biologically-inspired algorithms for further experimentation

The ATS has been demonstrated to be a technological envelope around an ecological system in which the various limiting growth factors of a component of that ecosystem can be easily and individually manipulated for experimental purposes. Somewhere in the state space defined by the range of all *n* limiting factors—for example, light, nitrogen, and flow turbulence—is a region or regions of intersection where algal metabolism is maximized (Figure 5. 23). Within this *n*-dimensional state space, there should exist local maxima as well as a global maximum of the performance of the algal turf.

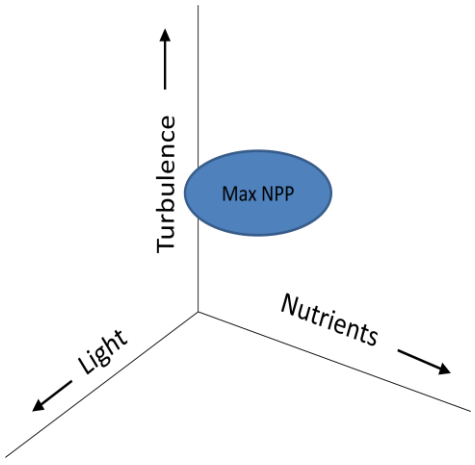

Figure 5. 23. The state space defined by the major limiting factors on the performance of the algal turf ecosystem in an ATS. Somewhere within the state space is a region at the intersection of defined levels of each factor where the productivity (NPP) of the algal turf is maximized.

Searching the state space to find these regions of maxima could require a tremendous number of replicates because of the large number of possible combinations of setpoint levels for each of the possible limiting factors. An alternate possibility for searching the state space is the use of a genetic algorithm, a type of artificial intelligence programming that takes biological evolution as its motivation, as it allows for random cross-over of characteristics between functional states, random mutation of states, and selection of robust states based upon fitness criteria (Hopgood 2001). A basic, generalized genetic algorithm flow chart is shown in Figure 5. 24, from which a summary of operation can be distilled from (Hopgood 2001). The algorithm requires that a search space be defined that includes each condition to be tested (in this case, each of the limiting factors). Each point in the search space is coded to be made up of "genes"—values addressing each point in the state space. Each point in the state space is to be evaluated for fitness according to a fitness function (in this case, possibly algal productivity). Upon randomly generating an initial population of state space points (representing various combinations of limiting factor setpoints), the points are evaluated according to fitness. Individual states are "mated" by combining portions of their genes, where those states evaluated as more fit, through the use of an objective "fitness" function, have a higher probability of genetic crossover. Random mutation of states is performed with another probability function, and then a new population is generated with the new set of states determined by the genes. The loop is iterated until all states converge upon an optimum best solution. Using this in an ATS control scenario as employed in this research, it might be expected that the state space of all possible combinations of limiting factors will converge upon the space of maximum net primary

productivity. The genetic algorithm mimics biological processes of evolution and thus incorporates a level of autonomy to the technoecosystem design; an algorithm as such would exhibit a measure of self-organization in response to the ecological organizational processes. The two components would self-organize around each other, in effect attaining a minimal level of 'homeostatic coupling' (Odum 1993) that is central to the technoecosystem concept.

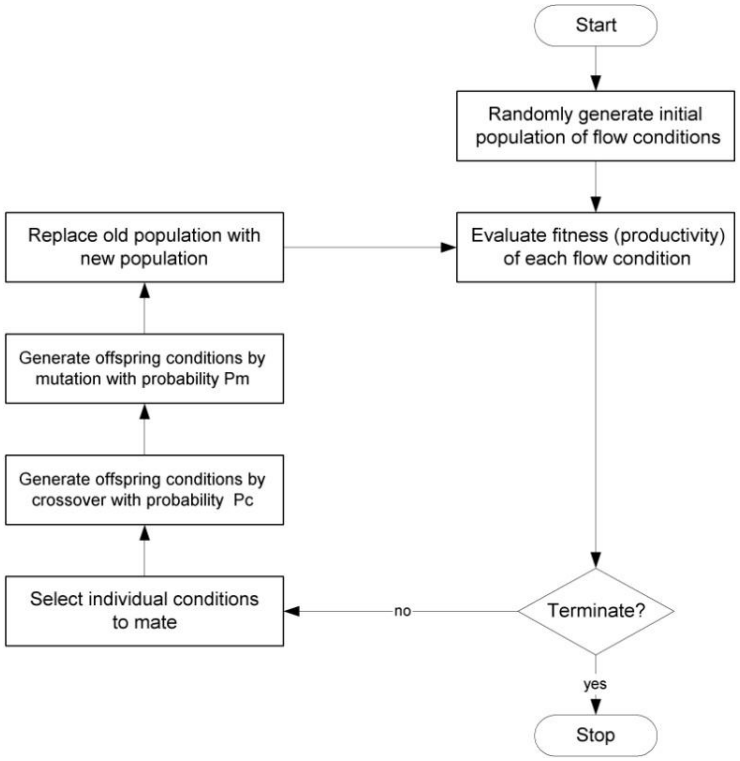

Figure 5. 24. Flow chart for general genetic algorithm that might be adapted for adaptive optimization of ATS productivity via flow rate manipulation (adapted from Hopgood (2001)).

For adequate performance of a genetic algorithm population of 50 to 500 replicates is needed (Hopgood, 2001), a prohibitive number for laboratory experimentation based upon availability of equipment and operator time. Thus, an autonomous ATS scenario employing a genetic algorithm might use a population of 50 virtual replicates generated using a calibrated systems model developed from that

proposed in Chapter 2. In this scenario, each virtual replicate might test a different set of light, flow rate, and nutrient loading conditions. Prior to the generation of the new population of operating conditions to be tested, a subset of the most fit combinations of conditions (based upon the fitness function) can be tested on a number of physical units in the laboratory, analyzing for average productivity. The most fit of these physical conditions would then be assigned an additional factor modifying and increasing the probability function that offspring from that set of conditions will be transferred to the new population of conditions. A new population is generated, and the genetic algorithm is run again on virtual replicates. This experiment might continue until convergence on a set of conditions for the limiting factors is seen. This type of system might also be adaptable to changing environmental conditions—for example, changing ambient temperatures that might make one algal species more competitive over another and affecting the ecosystem metabolism as measured by the pH diurnal.

Conclusions and Implications

The following conclusions can be made for this set of experiments:

- Experiments with the automated control system implemented on a physical ATS unit demonstrated that the control system operated as anticipated, seeking the highest net carbon productivity (NCP) at the lowest volumetric flow rate.
- The activity of the control algorithm was strongly dependent on the characteristics of the input distribution of NCP to flow rate, to the strength of this relationship, and to the variance in the measurement of the controlled parameter (NCP).
- The ATS technoecosystem did show signatures of convergence, as Pump State was minimized over a number of cycles. The system sought the energetic minimum for a

maximum level of bioproduction, amounting to a trajectory of development seeking the maximum efficiency for the bioproduction process.

- Each of the autonomously controlled ATS units showed a change in the relative abundance of algal species over time favoring the blue-green *Oscillatoria* over other green algal species.

The difficulties observed in operating the system suggest various avenues for improvement. For example, while it was expected that the distribution of NCP versus Pump State would follow a subsidy-stress relationship as observed in previous experimentation with the ATS units, the distribution of both NCP and biomass production rate seemed to be defined more as a distribution that was flat over most of the range of flow rate. Additionally, a large amount of measurement noise was expected and observed; these could be addressed and minimized through the adoption of better methodologies—for example, through more frequent titration for the IC-pH curve. The system also proved sensitive to false and inaccurate readings due to electrical noise or to drifting acid-base chemistry of the process water. Developing contingency operations for the algorithm for this situation is one recommendation for improvement of the system. Despite these difficulties in the engineering of the system, the ATS technoecosystem did show signatures of convergence, as Pump State was minimized over a number of cycles. Many more cycles than could be tested here, however, would be required to show the characteristics of convergence.

The shift in the relative abundance of algal species over time in each of the autonomously controlled ATS units is a promising avenue for further research. It was

noted that there was a trend developing throughout the number of cycles that favored the blue-green *Oscillatoria* over other green algal species. Although this trend was not reflected in the aggregate mean comparisons between standard and autonomous modes of operation, a trend analysis is warranted to determine the strength of this relationship; preliminary analsysis along these lines suggests that the increasing trend in *Oscillatoria* is significant. This leads to the implication that the ATS system is internally organizing through a change in the relative abundance of algal species such that the algal community can best take advantage of the engineered information feedback afforded by the control system. In this way, the ATS unit coupled with the feedback control system fits the minimal definition of a technoecosystem in which the subunits are homeostatically coupled. While improvements to the monitoring and control components of the system can certainly be suggested, the system in its current state can be considered to be a platform on which more complex decision-making algorithms can be developed and employed. This may help to increase the utility of the ATS in remote deployments as a caretaker technological system helps the ATS ecosystem maintain a homeostasis for maximized productivity in a changing environment. The ATS technoecosystem platform may also be developed into a standard experimental unit for testing of fundamental organizing principles of more complicated techno-ecological hybrids.

Chapter 6: Conclusions and Implications

Research Conclusions

With the engineering of complex self-organizing biosystems as a new field of endeavor, the design and constructions of complex systems that hybridize ecological entities within or coupled to a technological envelope is an emerging formal field of study in ecological engineering The research pursued here supports the development of an autonomous and internally-controlled technoecological hybrid, based on an algal turf ecosystem, which intermingles engineered feedback control programming with internal feedback patterns within the ecosystem. Following a mode of analysis that seeks to understand and merge systems-level principles for the component technological and ecological system, the research sought to investigate the characteristics of the ecosystem in response to potential limiting factors that were incident upon it, the nature of the technological system designed to interface with it to maximize ecosystem performance, and the characteristics of the combined techno-ecological hybrid as an internally-coupled self-organizing system.

Chapter 2: Preliminary Investigations

Preliminary investigations were undertaken to understand the role of bed turbulence, as determined by flow rate and wave surge frequency, as a limiting factor to the productivity of the algal turf in an algal turf scrubber receiving a range of nutrient-loading rates. Turbulence in the ATS unit was recognized to have components related to both volumetric flow rate and wave surge frequency, and each were manipulated independently on an algal turf scrubber operating under different nitrogen loading rates. The effects of different levels of turbulence on the rate of production of algal biomass

production rate were measured via regular periodic biomass harvest. Turbulence of the flow in an ATS was an important factor in the maximization of algal growth, acting as limiting to algal production when other factors were provided in abundance. The following conclusions were made based upon this set of experiments:

- Turbulence acts as a limiting factor to the algal biomass production in an ATS when other factors are provided in abundance.
- Wave amplitude is a stronger factor than wave frequency on determining the biomass production of algae in an ATS, and biomass production is maximized when the combination of wave surge amplitude and frequency is optimized.
- Increased turbulence affects the mass transfer at the scale of the algal turf thickness and is one mechanism for stimulating the overall biomass productivity, although it cannot be concluded that this is the only mechanism.

Chapter 3: The Ecosystem

This set of experiments was undertaken to investigate the effect of turbulence on the ecosystem metabolism—net primary production, respiration, and the ratio of these—of an algal turf in an ATS system. Measurements were design to measure the primary productivity (as net carbon productivity) and respiration of the ATS ecosystem and investigate its response to changes in turbulence levels. The wave surge frequency was manipulated on a set of ATS units while an automated monitoring system recorded the pH diurnal in each ATS, and then converted to an inorganic carbon concentration diurnal using information derived from titration of ATS process water and from which ecosystem metabolic measures were calculated. The data were used to investigate the relationship between the correlation between the metabolic measures and biomass production. Also,

the relative abundance of dominant algal genera were measured from each ATS growth bed for a preliminary investigation into their relative competitiveness under combinations of operating conditions. The following conclusions were made based on this set of experiments:

- Tturbulence was shown to be a limiting factor to productivity, respiration, and biomass production when light and nutrient loading rate are greater.
- Productivity and respiration were shown to follow a subsidy stress relationship, although the effect was more pronounced at lower light and nutrient loading conditions.
- The relative abundance of the dominant genera of algae where shown to be a function of the level of turbulence, with each of the main genera most dominant within a characteristic zone of flow rate.

Chapter 4: The Technosystem

Virtual testing was employed to experiment with and understand the behavior of the supervisory control algorithm for the technoecosystem, a simple seeking algorithm designed to find the maximum of a dependent variable over the range of variation of an independent variable subject to feedback control. The algorithm was tested using hypothetical stochastic distributions of ecosystem productivity versus flow turbulence as virtual input data to investigate the accuracy and rate of algorithm convergence on the expected solution for various conditions. The following conclusions were made from this set of experiments:

- The algorithm has the ability to seek for and find the maximum of a parameter at the lowest possible Pump State over a range of distribution relationships.

- The actions and effectiveness of the algorithm, as measured by the rate of convergence, are strongly influenced by the variance of the input data to which it responds and by the strength of the relationship between the controlled parameter and the measured variable.

Chapter 5: The Technoecosystem

Analysis of each of the component subsystems in previous sections led to assembly and testing of the full algal turf scrubber technoecosystem. The system was tested in multiple trials through numerous harvest cycles in which the Pump State and net primary productivity were recorded and analyzed for convergence. The expected behavior of the system was for it to track the subsidy-stress curve for net primary productivity related to flow turbulence to find the flow rate where net primary production was maximized. Analysis of the system behavior consisted of analyzing the convergence of the time-trace of productivity and Pump State and comparing them to those expected as determined by the virtual algorithm experiments. Also, the relative abundances of the dominant algal species were tracked throughout the trials and compared to those measured for ATS units operating in a standard mode without feedback control. The following conclusions can be made from this set of experiments:

- The automated control system implemented on a physical ATS unit operated as designed, seeking the highest productivity at the lowest volumetric flow rate.
- The activity of the control algorithm was found to be strongly dependent on the characteristics of the input distribution of productivity to flow rate, and this relationship was observed to be flat over most of the range of flow rate.

- The ATS technoecosystem showed rudimentary signatures of convergence, as Pump State was minimized over a number of cycles, and the system trended toward a state of maximum efficiency for the production of algal biomass.
- The relative abundance of algal species shifted over time in the autonomous units, seemingly in response to the novel engineered feedback loops.

Avenues for futher study

Based on the experiments pursued in this research, a number of avenues for further research can be recommended.

First, further investigation is necessary to confirm the mechanism by which turbulence increases overall algal production in an ATS. While the research here suggests that turbulence helps to overcome diffusion limitations into the algal turf, results of the experiments could not exclude the possibility that increased light availability in a turbulent environment was also a factor. More research is warranted to determine the relative contribution of these factors to overall productivity.

Second, the metabolic measurement were lower than expected and became more decoupled from the biomass production rate measurements as light and nutrient loading were increased. There was evidence that gas transfer across the air-water interface, assumed to be insignificant, may in fact be a consideration in measurements of metabolism during conditions of high turbulence. More research is necessary to determine the relative influence of air-water gas transfer on the pH diurnal method to refine the metabolism measurements.

The control system overall could be improved through the reduction of measurement noise, through improved filtering of the signal, and through the

improvement of core methodologies, such as more frequent titration for the pH diurnal method of metabolism. Additionally, the ATS technoecosystem might be run through longer and more harvest cycles to further investigate the trajectory of convergence.

Finally, it may be important to understand the role of the species-level organization in the aggregate metabolism of the ATS ecosystem for better understanding of the system-level operation of the ATS technoecosystem. More research is suggested to determine the importance in the shift of species abundance in response to the feedback control mechanisms engineered for the ATS system.

Overall Conclusions and Implications

The ATS technoecosystem is in its rudimentary stages of autonomy, as the coupling between technological and ecological remains mostly behavioral. Elements of this research, however, do suggest that the principles of self-organization apply to the hybridized self-organizing system and that complex internal organization is possible between the components of such a system. In these experiments, the algorithm showed signs of convergence that were reminiscent of the decision processes of a human operator, responding to the physiological condition of the ecological system in its care. The ecological system showed signs of internal organization in response to the novel feedback networks supplied to it that are expressed at the species level, similar to the dynamics found by other researchers in technoecosystem engineering. The changes in relative abundance of algal species observed in the automated ATS system suggest a measure of internal organizing such that the ecosystem can best take advantage of the engineered information feedback afforded by the control system. If these changes in internal structure in response to the presence of the technological system are indeed

persistent characteristics mediated by the competitive exclusion of one or a few dominant algal species, might these species be considered to be pre-adapted (Kangas 2004) to the information processing subcomponent of the technosphere? As invasive and weedy species are often interpreted to be pre-adapted to the unstable, disturbed environments created by human impact on the landscape, is there a class of species that are pre-adapted to take advantage of the increased rate and complexity of information processing in modern human society? Experiments with technoecosystem microcosms such as undertaken and further proposed in this research may supply a class of experimentation with complex adapting systems unavailable at the larger scale, yet which may provide understanding into the general rules of organization that must operate at scales ranging from the microscopic to the global.

Appendix A: Data Acquisition and Control Program

The pH data acquisition and control program is designed to monitor the net primary productivity of an aquatic system, based upon the pH diurnal method, and take action on a set of pumps to affect the turbulence within the aquatic system to optimize the flow turbulence regime for maximum net primary productivity. The algorithm of the control program may be considered to consist of two main parts—one that monitors the pH diurnal in an aquatic system and calculates the real-time change in net primary productivity, and one that takes control action on pumps (or other external 'motivator' mechanisms). The monitoring part of the algorithm is shown in Figure A. 1. The system takes user inputs, sets up the initial conditions for starting, and begins recording the pH diurnal. Using the CO_2-pH titration polynomial, it converts pH readings to inorganic carbon concentration (IC), and then tracks changes in IC as a measure of production and respiration. So long as total time since the start of the cycle is less than the user-defined N (the number of days to track P or R for comparison with the previous cycle), the algorithm loops back to record another pH data point; otherwise, it advances on to the flow control portion.

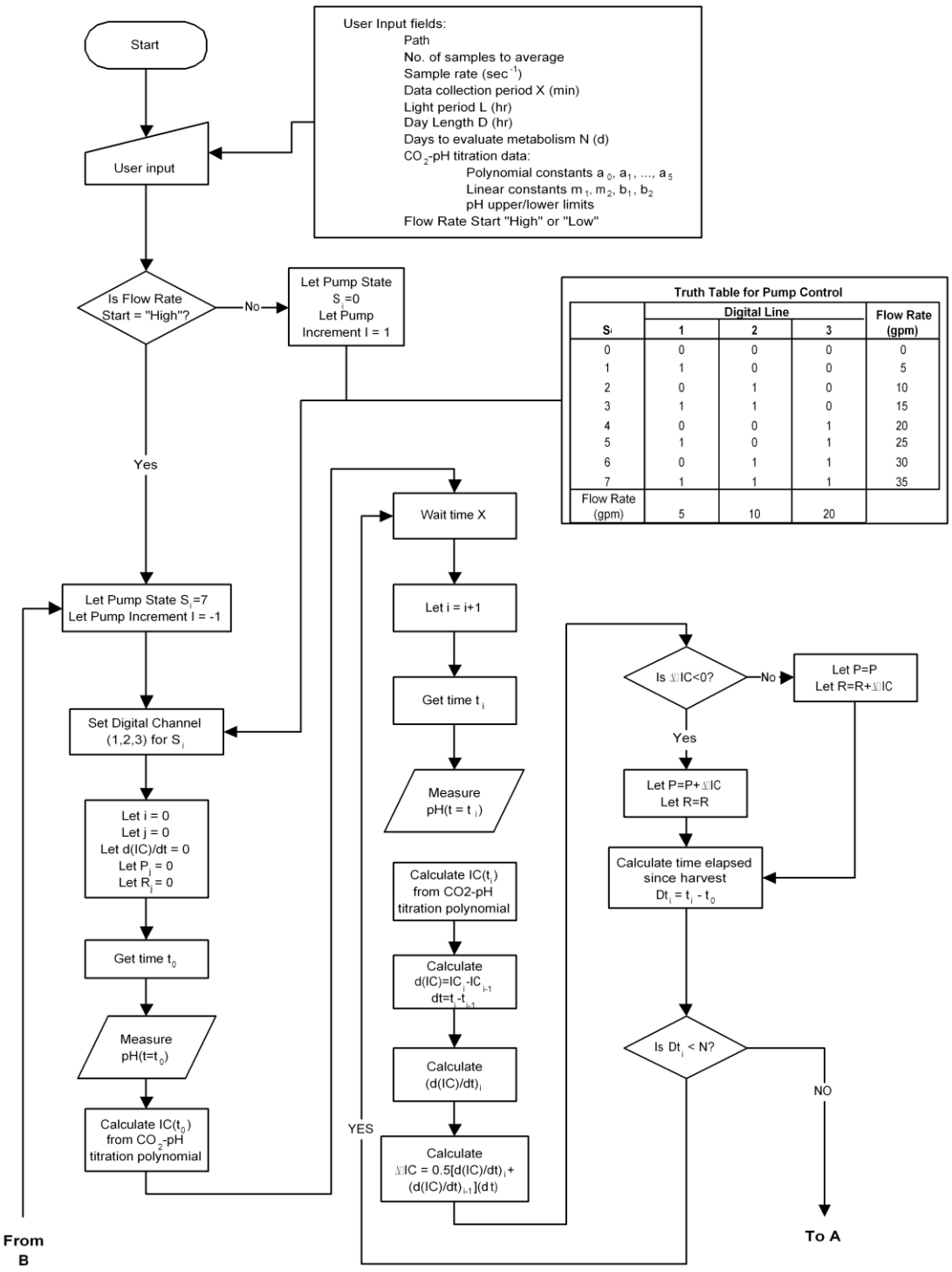

Figure A. 1. Detailed flow chart of the flow control algorithm at the core of the Labview control system, showing the portion that monitors the net primary productivity based on the pH diurnal method.

The flow control portion of the algorithm is shown in Figure A. 2. This portion activates following the completion of the data acquisition portion's cycle for collecting multi-day data on metabolism. Upon activation, it prints screen messages allowing for user input to update the IC-pH titration polynomial estimate, and then increments or decrements the Pump State based upon the value of productivity (P) this cycle compared to that determined for the previous cycle. Should the P measured this cycle be the same (within an arbitrary tolerance) to that of last cycle, the Pump State is automatically decremented, thus trending the flow rate to the least possible energy input for otherwise metabolically-equivalent conditions. Should the measured P be significantly different greater this cycle compared to last cycle, the Pump State is changed in the same direction as the previous change (I_i), otherwise the Pump State is changed in the opposite direction ($-I_i$). Following conventions on what to do at the extremes Pump States (0 and 7), the Pump State is returned to the start of the program for activation/deactivation of the appropriate digital lines, and the entire large loop of multi-day pH monitoring begins again.

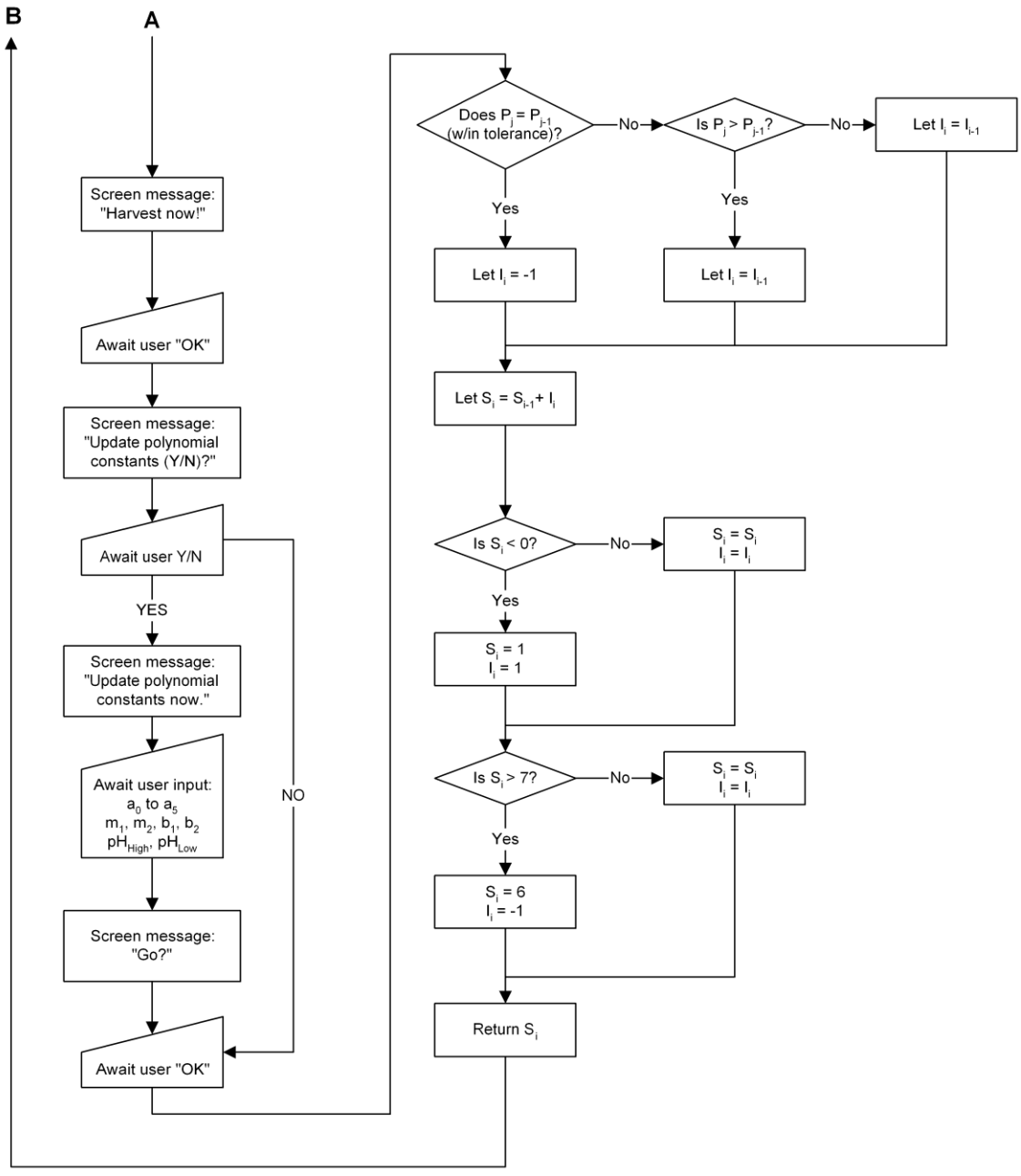

Figure A. 2. Flowrate control portion of the control algorithm employed in Labview. "A" and "B" connect to the corresponding terminals labeled in Figure A. 1.

Appendix B: Full Results for Subsidy-Stress Investigations

Subsidy-Stress Metabolic and Production measurements: Data Tables

Table B. 1. Table of results of calculated productivity (P), respiration (R), P/R ratio, and measured biomass for all replicates, means, and standard deviations (SD) at various flow rates and measured dump bucket tipping frequency for *low light/low NLR (manure)* conditions. Blank values indicate "no data" for that trial.

Parameter	Nom. Flow Rate (gpm)	Tip Freq. (min^{-1})		Trials								Statistics		
		Mean	SD	1	2	3	4	5	6	7	8	Mean	SD	n
Productivity ($gC\ m^{-2}\ d^{-1}$)	0.25	0.1	0.00	-1.00	-1.83	-1.01	-1.34	-1.16	-1.71	-1.07	-0.59	-1.21	0.40	8
	1	0.3	0.11	-1.22	-2.24	--	-1.11	-2.17	-1.31	-2.00	-1.68	-1.68	0.47	7
	7	2.7	0.16	-1.55	-1.23	-1.38	-1.90	-2.16	-1.77	-2.37	-2.16	-1.82	0.40	8
	35	11.5	NA	-0.46	--	-0.46	-0.63	-1.02	-0.72	-0.63	-0.67	-0.65	0.19	7
Respiration ($gC\ m^{-2}\ d^{-1}$)	0.25	0.1	0.00	0.91	1.64	1.09	1.34	1.11	1.61	0.99	0.62	1.16	0.35	8
	1	0.3	0.11	1.22	2.58	--	1.24	2.00	1.30	1.93	1.76	1.72	0.50	7
	7	2.7	0.16	1.60	1.40	1.43	2.07	2.23	1.89	2.49	2.30	1.93	0.41	8
	35	11.5	NA	0.46	--	0.50	0.59	0.94	0.67	0.64	0.64	0.63	0.16	7
P/R	0.25	0.1	0.00	1.10	1.11	0.93	1.00	1.04	1.06	1.09	0.95	1.04	0.07	8
	1	0.3	0.11	1.00	0.87	--	0.90	1.08	1.01	1.03	0.96	0.98	0.08	7
	7	2.7	0.16	0.97	0.88	0.97	0.92	0.97	0.94	0.95	0.94	0.94	0.03	8
	35	11.5	NA	1.00	--	0.93	1.07	1.09	1.06	0.98	1.04	1.02	0.06	7
Biomass Production ($gDW\ m^{-2}\ d^{-1}$)	0.25	0.1	0.00	7.8	9.0	9.5	8.6	10.4	9.2	5.8	8.0	8.5	1.4	8
	1	0.3	0.11	9.6	7.8	7.4	11.4	10.8	9.7	9.9	9.9	9.5	1.4	8
	7	2.7	0.16	11.0	12.5	8.3	13.5	14.0	11.9	9.0	8.0	11.0	2.4	8
	35	11.5	NA	11.1	8.7	8.8	9.3	5.2	3.7	3.0	--	7.1	3.1	7

Table B. 2. Table of results of calculated productivity (P), respiration (R), P/R ratio, and measured biomass for all replicates, means, and standard deviations (SD) at various flow rates and measured dump bucket tipping frequency for a *redo of low light/low NLR(manure)* conditions following the cutting and mixing of ATS growth screens. Blank values indicate "no data" for that trial.

Parameter	Nom. Flow Rate (gpm)	Tip Freq. (min^{-1})		Trials					Statistics		
		Mean	SD	1	2	3	4	5	Mean	SD	n
Productivity ($gC\ m^{-2}\ d^{-1}$)	0.25	0.1	0.0	--	-0.90	-1.07	-0.48	-0.84	-0.82	0.25	4
	1	0.4	0.1	-0.51	-0.76	-0.66	-0.71	--	-0.66	0.11	4
	7	2.6	0.1	-0.73	-0.97	-0.78	-0.84	-0.77	-0.82	0.09	5
	35	11.5	0.3	-0.17	-0.20	-0.19	-0.26	-0.23	-0.21	0.03	5
Respiration ($gC\ m^{-2}\ d^{-1}$)	0.25	0.1	0.0	--	0.54	0.92	0.60	0.57	0.66	0.18	4
	1	0.4	0.1	0.47	0.56	0.66	0.59	--	0.57	0.08	4
	7	2.6	0.1	0.65	0.80	0.72	0.70	0.67	0.71	0.06	5
	35	11.5	0.3	0.15	0.18	0.19	0.24	0.22	0.19	0.03	5
P/R	0.25	0.1	0.0	--	1.68	1.16	0.80	1.47	1.28	0.38	4
	1	0.4	0.1	1.10	1.36	1.01	1.22	--	1.17	0.15	4
	7	2.6	0.1	1.12	1.22	1.09	1.20	1.16	1.16	0.05	5
	35	11.5	0.3	1.15	1.09	1.03	1.09	1.04	1.08	0.05	5
Biomass Production ($gDW\ m^{-2}\ d^{-1}$)	0.25	0.1	0.0	6.4	12.4	13.3	8.6	13.0	10.8	3.1	5
	1	0.4	0.1	9.6	9.6	10.1	11.1	10.9	10.3	0.7	5
	7	2.6	0.1	11.0	13.0	11.8	12.8	11.4	12.0	0.9	5
	35	11.5	0.3	8.9	7.9	7.4	10.4	7.0	8.3	1.4	5

Table B. 3. Table of results of calculated productivity (P), respiration (R), P/R ratio, and measured biomass for all replicates, means, and standard deviations (SD) at various flow rates and measured dump bucket tipping frequency for *high light/low NLR (manure)* conditions. Blank values indicate "no data" for that trial.

Parameter	Nom. Flow Rate (gpm)	Tip Freq. (min^{-1})		Trials				Statistics		
		Mean	SD	1	2	3	4	Mean	SD	n
Productivity ($gC\ m^{-2}\ d^{-1}$)	0.25	0.04	0.01	-0.78	-1.14	-1.40	-2.44	-1.44	0.71	4
	1	0.3	0.0	-1.43	-1.42	-2.44	-1.79	-1.77	0.48	4
	7	2.7	0.0	-1.46	-0.86	-2.04	-1.49	-1.46	0.48	4
	35	11.5	0.6	-0.53	-0.38	-0.70	-0.91	-0.63	0.23	4
Respiration ($gC\ m^{-2}\ d^{-1}$)	0.25	0.04	0.01	0.55	0.88	1.12	1.71	1.06	0.49	4
	1	0.3	0.0	1.13	1.19	2.00	1.65	1.49	0.41	4
	7	2.7	0.0	1.17	0.80	1.90	1.45	1.33	0.47	4
	35	11.5	0.6	0.49	0.42	0.81	0.96	0.67	0.26	4
P/R	0.25	0.04	0.01	1.41	1.30	1.25	1.43	1.35	0.09	4
	1	0.3	0.0	1.26	1.20	1.22	1.08	1.19	0.08	4
	7	2.7	0.0	1.24	1.08	1.07	1.03	1.11	0.09	4
	35	11.5	0.6	1.09	0.91	0.87	0.95	0.95	0.10	4
Biomass Production ($gDW\ m^{-2}\ d^{-1}$)	0.25	0.04	0.01	15.6	11.2	11.9	12.0	12.7	2.0	4
	1	0.3	0.0	14.0	11.5	13.9	18.0	14.4	2.7	4
	7	2.7	0.0	15.8	11.4	16.4	13.7	14.4	2.3	4
	35	11.5	0.6	14.4	12.5	15.1	13.0	13.7	1.2	4

Table B. 4. Table of results of calculated productivity (P), respiration (R), P/R ratio, and measured biomass for all replicates, means, and standard deviations (SD) at various flow rates and measured dump bucket tipping frequency for *high light/medium NLR (manure)* conditions. Blank values indicate "no data" for that trial.

Parameter	Nom. Flow Rate (gpm)	Tip Freq. (min^{-1})		Trials								Statistics		
		Mean	SD	1	2	3	4	5	6	7	8	Mean	SD	n
Productivity ($gC\ m^{-2}\ d^{-1}$)	0.25	0.03	0.00	-0.47	-0.48	-0.36	-0.97	-0.80	-0.69	-0.67	-0.57	-0.63	0.20	8
	7	2.74	0.10	-1.57	-1.45	--	-1.08	-0.77	-1.19	-1.29	-1.42	-1.25	0.27	7
	35	10.10	1.09	-0.93	-0.92	-0.65	-1.02	-1.05	-1.07	-1.23	-1.24	-1.01	0.19	8
Respiration ($gC\ m^{-2}\ d^{-1}$)	0.25	0.0	0.00	0.41	0.53	0.48	0.96	0.81	0.75	0.62	0.56	0.64	0.19	8
	7	2.7	0.10	1.59	1.41	--	1.07	0.89	1.21	1.22	1.34	1.25	0.23	7
	35	10.1	1.09	0.79	0.82	0.67	1.00	1.06	1.03	1.12	0.89	0.92	0.15	8
P/R	0.25	0.0	0.00	1.14	0.92	0.75	1.01	0.99	0.92	1.08	1.02	0.98	0.12	8
	7	2.7	0.10	0.99	1.03	--	1.01	0.87	0.98	1.06	1.06	1.00	0.07	7
	35	10.1	1.09	1.17	1.11	0.98	1.02	1.00	1.04	1.09	1.40	1.10	0.14	8
Biomass Production ($gDW\ m^{-2}\ d^{-1}$)	0.25	0.0	0.00	19.8	17.2	18.5	18.0	16.4	21.6	24.0	19.5	19.4	2.5	8
	7	2.7	0.10	28.9	13.2	25.1	20.1	18.2	29.6	24.9	27.8	23.5	5.8	8
	35	10.1	1.09	27.9	22.1	28.7	24.7	21.3	33.0	25.5	35.7	27.4	5.1	8

Table B. 5. Table of results of calculated productivity (P), respiration (R), P/R ratio, and measured biomass for all replicates, means, and standard deviations (SD) at various flow rates and measured dump bucket tipping frequency for *high light/high NLR (manure)* conditions. Blank values indicate "no data" for that trial.

Parameter	Nom. Flow Rate (gpm)	Tip Freq. (min^{-1})		Trials						Statistics		
		Mean	SD	1	2	3	4	5	6	Mean	SD	n
Productivity ($gC\ m^2\ d^{-1}$)	0.25	0.03	0.00	-0.62	-1.66	-1.13	-0.46	-0.26	-0.47	-0.77	0.53	6
	7	2.73	0.00	-0.91	-0.57	-0.76	-1.13	-1.03	-0.97	-0.90	0.20	6
	35	11.00	1.41	-0.67	-0.82	-1.29	-0.86	-0.53	-0.48	-0.77	0.30	6
Respiration ($gC\ m^2\ d^{-1}$)	0.25	0.0	0.00	0.61	1.70	1.11	0.34	0.32	0.40	0.75	0.55	6
	7	2.7	0.00	0.93	0.58	0.83	1.05	1.16	0.87	0.90	0.20	6
	35	11.0	1.41	0.60	0.67	1.36	0.69	0.57	0.43	0.72	0.33	6
P/R	0.25	0.0	0.00	1.00	0.97	1.02	1.35	0.80	1.18	1.06	0.19	6
	7	2.7	0.00	0.98	0.99	0.91	1.08	0.89	1.12	0.99	0.09	6
	35	11.0	1.41	1.12	1.22	0.95	1.24	0.92	1.10	1.09	0.13	6
Biomass Production ($gDW\ m^2\ d^{-1}$)	0.25	0.0	0.00	21.3	16.2	23.1	27.6	21.9	29.0	23.2	4.6	6
	7	2.7	0.00	22.1	31.5	35.5	23.1	25.8	36.0	29.0	6.2	6
	35	11.0	1.41	32.5	43.2	41.6	35.3	--	30.5	36.6	5.6	5

Table B. 6. Table of results of calculated productivity (P), respiration (R), P/R ratio, and measured biomass for all replicates, means, and standard deviations (SD) at various flow rates and measured dump bucket tipping frequency for *high light/low NLR(Bristol's solution)* conditions. Blank values indicate "no data" for that trial.

Parameter	Nom. Flow Rate (gpm)	Tip Freq. (min^{-1})		Trials						Statistics		
		Mean	SD	1	2	3	4	5	6	Mean	Std Dev	n
Productivity ($g\ C\ m^2\ d^{-1}$)	0.25	0.1	NA	-0.58	-0.50	-0.54	-0.28	-0.30	-0.42	-0.44	0.13	6
	7	2.8	NA	-1.04	-0.68	-0.53	--	--	-0.36	-0.65	0.29	4
	35	11.7	NA	-0.31	-0.24	-0.23	-0.17	-0.14	-0.22	-0.22	0.06	6
Respiration ($g\ C\ m^2\ d^{-1}$)	0.25	0.1	NA	0.60	0.47	0.49	0.29	0.29	0.41	0.42	0.12	6
	7	2.8	NA	0.91	0.66	0.48	--	--	0.34	0.60	0.25	4
	35	11.7	NA	0.25	0.24	0.21	0.16	0.13	0.20	0.20	0.05	6
P/R	0.25	0.1	NA	0.97	1.08	1.11	0.96	1.03	1.02	1.03	0.06	6
	7	2.8	NA	1.14	1.04	1.10	--	--	1.03	1.08	0.05	4
	35	11.7	NA	1.24	1.01	1.13	1.10	1.10	1.10	1.11	0.07	6
Biomass ($g\ DW\ m^2\ d^{-1}$)	0.25	0.1	NA	2.9	3.8	8.4	5.3	6.0	8.6	5.9	2.3	6
	7	2.8	NA	5.8	6.4	7.2	6.8	8.2	10.4	7.5	1.7	6
	35	11.7	NA	10.2	7.5	8.3	6.9	7.9	8.1	8.1	1.2	6
NLR ($gN\ m^2\ d^{-1}$)	0.25	0.1	NA	0.24	0.54	0.32	0.29	0.64	0.82	0.47	0.23	6
	7	2.8	NA	0.31	0.54	0.86	0.71	0.64	0.86	0.65	0.21	6
	35	11.7	NA	0.31	0.54	0.89	0.86	0.86	1.19	0.77	0.31	6

Linear Regression Analysis of Metabolic versus Biomass Measurements

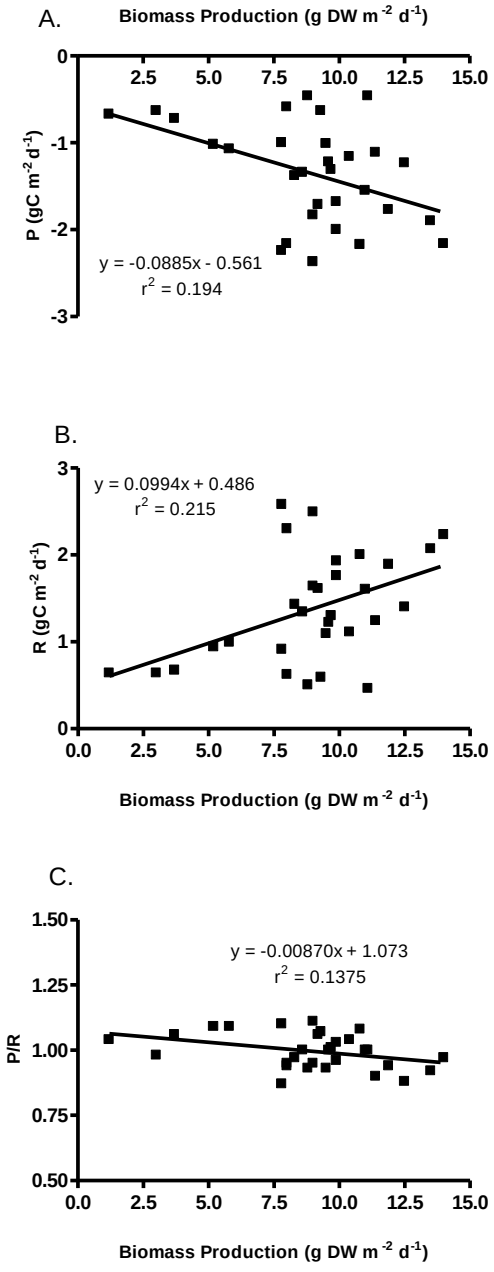

Figure B. 1. Linear regression analysis for operating conditions of (low light, low NLR, manure), showing the following metabolic measurements versus biomass production: (A) primary productivity (P); (B) respiration (R); (C) P/R ratio.

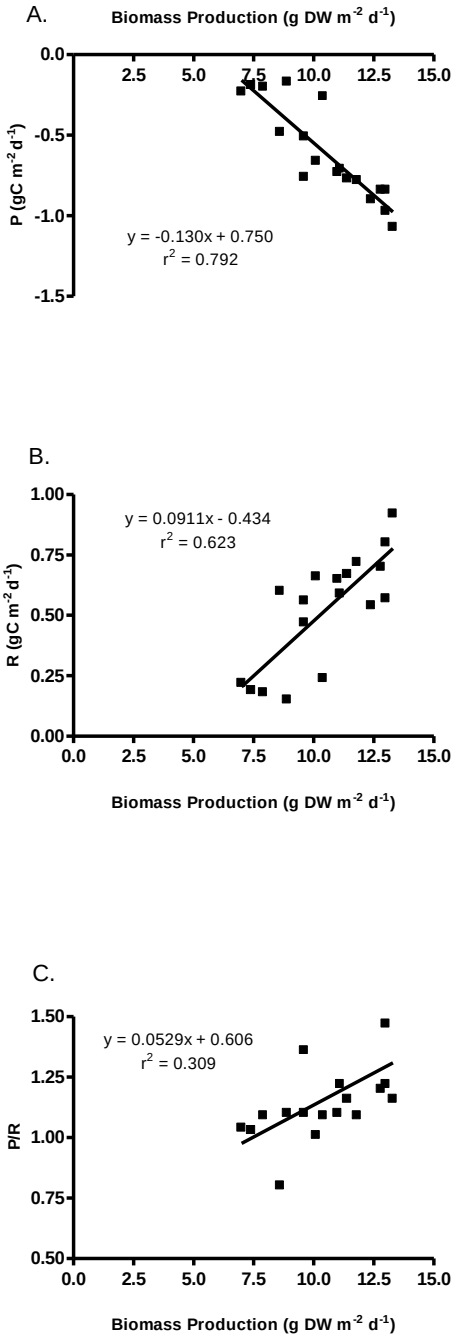

Figure B. 2. Linear regression analysis for the retesting of operating conditions of (low light, low NLR, manure), showing the following metabolic measurements versus biomass production: (A) primary productivity (P); (B) respiration (R); (C) P/R ratio.

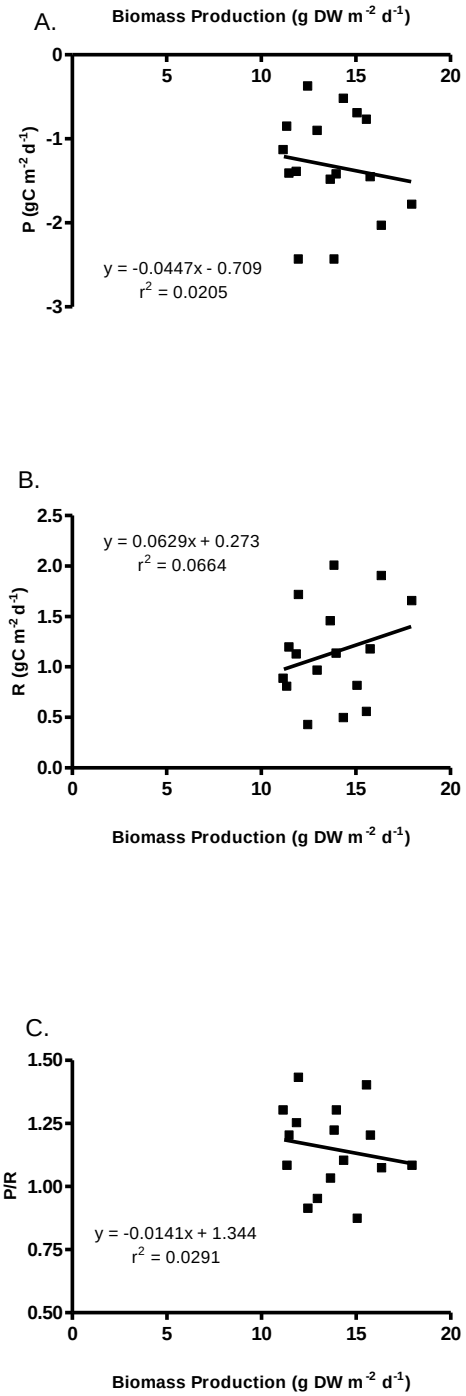

Figure B. 3. Linear regression analysis for the testing of operating conditions of (high light, low NLR, manure), showing the following metabolic measurements versus biomass production: (A) primary productivity (P); (B) respiration (R); (C) P/R ratio.

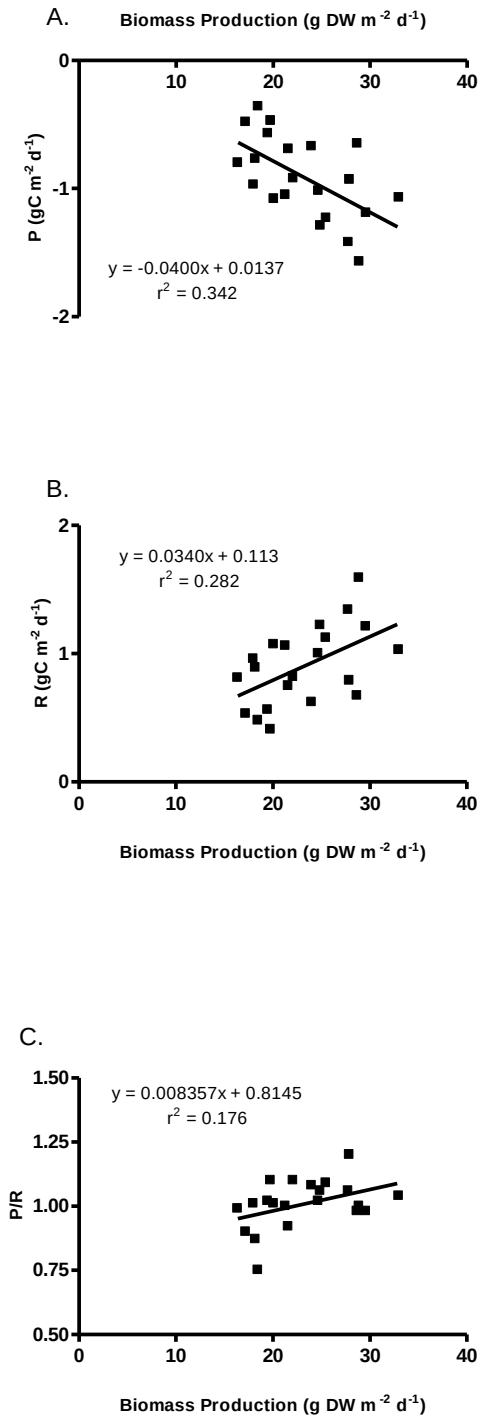

Figure B. 4. Linear regression analysis for the testing of operating conditions of (high light, medium NLR, manure), showing the following metabolic measurements versus biomass production: (A) primary productivity (P); (B) respiration (R); (C) P/R ratio.

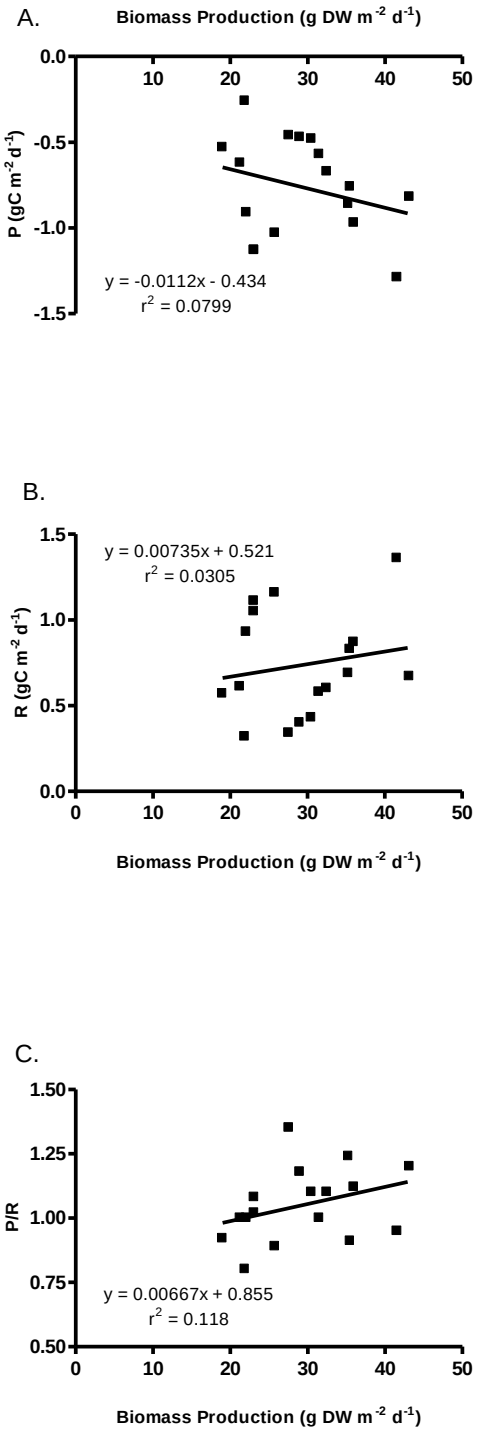

Figure B. 5. Linear regression analysis for the testing of operating conditions of (high light, high NLR, manure), showing the following metabolic measurements versus biomass production: (A) primary productivity (P); (B) respiration (R); (C) P/R ratio.

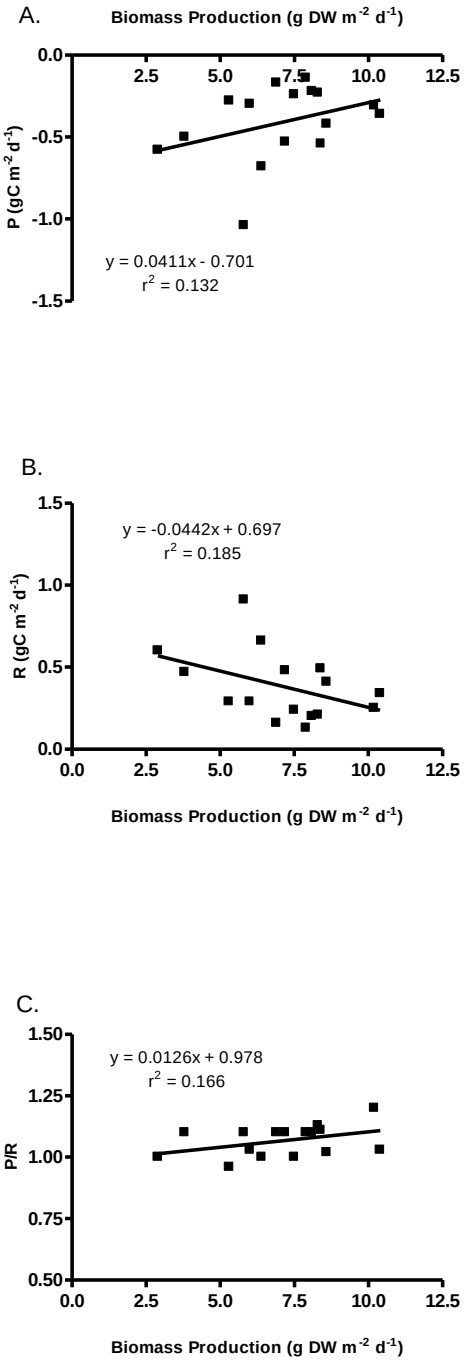

Figure B. 6. Linear regression analysis for the testing of operating conditions of (high light, low NLR, Bristol's), showing the following metabolic measurements versus biomass production: (A) primary productivity (P); (B) respiration (R); (C) P/R ratio.

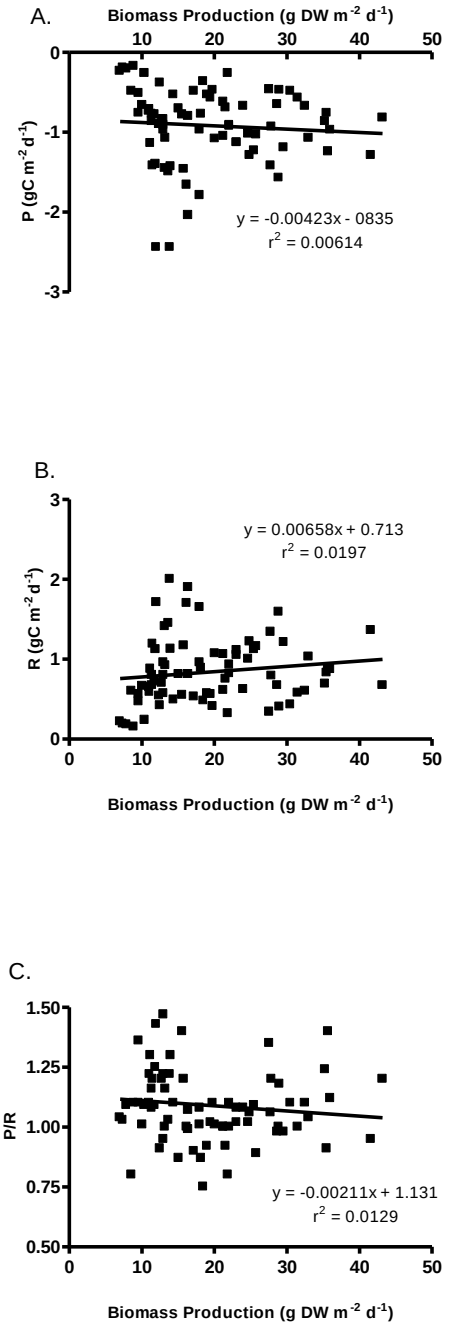

Figure B. 7. Linear regression analysis for all data samples from tests of all operating conditions except (low light, low NLR, manure) and (low light, low NLR, Bristol's), showing the following metabolic measurements versus biomass production: (A) primary productivity (P); (B) respiration (R); (C) P/R ratio.

Appendix C: Light Regimes Data for Subsidy-Stress Experiments

Measurements of the light intensity on each ATS unit were made periodically throughout all subsidy-stress experiments. In October 2007, it was observed that the intensity of the lights was lower than had been measured previously. Bulb age and wear were suspected to be the cause, and the bulbs were replaced with new bulbs at this time, resulting in the general division of experiments between low and high light conditions.

On each ATS unit, measurements of the light intensity were made at 25 locations evenly spaced in the ATS growth area. These were averaged for each ATS for each date of measurement using Theissen polygon weighting (Ward and Trimble 2004), the results of which are shown in Table C. 1.

Table C. 1. Weighted mean and standard deviation of light intensities for the set of ATS units in the lab measured at various times throughout the set of experiments. Means and standard deviations are calculated using Theissen polygon areal weighting of 25 measurements evenly distributed as a grid over the ATS growth area.

ATS No.	Light Intensity (μmol m^{-2} s^{-1}) at Date of Measurement			
	April 2007	**Oct. 2007**	**Nov. 2007**	**July 2008**
1	216 ± 107	186 ± 80	244 ± 129	227 ± 113
2	188 ± 84	167 ± 75	297 ± 143	--
4	259 ± 143	206 ± 108	326 ± 176	--
5	224 ± 104	169 ± 77	322 ± 166	--
7	231 ± 43	--	--	184 ± 40

A two-way ANOVA analysis (Table C. 2 and Table C. 3) on ATS1 through 5 for April, October, and November 2007 measurements of light intensity showed that "Date" accounts for 13.5% of the variation ($F=23.5$, $Df_n=2$, $Df_d=288$, $P<0.0001$); variation for "ATS no." or their interaction were not significant ($P>0.05$).

Table C. 2. Table of results of a two-way ANOVA analysis on average light levels measured on each ATS on different dates.

Source of Variation	Df	Sum-of-squares	Mean square	F
Interaction	6	81290	13550	0.9289
Date	2	685400	342700	23.50
ATS no.	3	114400	38120	2.614
Residual	288	4200000	14580	

Table C. 3. Table of results of a two-way ANOVA analysis on average light levels measured on each ATS on different dates, in which only the date of measure was significant.

Source of Variation	% of total variation	P value	Significant?
Interaction	1.60	0.4744	No
Date	13.49	<0.0001	Yes
ATS no.	2.25	0.0515	No

The means of the columns in Table C. 1 were tested using the student's t-test. Results for this test (Table C.4) show that the means between April and October 2007 were not significantly different (P=0.0688), but the means between October and November 2007 (after the new bulbs were installed) were significantly different (P=0.0053).

Table C. 4. Result of student t-tests between the first 3 columns of Table C. 1. Results show that the means of the light intensity are significantly different between Oct. and Nov. 2007, before and after light bulbs were replaced, but were not significantly different between April and October 2007 when no bulb changes were made.

Result	April 2007 vs Oct 2007	Oct 2007 vs Nov 2007
Unpaired t-test with Welch's Correction		
P value	0.0688	0.0053
Means signif. different? (P < 0.05)	No	Yes
One- or two-tailed P value?	Two-tailed	Two-tailed
Welch-corrected t, Df	t=2.311 Df=5	t=5.504 Df=4
How big is the difference?		
Mean ± SEM of first column	221.8 ± 14.62 N=4	182.0 ± 9.065 N=4
Mean ± SEM of second column	182.0 ± 9.065 N=4	297.3 ± 18.87 N=4
Difference between means	39.75 ± 17.20	-115.3 ± 20.94
95% confidence interval	-4.475 to 83.98	-173.4 to -57.13
R squared	0.5164	0.8834

The maximum light intensity levels as measured in the center of each ATS bed is also reported (Table C. 5). A two-way ANOVA analysis (Table C. 6 and Table C. 7) on ATS1 through 5 for April, October, and November 2007 measurements of maximum light intensity showed that "Date" accounts for 60.95% of the variation ($F=22.0$, $Df_n=2$, $Df_d=6$, $P=0.0017$), while "ATS no." accounts for 30.74% of the variation ($F=7.40$, $Df_n=3$, $Df_d=6$, $P=0.0193$).

Table C. 5. Maximum light intensity for each ATS unit in the lab measured at various times throughout the set of experiments. Maximum intensity was measured in the exact center of the ATS growth area.

ATS No.	Light Intensity (µmol m^{-2} s^{-1}) at Date of Measurement			
	April 2007	**Oct. 2007**	**Nov. 2007**	**July 2008**
1	357	277	378	416
2	316	270	464	--
4	477	385	553	--
5	392	265	527	--
7	272	--	--	255

Table C. 6. Table of results of a two-way ANOVA analysis on average light levels measured on each ATS on different dates.

Source of Variation	Df	Sum-of-squares	Mean square	F
Date	2	65750	32880	22.00
ATS no.	3	33160	11050	7.398
Residual	6	8966	1494	

Table C. 7. Table of results of a two-way ANOVA analysis on maximum light levels measured on each ATS on different dates, in which both date of measure and ATS number was significant.

Source of Variation	% of total variation	P value	Significant?
Date	60.95	0.0017	Yes
ATS no.	30.74	0.0193	Yes

The means between the columns in Table C. 5 were tested using the student's t-test. Results for this test (Table C. 8) show that the means between April and October 2007 were not significantly different (P=0.1113), but the means between October and November 2007 (after the new bulbs were installed) were significantly different (P=0.0133).

Table C. 8. Result of student t-tests between the first 3 columns of Table C. 5. Results show that the means of the light intensity are significantly different between Oct. and Nov. 2007, before and after light bulbs were replaced, but were not significantly different between April and October 2007 when no bulb changes were made.

Result	April 2007 vs Oct 2007	Oct 2007 vs Nov 2007
Unpaired t-test with Welch's Correction		
P value	0.1113	0.0133
P value summary	ns	*
Means signif. different? (P < 0.05)	No	Yes
One- or two-tailed P value?	Two-tailed	Two-tailed
Welch-corrected t, Df	t=1.931 Df=5	t=3.747 Df=5
How big is the difference?		
Mean ± SEM of first column	385.5 ± 34.23 N=4	299.3 ± 28.69 N=4
Mean ± SEM of second column	299.3 ± 28.69 N=4	480.5 ± 38.94 N=4
Difference between means	86.25 ± 44.66	-181.3 ± 48.37
95% confidence interval	-28.57 to 201.1	-305.6 to -56.90
R squared	0.4273	0.7374

Appendix D: Algal Species Abundances

To characterize the relative competitiveness of algae in the ATS systems throughout various trials, algae were sampled periodically from each of the ATS units throughout the experiments to determine the relative abundance of the various species in the ATS bed. The methods used for characterizing the algae in the ATS units were as follows: algae were sampled with tweezers from the screen bed of each ATS unit in three places, typically near the center of the growth area of the ATS bed, although the specific location of sampling was haphazardly selected. Sampling occurred just prior to a harvest and was performed numerous times throughout the term of operation of the ATS units. These samples were combined in a sample vial. The vial was shaken vigorously by hand to homogenize and was sub-sampled three times with tweezers; each subsample was then mounted on a microscope slide. Using a microscope, algae was keyed to the genus level for each subsample. It was known from prior studies (Mulbry and Wilkie 2001) that the ATS units were typically dominated by algae from the *Rhizoclonium*, *Microspora*, and *Oscillatoria* genera. For each subsample, an indication of the relative abundance of each of these genera of algae was made according to the following designations: (0) = Absent; (1) = Rare; (2) = Common; (3) = Abundant. Unknown genera of algae (typically one of many planktonic forms) were categorized as "Other" and ascribed an abundance designation. Analyses of these data included calculating the subsample mean and standard deviation of the abundance number designations for each algal genus in each ATS unit on each sample date. The mean was divided by the sum of all abundance means (across all genus designations) for that ATS unit and sample day to yield a percent abundance for each genus. The recorded data included sample date, nitrogen loading rate

(NLR) and feed type (i.e., manure, Miracle Gro®, urea solution, or Bristol's solution) for the harvest period, average flow rate and wave surge frequency for two weeks prior to sample date, and the relative abundance for each algal genus (Table D. 1).

Table D. 1.Master list of algal relative abundance under various ATS units and operating conditions.

ATS No.	Day	Flow Rate (gpm)	Tip Freq (min^{-1})	NLR (g N d^{-1})	Feed Type	NO_3 (mg/l)	Relative Abundance			
							Osc	Rhizo	Microsp	Other
1	0	15.0	5.0	0.70	M	2	0.206	0.441	0.353	0.000
1	3	10.0	3.3	0.70	M	1	0.067	0.533	0.400	0.000
1	19	1.0	0.3	0.70	M	0	0.056	0.000	0.549	0.394
1	24	2.3	0.8	0.70	M	0	0.154	0.154	0.615	0.077
1	34	3.7	1.2	1.20	U	7	0.056	0.333	0.500	0.111
1	44	13.3	4.4	0.72	U	0	0.235	0.294	0.471	0.000
1	59	21.7	7.2	1.20	U	47	0.171	0.390	0.390	0.049
1	89	17.5	5.8	0.98	MG	17	0.067	0.600	0.200	0.133
1	93	15.0	5.0	1.08	MG	44	0.333	0.389	0.278	0.000
1	101	16.7	5.6	0.73	MG	72	0.286	0.333	0.381	0.000
1	112	35.0	11.7	0.28	B	48	0.200	0.467	0.333	0.000
1	126	35.0	11.7	0.54	B	0	0.176	0.529	0.176	0.118
1	133	35.0	11.7	0.89	B	6	0.045	0.409	0.273	0.273
1	133	35.0	11.7	0.89	B	6	0.000	0.692	0.154	0.154
1	147	35.0	11.7	0.86	B	67	0.200	0.600	0.067	0.133
1	161	33.3	11.1	0.75	B	88	0.000	0.391	0.348	0.261
1	170	25.0	8.3	0.60	B	49	0.111	0.389	0.500	0.000
1	183	16.7	5.6	0.66	B	23	0.059	0.471	0.471	0.000
1	188	13.3	4.4	0.75	B	47	0.000	0.450	0.450	0.100
1	198	15.0	5.0	0.75	B	91	0.000	0.348	0.391	0.261
1	207	21.7	7.2	0.75	B	82	0.235	0.529	0.176	0.059
1	212	20.0	6.7	0.45	B	68	0.118	0.529	0.118	0.235
1	226	16.7	5.6	0.64	B	82	0.071	0.643	0.143	0.143
1	247	11.7	3.9	0.38	B	78	0.286	0.321	0.071	0.321
2	0	7	2.3	2.00	M	0	0.167	0.367	0.467	0.000
2	3	7	2.3	2.00	M	0	0.267	0.333	0.400	0.000
2	19	7	2.3	2.50	M	0	0.188	0.438	0.375	0.000
2	24	7	2.3	2.50	M	0	0.154	0.346	0.346	0.154
2	34	7	2.3	2.50	M	2	0.308	0.346	0.269	0.077
2	44	7	2.3	1.50	M	0	0.286	0.214	0.286	0.214
2	59	7	2.3	2.88	M	31	0.340	0.234	0.340	0.085
2	89	7	2.3	0.98	MG	87	0.238	0.333	0.429	0.000
2	93	7	2.3	0.73	MG	99	0.067	0.333	0.600	0.000
2	106	7	2.3	0.48	MG	63	0.317	0.195	0.439	0.049
2	112	7	2.3	0.33	MG	60	0.333	0.381	0.286	0.000
2	126	7	2.3	0.54	B	3	0.000	0.818	0.182	0.000
2	133	7	2.3	0.86	B	6	0.375	0.375	0.167	0.083
2	147	7	2.3	0.64	B	54	0.118	0.294	0.529	0.059
2	154	15	5.0	0.86	B	58	0.000	0.900	0.000	0.100
4	0	0.25	0.1	2.00	M	0	0.280	0.000	0.720	0.000
4	3	0.25	0.1	2.00	M	0	0.200	0.200	0.600	0.000
4	19	0.25	0.1	2.50	M	0	0.316	0.000	0.316	0.368
4	24	0.25	0.1	2.50	M	24	0.375	0.000	0.625	0.000
4	34	0.25	0.1	2.50	M	2	0.304	0.043	0.261	0.391
4	44	0.25	0.1	1.50	M	0	0.231	0.077	0.692	0.000
4	59	0.25	0.1	2.88	M	0	0.318	0.000	0.409	0.273
4	89	0.25	0.1	0.98	MG	34	0.273	0.045	0.409	0.273
4	93	0.25	0.1	0.73	MG	74	0.095	0.048	0.429	0.429
4	101	0.25	0.1	0.58	MG	68	0.421	0.105	0.421	0.053
4	112	0.25	0.1	0.73	MG	112	0.450	0.150	0.300	0.100
4	126	0.25	0.1	0.54	B	140	0.000	0.391	0.391	0.217
4	133	0.25	0.1	0.32	B	37	0.200	0.280	0.280	0.240
4	147	0.25	0.1	0.64	B	38	0.000	0.563	0.063	0.375
4	154	0.25	0.1	0.82	B	31	0.000	0.222	0.500	0.278
5	0	35	11.7	2.00	M	0	0.529	0.162	0.279	0.029

Table D.1. Continued.

ATS No.	Day	Flow Rate (gpm)	Tip Freq (min^{-1})	NLR (g N d^{-1})	Feed Type	NO_3 (mg/l)	Relative Abundance			
							Osc	Rhizo	Microsp	Other
5	3	35	11.7	2.00	M	0	0.412	0.235	0.353	0.000
5	19	35	11.7	2.50	M	3	0.450	0.150	0.300	0.100
5	24	35	11.7	2.50	M	26	0.391	0.000	0.217	0.391
5	34	35	11.7	2.50	M	54	0.360	0.120	0.280	0.240
5	44	35	11.7	1.50	M	5	0.290	0.194	0.226	0.290
5	59	35	11.7	1.50	MG	90	0.533	0.000	0.467	0.000
5	89	35	11.7	0.93	MG	4	0.268	0.439	0.293	0.000
5	93	35	11.7	1.08	MG	7	0.056	0.500	0.444	0.000
5	101	35	11.7	0.98	MG	2	0.286	0.429	0.286	0.000
5	105	35	11.7	1.10	MG	0	0.200	0.360	0.200	0.240
5	126	35	11.7	0.70	MG	0	0.278	0.444	0.167	0.111
5	133	25	8.3	1.00	MG	0	0.381	0.429	0.190	0.000
5	147	15	5.0	0.30	MG	45	0.300	0.400	0.200	0.100
7	34	11	3.7	0	U	120	0.450	0.100	0.050	0.400
7	44	11	3.7	0	U	90	0.500	0.200	0.300	0.000
7	59	11	3.7	0.70	MG	0	0.000	1.000	0.000	0.000
7	89	27	9.0	0.88	MG	9	0.364	0.409	0.227	0.000
7	93	35	11.7	1.08	MG	46	0.471	0.353	0.176	0.000
7	101	35	11.7	0.53	MG	61	0.300	0.450	0.250	0.000
7	105	35	11.7	0.35	B	13	0.400	0.150	0.400	0.050
7	126	4	1.2	0.65	B	15	0.333	0.333	0.333	0.000
7	133	7	2.2	0.90	B	12	0.410	0.410	0.179	0.000
7	147	17	5.6	0.90	B	56	0.000	0.900	0.100	0.000
7	161	8	2.8	0.75	B	106	0.125	0.563	0.125	0.188
7	170	12	3.9	0.60	B	56	0.000	0.667	0.333	0.000
7	183	12	3.9	0.66	B	89	0.133	0.600	0.267	0.000
7	188	13	4.4	0.75	B	73	0.000	0.600	0.400	0.000
7	198	10	3.3	0.75	B	79	0.000	0.750	0.250	0.000
7	207	10	3.3	0.75	B	65	0.250	0.450	0.200	0.100
7	212	12	3.9	0.45	B	50	0.167	0.375	0.208	0.250
7	226	12	3.9	0.64	B	77	0.250	0.563	0.125	0.063
7	247	7	2.2	0.38	B	84	0.333	0.259	0.074	0.333

References

Adey, W. H. 1982. Algal Turf Scrubber. U. S. Patent and Trademark Office, United States.

Adey, W. H. 1987. Marine microcosms. Pages 133-149 *in* W. R. I. Jordan, M. E. Gilpin, and J. D. Aber, editors. *Restoration Ecology*. Cambridge University Press, Cambridge, U.K.

Adey, W. H., and J. M. Hackney. 1989. The composition and production of tropical marine algal turfs in laboratory and field experiments. Pages 1-80 *in* W. H. Adey and D. F. Farrier, editors. *The Biology, Ecology and Mariculture of Mithrax Spinosissimus, Utilizing Cultured Algal Turfs*. Mariculture Institute, Los Angeles, CA.

Adey, W. H., and K. Loveland. 2007. *Dynamic Aquaria: Building and Restoring Living Ecosystems*, Third edition. Academic Press, San Diego, California.

Adey, W. H., C. Luckett, and K. Jensen. 1993. Phosphorus removal from natural waters using controlled algal production. *Restoration Ecology* **1**:29-39.

Adey, W. H., C. Luckett, and M. Smith. 1996. Purification of industrially contaminated groundwaters using controlled ecosystems. *Ecological Engineering* **7**:191-212.

Anonymous. 1995. Aquaricare™ Algae Scrubbers & Light-up™ Trays. Aquatic BioEnhancement Systems, Sugar Land, Texas.

Antoine, S. E., and K. Benson-Evans. 1982. The effect of current velocity on the rate of growth of benthic algal community. *Int. Revue ges. Hydrobiol.* **67**:575-583.

APHA. 1995. *Standard Methods for the Examination of Water and Wastewater*, 19th Edition edition. American Public Health Association, Washington, DC.

Barr, N. G., A. Kloeppel, T. A. V. Rees, C. Scherer, R. B. Taylor, and A. Wenzel. 2008. Wave surge increases rates of growth and nutrient uptake in the green seaweed Ulva pertusa maintained at low bulk flow velocities. *Aquatic Biology* **3**:179-186.

Beyers, R. J. 1963. The metabolism of twelve aquatic laboratory microecosystems. *Ecological Monographs* **33**:281-306.

Beyers, R. J. 1964. Measuring the carbon dioxide metabolism of aquatic organisms. *American Biology Teacher* **27**:499-510.

Beyers, R. J. 1965. The pattern of photosynthesis and respiration in laboratory microecosystems. Pages 63-74 *in* C. R. Goldman, editor. I.B.P. PF Symposium. University of California Press, Pallanza, Italy.

Beyers, R. J. 1974. Report of the Savannah River Laboratory. University of Georgia, Aiken, South Carolina.

Beyers, R. J., J. L. Larimer, H. T. Odum, R. B. Parker, and N. E. Armstrong. 1963. Directions for the determination of changes in carbon dioxide concentration from changes in pH. *Publications of the Institute of Marine Science Texas* **9**:454-489.

Beyers, R. J., and H. T. Odum. 1959. The use of carbon dioxide to construct pH curves for the measurement of productivity. *Limnology and Oceanography* **4**:499-502.

Beyers, R. J., and H. T. Odum. 1993. *Ecological Microcosms*. Springer-Verlag, New York.

Beyers, R. J., and R. W. Warwick. 1968. Production of carbon dioxide by *Rangia cuneata*. *Contributions in Marine Science* **13**:43-50.

Biggs, B. J. F., D. G. Goring, and V. I. Nikora. 1998. Subsidy and stress responses of stream periphyton to gradients in water velocity as a function of comunity growth form. *Journal of Phycology* **34**:598-607.

Biggs, B. J. F., and C. W. Hickey. 1994. Periphyton responses to a hydraulic gradient in a regulated river in New Zealand. *Freshwater Biology* **32**:49-59.

Blersch, D. M. 2004. *Investigations into the system dynamics of a wetland soil technoecosystem using redox potential as a metabolic indicator and feedback control parameter.* M.S.Thesis, University of Maryland, College Park, MD.

Blersch, D. M., and P. C. Kangas. 2006. Autonomous behaviour of a wetland soil technoecosystem. *Environmental Engineering Science* **23**:285-295.

Bothwell, M. L. 1988. Growth rate responses of lotic periphytic diatoms to experimental phosphorus enrichment: The influence of temperature and light. *Can. J. Fish. Aquat. Sci.* **45**:261-270.

Bott, T. L. 1996. Primary productivity and community respiration. Pages 533-556 *in* F. R. Hauer and G. A. Lamberti, editors. *Methods in Stream Ecology*. Academic Press, San Diego.

Broad, W. J. 2005. A web of sensors, taking Earth's pulse. Page 1 *in* The New York Times, New York City.

Brooks, R. A. 2002. *Flesh and Machines: How Robots Will Change Us*. Pantheon Books, New York.

Cai, T. 2002. *The Maximum Power Principle: An Empirical Investigation*. Ph.D. Dissertation, University of Florida, Gainesville, Florida.

Cai, T. T., C. L. Montague, and J. S. Davis. 2006. The maximum power principle: An empirical investigation. *Ecological Modelling* **190**:317-335.

Camazine, S., J. Deneubourg, N. R. Franks, J. Sneyd, G. Theraulaz, and E. Bonabeau. 2001. *Self-Organization in Biological Systems*. Princeton University Press, Princeton, New Jersey.

Carignan, R. 1998. Automated determination of carbon dioxide, oxygen, and nitrogen partial pressures in surface waters. *Limnology and Oceanography* **43**:969-975.

Carpenter, R. C., H. T. P. Williams, and W. H. Adey. 1991. Measurements of primary productivity and nitrogenase activity of coral reef algae in a chamber incorporating oscillatory flow. *Limnology and Oceanography* **36**:40-49.

Carpenter, R. C., and S. L. Williams. 1993. Effects of algal turf canopy height and microscale substratum topography on profiles of flow speed in a coral forereef environment. *Limnology and Oceanography* **38**:687-694.

Carpenter, R. C., and S. L. Williams. 2007. Mass transfer limitation of photosynthesis of coral reef algal turfs. *Marine Biology* **151**:435-450.

Clark, O., and R. Kok. 1998. Engineering of highly autonomous biosystems: Review of the relevant literature. *International Journal of Intelligent Systems* **13**:749-783.

Clark, O., R. Kok, and R. Lacroix. 1999. Mind and autonomy in engineered biosystems. *Engineering Applications of Artificial Intelligence* **12**:389-399.

Clark, O. G., and R. Kok. 1999. Characterizing biosystems as autopoietic entities. Unpublished manuscript, Dept. Agricultural and Biosystems Engineering, McGill University.

Craggs, R. J., W. H. Adey, B. K. Jessup, and W. J. Oswald. 1996. A controlled stream mesocosm for tertiary treatment of sewage. *Ecological Engineering* **6**:149-169.

DeAngelis, D. L., M. Loreau, D. Neergaard, P. J. Mulholland, and E. R. Marzolf. 1995. Modelling nutrient-periphyton dynamics in streams: The importance of transient storage zones. *Ecological Modelling* **80**:149.

DeGrandpre, M. D., T. R. Hammar, S. P. Smith, and F. L. Sayles. 1995. In-situ measurements of seawater P(CO_2). *Limnology and Oceanography* **40**:969-975.

Doty, M. S. 1971. Measurement of water movement in reference to benthic algal growth. *Botanica Marina* **14**:32-35.

Duffield, C. 1976. *Geothermal Technoecosystems and Water Cycles in Arid Lands*, University of Arizona Office of Arid Lands Studies, Tucson, Arizona.

Falter, J. l., M. J. Atkinson, and C. F. M. Coimbra. 2005. Effects of surface roughness and oscillatory flow on the dissolution of plaster forms: Evidence for nutrient mass transfer to coral reef communities. *Limnology and Oceanography* **50**:246-254.

Fernando, C., and A. Penn. 2006. The origin of autonomy at the chemical and ecosystem levels. Autonomy Workshop Paper, Artificial Life X, Bloomington, Indiana.

Griffith, P. C., J. D. Cubit, W. H. Adey, and J. N. Norris. 1987. Computer-automated flow respirometry--Metabolism measurements on a Caribbean reef flat and in a microcosm. *Limnology and Oceanography* **32**:442-451.

Hopgood, A. A. 2001. *Intelligent Systems for Engineers and Scientists*, 2nd edition. CRC Press, Boca Raton, Florida.

Horner, R. R., and E. B. Welch. 1981. Stream periphyton development in relation to current velocity and nutrients. *Canadian Journal of Fisheries and Aquatic Sciences* **38**:449-457.

Horner, R. R., E. B. Welch, M. R. Seeley, and J. M. Jacoby. 1990. Responses of periphyton to changes in current velocity, suspended sediment and phosphorus concentration. *Freshwater Biology* **24**:215-232.

Hydromentia. 2005. S-154 Pilot Single Stage Algal Turf Scrubber (ATS^{TM}) Final Report. South Florida Water Management District.

Ieropoulos, I. A., J. Greenman, C. Melhuish, and I. Horsfield. 2009. Artificial symbiosis in EcoBots. Pages 185-211 *in* A. Adamatzky and M. Komosinski, editors. *Artificial Life Models in Hardware*. Springer, London.

Izquierdo, L. R., S. S. Izquierdo, J. M. Galán, and J. I. Santos. 2009. Techniques to understand computer simulations: Markov chain analysis. *Journal of Artificial Societies and Social Simulation* **12**(1):6.

Jokiel, P. L., Morrissey, J.I. 1993. Water motion on coral reefs: evaluation of the 'clod card' technique. *Marine Ecology Progress Series* **93**:175-181.

Kangas, P. C. 2004. *Ecological Engineering: Principles and Practice*. Lewis Publishers, Boca Raton, Florida.

Kania, H. J., and R. J. Beyers. 1974. Feedback control of light input to a microecosystem by the system. Savannah River Ecology Laboratory Report, Aiken, SC.

Kebede-Westhead, E., C. Pizarro, W. W. Mulbry, and A. C. Wilkie. 2003. Production and nutrient removal by periphyton grown under different loading rates of anaerobically digested flushed dairy manure. *Journal of Phycology* **39**:1275.

Kemeny, J. G., and J. L. Snell. 1960. *Finite Markov Chains*. D. Van Nostrand Co., Inc., Princeton, NJ.

Kok, R., and R. Lacroix. 1993. An analytical framework for the design of autonomous, enclosed agroecosystems. *Agricultural Systems* **43**:235-260.

Krebs, C. J. 1994. *Ecology: The Experimental Analysis of Distribution and Abundance*, 4th edition. HarperCollins College Publishers, New York.

Larned, S. T., V. I. Nikora, and B. J. F. Biggs. 2004. Mass-transfer-limited nitrogen and phosphorus uptake by stream periphyton: A conceptual model and experimental evidence. *Limnology and Oceanography* **49**:1992-2000.

Lau, Y. L., and D. Liu. 1993. Effect of flow rate on biofilm accumulation in open channels. *Water Research* **27**:355-360.

Lewis, J. B. 1977. Processes of organic production on coral reefs. *Biological Reviews* **52**:305-347.

Liebig, J. 1840. *Organic Chemistry in its Applications to Agriculture and Physiology*.

Lin, K.-C., Y.-L. Lee, and C.-Y. Chen. 2007. Metal toxicity to Chlorella pyrenoidosa assessed by a short-term continuous test. *Journal of Hazardous Materials* **142**:236-241.

Lotka, A. J. 1922. Contribution to the energetics of evolution. *Proc. Natl. Acad. Sci. USA* **8**:147-151.

Marsh, J. A. 1970. Primary productivity of reff-building calcareous red algae. *Ecology* **51**:256-263.

Masters, G. M. 1991. *Introduction to Environmental Engineering and Science*. Prentice Hall, Englewood Cliffs, New Jersey.

Mcintire, C. D. 1966a. Some effects of current velocity on periphyton communities in laboratory streams. *Hydrobiologia* **27**:559-570.

McIntire, C. D. 1966b. Some factors affecting respiration of periphyton communities in lotic environments. *Ecology* **47**:918-930.

Mitsch, W. J., and S. E. Jorgensen. 2004. *Ecological Engineering and Ecosystem Restoration*. John Wiley and Sons, Inc., Hoboken, Nw Jersey.

Momo, F. R. 1995. A new model for periphyton growth in running waters. *Hydrobiologia* **299**:215-218.

Mulbry, W., E. K. Westhead, C. Pizarro, and L. Sikora. 2005. Recycling of manure nutrients: use of algal biomass from dairy manure treatment as a slow release fertilizer. *Bioresource Technology* **96**:451.

Mulbry, W. W., and A. C. Wilkie. 2001. Growth of benthic freshwater algae on dairy manures. *Journal of Applied Phycology* **13**:301-306.

Myers, J., and L. B. Clark. 1944. Culture conditions and the development of the photosynthetic mechanism. II. An apparatus for the continuous culture of *Chlorella*. *J. Gen. Physiol.* **28**:103-112.

Nelson, M., T. L. Burgess, A. Alling, N. Alvarezromo, W. F. Dempster, R. L. Walford, and J. P. Allen. 1993. Using a closed ecological system to study earth's biosphere. *Bioscience* **43**:225-236.

Nikora, V. I., D. G. Goring, and B. J. F. Biggs. 1998. A simple model of stream periphyton-flow interactions. *Oikos* **81**:607-611.

Odum, E. P. 1969. The strategy of ecosystem development. *Science* **164**:262-270.

Odum, E. P., and G. W. Barrett. 2005. *Fundamentals of Ecology*, 5th Edition edition. Thomson Brooks/Cole, Belmont, California.

Odum, E. P., J. T. Finn, and E. H. Franz. 1979. Perturbation theory and the subsidy-stress gradient. *Bioscience* **29**:349-352.

Odum, H. T. 1956. Primary production in flowing waters. *Limnology and Oceanography* **1**:102-117.

Odum, H. T. 1971. *Environment, Power and Society*. Wiley Interscience, New York.

Odum, H. T. 1975. Combining energy laws and corollaries of the maximum power principle with visual system mathematics. Pages 239-263 *in Ecosystem Analysis and Prediction*: Proceedings of the Conference on Ecosystems at Alta, Utah. SIAM Institute for Mathematics and Society, Philadelphia.

Odum, H. T. 1993. *Ecological and General Systems,* Second edition. University of Colorado Press, Niwot, Colorado.

Odum, H. T. 1996. *Environmental Accounting: EMERGY and Environmental Decision Making*. John Wiley & Sons, Inc., New York.

Odum, H. T. 2007. *Environment, Power, and Society for the Twenty-first Century : The Hierarchy of Energy*. Columbia University Press, New York.

Odum, H. T., and C. M. Hoskin. 1957. Metabolism of a laboratory stream microcosm. *Publications of the Institute of Marine Science University of Texas* **4**:16-46.

Odum, H. T., and R. C. Pinkerton. 1955. Time's speed regulator: The optimum efficiency for maximum power output in physical and biological systems. *American Scientist* **43**:321-343.

Park, K., D. W. Hood, and H. T. Odum. 1958. Diurnal pH variation in Texas Bays, and its application to primary production estimation. *Publications of the Institute of Marine Science Texas* **5**:47-64.

Petersen, J. E. 1998. *Scale and Energy Input in the Dynamics of Experimental Estuarine Ecosystems*. Ph.D. Dissertation, University of Maryland, College Park, Maryland.

Petersen, J. E. 2001. Adding artificial feedback to a simple aquatic ecosystem: the cybernetic nature of ecosystems revisited. *Oikos* **94**:533-547.

Phillips, O. M. 1977. *The Dynamics of the Upper Ocean,* Second edition. Cambridge University Press, Cambridge.

Porter, E. T., L. P. Sanford, and S. E. Suttles. 2000. Gypsum dissolution is not a universal integrator of 'water motion'. *Limnology and Oceanography* **45**:145-158.

Porter, J., P. Arzberger, H. Braun, P. Bryant, S. Gage, T. Hansen, P. Hanson, C. Lin, F. Lin, T. Kratz, W. Michener, S. Shapiro, and T. Williams. 2005. Wireless sensor networks for ecology. *Bioscience* **55**:561-572.

Premazzi, G., O. Ravera, and A. Lepers. 1978. A modified turbidostatic system for algal population studies. *Mitt. Internat. Verein. Limnol.* **21**:42-49.

Pulliam, H. R., and B. R. Johnson. 2002. Ecology's new paradigm: What does it offer designers and planners? Pages 51-84 *in* B. R. Johnson and K. Hill, editors. *Ecology and Design: Frameworks for Learning*. Island Press, Washington, DC.

Ruiz-Mirazo, K., J. Pereto, and A. Moreno. 2004. A universal definition of life: Autonomy and open-ended evolution. *Origins of Life and Evolution of the Biosphere* **34**:323-346.

Ryther, J. H. 1956. The measurement of primary production. *Limnology and Oceanography* **1**:72-84.

Sanford, L. P. 1997. Turbulent mixing in experimental ecosystem studies. *Marine Ecology Progress Series* **161**:265-293.

Saravia, L. A., F. Momo, and L. D. B. Lissin. 1998. Modelling periphyton dynamics in running water. *Ecological Modelling* **114**:35-47.

Sellers, P., R. H. Hesslein, and C. A. Kelly. 1995. Continuous measurement of CO_2 for estimation of air-water fluxes in lakes--An in-situ technique. *Limnology and Oceanography* **40**:575-581.

Silvester, N. R., and M. A. Sleigh. 1985. The forces on microorganisms at surfaces in flowing water. *Freshwater Biology* **15**:433-448.

Son, D. H., and T. Fujino. 2003. Modeling approach to periphyton and nutrient interaction in a stream. *Journal of Environmental Engineering* **129**:834-843.

Steinman, A. D., and G. A. Lamberti. 1996. Biomass and pigments of benthic algae. Pages 295-313 *in* F. R. Hauer and G. A. Lamberti, editors. *Methods in Stream Ecology*. Academic Press, San Diego.

Stevenson, R. J. 1996. The stimulation of drag and current. Pages 321-340 *in* R. J. Stevenson, M. L. Bothwell, and R. L. Lowe, editors. *Algal Ecology: Freshwater Benthic Ecosystems*. Academic Press, San Diego, California.

Streeter, V. L., and E. B. Wylie. 1975. *Fluid Mechanics*, 6th edition. McGraw-Hill Book Company, New York.

Stumm, W., and J. J. Morgan. 1995. *Aquatic Chemistry*, 3rd edition. John Wiley & Sons, New York.

Thomas, F. I. M., and C. D. Cornelisen. 2003. Ammonium uptake by seagrass communities: effects of oscillatory versus unidirectional flow. *Marine Ecology Progress Series* **247**:51-57.

Todd, J., and B. Josephson. 1996. The design of living technologies for waste treatment. *Ecological Engineering* **6**:109-136.

Trainor, F. R., and L. E. Shubert. 1974. Scenedesmus morphogenesis. Colony control in dilute media. *Journal of Phycology* **10**:30-33.

Vanriel, P., and L. Johnson. 1995. Action principles as determinants of ecosystem structure: The autonomous lake as a reference system. *Ecology* **76**:1741-1757.

Vernon, D., and D. Furlong. 1992. Relativistic ontologies, self-organization, autopoiesis, and artificial life: A progression in the science of the autonomous. Part I--The Philosophical Foundations. Pages 26-40. *in* B. McMullin, editor. *Autopoiesis and Perception*, Dublin City University.

Ward, A. D., and S. W. Trimble. 2004. *Environmental Hydrology*, Second edition. Lewis Publishers, Boca Raton, Florida.

Whitford, L. A. 1960. The current effect and growth of fresh-water algae. *Transactions of the American Microscopical Society* **79**:302-309.

Wilkie, A. C., and W. W. Mulbry. 2002. Recovery of dairy manure nutrients by benthic freshwater algae. *Bioresource Technology* **84**:81-91.

Wilkinson, S. 2001. Hungry for success--future directions in gastrobotics research. *Industrial Robot* **28**:213-219.

Williams, S. L., and R. C. Carpenter. 1998. Effects of unidirectional and oscillatory water flow on nitrogen fixation (acetylene reduction) in coral reef algal turfs, Kaneohe Bay, Hawaii. *Journal of Experimental Marine Biology and Ecology* **226**:293-316.